UNIVERSITY OF MIAMI

A Hydrologic and Stable Isotope Study of East Everglades National Park and the West Wellfield of Miami-Dade County, Florida

By

Walter Mark Wilcox

A THESIS

Submitted to the Faculty

of the University of Miami

in partial fulfillment of the requirements for

the degree of Master of Civil Engineering

Coral Gables, Florida

August 2000

UNIVERSITY OF MIAMI

A thesis submitted in partial fulfillment of
the requirements for the degree of
Master of Civil Engineering

A Hydrologic and Stable Isotope Study of East Everglades National Park and the West Wellfield of Miami-Dade County, Florida

Walter Mark Wilcox

Approved:

Dr. Helena Solo-Gabriele Assistant Professor of Civil Engineering	Dr. Steven G. Ullmann Dean of the Graduate School
Dr. Leonel Sternberg Professor of Biology	Dr. Frederick Nagle Professor of Geological Sciences

Walter Mark Wilcox (M.S., Civil Engineering)
A Hydrologic and Stable Isotope Study of East Everglades National Park and the West Wellfield of Miami-Dade County, Florida (August 2000)

Abstract of a master's thesis at the University of Miami.

Thesis supervised by Professor Helena Solo-Gabriele.

No. of pages in text: 177

An isotopic study was performed to assess the movement of groundwater for a site located in Miami-Dade County, Florida. The site encompasses portions of northeast Everglades National Park and western suburban Miami, incorporating the West Wellfield municipal pumping wells, a part of Levee 31N (L-31N) and lakes formed by rock mining. Hydrogeology of the area was evaluated through a review of available data including technical reports and geologic cores. Samples of ground, surface, and rain water were collected over a period from January 1996 to December 1998 and were analyzed for their isotopic composition. Various analytical and graphical techniques were used to analyze this data and two conceptual box models were developed to quantify flows between different regions within the site.

The hydrogeologic review indicates that the portion of the Biscayne Aquifer underlying the study site is, in general, highly transmissive with the exception of two semi-confining layers of reduced hydraulic conductivity. Isotopic results show that local rainfall is the predominant source of water to the

study site with additional water provided by Water Conservation Areas northwest of the site. Everglades surface water infuses into the aquifer and migrates east in the vicinity of Levee 31N. On the urban side of L-31N, “shallow” groundwater (above the deeper semi-confining layers) is substantially affected by urban rainfall while “deep” groundwater (below the deeper semi-confining layers) maintains a composition similar to that of Everglades water. Rock mining lakes in the area provide “breaks” in the semi-confining layers that allow for mixing of “shallow” and “deep” water. As water travels eastward, municipal well intakes, screened to a depth below the deeper semi-confining layer, draw upon not only “shallow” urban water (predominantly comprised of urban rainfall) and lake water (having influences from both urban rainfall and Everglades water) but also “deep” water that originated in the Everglades. Results from one of the box models estimate that over sixty percent of the water being removed by municipal pumping originated in the Everglades. These conclusions suggest that Everglades water, both directly through “deep” groundwater flow and indirectly through mixing with rock-mining lakes, is being drawn into the operating municipal wellfield.

Acknowledgments

I gratefully acknowledge a number of people without whom, the completion of this thesis could not have been accomplished. My committee chairperson, Dr. Helena Solo-Gabriele, was irreplaceable as a mentor, teacher, advisor and provider of much needed assistance. Her guidance and aid through every portion of the project was exceptional and appreciated.

My other committee members were also of great assistance. I owe a debt of gratitude to Dr. Leonel Sternberg, who spent many hours teaching me the nuances of stable isotope study and analysis. Dr. Frederick Nagle greatly expanded my knowledge of geology, a subject that, as an engineer, was very foreign to me at first.

A special thanks to Albert Herrera for providing data from the rock mining lakes for the isotope study. Technical assistance was provided by several other people as well, including Mark Nemeth, Tim Desmarais, Naila Hosein, Gudrun Ibler, Sharon Ewe, Kevin Cunningham, Angela Chong, Dr. David Chin and Margarida Masden.

Last, but certainly not least, for without these organizations there would have been no project whatsoever, I would like to thank Everglades National Park, the South Florida Water Management District and the United States Geological Survey for funding the study.

Table of Contents

Table of Contents (continued)

List of Figures

List of Figures (continued)

List of Tables

1

Motivation and Project Description

South Florida faces the constant problem of trying to find a balance between the water needs of its natural ecosystem, its population, and its industries and agriculture. Urban and agricultural expansion cause an ever growing need for water while at the same time put a strain on the existing fresh water supply by draining wetland areas for other uses and facilitating saltwater intrusion into the aquifer system through municipal pumping. In response to increasing water and land demands, the municipal wellfields of Miami-Dade County have progressively moved further west toward the Everglades. This expansion has raised concerns relating to the effect that municipal wellfields have on Everglades hydrology (Solo-Gabriele, 1998).

Already, nearly fifty percent of the historic Everglades have been destroyed or drained (Sonenshein, 2000). As the municipal wells draw water from a very highly transmissive aquifer, they could, depending on pumping rates, conceivably impact the flow of water in the Everglades. At this time, the relationship between Everglades flow and the municipal wells is poorly understood. This thesis will analyze this relationship by examining a study area in Miami-Dade County Florida.

The study site for this thesis will include parts of northeast Everglades National Park and western suburban Miami. This site incorporates the West Wellfield municipal pumping wells of Miami-Dade County, lakes formed by rock mining, a part of Levee 31N (L-31N) and a segment of the L-31N canal located just east of the levee between Everglades and urban waters. This area is hydraulically inter-connected, with changes to any part of the surface water or groundwater systems affecting the hydrology of the entire site. The extent to and the means by which these changes occur is unclear at this time. Due to the water management concerns previously outlined, the hydrologic impact of the municipal wellfield, located within two miles of the Everglades border, on the study site is of particular importance. Additional questions relating to the impact of rock mining in the area, the amount of seepage under the levee system and the possible effect of the canal as a boundary between Everglades and urban waters are all to some degree unanswered.

Taking into account all of these questions, the primary goal of this project is to determine whether Everglades water is being drawn into the municipal pumping wells of the West Wellfield. Additional goals will be to assess whether rock-mining lakes in the area have an effect on site hydrology, to determine if significant seepage under L-31N is occurring and to evaluate the extent to which the L-31N canal acts as a hydrologic boundary between Everglades and urban water. These goals will be accomplished by performing a thorough

hydrogeologic review of the study area through examination of technical papers and geologic cores as well as through a hydrologic study using stable isotopes of oxygen-18 and deuterium as tracers (Solo-Gabriele and Sternberg, 1998). This isotope study will incorporate data collected over a period from January 1996 to December 1998, incorporating water samples taken for use in this thesis with that of both previous and concurrent isotope work in the area (Solo-Gabriele, 1998, Ibler et al., 1999 and Herrera, 2000). Analytical and graphical techniques will be used to analyze this data and conceptual box models will be developed to quantify flows between different regions within the site. Additionally, a MODBRANCH computer model of a portion of the study site as developed by Nemeth (2000) and modified by Herrera (2000) exists. This model will be utilized to provide a means of comparison for the flow terms from the conceptual box models.

2

Description of Study Site

2.1 Overview of Study Site

The study area (Figure 2.1.1) is located in the western part of Miami-Dade County, Florida and is comprised of a wetland region in the northeastern corner of Everglades National Park as well as residential and agricultural areas of suburban Miami. The site is divided longitudinally by Levee 31N (L-31N) into what will be referred to as “Everglades” in the west and “urban” in the east (Figure 2.1.2). The area is bounded on the north by the Tamiami Canal (also designated as the L-29 and C-4 Canals). Near the southern boundary lies the C-1W Canal. Low topographic relief characterizes the study area. Land-surface elevations in the site range from 4 to 8 ft above sea level with the Everglades side being in general higher than the urban side.

Wetland areas inundated with surface water characterize land on the Everglades side of L-31N. Surface water in this part of the study area is on the order of 3 ft deep during most of the year. However, it is possible for decreased rainfall and gate operations within the southern Florida canal system to cause this water level to decline significantly. In fact, during the dry season from November to May, water may recede to the point that much of the area is left

completely dry for months at a time. While this condition was observed during 1996, it was not observed during 1997 and 1998 and is not a regular yearly event.

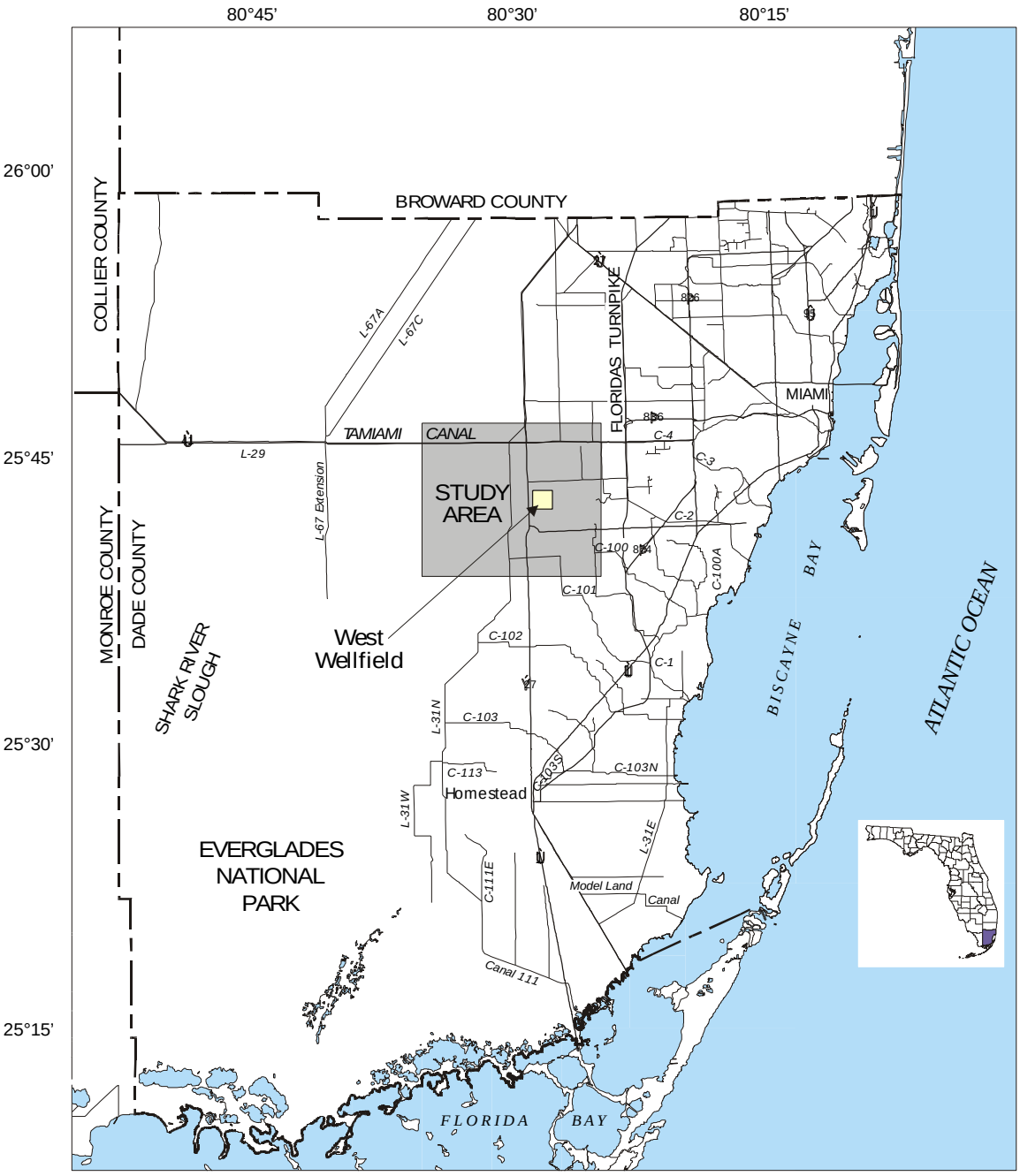

Figure 2.1.1 Location of Study Area (modified from Nemeth et al., 2000)

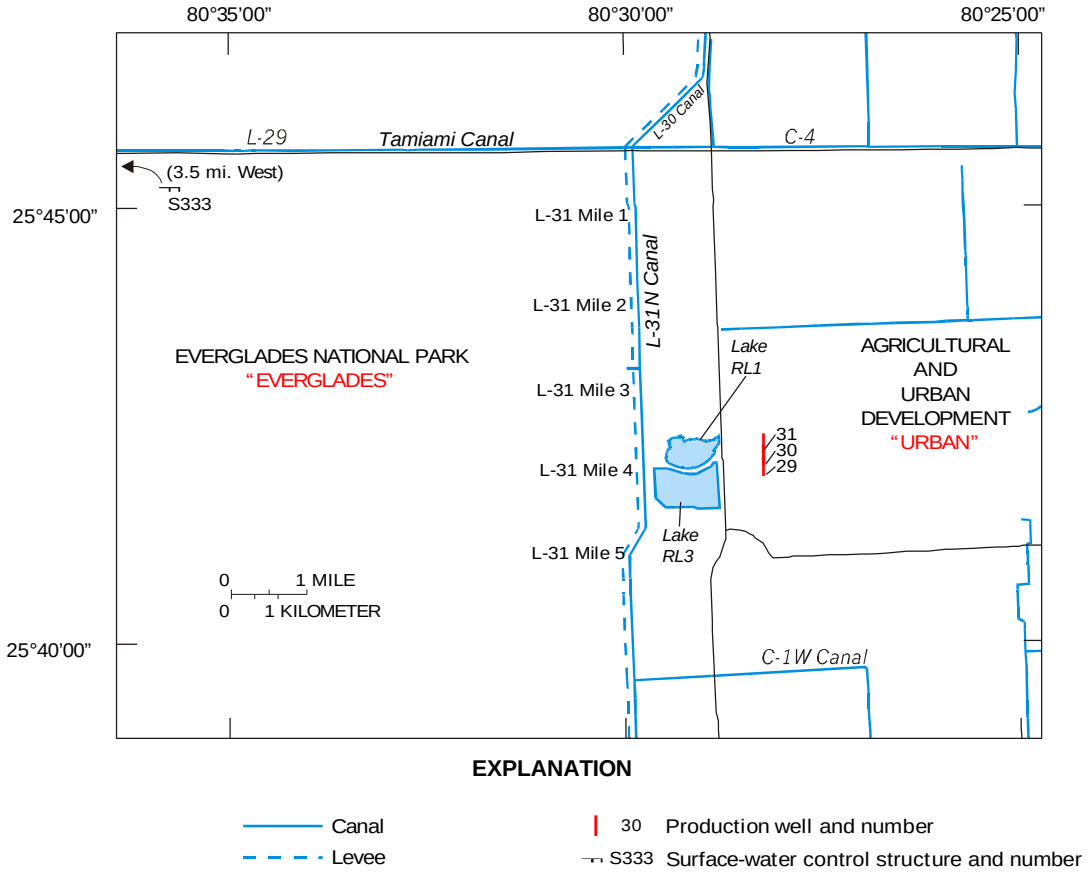

Figure 2.1.2 Study Area

The major structure of importance to this study on the Everglades side of L-31N is gate S333. This gate is located on Levee 67 at the Tamiami Canal. When in operation, it can deliver up to 1350 cfs from Conservation Area 3 into the Tamiami Canal and ultimately the Shark River Slough. The Shark River Slough runs through the western edge of the study site (Figure 2.1.3) and as a result, gate operations at S333 can affect water migration in the study area.

The urban (eastern) side of the study site encompasses the West Wellfield of Miami-Dade County. This wellfield draws water from the Biscayne aquifer at depths between 40 and 70 ft below land surface and is comprised of pumping

wells 29, 30 and 31. The wells are permitted for pumping rates of 10, 5 and 1 million gallons per day, respectively. The three wells are usually not operated simultaneously.

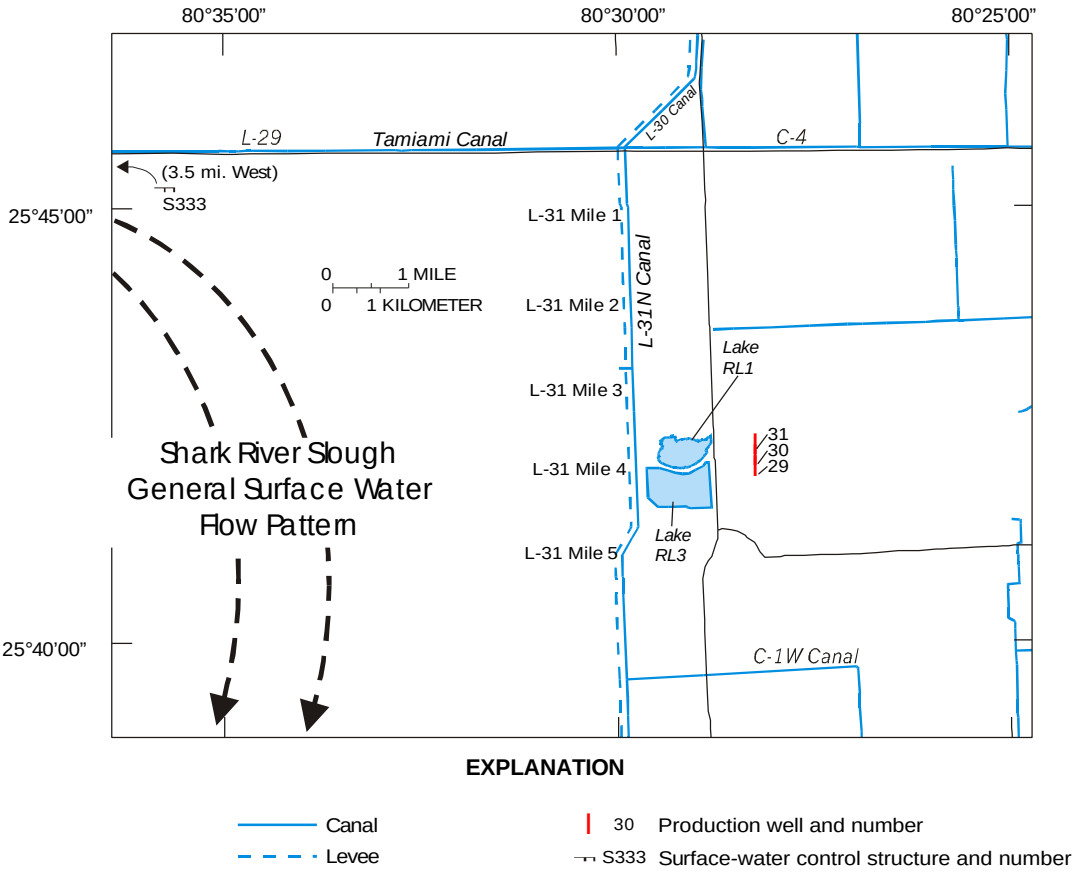

Figure 2.1.3 Shark River Slough

The L-31 N Canal (Figure 2.1.4) is located just to the east of the levee and flows from north to south, joining the Tamiami (L-29 and C-4) and L-30 Canals at the northern edge of the study area and the C-1W Canal at the area's southern boundary. This canal, having a depth of about 20 ft and a top width of about 100 ft, is the primary surface water canal within the study area. The stage of the canal generally does not vary by more than 3 ft.

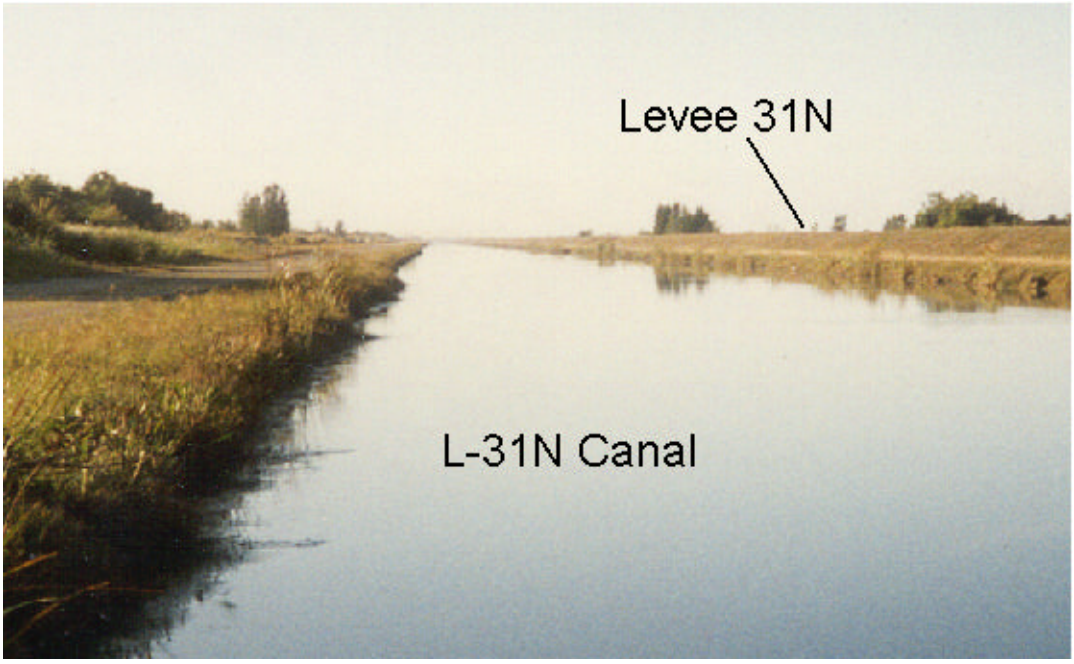

Figure 2.1.4 L-31N Canal

Several lakes are also present in the urban side of the study area. For the purposes of this investigation, two lakes, designated RL1 and RL3 in Figure 2.1.2, were examined. Both of these lakes are the result of rock mining and are somewhat variable in depth. RL1 increases in depth in a concentric fashion skewed towards the southeast corner of the lake. The greatest depths are on the order of 40 ft below ground surface elevation. RL3 is much more variable having bottom depths ranging from 30 ft to 55 ft in non-uniform patterns. On the eastern (outflow) side of the lakes, the groundwater table is generally lower than the lakes' water surface elevation, indicating that the lakes appear as a "stair step" where groundwater flows in on the west and out on the east (Herrera, 2000).

Many monitoring wells equipped with stage recorders are located within the study area. All wells utilized in this study are operated by the United States Geologic Survey

(USGS). Data from rain gages located at S336, S338 and G-3553 within the study area (Figure 2.1.5) were also used. The S336 and S338 gages are operated by the SFWMD while G-3553 is maintained by the USGS. Only daily values are available for S338 and G-3553 while both daily and hourly values are available for S336. Data from the three rain gages indicate that rainfall within the study site is highly variable. Averages of available rainfall data from the three sites were used in this thesis as outlined in Table 2.1.1. In the table, all values are the average of monthly data from S338, S336 and G-3553, unless otherwise noted. All data are reported in inches. Potential evaporation values were obtained from a weather station on Tamiami Trail located fifteen miles west of the study site. This station is operated by the SFWMD. Potential evaporation values in inches are provided in Table 2.1.2.

Table 2.1.1 - Rainfall Data (in)

Year	Month												Sum
	Jan	Feb	Mar	Apr	May	Jun	Jul	Aug	Sep	Oct	Nov	Dec	
1996	1.17	0.23	0.89	1.32	8.36	10.81	5.26	6.77[2]	4.82[2]	5.55[3]	0.41[3]	0.79[1]	**46.37**
1997	1.15[2]	1.27	2.97	5.72	4.22	11.13	4.66[2]	6.35[2]	11.38	0.72	3.34[4]	1.79	**54.68**
1998	1.34	5.12[2]	5.30[2]	0.43	3.22	5.36	6.06[2]	7.68	9.49	2.45[2]	4.44[2]	1.57[1]	**52.46**

[1] S338 Only
[2] Average of S338 and S336 only
[3] Average of S338 and G-3553 only
[4] Average of S336 and G-3553 only

Table 2.1.2 – Potential Evaporation Data (in)

Year	Month												Sum
	Jan	Feb	Mar	Apr	May	Jun	Jul	Aug	Sep	Oct	Nov	Dec	
1996	3.31	3.69	5.05	6.13	6.29	6.10	6.58	4.05	5.92	4.7	4.19	3.12	**59.30**
1997	3.03	3.28	5.22	5.68	6.17	5.66	5.99	5.31	4.78	4.89	3.2	2.98	**56.19**
1998	3.15	4.33	5.44	6.12	8.11	7.09	4.88	6.23	7.02	3.17	4.68	-	**60.22**

Reference will be made in later sections to the “focus area” of the study site. This designation was initially derived for the area of increased discretization in a MODBRANCH model of the site created in a related part of this project (but not within

the scope of this thesis) and outlined in Nemeth et al. (2000). In this thesis, it is used to refer to the general area of interest for water migration into the West Wellfield (Figure 2.1.6). This area stretches from L-31N mile 3 to L-31N mile 5 and encompasses the West Wellfield and its immediate surrounding urban areas, lakes RL1 and RL3 and the easternmost portions of the Everglades extending roughly two miles west of Levee 31N.

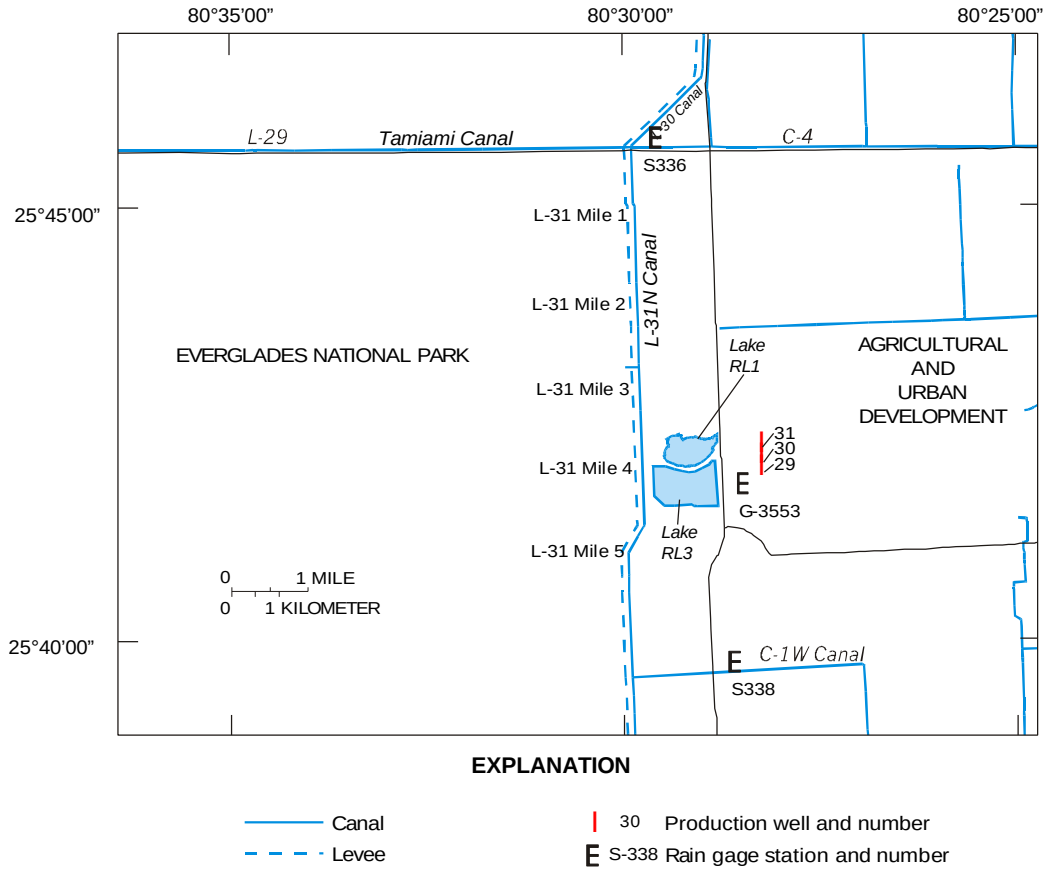

Figure 2.1.5 Rain Gages

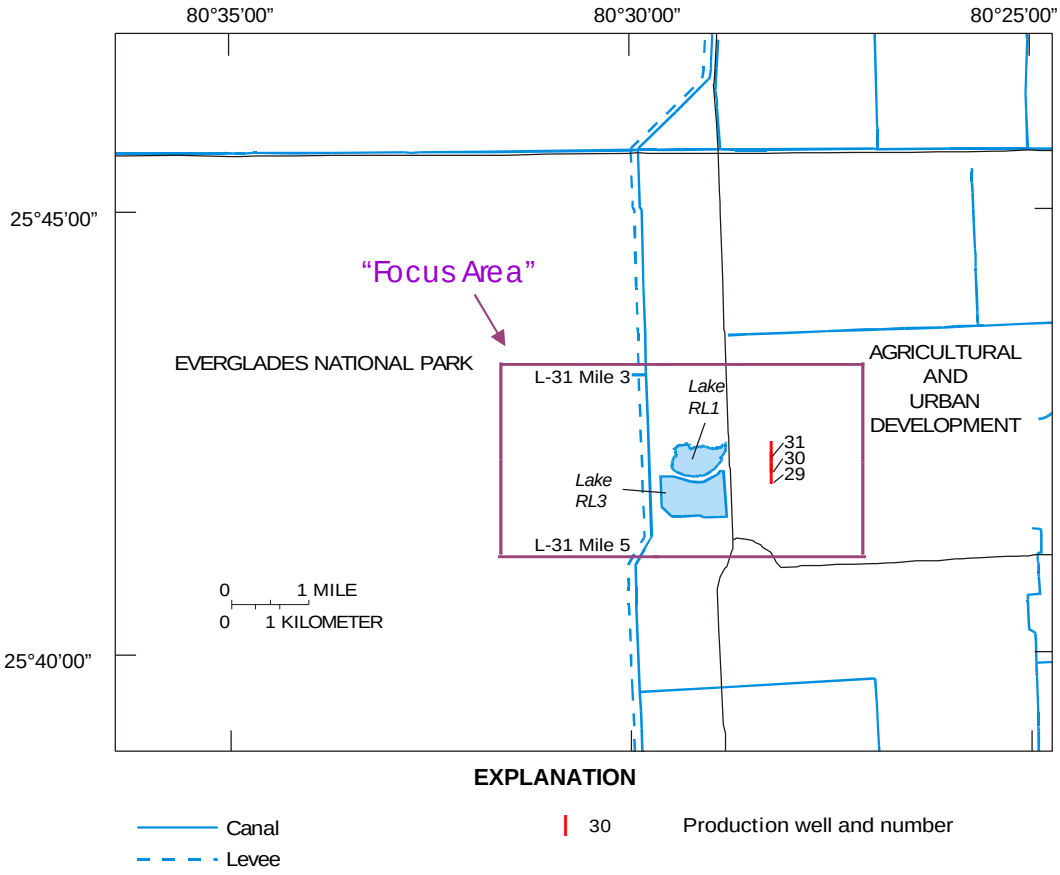

Figure 2.1.6 Focus Area

2.2 Geologic Background

The surficial aquifer system underlying South Florida extends to a depth of approximately 180 feet below mean sea level in the study area and is generally bounded on the lower end by the confining clays and silts present in the top portion of the Hawthorn Formation. In the Miami area, the unconfined Biscayne aquifer, the most important aquifer in the South Florida area from a water supply perspective, is found in the upper part of this surficial aquifer system. The Biscayne aquifer as defined by Fish and Stewart (1991) comprises

various portions of the Pamlico Sand, Miami Oolite (Miami Limestone), Anastasia Formation, Key Largo Limestone, Fort Thompson Formation, and highly permeable regions of the Tamiami Formation. The base of the Biscayne aquifer in the study site as determined using cross sections developed by Fish and Stewart (1991), is located at “the top of the low permeability sand (marl) of the Tamiami Formation” and slopes from a high point of approximately 44 feet below mean sea level in the southwest corner of the study area down to an elevation of roughly 84 feet below sea level in the northeast corner.

The portion of the Biscayne aquifer located in the study area mostly consists of highly permeable limestone having a very high hydraulic conductivity and includes three formations: the Tamiami Formation, the Fort Thompson Formation, and Miami Limestone (Figure 2.2.1). The Fort Thompson and Miami Limestone are of Pleistocene age, whereas the Tamiami Formation Formation is of the Pliocene and late Miocene ages (Randazzo, 1997).

The Tamiami Formation extends to a depth well below the base of the Biscayne aquifer (Causaras, 1987). The sandstone portion of the Tamiami Formation below the base of the Biscayne aquifer is not nearly as permeable as the formations above it and does not permit significant vertical flow (Fish and Stewart, 1991). The portion of the Tamiami Formation above the base of the Biscayne aquifer comprises highly permeable limestones as found in the Fort Thompson Formation or calcareous sandstones, which are also very porous. The

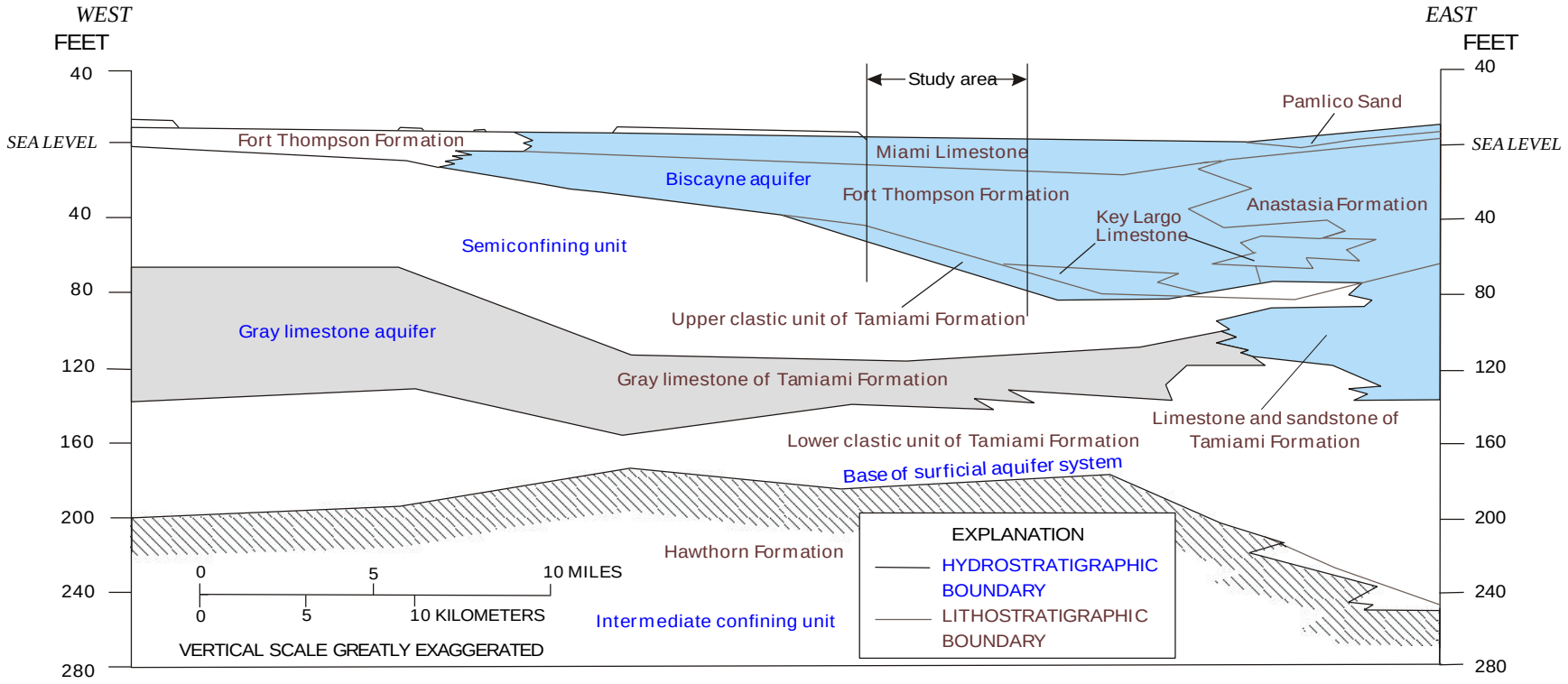

Figure 2.2.1 Hydrogeologic Section Showing Formations, Aquifers, and Confining Units of the Surficial Aquifer System in Central Miami Dade County, (modified from Fish and Stewart, 1991). Section extends along Tamiami Trail.

contact between the Fort Thompson Formation and the Tamiami Formation slopes from about 32.5 feet below sea level in the northwestern corner of the study area to 52.5 feet below sea level in the southeastern corner. The Fort Thompson Formation predominantly consists of marine and freshwater limestones riddled with secondary-solution cavities. Although these cavities are usually less than 2 in. (inches) in diameter, they are sufficiently abundant so as to make the formation very highly permeable (Fish and Stewart, 1991). The Fort Thompson Formation is between the Tamiami Formation and the Miami Limestone. Both the Fort Thompson Formation and the Tamiami Formation of the Biscayne aquifer are composed of highly permeable material and have estimated hydraulic conductivities of at least 20,000 ft / d (feet per day). In the study area, land surface elevation is approximately 6 to 8 ft above sea level. The Miami Limestone generally is found from surface elevation to about 8 to 12 ft below ground level (Causaras, 1987). The overall hydraulic conductivity of the Miami Limestone at 1000 ft / d to 5000 ft / d generally is lower and more variable than that of the Fort Thompson Formation and the portion of the Tamiami Formation above the base of the Biscayne aquifer. The slightly lower range of hydraulic conductivity values for the Miami Limestone, as compared to the rest of the Biscayne aquifer, may be due to variability in this formation as a consequence of soft layers within the limestone that have only minor development of secondary-solution porosity. Additionally, the presence of sand,

lime, mud, muck or marl found in this topmost formation can hinder ground-water flow (Fish and Stewart, 1991).

Recently, geologic study in the area has turned to determining the existence of semi-confining layers within the Biscayne aquifer. In the study area, there are two semi-confining layers of low-permeability limestone (Figure 2.2.2). The shallower of these layers is located near the top of the Fort Thompson Formation, just below the Miami Limestone, and is most likely the result of surface exposure caused by sea-level regression following the deposition of the formation. From a compilation of existing data, it has been determined that this layer begins about 10 ft below ground elevation and is roughly 2 feet thick, extending to a depth of 12 ft below ground elevation. This layer is very consistently found at this depth within the focus area of the study site and can be taken to be horizontal with only very localized variations.

The deeper semi-confining layer was not found to be as regularly horizontal as the first. On average, the layer is 5 feet thick and begins at a depth of 35 to 40 feet below ground surface elevation (and approximately 30 to 35 feet below mean sea level) in the focus area. Across the entire study site, this deeper layer slopes from a top elevation of 22.5 ft below sea level in the northwestern corner of the area to 42.5 ft below sea level in the southeastern corner and is taken as five feet thick. From available data, this layer appears to have roughly the same slope as the contact between the Tamiami Formation and the Fort

Thompson Formation, as outlined by Causaras (1987). This seems reasonable as the contact of the Tamiami Formation and the Fort Thompson Formation is only about approximately five feet deeper than the bottom of the semi-confining layer.

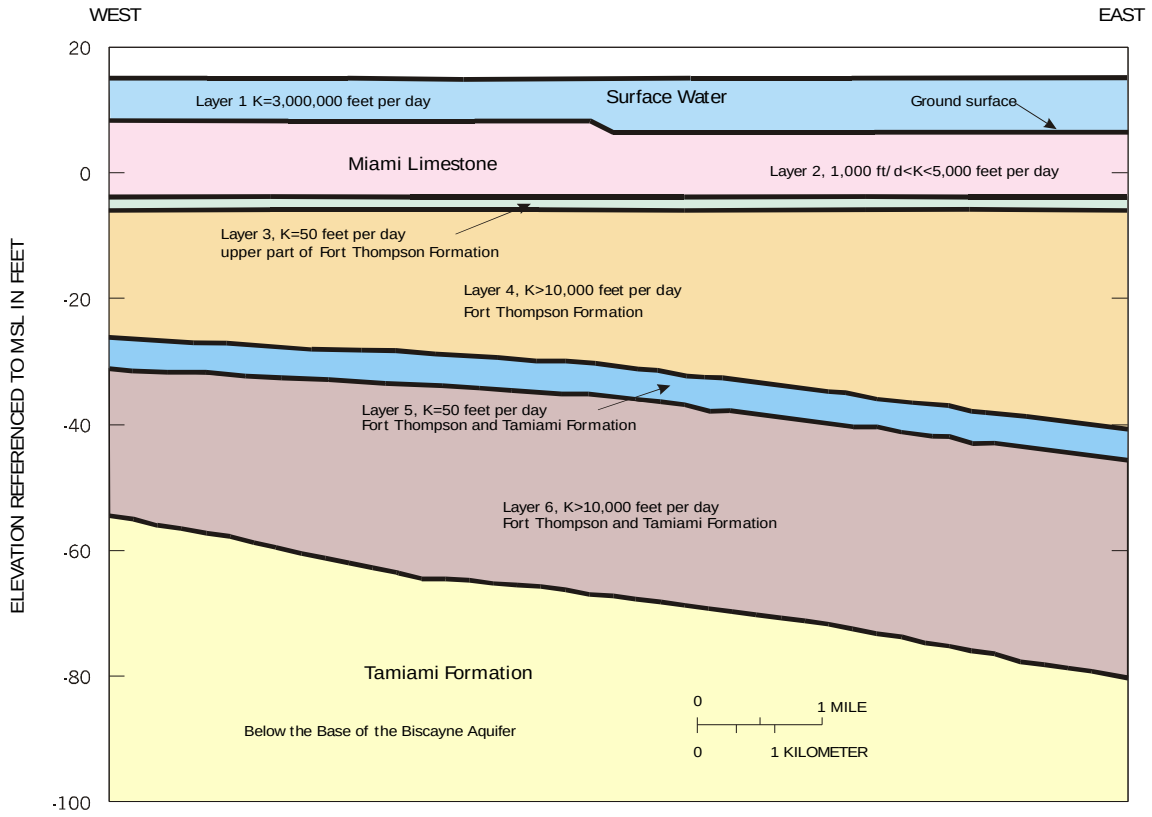

Figure 2.2.2 Hydrogeologic Layers of the Biscayne Aquifer (modified from Nemeth et al., 2000) Section extends west to east just south of Lake RL3

The existence of the semi-confining layers is indicated by information from many sources. Many geologic cores from the study area have been analyzed. During the mid to late 1970s, General Portland Inc. cored numerous holes in township sections 24, 25, and 36 east of Levee 31N and sections 26 and 35 west of the levee (Bill Murphy, Kendall Properties, personal communication,

1997). Several holes were also cored from the bottom of a rock mining lake east of the levee (designated RL1 in Figure 2.1.2). These holes are all located within the study area and several are found within the focus area. These cores were extracted for mineral analysis in order to assess the feasibility of rock mining, not for hydrogeologic analysis. However, data obtained from them support the existence of semi-confining layers. The method used to bore the holes involved applying hammer blows to the sampler and recording the depth of penetration. Consequently, when a dense, less vacuous and permeable layer, was encountered, a greater number of hammer blows were needed to penetrate a given thickness. An examination of the boring records from General Portland Inc.'s studies provides extensive support for the inclusion of two low-permeability layers in the study area. Nearly all borings show a substantial increase in hammer blows in the region about 10 ft below surface elevation, indicating that the shallower semi-confining layer is indeed present. These data also provide support for the deeper low-permeability layer in the Biscayne aquifer. The sample borings taken from the rock mining lake (which penetrate to deeper elevations than other holes using this method of boring) clearly record an increase in the number of hammer blows at a depth of 35 to 40 feet below surface elevation. This depth corresponds to the proposed depth of the top of the deep semi-confining layer.

United States Geologic Survey continuous core samples were obtained for wells G-3663 and G-3664 (Figure 2.2.3), located about 0.5 miles and 1.5 miles west of L-31N mile 4, respectively (Figure 2.2.4), and were examined to determine their properties. Intervals having “low” hydraulic conductivity values relative to the predominant characteristics of the extracted sample were found in each core and a correlation between the two sites was made approximating the location of probable semi-confining layers. Support for the existence of semi-confining layers is based on hydraulic conductivity estimates, and on data relating to lithology, color, fossils, sedimentary structures, and depositional environments (Kevin Cunningham, USGS, personal communication 1998). To develop the ranges of hydraulic conductivity presented in Figure 2.2.3, the core samples from G-3663 and G-3664 were analyzed using data reported by Fish and Stewart (1991). Based on the observed characteristics of core sample fragments, the semi-confining layers were estimated to have core-scale hydraulic conductivity values of less than 10 ft/d. However, the field scale value is higher as a result of fractures, solution cavities, or other discontinuities in the sedimentary aquifer material that were not represented in the core sample. These local variations significantly increase the transmissivity of the aquifer, so a hydraulic conductivity of 50 ft/d was considered to be an acceptable value for the semi-confining layers.

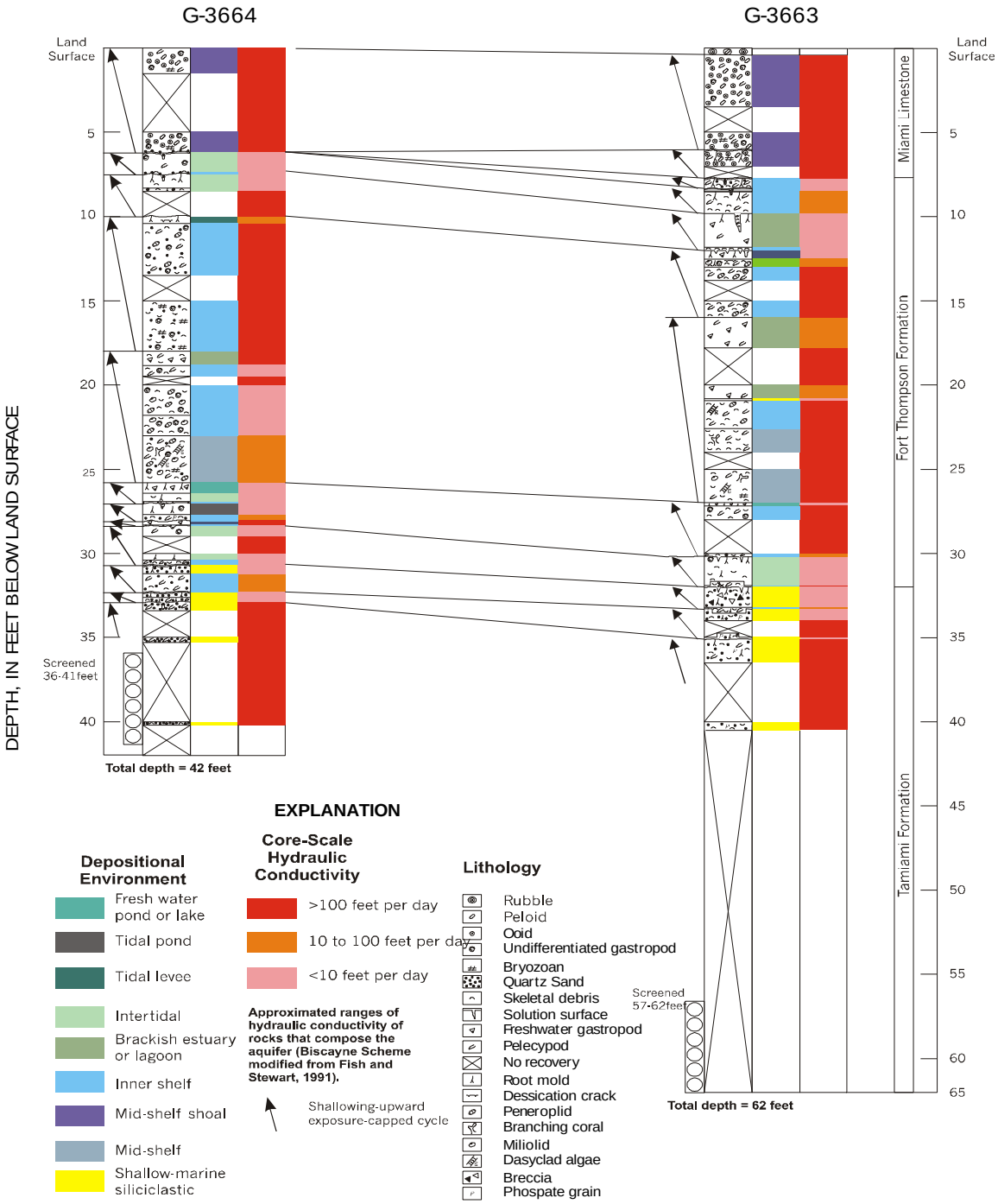

Figure 2.2.3 Lithology, Depositional Environment, and Hydraulic Conductivity for Wells G-3663 and G-3664. Wells logged and plotted in 1998 by K.J. Cunningham of the U.S. Geological Survey.

Another important feature is evident in the G-3663 core (Figure 2.2.3). This is the existence of a large underground cavern extending from about 40 ft. to at least 62 ft. (the total depth of the core) below ground surface. Localized disturbances such as this are commonly found in predominantly limestone aquifers and are most commonly in the form of dissolution cavities or karst collapses (i.e. sinkholes). These types of features may have significant impacts on groundwater flow patterns, acting as flow conduits that greatly increase the hydraulic conductivity within a localized area.

Descriptions of a group of reverse-air cores extracted along Levee 31N also were examined for evidence of the semi-confining layers. These wells (which have been filled in) were designated as G-3665, G-3666, G-3667, G-3668, G-3669 and G-3670; they were located along L-31N at distances of 0.5, 1.0, 1.5, 2.0, 2.5, and 3.0 mi., respectively, south of structure S-24A (Figure 2.2.4). Some correlation problems were encountered as the core samples were not specifically described with hydraulic conductivity values in mind and sampling intervals did not necessarily correspond to regions of interest for this study. Despite these difficulties, evidence of the shallower low-permeability layer is clearly present in all six wells. Descriptions of intervals of “very dense” and “well cemented” bedrock are found at depths varying from as shallow 10 ft to as deep as 15 ft. The deeper semi-confining layer is only clearly present at G-3666, G-3667 and G-3668. These wells show intervals of dense rock in the range of 32 to 36 ft deep. The lack

of evidence in the other wells can be attributed to the fact that the total depth of the cores only goes to 36 or 37 feet. As a result, the decreasing slope of the deeper semi-confining layer in the southerly direction may very well have taken it below the sample range of cores G-3669 and G-3670.

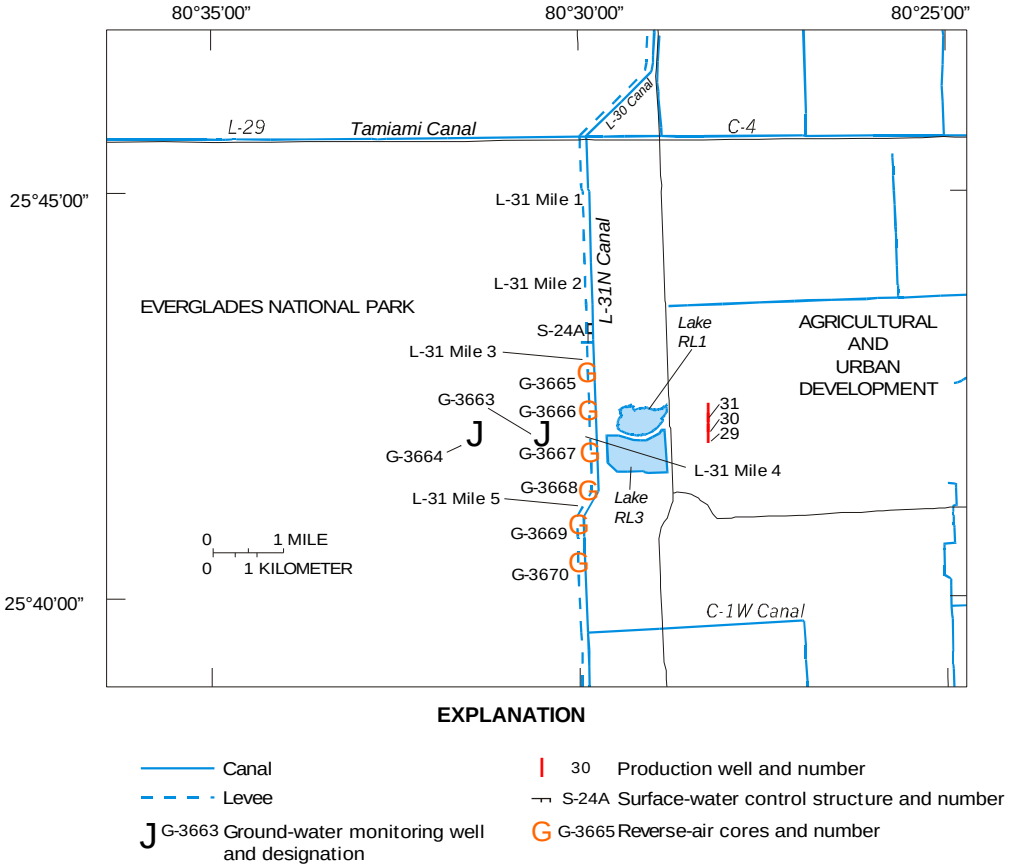

Figure 2.2.4 Location of Examined Geologic Cores

Further justification for the existence of these semi-confining layers can be found through a literature review of various sources of geologic data. A report by Amanda Krupa (SFWMD, personal communication, 1997) attempts to assess the existence of semi-confining layers within the Biscayne aquifer in the Pennsuco area of Dade County near Levee 30, located immediately north of

Levee 31N. While this project focuses primarily on the upper portion of the Biscayne aquifer and does not specifically address the exact location of the study area for this thesis, several of the justifications for the existence of semi-confining layers that are made in the report (for example, “a two-foot thick layer of the dense limestone conglomerate… at the contact of the Miami Limestone and the Fort Thompson Formation”) are also applicable at this site. Additionally, this report serves to summarize and analyze several sources of literature available concerning the presence of semi-confining layers in the Biscayne aquifer. Sources for Krupa’s report include Fish and Stewart (1991), Swain et al. (1996), Labowski (1988), Causaras (1987), Maurrasse (1976), Klein and Sherwood (1961), Shroeder et al. (1958), and several core sample logs obtained from the US Army Corps of Engineers (1951 to 1976), the SFWMD (Switanek, 1997), and the USGS. All of these sources provide at least some measure of justification for the inclusion of semi-confining layers in the Biscayne aquifer and lead Krupa to conclude that a low-permeability layer exists near the contact of the Miami Limestone and the Fort Thompson Formation.

2.3 Groundwater Flow / Seepage

While the presence of the Shark River Slough and the presence of L-31N as a boundary significantly impact surface water flow patterns in the Everglades, groundwater movement in the study site is more complicated.

Ground-water flow characteristics for the area are available in several forms. Regional water table maps indicate a ground-water flow pattern from west to east within the study area (Fish and Stewart, 1991 and Meritt, 1995). As the site incorporates the West Wellfield of Miami-Dade County, ground-water flow in the area is affected by operation of the wells. In addition, the several lakes formed as a result of rock mining also affect flow patterns throughout the region. A representative example of ground-water contours in the study area is provided in Figure 2.3.1.

Seepage meter tests were performed (Nemeth et al., 2000) at several sites in the vicinity of L-31N (Figure 2.3.2). SM1 is located the farthest west within the Everglades at about 1.5 miles west of L-31N while SM6 is located the farthest east at .3 miles west of L-31N. A portion of these results is provided in Table 2.3.1 for comparison. These tests show that the largest seepage values are found at SM4 (located at G-3577, a shallow well located approximately 0.5 miles west of Levee 31N mile 4 at the same location as G-3663) and at SM5 and SM6, located at a point midway between G-3577 and Levee 31N. These results are consistent with the geologic makeup of the area that would indicate a localized area of high flow near the cavern found below G3577 as well as increased seepage as L-31N is approached from the west.

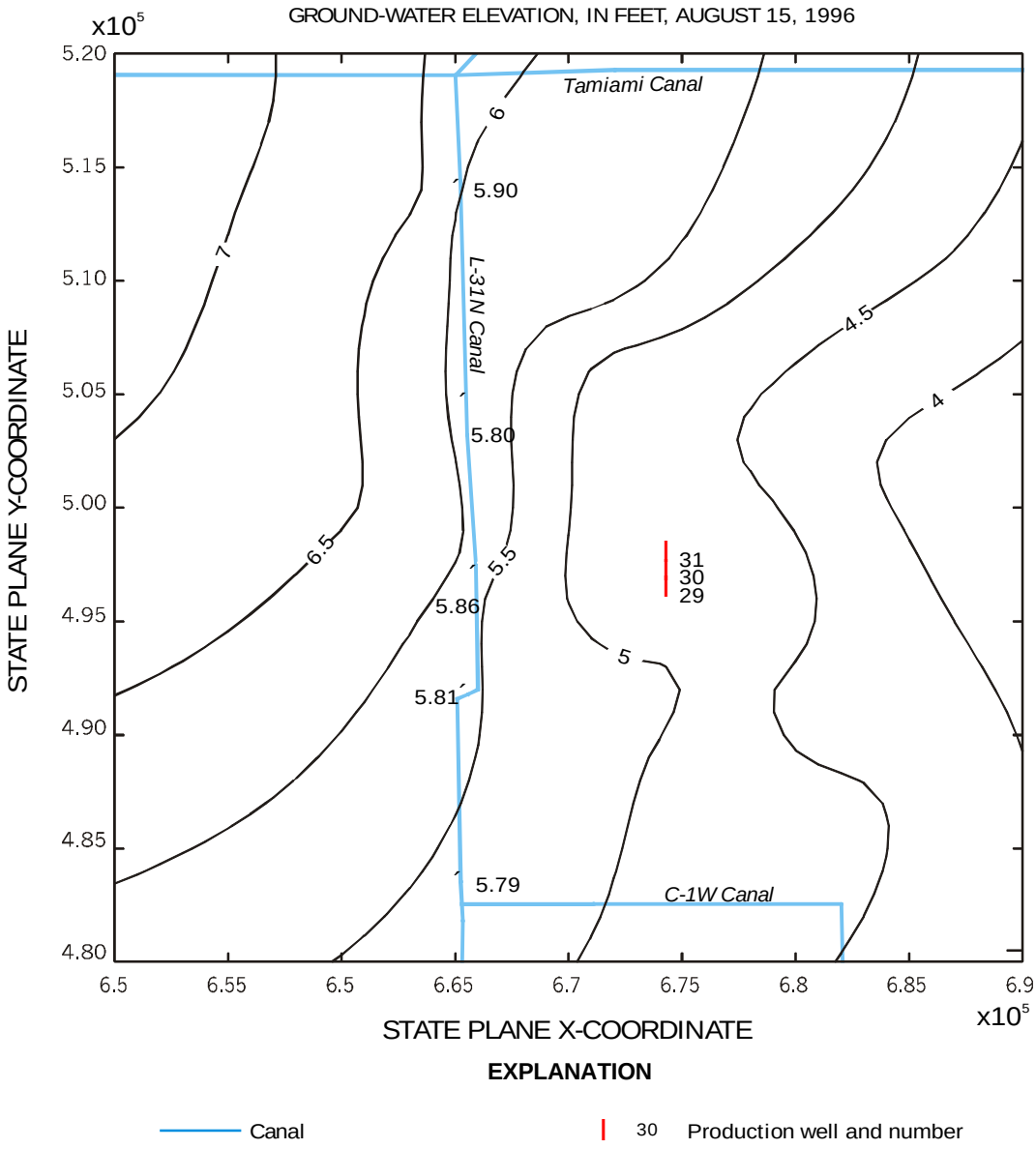

Figure 2.3.1 Groundwater Contours at the Levee 31N Site, August 15, 1996 (taken from Ibler et al., 1999)

Table 2.3.1 Seepage Meter Test Results (taken from Nemeth et al., 2000)

Test Period	Total Hours	Seepage (ft / day)					
		SM1	SM2	SM3	SM4	SM5	SM6
10-16-97 to 10-23-97	168	.00104[1]	.00099[1]	.00124[1]	.00179	.00172	.00132
10-30-97 to 11-04-97	123	.00117[1]	.00190	.00202	.00257[2]	.00457[2]	.00417[2]
2-10-98 to 2-25-98	357	.00021[1]	.00053[1]	.00021[1]	.00106[1]	.00159	.00166
3-03-98 to 3-10-98	165	.00097[1]	.00115[1]	.00106[1]	.00195	.00167	.00166

[1] Below detection limit of 0.00130

[2] Water level declined below the operational limit of the seepage meter. Actual seepage rates are greater than values reported in table.

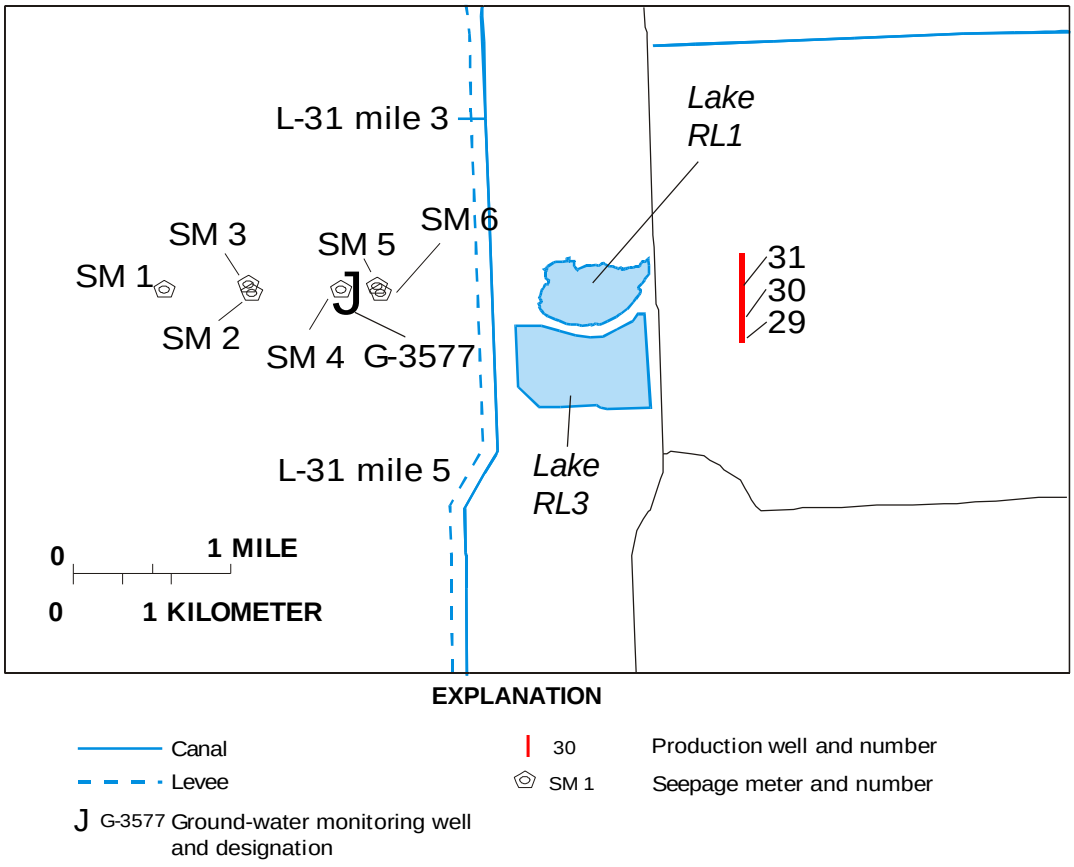

Figure 2.3.2 Location of Seepage Meters

3

Stable Isotopes

3.1 Background on Stable Isotopes

3.1.1 General Characteristics of Stable Isotopes

Isotopes are atoms having the same number of protons in their nucleus (and hence the same atomic number), but a different number of neutrons (and hence different atomic weights). In fact, the word isotope means “same place” describing the fact that isotopes occupy the same position on the periodic table, having nearly identical chemical properties but different masses (Oxtoby et al., 1990 and Ibler et al., 1999). Nuclides are isotope-specific atoms, distinguished by one another by the number of protons (Z) and the number of neutrons (N) in their nuclei. For a nuclide, the generalized methodology defines the sum of the protons and the neutrons in its nucleus (Z + N) as its mass or atomic weight (Clark and Fritz, 1997). However, in actuality, the atomic weight is slightly smaller than this sum. This difference can be attributed to the binding energy required to break the nucleus into its constituent nucleons.

There are two fundamental types of isotopes, stable and unstable (radioactive) species. While stable isotopes maintain a constant nucleic form, radioactive isotope decay spontaneously over time to form new nuclides. There

are various criteria that assess whether particular nuclides will be stable. All of these criteria indicate that the relative stability of a nuclide is dependent upon the number of neutrons present in the nucleus. The “Symmetry Rule” states that in general elements having low atomic numbers have stable nuclides when the number of neutrons is approximately equal to the number of protons (N:Z is close to 1) (Hoefs, 1997 and Oxtoby et al., 1990). As atomic weights increase, this ratio can approach a maximum value of 1.5 (for the heaviest element) and still remain stable (Hoefs, 1997). Another criterion that helps to explain isotope stability is the “Oddo-Harkins Rule”. This rule states that nuclides of even atomic numbers are more abundant than are those with odd numbers. For the purposes of this thesis, only stable isotopes are important.

3.1.2 Elemental Characteristics

As water is made up of hydrogen and oxygen, the isotopes of these two elements will be studied in this thesis. Hydrogen is one of the most abundant elements on the planet, comprising approximately 15% of all the atoms present in the crust, bodies of water, and atmosphere of the earth (Ibler et al., 1999). There are three isotopes of hydrogen, but only two are stable. The two stable isotopes are hydrogen and deuterium. Hydrogen has an atomic mass of approximately one (^{1}H) while deuterium has a neutron in its nucleus causing it to have an atomic mass of two (^{2}H or D). The relative abundances of these two stable isotopes are 99.9844% for ^{1}H and 0.0156% for D as reported by Way et al.

(1950). It is interesting to note that since hydrogen has the largest relative mass difference by far between its two stable isotopes, the largest variations in stable isotope ratios are also observed in hydrogen. The third isotope of hydrogen is a naturally occurring radioactive isotope with a half-life of 12.5 years. It is called tritium (Hoefs, 1997). For the purposes of this thesis, only hydrogen and deuterium are important.

Like hydrogen, oxygen is almost omnipresent on Earth, occurring in many compounds of any phase (gaseous, liquid or solid). In fact, oxygen is the most abundant element on earth (Ibler et al., 1999). There are three stable isotopes of oxygen. Oxygen-16 (^{16}O) is the most common form. This atom contains eight protons and eight neutrons for an atomic mass of sixteen. The other two isotope species are oxygen-17 (^{17}O) and oxygen-18 (^{18}O), which have one and two additional neutrons in the nucleus, respectively. The average abundances of oxygen according to Garlick (1969) are 99.763% for ^{16}O, 0.0375% for ^{17}O and 0.1995% for ^{18}O. In isotope studies, the ratio of $^{18}O/^{16}O$ is usually reported due to the greater abundance of oxygen-18. Additionally, a greater relative mass difference is observed between oxygen-18 and oxygen-16 than between oxygen-17 and oxygen-16 allowing for greater variation in isotope ratios (Hoefs, 1987).

3.1.3 Isotope Effects

The differences in atomic weight (due to variation in nuclear makeup) of differing isotope species gives rise to variance in the physiochemical properties

of isotopes. For example, the replacement of an atom in a molecule by one of its isotopes can change physical properties such as viscosity, boiling point, and vapor pressure as well as cause variations in chemical reaction time (Hoefs, 1997). These dissimilarities in physiochemical properties arising from differences in the atomic mass of an element are called isotope effects. In lighter weight elements such as oxygen and hydrogen, isotope effects are even more pronounced due to the large relative change in mass.

Isotope effects arise from quantum mechanical effects, specifically the vibrational motions of isotopes. The energy of a molecule varies with inter-atomic distance and is confined to certain discrete levels. The lowest energy level is not at the minimum of the energy curve, but above the curve minimum by an amount equal to ½ hv where h is Planck's constant and v is the frequency of the atoms in the molecule vibrating with respect to one another (Hoefs, 1997). As a result, in the ground state at absolute zero temperature (0 Kelvin), the molecule still possesses energy above the minimum of the curve. As this "zero-point energy" is dependent of vibrational frequency, which is subsequently dependent on mass, different isotope species will have different zero-point energies. A molecule of a heavy isotope will have a lower zero-point energy than that of a molecule of a light isotope. This is evident in Figure 3.1.1, which depicts potential energy as a function of the distance in a diatomic molecule. E_H refers to the dissociation energy of heavy molecule and E_L refers to the dissociation energy of

light molecule. As a result of the difference in zero-point energies, the heavy isotope not only has greater atomic weight than that of the lighter isotope, but also has greater bond strength. Both of these factors help to contribute to isotope effects that result in differences in the physiochemical properties of isotope species.

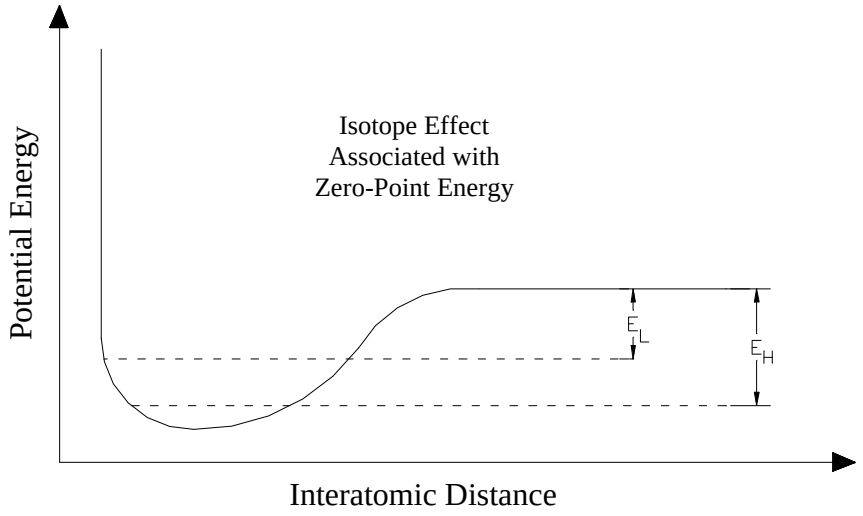

Figure 3.1.1 Schematic Potential Energy Curve Showing Isotope Effect Associated with Zero-Point Energy (taken from Hoefs, 1997)

3.1.4 Fractionation Processes

Obviously, not all substances have the same isotopic makeup. Frequently, the ratios of the different isotope species within different substances or even two substances of the same chemical makeup but of differing origin or phase are quite different. “Isotope fractionation” refers to the partitioning of isotopes between two substances or two phases of the same substance with different

isotope ratios. The two main phenomena that cause fractionation are isotope exchange reactions and kinetic processes.

Isotope exchange reactions refer to those processes in which there is no net reaction, but the isotopic distribution changes between different chemical substances, phases, or individual molecules (Hoefs, 1997). Isotope exchange reactions occur at chemical equilibrium and can be written as the reaction:

$$aA_1 + bB_2 \Leftrightarrow aA_2 + bB_1 \qquad \text{(Equation 3.1.1)}$$

in which species A and B contain either the light or heavy isotopes 1 or 2, respectively. For this equation, the equilibrium constant (K) is given by:

$$K = ([A_2]^a[B_1]^b) / ([A_1]^a[B_2]^b) = [A_2 / A_1]^a / [B_2 / B_1]^b \qquad \text{(Equation 3.1.2)}$$

When examining isotopes, the "fractionation factor" (α) is used more frequently than the equilibrium constant. This term is the relationship of the isotope ratios between two chemical compounds (Clark and Fritz, 1997) and is related to K by the equation:

$$\alpha = K^{1/n} \qquad \text{(Equation 3.1.3)}$$

where n is the number of atoms exchanged. Typically, isotope exchange reactions are written such that only one atom is exchanged (n=1) thereby making $K=\alpha$ (Hoefs, 1997).

While isotope exchange reactions occur at chemical equilibrium, this is not the case with kinetic fractionation processes. These effects are seen in incomplete and unidirectional processes not at equilibrium including evaporation, biologic

reactions and diffusion (Hoefs, 1997). In these types of reactions, isotope effects in different isotopic species, which result in variations in physical properties and chemical bond strength, cause a fractionation process to occur during the reaction. Of special interest to this thesis are evaporative processes on account of the presence of evaporated surface waters in the Everglades. In these evaporative processes, significant fractionation occurs as a result of differences in the vapor pressures of isotopic compounds stemming from differences in atomic weight. As evident in Table 3.1.1, lighter molecular species are preferentially enriched in the vapor phase. Conversely, this causes an enrichment of heavy isotopes in the water source being evaporated (in the case of this thesis, surface water in the Everglades) (Hoefs 1997).

Table 3.1.1 Vapor Pressures of Selected Isotopic Species

Isotope Species	Vapor Pressure (at 100°C, in Torr)
$H_2{}^{16}O$	760.00
$D_2{}^{16}O$	721.60

3.1.5 Measurement Convention (δ Values)

Measurement of isotopes is performed through the use of delta values (δ). These δ values are not a direct measure of isotopic variation in a particular sample but rather serve to compare the isotopic composition of a sample to a known standard. Motivation for this type of convention comes from several factors. The delta convention is primarily used to compensate for the fact that one isotope typically dominates a direct ratio comparison (R) due to differences

in natural abundances. This can result in changes due to fractionation being too small to measure accurately. δ value calculations compensate for this problem. Additionally, the comparison to established standards incorporated into the δ value calculation provide a universal reference for isotope enrichment, allowing for comparison of data from several studies.

As an example, the isotopic ratio (R) for two of the oxygen isotopes (^{18}O and ^{16}O) would be given by the equation:

$$R = {}^{18}O / {}^{16}O \qquad \text{(Equation 3.1.4)}$$

This value can be experimentally obtained through use of a mass spectrometer. However, as the abundance of ^{18}O relative to ^{16}O is very small, this number would not be of much practical use. Rather, it is used to calculate delta values as follows:

$$\delta = [(R_{sample} - R_{standard}) / R_{standard}]*1000 \qquad \text{(Equation 3.1.5)}$$

where δ is reported as permil ($^{0}/_{00}$) and represents the positive or negative deviation from a chosen standard (Clark and Fritz, 1997). For each batch of sample preparation, a known standard is also tested so as to provide $R_{standard}$ values for calculation of δ. A more in depth outline of calculations used to obtain the delta values reported in this study is provided in Appendix A.

As previously indicated, measurement of delta values does not occur on an absolute scale, but rather depends upon a reference standard. Several standards are employed on a regular basis in isotope research. The original

standard which was used for the calibration of meteoric water was NBS-1. This was a water sample collected in the Potomac River and catalogued by the National Bureau of Standards. In 1961, Craig introduced a new standard. This standard was labeled SMOW for Standard Mean Ocean Water, as the oceans are the basis of the meteorological cycle, and was calibrated to the isotopic content of NBS-1. Craig (1961) defines SMOW as:

$$(^{18}O / ^{16}O)_{SMOW} = 1.008\ (^{18}O / ^{16}O)_{NBS\text{-}1} = (1993.4 \pm 2.5) \times 10^{-6} \quad \text{(Equation 3.1.6)}$$

$$(D / H)_{SMOW} = 1.050\ (D / H)_{NBS\text{-}1} = (158 \pm 2) \times 10^{-6} \quad \text{(Equation 3.1.7)}$$

Later, as demand for universal standard water for calibration and quality assurance increased, another standard was developed by the United Nations International Atomic Energy Agency (IAEA). This standard was prepared from distilled seawater that was modified to have an isotopic composition close to SMOW and was called Vienna Standard Mean Ocean Water (VSMOW). Measurements on VSMOW (Baertchi, 1976 and Hagemann et al., 1970) indicate that it can be defined as:

$$(^{18}O / ^{16}O)_{VSMOW} = (2005.2 \pm 0.45) \times 10^{-6} \quad \text{(Equation 3.1.8)}$$

$$(D / H)_{VSMOW} = (155.76 \pm 0.05) \times 10^{-6} \quad \text{(Equation 3.1.9)}$$

VSMOW has been the internationally accepted reference for ^{18}O and D for nearly thirty years and as such was used as the primary reference for this study. This was done by calibrating a lab standard to VSMOW during a yearly calibration as outlined in Appendix A. Individual batch samples were then compared to the lab

standard. During the course of this thesis, descriptive terms will be used to refer to various isotopic conditions relative to the universal VSMOW standard. The terms “isotopically light” and “isotopically heavy” denote a depletion or enrichment, respectively, of heavy isotopes (oxygen-18 and deuterium) as compared to VSMOW.

While all delta values for the study are referenced to VSMOW, an additional standard, Standard Light Antarctic Precipitation (SLAP), was employed in performing the quality assurance quality control (QAQC) calibration (as outlined in Appendix A) for the study. It is commonly used for waters that are very depleted from ocean waters, and is calibrated with respect to VSMOW as the following:

$$\delta^{18}O_{SLAP} = -55.50\ ^{0}/_{00}\ VSMOW \qquad \text{(Equation 3.1.10)}$$

$$\delta D_{SLAP} = -428.0\ ^{0}/_{00}\ VSMOW \qquad \text{(Equation 3.1.11)}$$

3.1.6 Meteoric and Evaporated Waters

The name “meteoric” refers to water that has gone through at least a portion of the meteorological cycle (i.e. evaporation, condensation, precipitation, etc.). All water in this study is considered to be meteoric water. Meteoric water is characterized by an observed relationship between hydrogen and oxygen isotope ratios. This relationship can be quantified by what is known as the “global meteoric water line” (Craig, 1961) which states that:

$$\delta D = 8\delta^{18}O + 10 \qquad \text{(Equation 3.1.12)}$$

Neither the slope nor the intercept coefficients of this equation are truly constant as they are seen to vary based on localized changes in atmospheric conditions and temperature. However, as observed in Figure 3.1.2, data collected from several points around the world indeed supports the assertion that the global meteoric water line can indeed be applied almost universally.

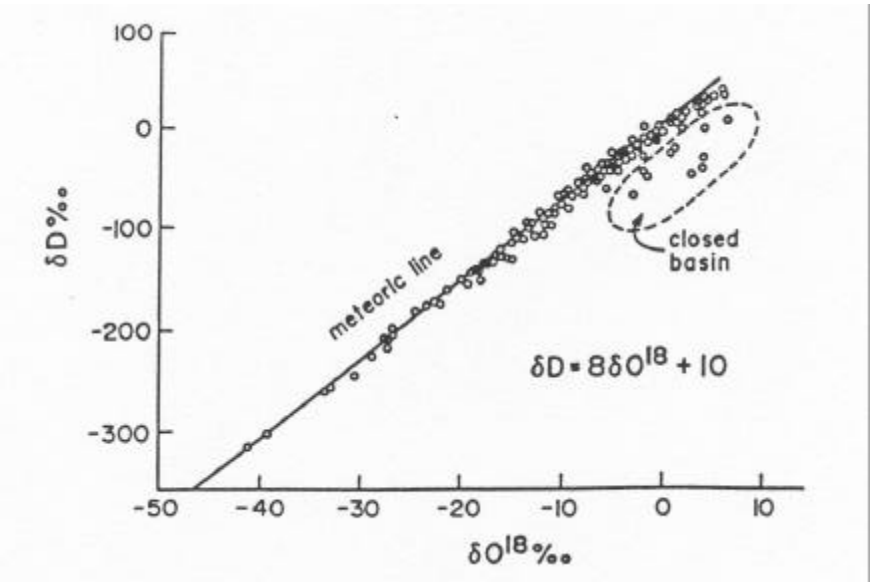

Figure 3.1.2 Isotopic Data of Rivers, Lakes and Precipitation from Various Parts of the World (taken from Mazor, 1991)

As outlined previously in section 3.1.4, waters undergoing evaporative processes will become enriched in heavy isotopes. In contrast to the meteoric water line, the relationship between oxygen-18 and deuterium for water bodies that have undergone evaporation is predicted by:

$$\delta D = M\delta^{18}O + I \qquad \text{(Equation 3.1.13)}$$

where $M<8$ (Sternberg, Personal Communication, 1999). As the slopes of the line for evaporated water and meteoric water are different, it is possible to identify

evaporated water on the basis of its δD and $\delta^{18}O$ values and its deviation from the meteoric water line. The point of intersection for these two lines would indicate the isotopic composition of the rainfall source from which the evaporated water originated prior to experiencing kinetic fractionation effects.

3.1.7 Rayleigh Distillation

The fractionation processes outlined in Section 3.1.4 lead to a phenomena in meteoric waters that results in rainfall becoming increasingly light during progression inland. This effect is known as “Rayleigh Distillation”. In this process (Figure 3.1.3), meteoric rainfall is evaporated from ocean water having a delta value of zero. Fractionation during evaporation results in the airborne water vapor becoming isotopically light as previously outlined. As the water vapor moves over land, it cools, condenses and begins to precipitate. During this phase, any heavy isotopes present in the water vapor are preferentially lost as rainfall. Since the number of heavy isotopes in the vapor is relatively small to begin with due to the initial evaporation process, the rainfall still remains light compared to ocean waters. The loss of a greater ratio of heavy isotopes to light isotopes during the first rainfall event result in the remaining water vapor being even lighter than after evaporation from the ocean. Consequently, during the next rainfall event, less heavy isotopes are present in the water vapor and rainfall in the second precipitation event is lighter than rainfall in the first precipitation

event. This process continues with subsequent rainfall events becoming increasingly light as the vapor moves inland.

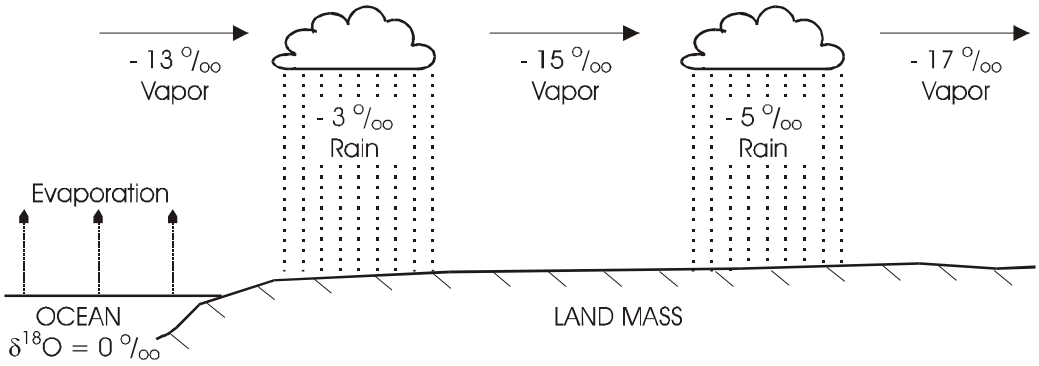

Figure 3.1.3 Rayleigh Distillation Effect (modified from Hoefs, 1987)

This type of distillation process can be written in equation form expressing the instantaneous isotopic ratios of remaining vapor and condensate liquid (R_v and R_l ,respectively) as functions of the isotope fractionation factor (α) and the fraction of residual vapor (*f*):

$$R_v / R_l = \alpha^{-1} * f^{(1/\alpha - 1)} \qquad \text{(Equation 3.1.14)}$$

Graphically, this relationship shows the decreasing trend in delta values with loss of vapor as in Figure 3.1.4.

3.2 Stable Isotopes Use in Study

3.2.1 The Use of Stable Isotopes at the Study Site

Stable isotopes have frequently been used in the analysis of groundwater. (Mazor, 1991). In the study area for this thesis, an isotopic difference can be observed between water derived from the Everglades and water that is recharged in urban areas. It is therefore feasible to use stable isotopes to trace the

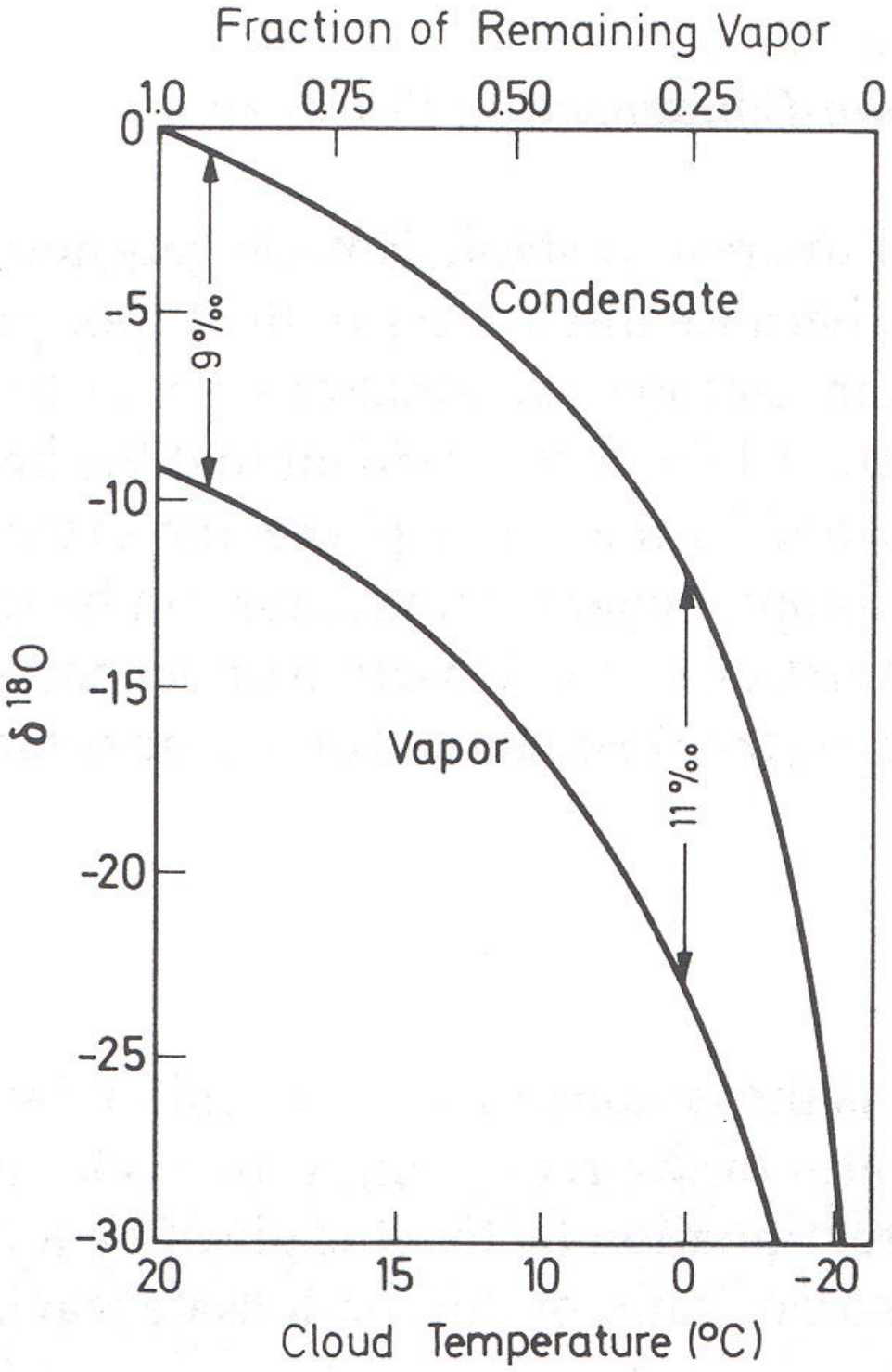

Figure 3.1.4 $\delta^{18}O$ in Cloud Vapor and Condensate as a Function of Remaining Vapor in the Cloud (taken from Hoefs, 1997)

flow of water within the study site. Since surface water in the Everglades is shallow and experiences considerable heat and solar radiation, it is subject to fractionation processes due to evaporation effects previously outlined. As a consequence, this surface water (and therefore Everglades groundwater that is recharged by seepage from evaporated surface water) becomes enriched in heavier isotopes. In contrast, urban waters are recharged by rainwater that infiltrates into the groundwater system relatively quickly as a result of the extensive drainage network present in these areas. As a result of this rapid infusion, urban waters maintain isotopic characteristics similar to that of meteoric rainwater. Urban water is therefore isotopically lighter than the isotopically heavy evaporated waters found within the Everglades. This difference allows for the flow of Everglades water to be traced through urban areas (Solo-Gabriele and Wilcox, 2000).

3.2.2 Isotope Monitoring Network

For the isotopic tracing part of the study, a monitoring network was established over time with an emphasis being placed on sites within the focus area. Initially, in early 1996, only a few sites were tested on a non-regular basis. However as the research continued, sites were continually added until the completion of sampling in December 1998. All told, approximately 430 samples were collected at 24 different sites. In addition, average monthly isotope values were obtained from a related study for lakes RL1 and RL3 for the period from

December 1997 to December 1998 (Herrera 2000). A summary of the isotope monitoring site characteristics is provided in Table 3.2.1. As can be seen, samples can be grouped into categories of shallow wells, deep wells, surface water (excluding lakes), lake water and rainwater. Additionally, water was sampled from the West Wellfield production wells. Sampling sites within the focus area are shown in plan view in Figure 3.2.1. For a complete set of isotope data for all sites, please see Appendix A.

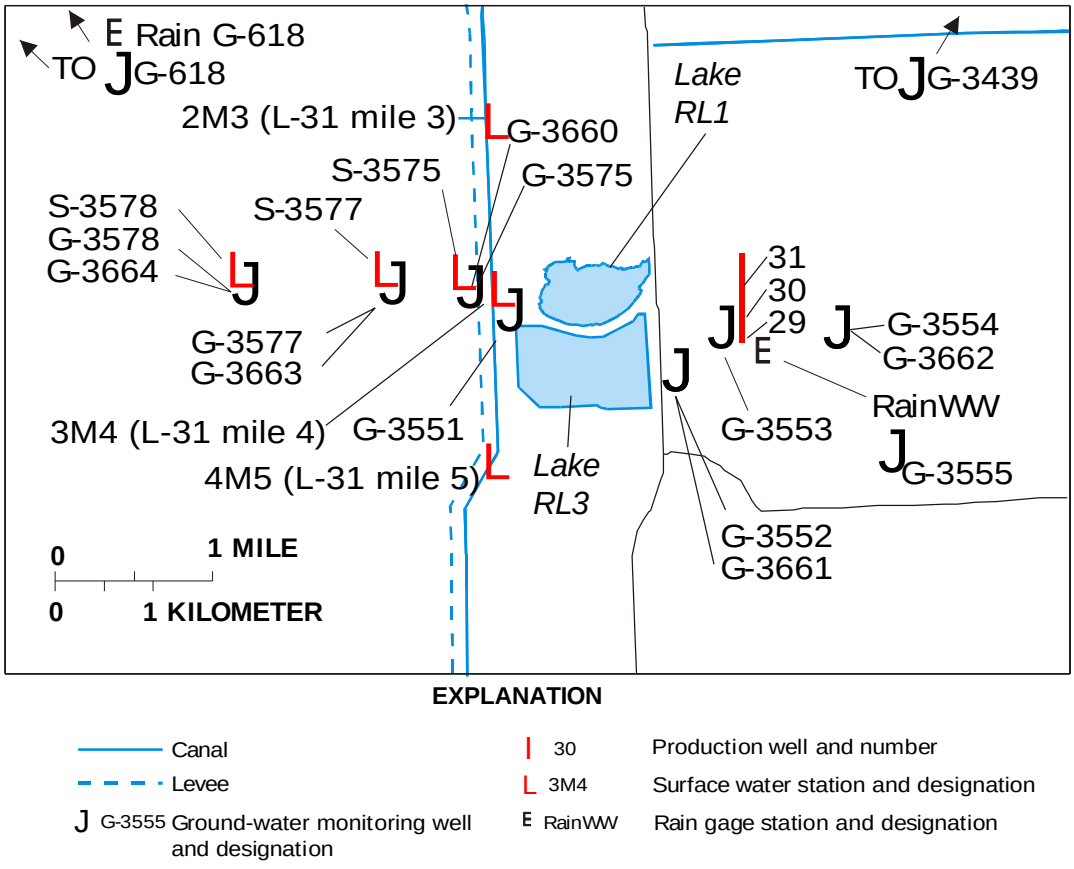

Figure 3.2.1 Isotope Monitoring Network

Table 3.2.1 Isotope Monitoring Station Site Descriptions

Site	Type of Station	Latitude	Longitude	State Plane X Coordin -ate	State Plane Y Coordin -ate	Agency	Station Identification Number	Land Surface Elevation (feet above sea level)	Drilled Depth (feet below land surface)	Casing Depth (feet below land surface)	Casing Diameter (inches)
G-3551	Shallow Well	25°41’58”	80°29’45”	666017	496749	USGS	254158080294501	6.57	18.3	13.3	5
G-3552	Shallow Well	25°41’38”	80°28’44”	671605	494752	USGS	254153808284401	7.41	19.4	14.4	5
G-3661	Deep Well	25°41’38”	80°28’44”	671605	494752	USGS	254138080284401	7.41	55.0	50.0	2
G-3553	Shallow Well	25°41’52”	80°28’21”	673703	496173	USGS	254152080282101	6.23	19.9	14.9	5
G-3554	Shallow Well	25°41’52”	80°27’45”	676996	496187	USGS	254152080274501	7.36	20	15	5
G-3662	Deep Well	25°41’52”	80°27’45”	676996	496187	USGS	254152080274501	9.40	55.0	50.0	2
G-3555	Shallow Well	25°41’11”	80°27’25”	678843	492055	USGS	254111080272501	8.25	19	14	5
G-3439	Deep Well	25°44’21”	80°26’02”	686353	511268	USGS	254421080260201	5.79	12	10	4
Well 29/30	Production Well	25°41’56”	80°28’18”	673978	496195	Miami-Dade WASA	BA-2, BA-3	6.50, 6.48	67, 70	39, 41	54, 54
G-618	Shallow Well	25°45’40”	80°36’00”	631648	519043	USGS	254500080360001	7.40	20	11	6
G-3575	Shallow Well	25°42’06”	80°29’47”	665831	497556	USGS	254206080294701	5.94	9.0	9.0	4
S3575	Surface Water	25°42’06”	80°29’47”	665831	497556	-	-	5.94	-	-	-
G-3660	Deep Well	25°42’06”	80°29’47”	665831	497556	USGS	254229080294801	-	57.0	47.0	6
G-3577	Shallow Well	25°42’07”	80°30’02”	664459	497652	USGS	254207080300201	6.00	8.0	8.0	4
S3577	Surface Water	25°42’07”	80°30’02”	664459	497652	-	-	6.00	-	-	-
G-3663	Deep Well	25°42’07”	80°30’02”	664459	497652	USGS	254207080300201	6.00	62.0	57.0	1.5
G-3578	Shallow Well	25°42’10”	80°30’48”	660250	497939	USGS	254210080304801	6.00	6.0	6.0	4
S3578	Surface Water	25°42’10”	80°30’48”	660250	497939	-	-	6.00	-	-	-
G-3664	Deep Well	25°42’10”	80°30’48”	660250	497939	USGS		6.00	41.0	36.0	1.5
2M3 (L-31N Canal mile 3)	Surface Water	25°43’02”	80°29’50”	665535	503208	USGS	02290765	-	-	-	-
3M4 (L-31N Canal mile 4)	Surface Water	25°42’06”	80°29’46”	665923	497556	USGS	02290766	-	-	-	-
4M5 (L-31N Canal mile 5)	Surface Water	25°41’09”	80°29’50”	665244	483521	USGS	02290767	-	-	-	-
Rain G-618	Rain Water	25°45’40”	80°35’14”	635857	519043	-	-	-	-	-	-
RainWW	Rain Water	25°41’56”	80°28’18”	673978	496195	-	-	-	-	-	-
RL1	Lake	25°42’06”	80°29’15”	668811	497556	-	-	-	-	-	-
RL3	Lake	25°41’38”	80°29’15”	668811	494752	-	-	-	-	-	-

3.2.3 Sample Collection

As previously stated, samples were collected during a period ranging from January 1996 to December 1998. Beginning in February 1997, samples were collected on a regular monthly schedule. All samples were collected in duplicate using glass scintillation vials. These vials were filled to the top with sample water and sealed with a screw-on top. A layer of parafilm was then wrapped around the vials in order to prevent evaporation and interaction with air from affecting the delta values of stored samples.

While all samples were stored in a consistent manner, the dissimilar nature of the sampling locations required different collection methods to be employed in obtaining samples from the diverse types of sites. Groundwater well samples were collected using a portable pump connected to a 12-volt battery (Figure 3.2.2). The intake end of the pump hose was lowered into the well casing while the outflow end was allowed to flow into the scintillation vial for sample collection. For shallow wells, the pump was allowed to draw water from the well for five minutes prior to sample collection. This was done in order to assure that the collected sample did indeed come from water at the casing depth of the well and was not affected by rainwater inflow into the casing or other factors. For deep groundwater sites, the pump was allowed to purge the well for fifteen minutes ensuring that the additional volume in a deeper well casing was indeed removed. The production well samples were taken directly from a spigot

attached to the pumping well. These samples were obtained from either Well 29 or Well 30 at the West Wellfield, depending upon which pump was in operation on the day of sampling.

Figure 3.2.2 Sampling from G-3552 (left), a Shallow Well, and G-3663 (right), a Deep Well

Surface water samples for sites other than the rock mining lakes were taken by immersing the scintillation vials below water surface in order to collect the samples. At the lakes, a pump was used to collect water from ten-foot depth intervals from the approximate center of each lake. These samples were analyzed independently and overall monthly average values were provided for use in this study (Herrera 2000).

Rainwater collection for isotope analysis provided a somewhat unique problem, as collected rainwater must be shielded from evaporation effects. In order to accomplish this, rainwater collection bottles were filled with a two-inch

deep layer of mineral oil prior to use (Figure 3.2.3). These bottles were fitted with a collection funnel and an air release port. As rain entered the collection apparatus, the buoyant mineral oil floated on top of the collected rain, preventing rainwater interaction with the air and insuring the isotopic integrity of the sample. At collection time, a syringe was used to transfer the rainwater from below the mineral oil layer and deposit the sample into scintillation vials. Collection basins were then replaced with fresh bottles with mineral oil for the next sampling period.

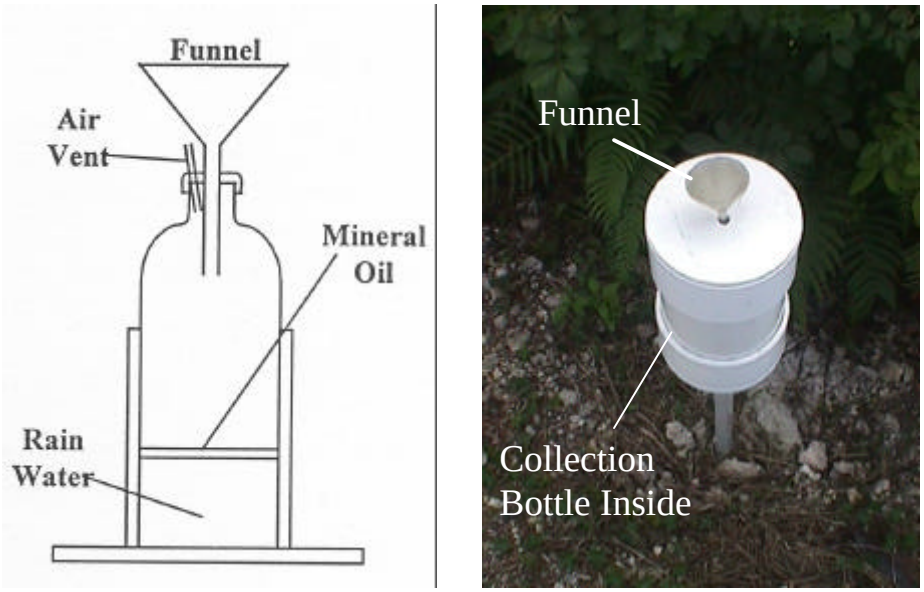

Figure 3.2.3 Rainwater Sampling Apparatus, Picture of Installation at G-618

3.3 Preparation/Analysis Techniques

3.3.1 Oxygen-18 Sample Preparation with CO_2

In order to determine oxygen 18 delta values for the study, carbon dioxide samples were prepared for introduction into the mass spectrometer. This

preparation was accomplished by the equilibration of 4 ml of carbon dioxide gas with 1 ml of water sample as per the syringe method proposed by Matsui (1980). In order for the carbon dioxide gas to come into complete equilibrium with the water, the syringes are then left standing with the plunger up for a period of three days in an incubator set at 25°C (Sternberg, Personal Communication, 1999). The fractionation value between carbon dioxide and water during this period is taken to be 1.0412. In other words, carbon dioxide, which is in equilibrium with sample water, will have a delta value of 41.2 $^{0}/_{00}$ relative to the water. Due to this fractionation, a correction must be made in the delta calculation for oxygen 18 as outlined in Appendix A.

After the incubation period is over, the gas contained in the syringe is injected into the carbon dioxide extraction apparatus for oxygen-18 analysis (Figure 3.3.1). The gas is sent to trap A where it is condensed by the use of liquid nitrogen. Any excess air is evacuated through the vacuum stopcock S_A. The liquid nitrogen is then replaced with the “slush” which is produced by mixing liquid nitrogen with alcohol to produce a solution at -80^{0}C. This solution keeps water vapor condensed in trap A, but releases the carbon dioxide gas. This gas is transferred to the carbon dioxide finger by placing the liquid nitrogen dewar on it. During the migration to the carbon dioxide finger, gas in the system is transferred through trap B, which has a permanent “slush” on it. This trap serves as a backup to trap A, insuring that all water vapor is indeed removed from the

carbon dioxide gas. Once the carbon dioxide gas has been collected in the finger, stopcock C is closed and the glass tubules are fully evacuated, removing any excess air or water that may have been in the system. After the vacuum source is closed, the stopcock is reopened and the nitrogen is moved and placed on any one of four given glass tubules. This causes the transfer of gas from the carbon dioxide finger to the chosen tubule. This tubule is flamed and sealed off for later analysis by the mass spectrometer (Herrera, 2000, Sternberg, Personal Communication, 1999).

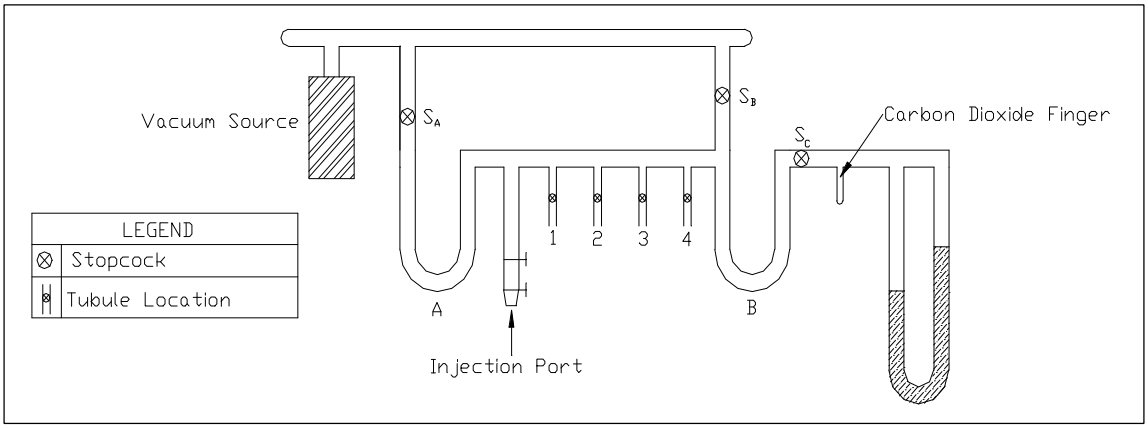

Figure 3.3.1 Carbon Dioxide Extraction Apparatus for Oxygen-18 Analysis

(taken from Herrera, 2000)

3.3.2 Deuterium Sample Preparation with H_2

During the course of this study, two different methods were used to prepare samples for deuterium analysis in the mass spectrometer. Both methods involve reducing sample water into elemental hydrogen through use of a heated furnace packed with oxidizable material. Vaporized water is allowed to oxidize the furnace medium thereby leaving only the hydrogen portion of the water

vapor to be collected. These processes result in no fractionation since all of the water is reduced.

The first method employed involved the use of a uranium furnace as outlined by Bigeleisen et al. (1952). This procedure was initially chosen due to its established accuracy in analyzing for deuterium in isotopic studies. In the uranium furnace method, capillaries are prepared which contain a small amount of sample water. These capillaries are then cracked and released into the hydrogen extraction apparatus (Figure 3.3.2). Vaporized water is condensed into trap A by the use of liquid nitrogen. Any excess air that was present in the capillary is pumped out through the vacuum stopcocks labeled S_V. Trap A is then heated while the liquid nitrogen is placed on trap B. Once transfer from A to B has been completed, the liquid nitrogen is placed on trap C. The gas then migrates from B to C and flows through the uranium furnace kept at 750°C where it reacts with the depleted uranium to produce pure hydrogen. In order to assure that all the water is converted to hydrogen, the water is sent from trap C back through the furnace to trap B. The hydrogen gas formed is then pumped by a toeppler pump and collected in a glass tubule. Finally, the glass tubule is flamed and sealed off for later analysis on the mass spectrometer (Herrera, 2000 and Sternberg, Personal Communication, 1999).

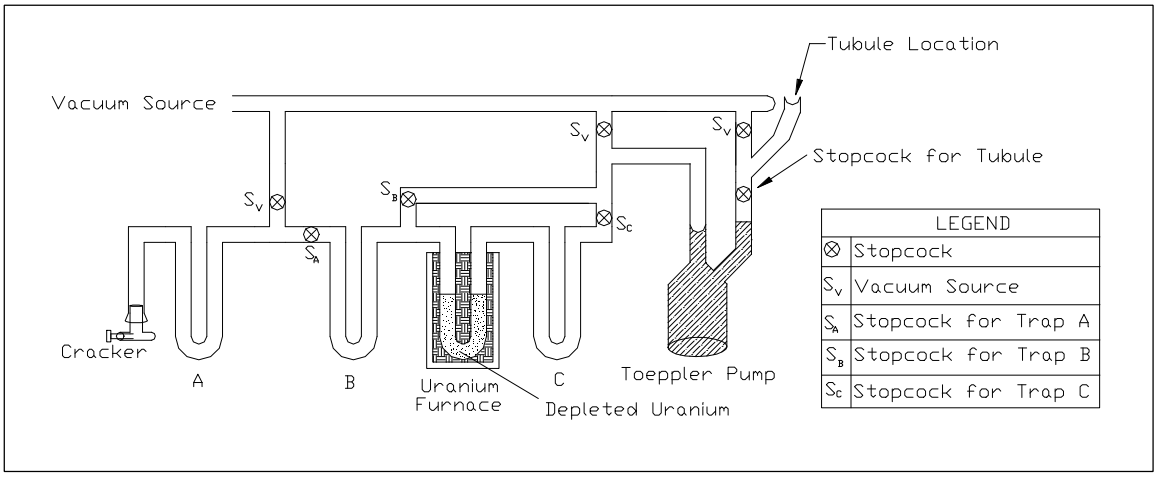

Figure 3.3.2 Hydrogen Gas Extraction Apparatus for Deuterium Analysis (Uranium Method) (modified from Herrera, 2000)

The second method (Gehre et al., 1996) is similar in conception, but relies on the use of a chromium furnace rather than a uranium furnace. In this procedure the hydrogen extraction apparatus is connected directly to the mass spectrometer inlet system (Figure 3.3.3). As a result, hydrogen gas is extracted from the furnace through use of the vacuum present in the mass spectrometer rather than through the use of a toeppler pump. This method proved to be a much faster means of analyzing samples while maintaining the accuracy of the uranium furnace method. In the chromium furnace method, 1 μL of sample water is injected through a septum into the chromium furnace at 850°C. Here, it is allowed to react for two minutes before the mass spectrometer computer opens the valve, admitting the sample into the ion source for mass analysis (Sternberg, Personal Communication, 1999).

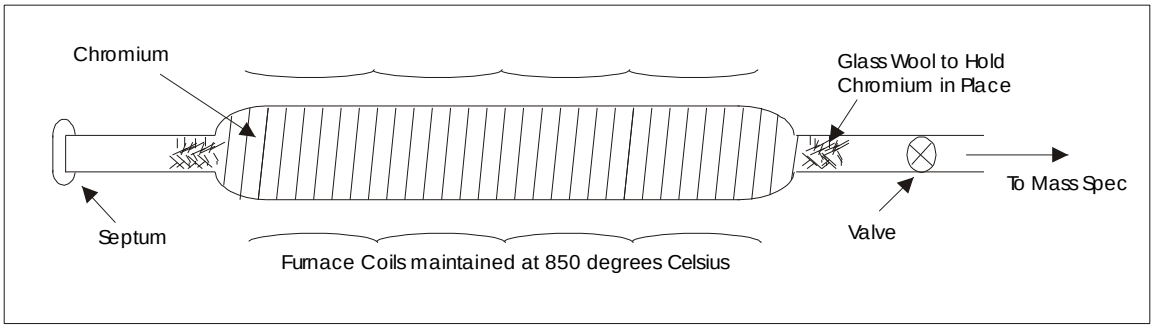

Figure 3.3.2 Hydrogen Gas Extraction Apparatus for Deuterium Analysis (Chromium Method)

3.3.3 Mass Spectroscopy

A mass spectrometer is used to determine the isotopic ratios (R values) of the oxygen and hydrogen samples that are needed for the calculation of delta values. It does this by separating particles on the basis of mass by imparting a charge to them, accelerating the ionized particles across a voltage difference and then observing their behavior in a magnetic field. A valid numeric scaling of mass ratio differentials for this procedure is accomplished by comparing the behavior of sample gasses to that of a reference gas of known isotopic composition.

When a mass spectrometer was employed in this study, water in vapor form was not directly injected into the inlet system of the mass spectrometer. Rather, carbon dioxide gas and hydrogen gasses were used to find the R_{sample} for oxygen-18 and deuterium analysis, respectively. This is due to the fact that water samples cannot be directly injected into the mass spectrometer as a result of the large “memory effects” associated with water that is absorbed by the walls of

combustion trains and vacuum systems. These “memory effects” can cause cross-sample contamination. In order to prevent this from occurring, water from collected samples was converted into gas carbon dioxide and hydrogen gas by the procedures outlined in the previous sections.

The principle components of a mass spectrometer include the inlet system, the ion source, the mass analyzer and the ion detector (Hoefs, 1987) (Figure 3.3.4). In the inlet system, sample and reference gasses are alternately allowed to enter the ion source, ensuring a continual comparison of the sample to a known reference. The ion source is a high vacuum area separated from the inlet system by a series of valves. As these valves are opened and closed, sample and reference gasses alternately enter the vacuum where they are bombarded by electrons emanating from a heated tungsten-coated iridium filament under a weak magnetic field. In order to maximize the efficiency of single ionization, energy of electrons used for ionization is on the order of 50 to 70 V. Collisions of the gaseous sample with electrons in this energy range serve to ionize the molecules into single positively charged particles.

An electric field draws the ions out of the filament-produced electron beam and accelerates them across a voltage difference into the mass analyzer. Particles leaving the ion source are imparted with a kinetic energy given by the equation:

$$\tfrac{1}{2} mv^2 = eV \qquad \text{(Equation 3.3.1)}$$

in which m is mass, v is velocity and eV is kinetic energy in electron volts. In the mass analyzer, a magnetic field is applied to the ion beam, which causes separation of the ions into a spectrum of masses according to a particular mass/charge (M/e) ratio. The different masses of the spectrum are deflected into circular paths whose radii are related to the value of M/e as given by the equation:

$$r \sim (M/e)^{1/2} \qquad \text{(Equation 3.3.2)}$$

in which r is the radius of the path (Hoefs, 1987). In the final part of the mass spectrometer, ion detectors are placed in line with the paths of the separated ionized particles of interest. These detectors collect the ions and convert the ionic current into an electrical impulse. This impulse is amplified and sent to a computer where the data from the sample and reference gasses are measured, compiled and then expressed a ratio of masses (R_{sample}) (Clark and Fritz, 1997).

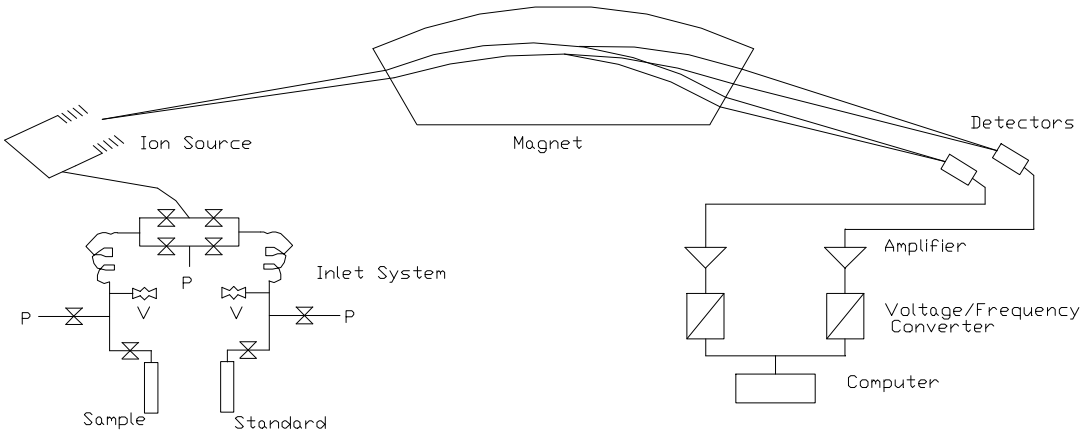

Figure 3.3.4 Schematic Drawing of a Mass Spectrometer
(taken from Hoefs, 1987)

As seen in Equation 3.3.2, adjusting the magnetic field applied to the ion beams will result in changes to the radii of the mass spectrum. As such, it was possible to use the same mass spectrometer for analysis of particles having different M/e ratios by adjusting the magnetic field in the mass analyzer. It is also common to change the electric field in the ion source to affect M/e ratios and optimize mass spectrometer performance (Hoefs, 1987). Therefore, different settings were used on the mass spectrometer to perform analysis on oxygen-18 and deuterium samples.

When working with carbon dioxide and hydrogen gas, the mass spectrometer specifically attempts to find the ratio of mass 46/44 (or the ratio of $^{12}C^{16}O^{18}O$ to $^{12}C^{16}O^{16}O$) for carbon dioxide and mass 3/2 (or the ratio of HD to H_2) for hydrogen gas. However, the existence of other molecular species can incorrectly inflate these ratios. These species include the mass 45 ions (e.g. $^{12}C^{16}O^{17}O$) for carbon dioxide and H^+_3 ion for hydrogen. Corrections for interference caused by the contributions of these increased-mass ions are made automatically by mass spectrometers.

In the case of carbon dioxide, a supplementary ion detector is designated to measure the mass 45/44 in addition to the mass 46/44 ratio. A correction equation is then applied by the computer to remove mass 45/44 effects from the final reported R_{sample}. For hydrogen gas, a different approach must be used, as the mass 3/2 ratio cannot distinguish between HD and H^+_3. It is known that the

production of H^{+}_{3} is proportional to both H^{+}_{2} production and the pressure of H_2. This pressure proportionality of H^{+}_{3} causes the plot of the mass 3/2 ratio vs. pressure to obtain a positive slope with increasing pressure (Figure 3.3.5). As the mass 3/2 ratio should not vary with pressure, it is possible for the computer to flatten the line by either adding to or subtracting from the sample ratio obtained at a known pressure. This correction requires an additional calibration step of the reference gas prior to each group sample run in order to determine the slope of the pressure related line (Clark and Fritz, 1997). In order to assure that accuracy of methods employed to analyze stable isotope ratios, a quality assurance / quality control (QAQC) assessment was performed as outlined in Appendix A.

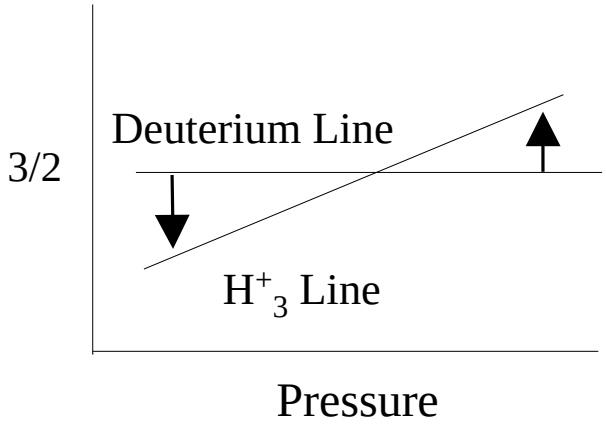

Figure 3.3.5 H^{+}_{3} Correction Line (taken from Herrera, 2000)

4

Isotope Data Analysis

4.1 Comparison to the Meteoric Water Line

A regression analysis was performed on the rainfall data collected at the RainWW and RainG-618 sites (Figure 4.1.1), in order to assure correlation between sampled data and the global meteoric water line (MWL) (Craig, 1961). The equation for the MWL obtained from the samples does indeed correlate well with the expected equation. The MWL has an equation of:

$$\delta D = 7.9550\delta^{18}O + 8.9211 \qquad \text{(Equation 4.1.1)}$$

as compared to the global MWL equation of:

$$\delta D = 8\delta^{18}O + 10 \qquad \text{(Equation 4.1.2)}$$

Specific $\delta^{18}O$ and δD values were found to be within acceptable ranges as $\delta^{18}O$ values were found to vary between –4.70 $^{o}/_{oo}$ to –0.29 $^{o}/_{oo}$ and δD values ranged from –32.93 $^{o}/_{oo}$ to 8.78 $^{o}/_{oo}$. It is also seen graphically that the fitted rain line is nearly identical to the global meteoric water. This is evidenced by the fact that the 95% confidence bounds of the fitted line encompass the global line MWL. Since the two lines are so close to each other, the global MWL was used in analysis of other meteoric plots. Further examination of the regression analysis is performed in Appendix B.

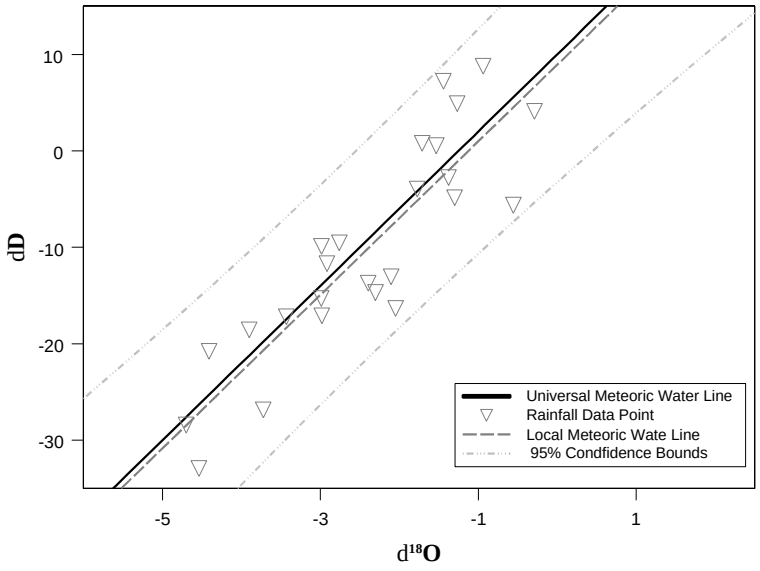

Figure 4.1.1 Local MWL vs. Global MWL

Once the decision to use the global MWL was made, a plot of $\delta^{18}O$ vs. δD of all collected samples excluding those from rainwater sites was created (Figure 4.1.2). This plot consists of over 430 data points. In all plots, data points having the same symbol shape belong to the same generalized categories as outlined in Table 4.1.1. The values plotted below the MWL, showing that the samples were enriched in ^{18}O values as compared with deuterium values. This would indicate that the waters within the study site were subjected to an evaporative process.

Table 4.1.1 Graphical Symbols

Symbol	Site Description
■	Shallow Well
◆	Deep Well
✠	Production Well
●	Surface Water
▲	Lake Water
▼	Rain Water

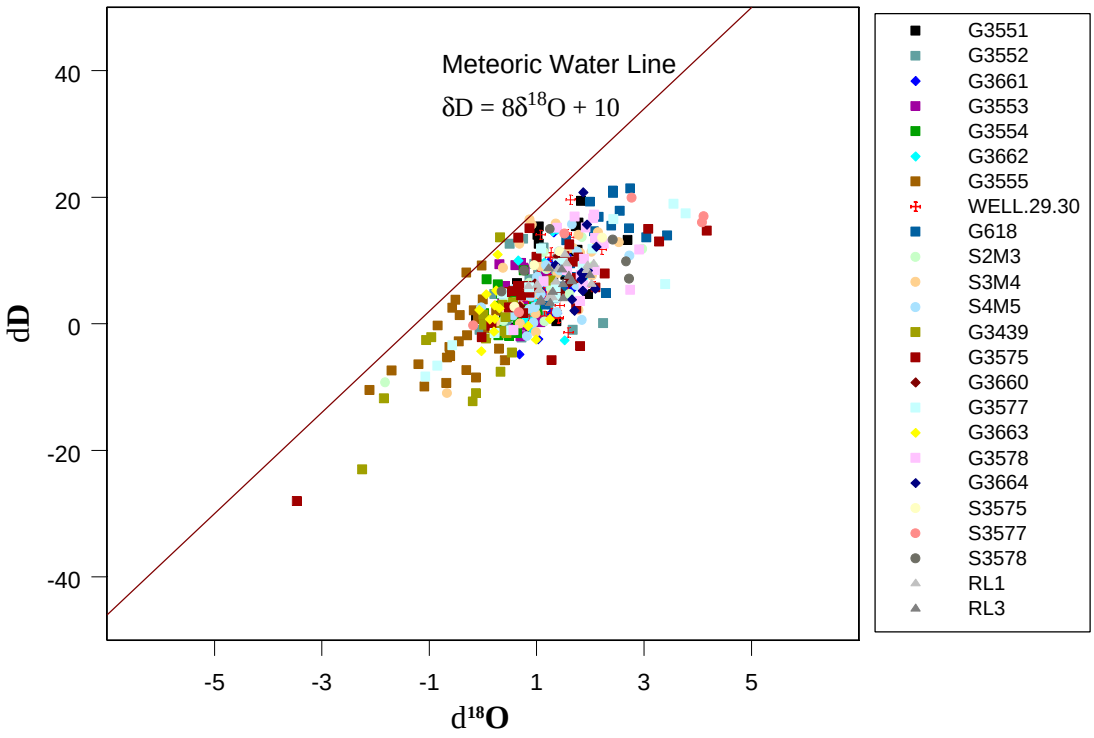

Figure 4.1.2 Meteoric Water Plot (All Analyzed Data Points Excluding Rainfall)

In order to further examine the structure of the collected data and the specifics of the evaporative process at work, the average delta values of all sites were plotted versus the MWL (Figure 4.1.3). As can be seen, rainwater is significantly lighter than the other water samples collected. Of the other sites (Figure 4.1.4), G-3555 and G-3439 are the lightest. These sites are the furthest east and consequently the most removed from the Everglades. G-618 and S3577, both located in the Everglades, are the heaviest. In agreement with the data points on the extremities, an overall pattern is observed from relatively heavy to relatively light as the sites progress geographically from west to east. To emphasize this point, wells have been grouped into Everglades wells (those west of L-31N) and

urban wells (those east of L-31N) (Figure 4.1.5). With the exception of G-3663, the Everglades wells are in general heavier than the urban wells.

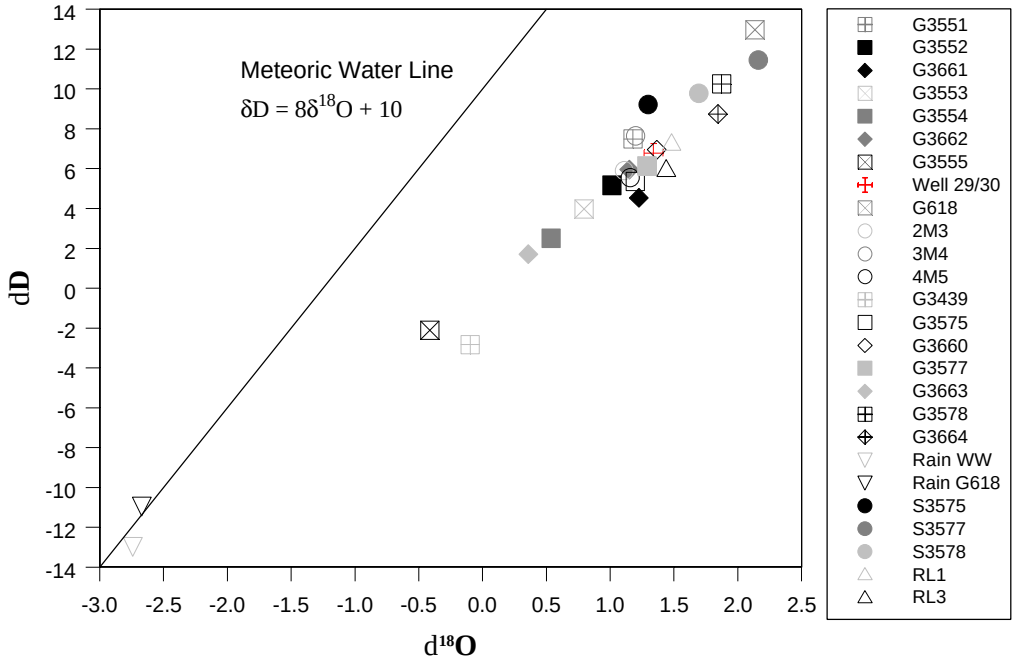

Figure 4.1.3 Average Values of Study Sites Including Rainfall

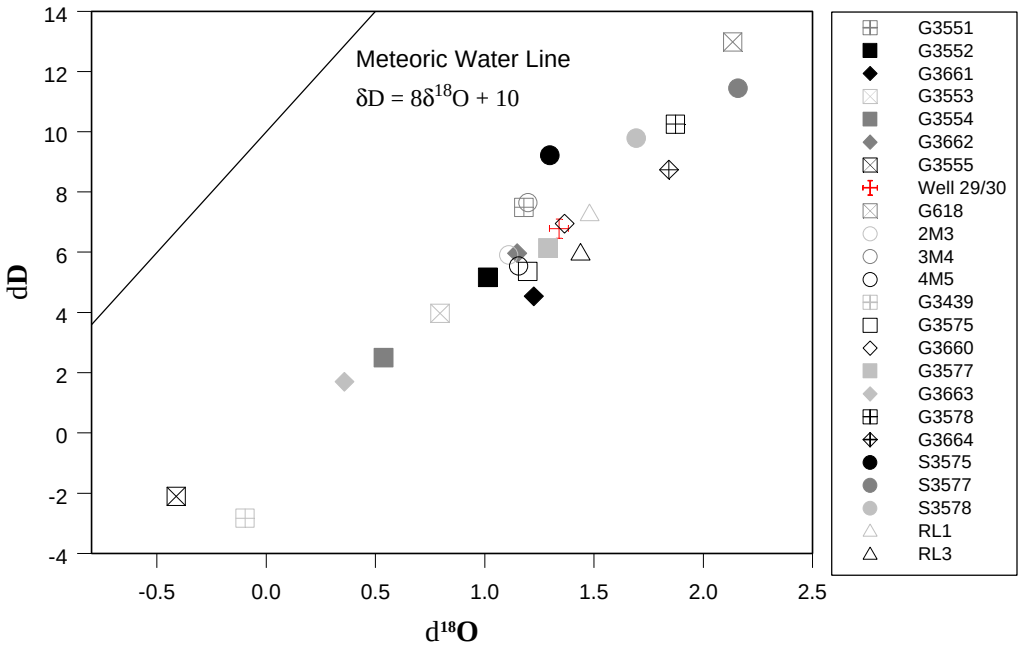

Figure 4.1.4 Average Values of Study Sites Excluding Rainfall

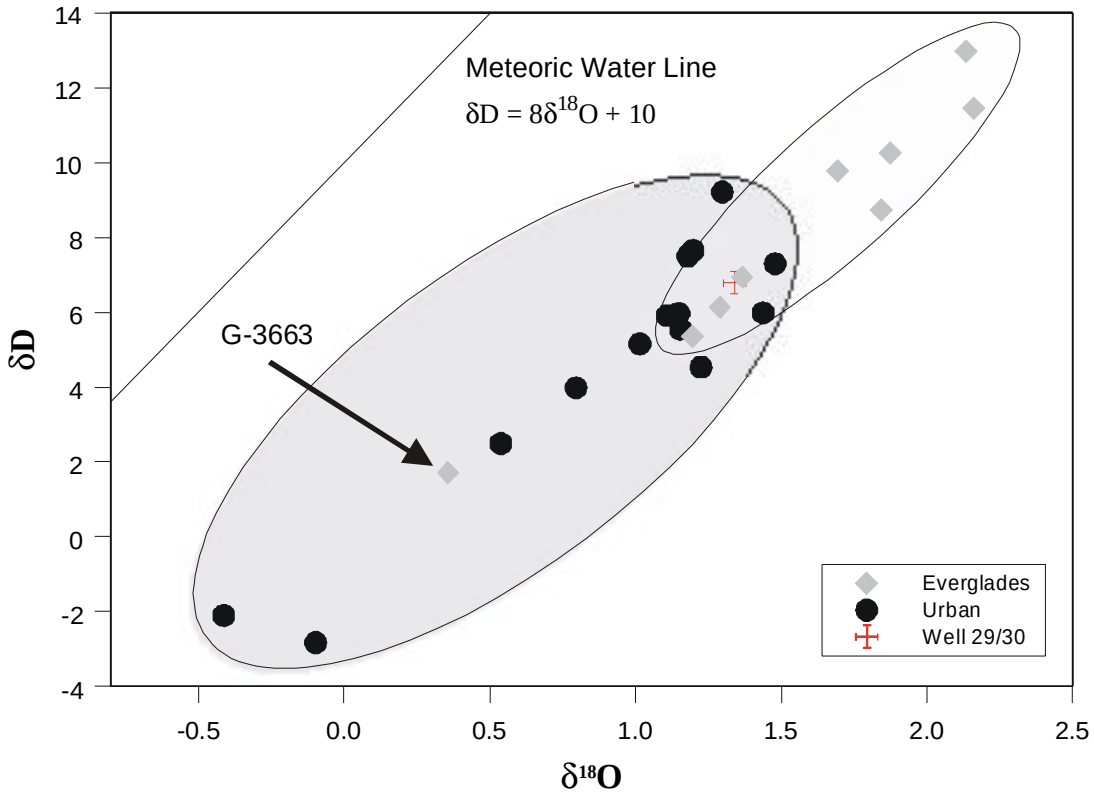

Figure 4.1.5 Everglades Wells vs. Urban Wells

In Figure 4.1.6, wells located at the same horizontal coordinates have been given the same color while wells of roughly the same depth have been assigned the same symbol. This was done in order to emphasize the fact that at specific geographic locations the deep wells are in most cases heavier than the shallow wells. This especially holds true on the urban (eastern) side of Levee 31N where, for example, G-3662 plots heavier than G-3554, even though both wells are located at the same location. While G-3664 does plot slightly lighter than G-3578, the primary exception to this general trend occurs at G-3577/G-3663 where the deeper well is significantly lighter than the shallow well. Further discussion of these observations is incorporated in Section 4.3.

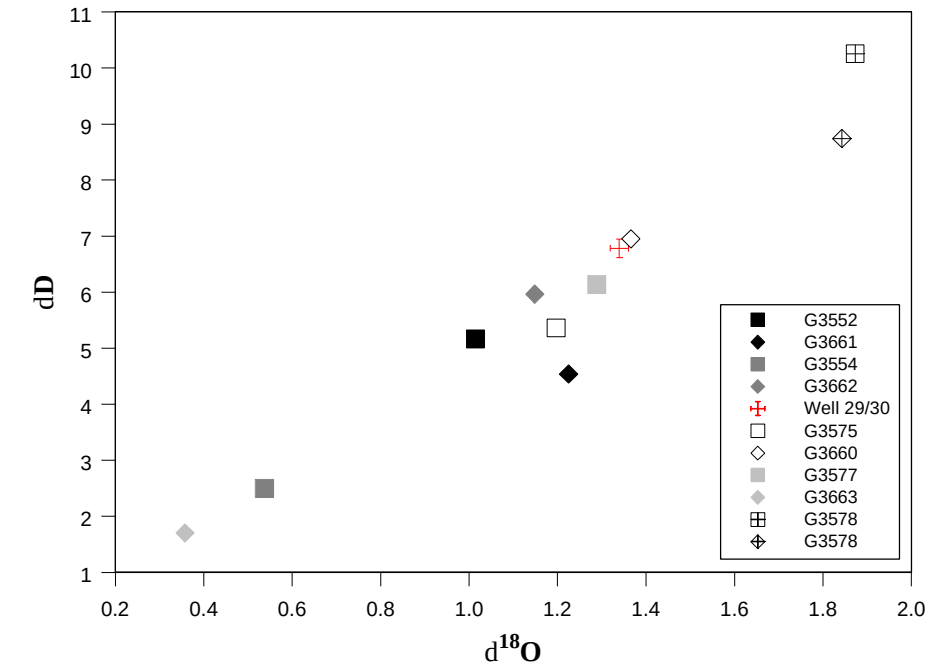

Figure 4.1.6 Shallow Wells vs. Deep Wells

Fitting a regression line that incorporates the average values of the specific sites allows for an examination of the effect of evaporation on the isotopic composition of waters in the study area as previously outlined in Chapter 3. An intersection of the regression line with the MWL would indicate that the rainfall feeding the system came from a location having an isotopic composition similar to the intersection point. In Figure 4.1.7, it can be seen that rainfall within the study area (the RainWW and Rain G-618 sites) falls within the 99% confidence limits. The assertion that local rainfall strongly contributes water to the system becomes even more convincing when 95% standard deviation bars are shown for the averaged values of individual sites (Figure 4.1.8). The variation of the rainfall data and the regression line confidence bounds overlap greatly.

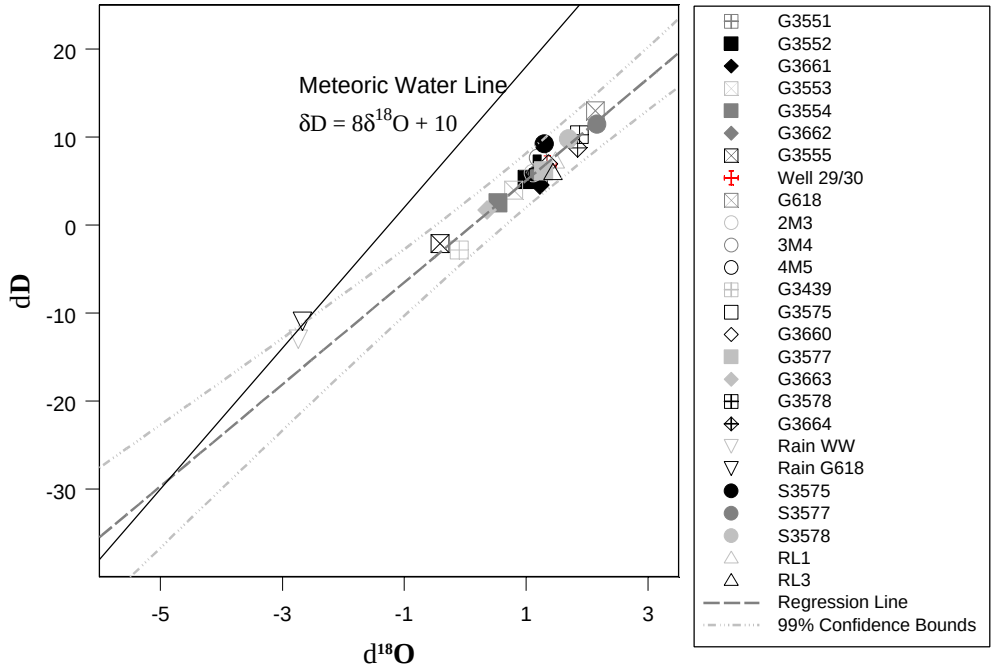

Figure 4.1.7 Sites Regression

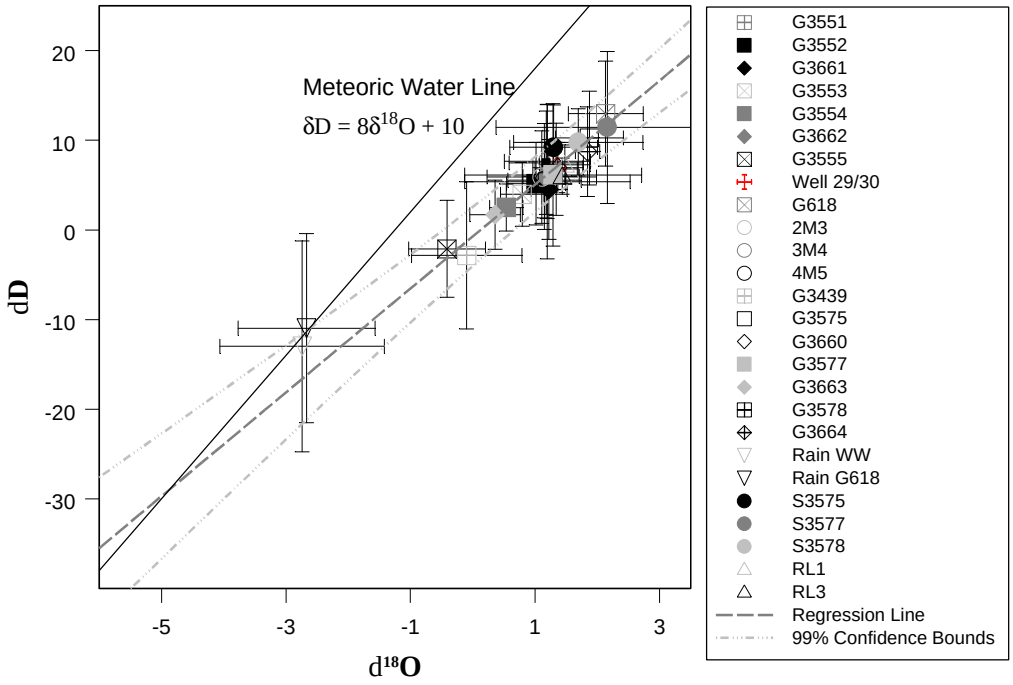

Figure 4.1.8 Sites Regression Analysis with Confidence Boundaries

The fact that the sampled rainfall plots near the outer bounds of the confidence limits of the study sites regression would seem to indicate that although rainfall in the study area is the primary source of water in the system there may be another, slightly lighter source of water as well. This influence can be attributed to the fact that water does indeed enter the study site from another source. The operation of water control gate S333 results in the infusion of water from an Everglades conservation area to the north of the study area. This conservation area collects water from rainfall points further north as well as more inland. While no isotope data is available in this area, it is conceivable that due to the Rayleigh distillation effects (as outlined in section 3.1.7), this water would trace back to a point that was lighter on the meteoric water line. This infusion of water could therefore have an influence on the sampling points in the study area and affect the regression line. However, it is important to make a distinction here that while the evaporation regression may point to a supplemental, lighter initial source of water (lighter rainfall) to the conservation area, this does not mean that water entering the study area through the gate is light. This water is in fact very heavy as a result of evaporation effects. In other words, while the regression analysis gives insight into the initial source of water (e.g. rainfall location) to a system, it does not indicate the state of the water in the system at a given time. Water that may have initially been isotopically light rainfall could in fact be heavy at a given time due to evaporation effects.

4.2 Distance Plot

To further emphasize the spatial effect of west to east migration on isotope values in the study area, plots of $\delta^{18}O$ values vs. distance from pumping wells were produced. 95% confidence intervals have been incorporated into the plots to show the effect that seasonal variations can have in delta values. The plot of average values shows a general trend of decreasing $\delta^{18}O$ values when moving from west to east in the study site (Figure 4.2.1). This trend is due to the mixing of isotopically light infiltration (primarily from urban areas) with evaporated Everglades water as the water migrates from west to east. Infiltration is lighter on the urban side due to rapid drainage of rainwater through an infrastructure designed to prevent flooding of these areas. Water is heavy on the Everglades side due to evaporation effects on the standing surface water west of Levee 31N. The mixing of these two water sources results in the $\delta^{18}O$ values becoming increasing lighter with distance from the Everglades. The predominant portion of this trend is seen in the vicinity of L-31N, along the border between the Everglades and urban areas. In the Everglades, the trend is much less pronounced once far removed from this border as evidenced by the relatively small change from G-618 to G-3578 over a large distance. The average value for L-31N canal sites is seen to lie immediately between G-3575 and G-3551, the shallow wells immediately west and east of the canal, respectively. This illustrates that canal water is not significantly different from the shallow wells.

This observation seems to indicate that the canal water is mixing with surrounding groundwater and therefore not acting as a boundary between Everglades and urban water.

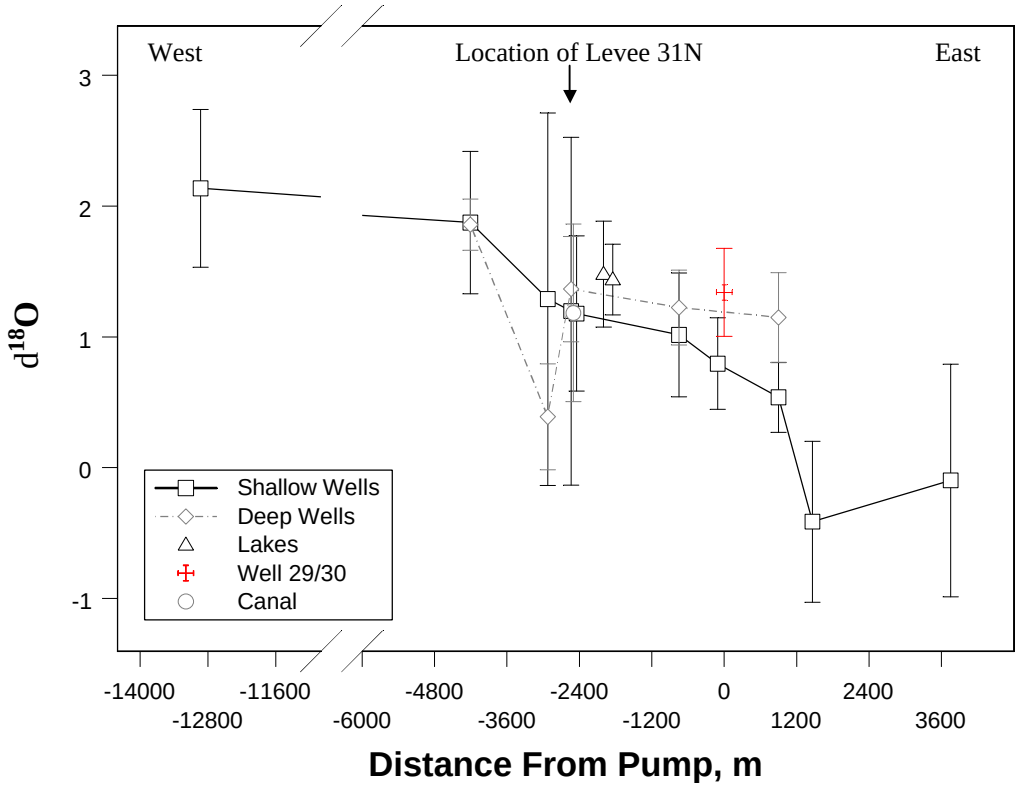

Figure 4.2.1 Distance Plot
Order of deep wells from west to east: G-3664, G-3663, G-3660, G-3661, G-3662
Order of shallow wells from west to east: G-618, G-3578, G-3577, G-3575, G-3551 G-3552, G-3553, G-3554, G-3555, G-3439

Also evident in Figure 4.2.1 are the previously alluded to trends of relatively isotopically heavy deep water to shallow water on the urban side of Levee 31N and the extremely light $\delta^{18}O$ values present at G-3663. The deep water begins to diverge from shallow water at G-3575/G-3660, the easternmost of the

Everglades wells. This divergence can be explained due to the mixing effect of light rainwater that rapidly infuses into the Biscayne Aquifer on the urban side of Levee 31N. While the shallow wells are significantly impacted by this infusion of rainfall, the deep wells do not show this effect as strongly (although a decreasing delta trend is still evident with eastward migration). This is most likely due to hydraulic head differences on the urban side of the levee that tend to promote predominantly horizontal flow in the aquifer. The presence of the semi-confining layers outlined in Section 2.2 may also be playing a role in inducing horizontal flow. The only clear divergence from these explanations occurs at G-3663. Reasons for variations from general trends evident at G-3663 will be addressed in Section 4.3.

Further examination of the plot indicates that the rock mining lakes and the pumping well are heavy for both their location and depth. The most likely reason for this observation at the lakes is evaporation. Evaporation results in enrichment of heavy isotopes at the surface of the lakes. It is likely that the lakes also are influenced by the inflow of deep heavy water that originated in the Everglades since evapo-transpiration effects alone would most likely not result in as large an enrichment over shallow water as that observed (Herrera, 2000). The pumping wells mirror the enrichment of the lake water supporting the hypothesis that water is being drawn into the wells from the rock mining lakes directly west of the wellfield. The only other source of such heavy water to the

pumping wells could be Everglades water and it is unlikely that the municipal wellfield is drawing water directly from sites such as G-3578 and G-3664. This is not to say that water from these sites does not migrate to the wellfield. However, the time required for this migration would result in at least some mixing with lighter, rain influenced water as is observed in the deep wells trendline. As such, the distance plot would seem to support the hypothesis that lake water is being drawn into the pumping wells.

It is important to note here that while the pumping well on average is heavy for its location and depth indicating an influence of lake water, this does not mean that it is not influenced by both deep and shallow water in its immediate location. The confidence interval for the pumping well clearly encompasses the deep well average line indicating that the pumping wells are most likely influenced by deep water. The shallow water in the area also asserts an influence as evidenced by the fact that the confidence interval of the pumping well overlaps at least partially the confidence intervals of surrounding shallow wells G-3553 and especially G-3552.

4.3 Three Dimensional Plots

The relative impact of rainfall events and S333 gate operation on the isotope delta values in the study area was assessed through the production of three-dimensional plots. These graphs plotted $\delta^{18}O$ vs. rainfall in inches vs.

average flow in cubic feet per second at gate S333. In order to compare short and longer term effects, two sets of plots were made, one incorporating values for the previous five days and one incorporating values for the previous thirty days to sampling. Plots of this nature produce graphical surfaces that react to the effects of both rainfall and gate operations on delta values. Heavier isotope values result in a darker color while lighter values result in lighter shading. If no significant impact by these variables is observed, a nearly flat, uniformly shaded plane having very little slope or surface distortion would be produced. On the other hand, if rainfall and gate operations do have an influence on delta values, the graphical surface will appear to bend and distort from a planar shape and will contain both darker and lighter shadings.

The five-day graphs show several interesting features. First, the plots once more confirm that sites in the west (Everglades) were in general heavier than sites in the east (urban) (Figure 4.3.1). Also evident is the fact that sites reacted differently to rainfall influences and influences from the operation of gate S333. For example, in G-618, an Everglades shallow well, the sloping transition from dark shading to light shading towards lighter $\delta^{18}O$ values as rainfall increases under low flow conditions indicates that at greater rainfall events, the $\delta^{18}O$ values are lighter. However, in the presence of flow through gate S333, these rainfall influences are negated and $\delta^{18}O$ values remain heavy. A more consistent pattern is observed in urban wells and urban surface waters (the lakes and canal)

where high rainfall events resulted in lighter $\delta^{18}O$ values. This type of pattern is consistent with the expected outcome as light rainfall should cause a decrease in site delta values as it mixes with heavier *in situ* water.

Additionally, the five-day plots show that the shallow wells and the deep wells were affected differently in the short term by rain and gate operations (Figure 4.3.2). The deep wells maintain a pattern similar to that of Everglades water indicating that in the short term, they were not as affected by rainwater as the shallow wells. This result makes sense due to the fact that travel time to the deep wells is most likely greater than five days.

Overall, it was observed that the graphical surface in many plots predominantly slopes along the rainfall axis rather than the flow axis. This indicates that flow through gate S333, though certainly a source of water to the system, did not result in fluctuations in $\delta^{18}O$ values comparable to those caused by rainfall in the short term at most sites. The only plots that significantly show the influence of gate S333 in the short term are the Everglades sites (as previously mentioned at G-618), especially the surface waters. S3578 is provided as a representative plot (Figure 4.3.3).

The noticeable exceptions to these general trends occurred at G-3577/G-3663 and at the pumping well (Figures 4.3.4 and 4.3.5) where the immediate influence of rainfall was observed despite the fact that these wells should show a pattern similar to that of G-618 due to their location or depth. For G-3663, this

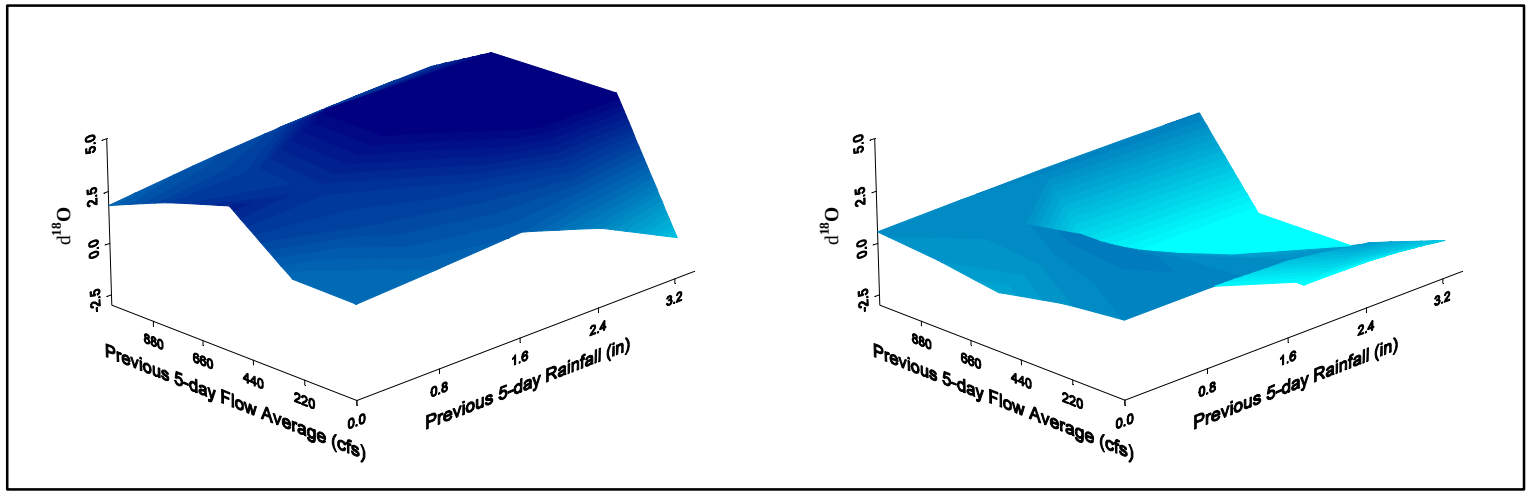

Figure 4.3.1 Everglades Well G-618 (left) vs Urban Wells G-3553 (right) 5-Day

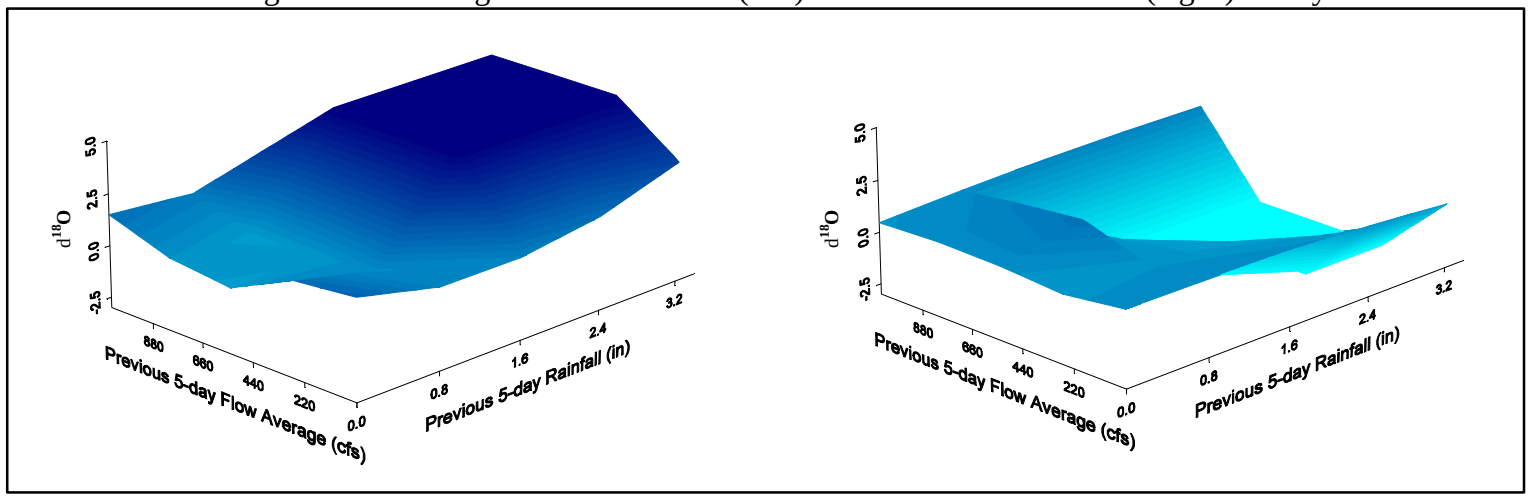

Figure 4.3.2 Deep Well G-3662 (left) vs Shallow Well G-3554 (right) 5-Day

divergence can be explained by the presence of a large open cavity encountered during the drilling of the well. The increased hydraulic conductivity associated with the existence of this cavity supports the hypothesis that rain influenced water travels through the aquifer at this location more quickly than at other locations. As a result, in the short term, $\delta^{18}O$ values at G-3577 and G-3663 are significantly decreased by rainfall events. This observation also explains the extremely light delta values observed in the meteoric (Figure 4.1.6) and distance plots (Figure 4.2.1).

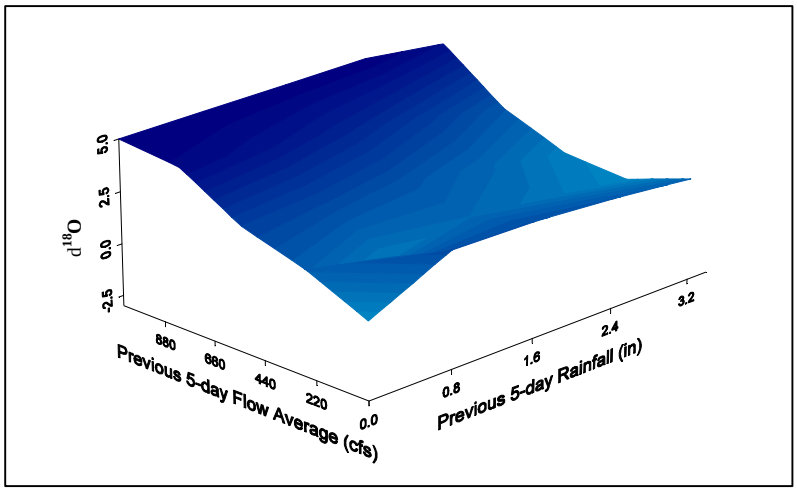

Figure 4.3.3 S3578, Everglades Surface Water 5-Day

In contrast, at the pumping well, the very nature of the well itself will give insight into the variation. The fact that the well is drawing large quantities of water from the surrounding aquifer medium is the direct cause of observed differences from other deep (non-pumping) wells. The pumping well pulls water not only horizontally, but also vertically from more shallow areas than its screened intake. However, it is important to note that while the shape of the

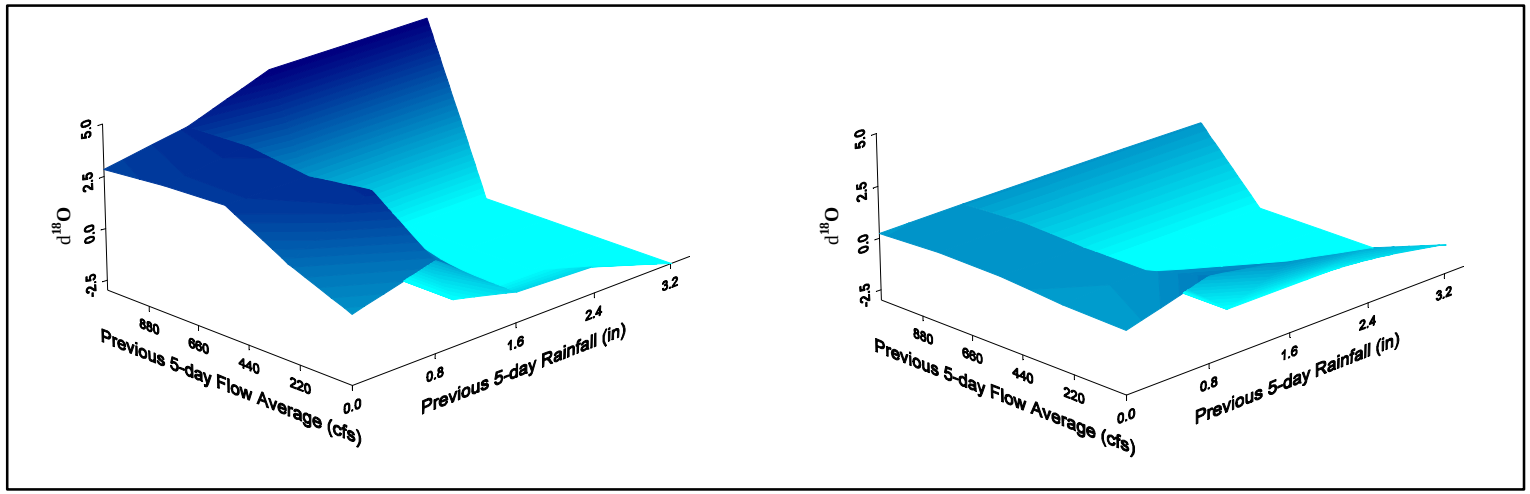

Figure 4.3.4 G-3577 (left) and G-3663 (right) 5-Day

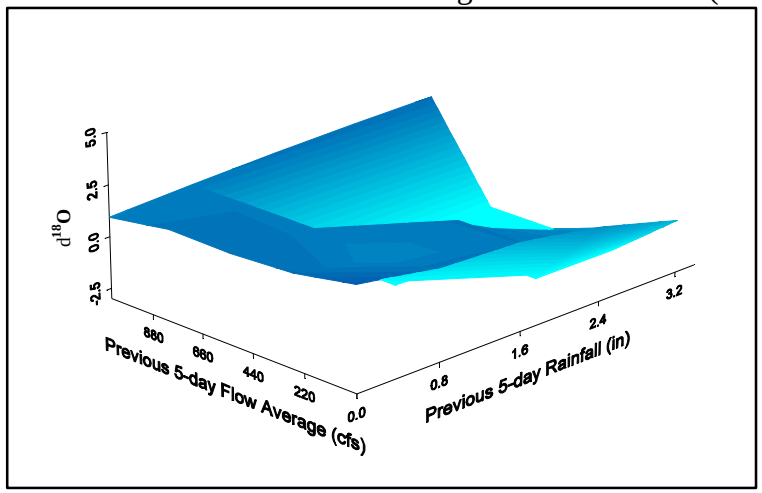

Figure 4.3.5 Well 29/30, Pumping Well 5-Day

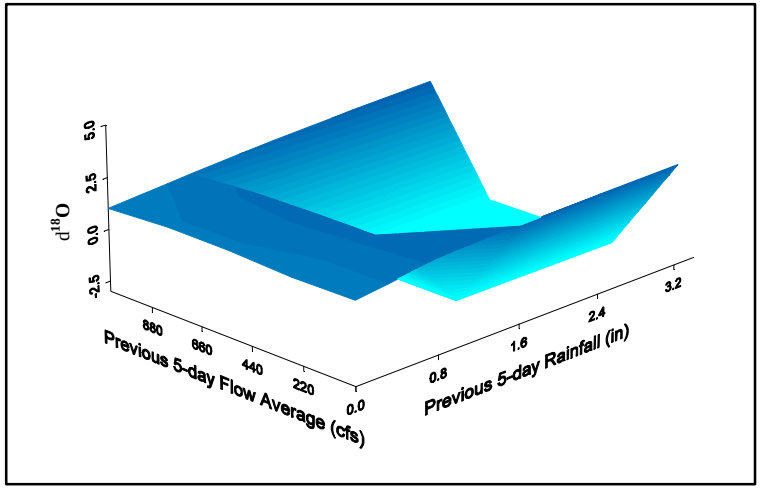

Figure 4.3.6 RL3, Rock-mining Lake 5-Day

three-dimensional plot points to a short-term rainfall influence similar to that of urban shallow wells, the overall values are heavier than surrounding shallow wells. This would indicate that the pumping well draws a mix of both shallow and deep waters. It is also interesting to note that the pumping well plot is similar to that of RL3 (Figure 4.3.6). Like the pumping well, RL3 exhibits a short-term rainfall influence, but overall is heavier than shallow wells in its vicinity. This observation suggests that the lakes may also have an influence on the pumping well.

The thirty-day plots are in general much more planar than the five-day plots as the greater time scale results in less drastic fluctuations in rainfall and flow measurements. The same sites as those examined in the five-day plots are provided in Figures 4.3.7 through 4.3.12.

As can be seen, the previous observations are further validated by these graphs. The important things to notice once again are the differences between Everglades (western) and urban (eastern) sites as well as the divergence between shallow and deep wells, specifically, the height of the plane on the vertical axis. In shallow Everglades and deep urban wells, the graphical surfaces plot at heavier $\delta^{18}O$ values than in urban, shallow wells. The thirty-day plots also confirm that the pumping well and lake RL3 do indeed plot heavy for their location.

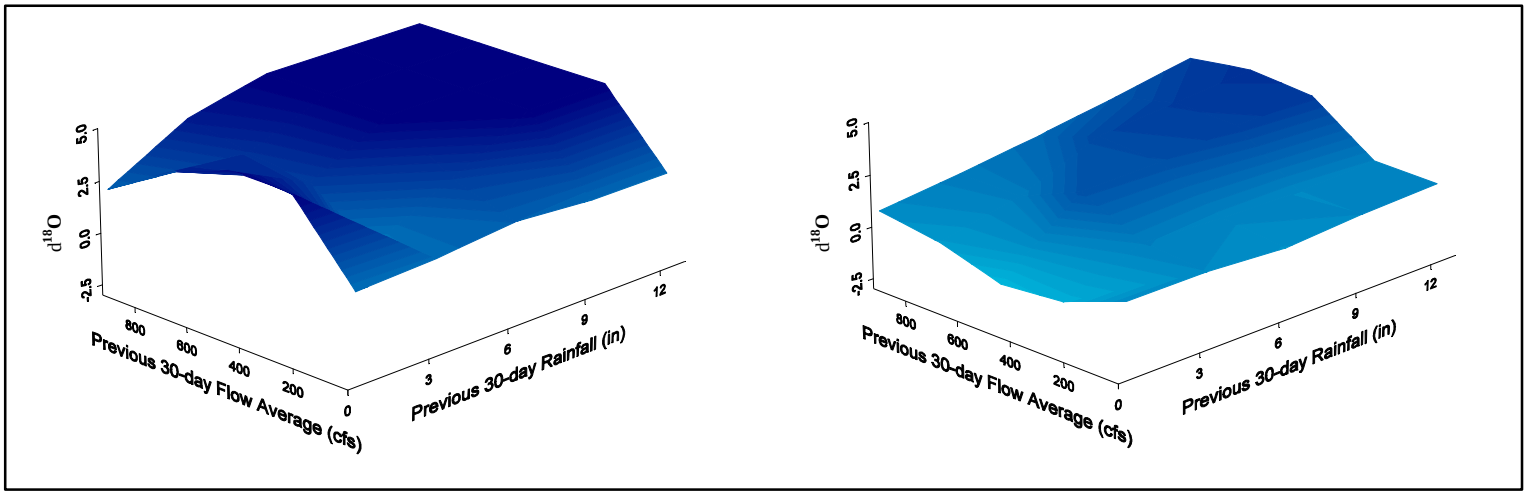

Figure 4.3.7 Everglades Well G-618 (left) vs Urban Well G-3553 (right) 30-Day

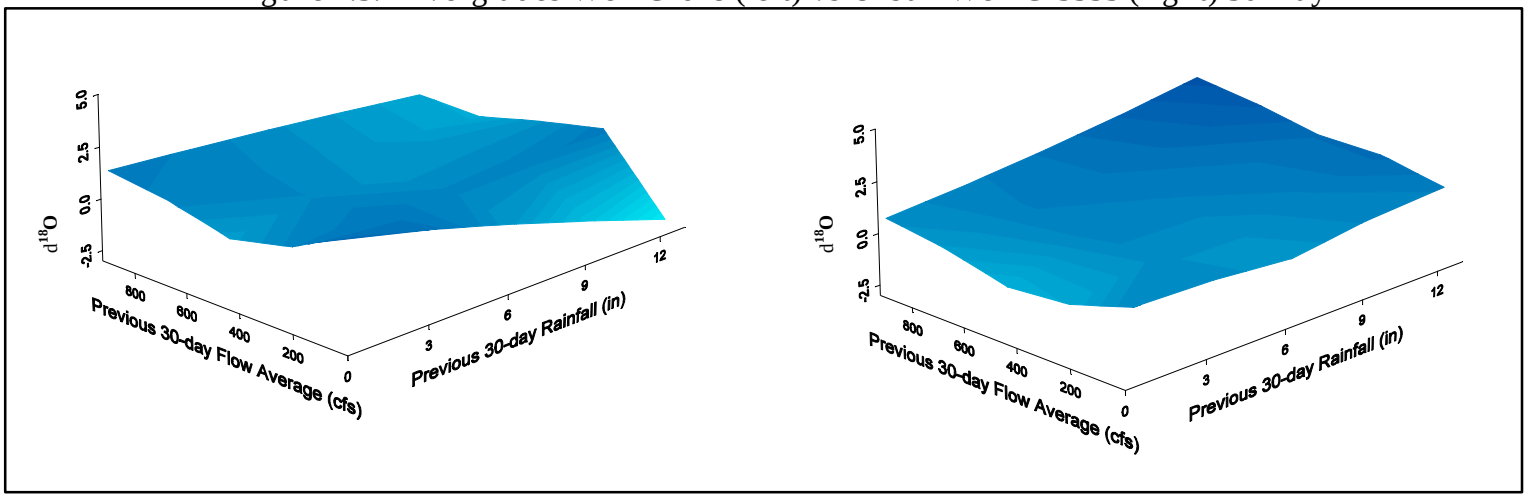

Figure 4.3.8 Deep Well G-3662 (left) vs Shallow Wells G-3554 (right) 30-Day

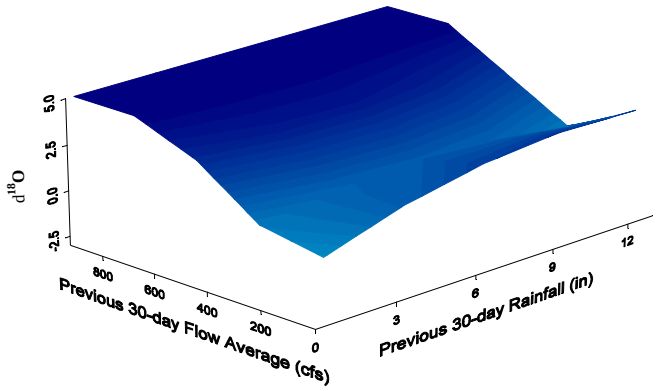

Figure 4.3.9 S3578, Everglades Surface Water 30-Day

Once again, the operations of gate S333 were examined and it appears that over the larger time scale, there is a significant correlation between gate operations and delta values in the Everglades. Everglades surface waters and shallow Everglades wells such as G-3575 and G-3578 (Figure 4.3.13) show a correlation between high flow conditions and heavy $\delta^{18}O$ values over thirty days. This serves to support the interpretation of the data in Section 4.1, which indicated that the operation of S333 is important in terms of providing a source of water to the Biscayne Aquifer system.

The thirty-day plots of G-3577 and G-3663 once again show a pattern that is irregular compared to the other sampled sites. It has already been observed in the five-day plots that rainwater infuses very quickly at this location. The thirty-day plots support this assertion, as for nearly any amount of rainfall and intermediate flow values (the most prevalent condition found throughout the course of the study) there is a sharp decline in $\delta^{18}O$ values at G-3577. It is also evident in this plot that at high flow conditions, $\delta^{18}O$ values increase

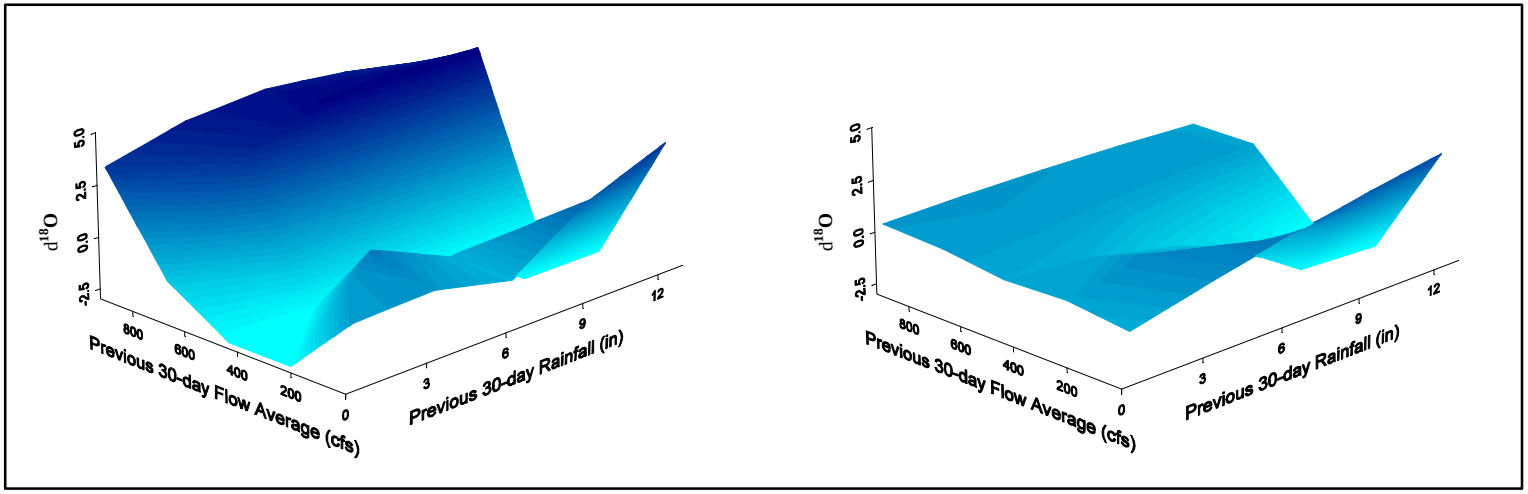

Figure 4.3.10 G-3577 (left) and G-3663 (right) 30-Day

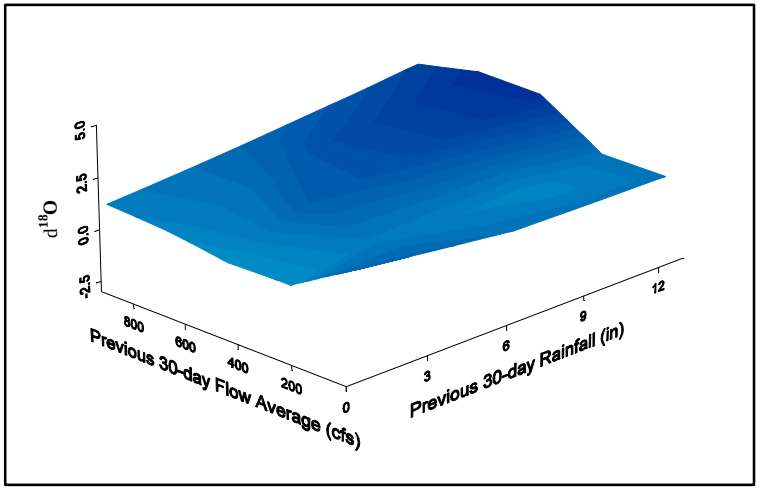

Figure 4.3.11 Well 29/30, Pumping Well 30-Day

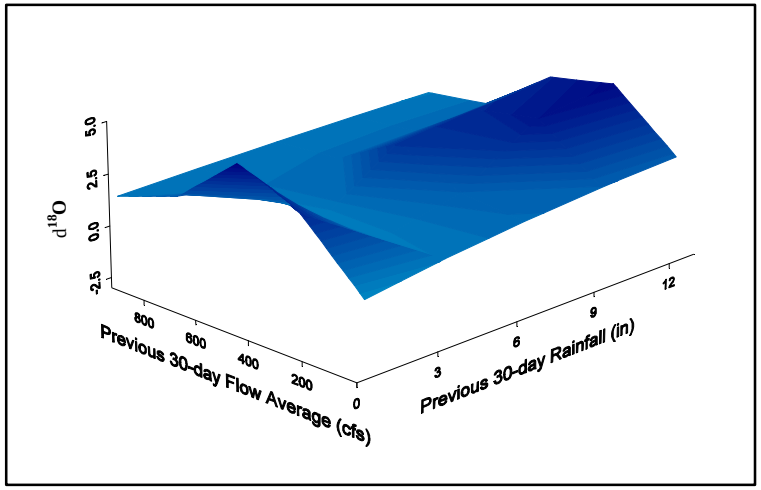

Figure 4.3.12 RL3, Rock-mining Lake 30-Day

dramatically indicating a correlation with operations of gate S333. It appears that the area directly beneath and immediately surrounding G-3577 acts as a sink for Everglades surface water. Over the larger time scale of thirty days, this collected water that infuses so rapidly is gradually mixed with the *in situ* ground water. This is evidenced by the decrease in delta values under heavy rainfall conditions observed below G-3577 at G-3663 and at other surrounding wells including G-3578 and G-3575 (Figure 4.3.13).

To make this concept clearer, a cartoon sketch is provided (Figure 4.3.14). The extremely high seepage into the underground cavern beneath G-3577 flows into a "conduit" of water that is isotopically different from surrounding groundwater. This "conduit" responds quickly to the composition of the surface water feeding the seepage. Over time, the predominant groundwater flow (moving from northwest to southeast) and further infusion of surface water cause water in this "conduit" to mix with surrounding groundwater, eventually reaching isotopic equilibrium and becoming indistinguishable from the groundwater. When the volume of seepage feeding the "conduit" is less, its range of influence is reduced. The predominant groundwater flow direction at this point is toward the southeast. It is therefore likely that this "conduit" takes water to the south of other sampling sites and does not regularly affect the delta values of other sampling sites. In fact, it is only under heavy rain conditions when increased volumetric input to the "conduit" results in a greater east/west

spreading of surface water influenced flow that mixing effects are observed in adjacent wells as mentioned above.

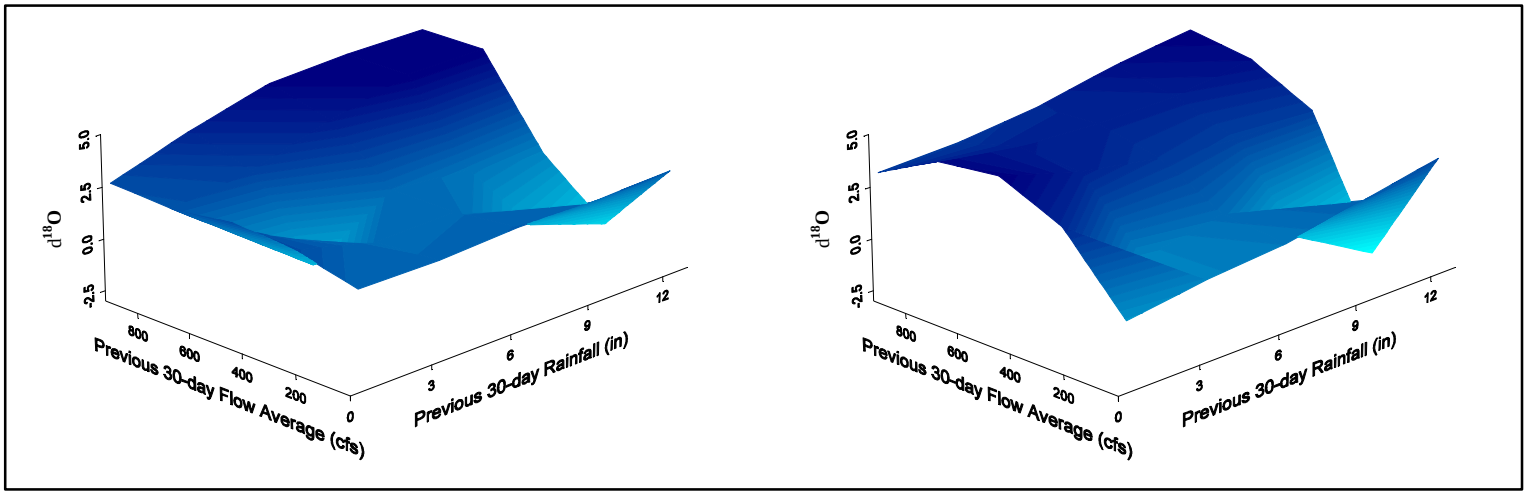

Figure 4.3.13 G-3578 (left) and G-3575 (right), Wells Near G-3577

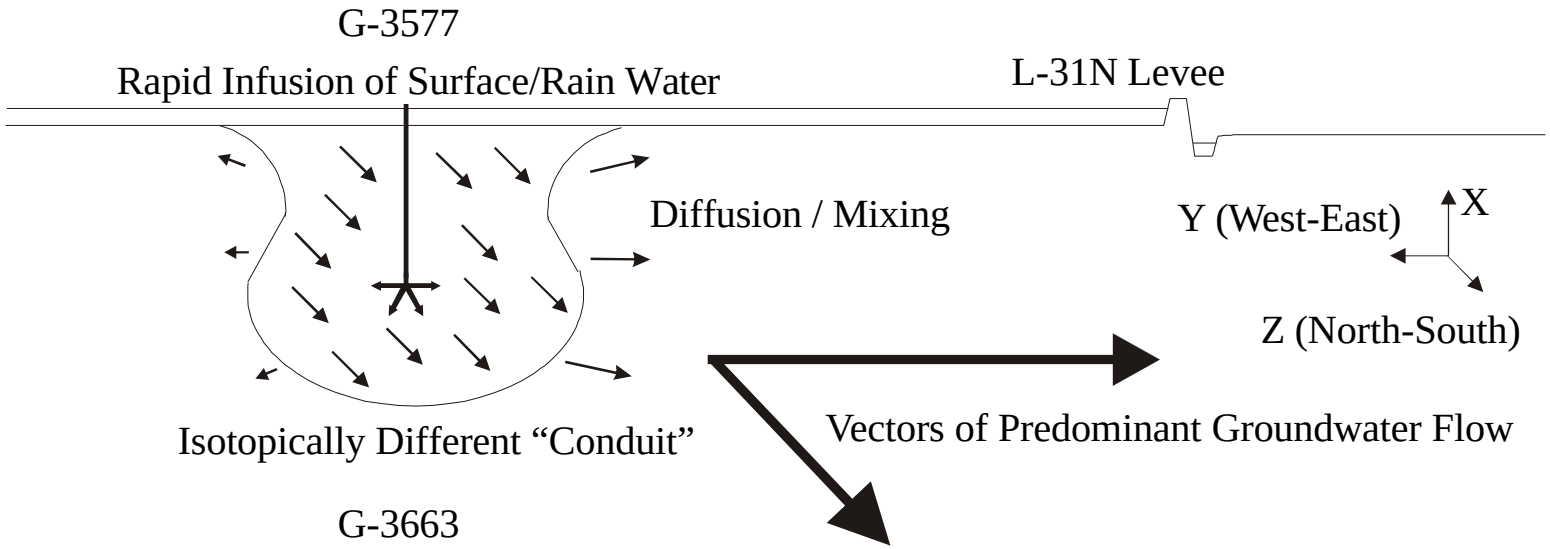

Figure 4.3.14 Cartoon Sketch of Rapid Everglades Surface Water into Flow "Conduit"

5

Modeling Based on Stable Isotopes

5.1 Simple Box Model

A simple box model was created in order to test the hypothesis that the mixing of Everglades and urban water is indeed occurring at the West Wellfield pumping stations. The conceptualization of this model involves the assumption that two isotopically different waters are being drawn to and mixed at the pumping well site. These waters include Everglades type water and urban type water (Figure 5.1.1).

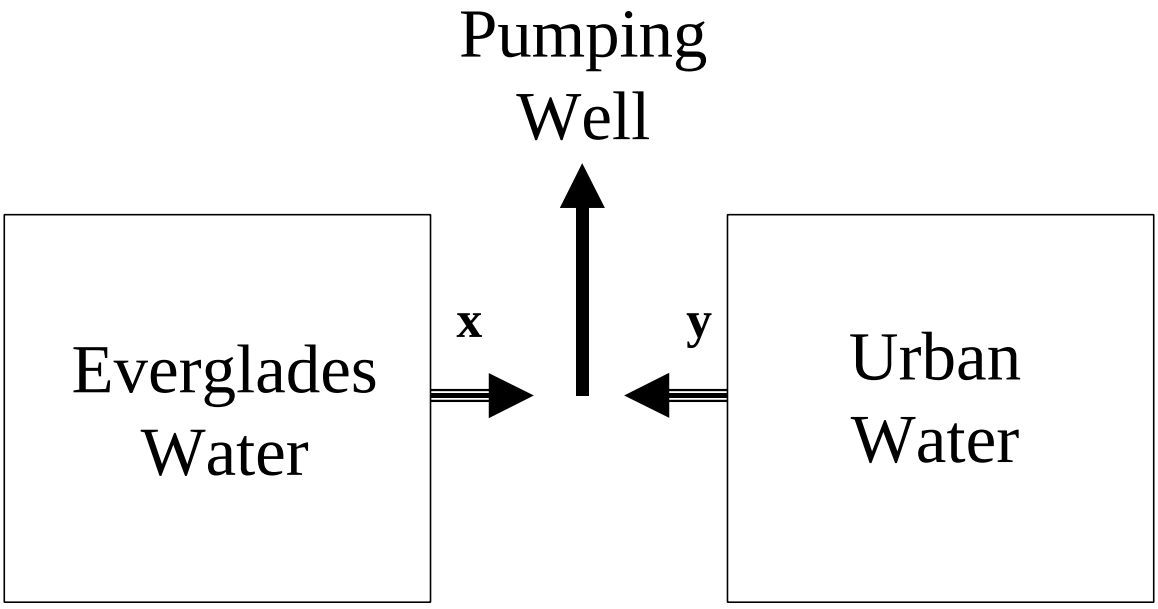

Figure 5.1.1 Simple Box Model Conceptualization

An isotopic balance of the conceptual model is represented by the following two equations:

$$x + y = 100\ \% \qquad \text{(Equation 5.1.1)}$$

$$(\delta^{18}O_x)x + (\delta^{18}O_y)y = (\delta^{18}O_p)100 \qquad \text{(Equation 5.1.2)}$$

in which x is the percentage of Everglades water at the pumping well, y is the percentage of urban water at the pumping well, $\delta^{18}O_x$ is the $\delta^{18}O$ value of Everglades water (taken as the $\delta^{18}O$ value at G-618), $\delta^{18}O_y$ is the $\delta^{18}O$ value of urban water (taken as the $\delta^{18}O$ value at G-3555) and $\delta^{18}O_p$ is the $\delta^{18}O$ value of water at pumping well 29/30.

This model was evaluated using different sets of input data. These sets included the overall average of all samples, the 1998 yearly data average, and the 1996/1997 combined data average. Also used as input for model runs were the averages of "Summer" months (considered to be May through October), "Winter" months (November through April), "Dry" months (those having less than a total of four inches of rainfall during the thirty days prior to sampling), and "Wet" months (those having more than a total of four inches of rainfall during the thirty days prior to sampling). Rainfall data for making the distinction between "wet" and "dry" months was measured at S338. It is important to note that the "wet" and "dry" terms refer to rain totals during the previous thirty days to sampling and not to the total for the month during which sampling

occurred. Results of the model for these data sets are provided in Table 5.1.1 for these various scenarios.

Table 5.1.1 Simple Box Model Results

	% Everglades Water	% Urban Water
Overall Average	68.9	31.1
1998 Average	65.7	34.3
1996-1997 Average	72.0	28.8
“Summer” Months	59.6	40.4
“Winter” Months	86.4	13.6
“Dry” Months	73.8	26.2
“Wet” Months	66.4	33.6

This model, using data for the entire study period, shows that 69% of the water being pumped from the well is indicative of Everglades water while only 31% is indicative of urban water. This supports the hypothesis that Everglades type water is indeed reaching the pumping well and in fact may be the major contributing source. This assertion is further strengthened by the fact that for all conditions, over 50% of the water at the pumping well is Everglades type. The simple model results also show that during “dry” conditions, when a smaller quantity of recharge is available, a greater demand is placed upon the contribution from Everglades groundwater. This causes the percent composition of Everglades water in the pumping well to increase. This observation also holds true when comparing summer and winter months. Summer months in general correlate to the wet season in South Florida during which rainfall would be recharging the urban water more consistently than during winter months.

Consequently, an increase in quantity of Everglades water reaching the pumping well is observed during the dryer winter conditions. The difference between the 1998 Average model results and those of the 1996-1997 Average is also most likely the result of rainfall differences. On average, there was less rainfall during 1996 and 1997 (50.52”) than in 1998 (52.46”) in the study area. Accordingly, the percentage of Everglades water returned by the model is higher in the drier 1996-1997 years.

While this simple box model is useful in assessing general trends, certain conceptual problems are inherent as a result of the simplicity of this type of model. These include the lack of compensation for the direct isotopic influence of rainfall and inflow from water conservation areas at gate S333 on the system as well as the influence of any mixing across geologic layers in the rock mining lakes and evaporation of water at the lake surface. There is no simple way to redress these problems within the framework of the simple model. While introducing only rainfall to the model would result in a higher Everglades influence (as additional heavy Everglades water would be needed to balance the light rain input in the isotope balance), introducing only isotopically heavy lake water as an inflow would cause an increase in the observed urban influence. In order to combat some of these problems, a more complex box model was developed. Results of this conceptualization are provided in the next section.

5.2 Complex Box Model

For the complex box model, a two-mile by four-mile rectangular area (Figure 5.2.1) within the focus area was selected and broken into five conceptual boxes (Figure 5.2.2). Specifications for these boxes are provided in Table 5.2.1.

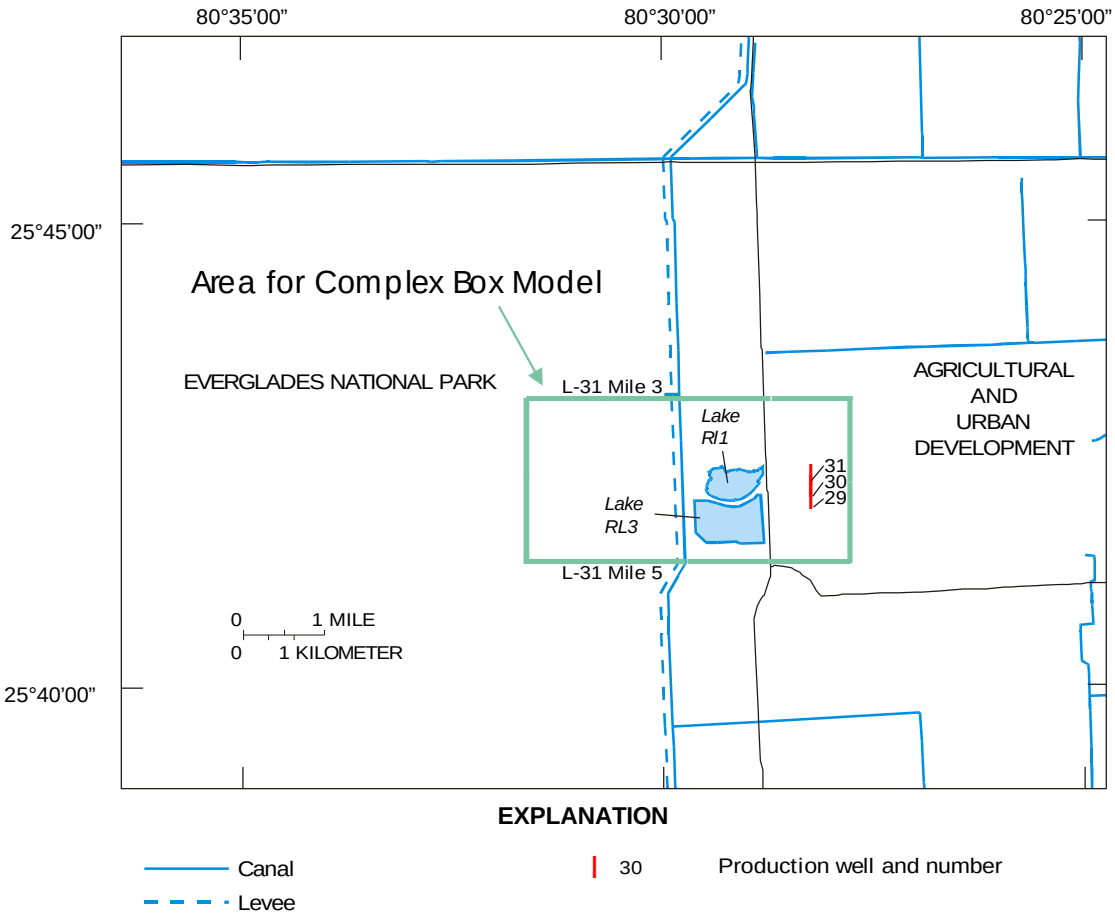

Figure 5.2.1 Area for Complex Box Model

In Table 5.2.1, R refers to rainfall, A refers to area, ET refers to evapo-transpiration, P refers to the pumping well and subscripts to the delta notation indicate location of a collected isotopic sample (e.g. δ_{G618} would refer to the average isotopic value of samples collected at the G-618 monitoring site). $\delta_{E\#}$ (the

Table 5.2.1 Complex Box Model Conceptualization

Box #	Box Description	Inputs	Corresponding δ Values Used	Outputs	Corresponding δ Values Used
1	Everglades	• Everglades water including inflow from S333 (E) • Rainfall (R1) over A1, a 2.00 mile by 2.00 mile area (111,513,600 sq. ft)	• G618 • Rain G618	• Evapo-transpiration (ET1) over A1, a 2.00 mile by 2.00 mile area (111,513,600 sq. ft) • "Shallow" Groundwater (X) • "Deep" Groundwater (Y)	• δ_{E1} from Rain G618, S3575, S3577 & S3578 • G3575 • G3660
2	Canal	• "Shallow" Groundwater (X) • Rainfall (R2) over A2, a 2.00 mile by 0.02 mile area (1,056,000 sq. ft)	• G3575 • Rain WW	• Evapo-transpiration (ET2) over A2, a 2.00 mile by 0.02 mile area (1,056,000 sq. ft) • "Shallow" Groundwater (Z)	• δ_{E2} from Rain WW, 2M3, 3M4 & 4M5 • G3551
3	Lakes	• "Shallow" Groundwater (Z) • Rainfall (R3) over A3, a 2.00 mile by 0.22 mile area (12,408,000 sq. ft)	• G3551 • Rain WW	• Evapo-transpiration (ET3) over A3, a 2.00 mile by 0.22 mile area (12,408,000 sq. ft) • "Shallow" Groundwater (L) • Seepage (S)	• δ_{E3} from Rain WW, RL1 & RL3 • δ_L from RL1 & RL3 • δ_L from RL1 & RL3
4	Deep Groundwater	• "Deep" Groundwater (Y) • Seepage from lakes (S)	• G3660 • δ_L from RL1 & RL3	• "Deep" Groundwater (D)	• G3662
5	Urban	• "Shallow" Groundwater (L) • "Deep" Groundwater (D) • Rainfall (R5) over A5, a 2.00 mile by 1.76 mile area (98,049,600 sq. ft)	• δ_L from RL1 & RL3 • G3662 • RainWW	• Pumping Well (P) • Urban Water (U)	• Well 29/30 • G3555

delta value of evaporated air leaving a surface water in box "#") is calculated using the method proposed by Gonfiantani (1986) and δ_L is the average of the $\delta^{18}O$ values for RL1 and RL3. The calculation of δ_E using the method as proposed by Gonfianitini is provided in appendix C. Also found in the table are the terms "shallow" groundwater and "deep" groundwater. This distinction is designed to distinguish between water moving in the Biscayne Aquifer above the deeper semi-confining layer ("shallow" corresponding to layers 2, 3 and 4 in Figure 2.2.2) and water moving between the deeper semi-confining layer and the base of the Biscayne Aquifer ("deep" corresponding to layer 6 in Figure 2.2.2).

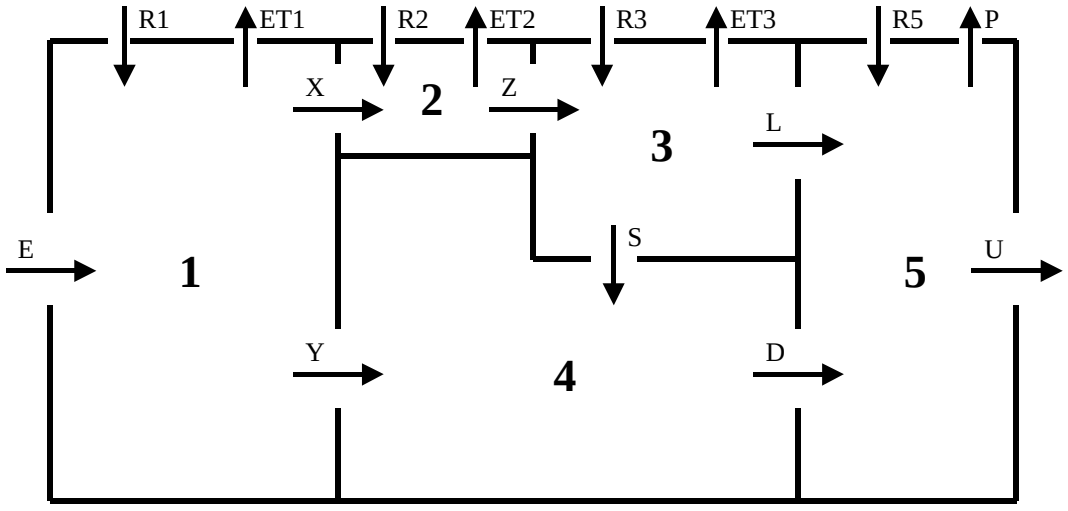

Figure 5.2.2 Complex Box Model Conceptualization

The measured and model obtained variables in the complex box model are outlined in Table 5.2.2. All variables in Table 5.2.2 are defined in Table 5.2.1. The unknown flow values were calculated in the model by simultaneously

solving equations created by performing isotopic and volumetric balances assuming steady state conditions and using six control volumes (Figure 5.2.3). A complete list of these computations is provided in Appendix C. Take for example the equations used in the balance of control volume one surrounding box one:

Volumetric Balance:

$$E + R1*A1 - ET1*A1 - X - Y = 0 \qquad \text{(Equation 5.2.1)}$$

Isotopic Balance:

$$E*\delta_{G618} + R1*A1*\delta_{Rain\ G618} - ET1*A1*\delta_{E1} - X*\delta_{G3575} - Y*\delta_{G3660} = 0$$

(Equation 5.2.5)

For these equations, all variables are defined in Table 5.2.1. All flows are measured in cubic feet per year (cfy), all areas are in square feet (sq. ft) and rainfall / evapo-transpiration values are measured in feet per year (ft / yr).

Table 5.2.2 Measured and Model Calculated Values

Box #	Measured Variables	Model Calculated Variables
1	R1, ET1, A1, δ_{G618}, $\delta_{Rain\ G618}$, δ_{E1}, δ_{G3575}, δ_{G3660}	E, X, Y
2	R2, ET2, A2, δ_{G3575}, $\delta_{Rain\ WW}$, δ_{E2}, δ_{G3551}	X, Z
3	R3, ET3, A3, δ_{G3551}, $\delta_{Rain\ WW}$, δ_{E3}, δ_{L}	Z, L, D
4	δ_{G3660}, δ_{L}, δ_{G3662}	Y, S, D
5	R5, A5, P, δ_{L}, δ_{G3662}, $\delta_{Rain\ WW}$, $\delta_{Well\ 29/30}$, δ_{G3555}	L, D, U

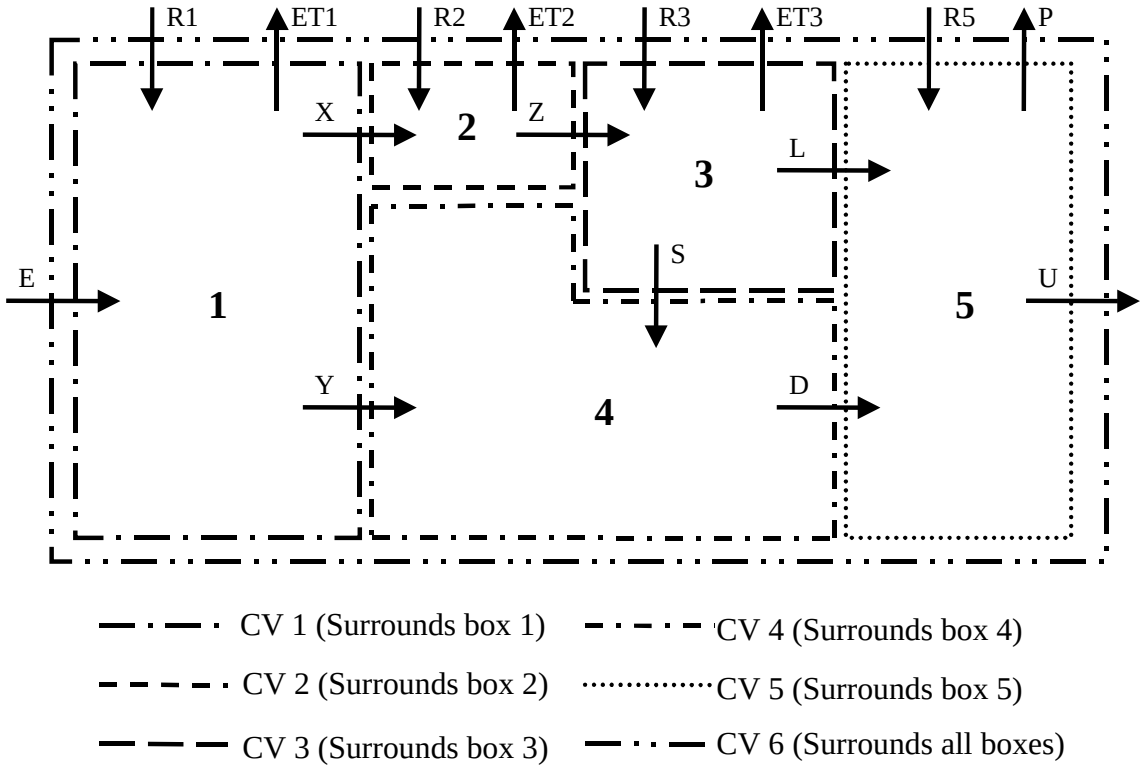

Figure 5.2.3 Control Volumes for Complex Box Model

Additional description of the lakes box (box 3) is needed in order to understand the model conceptualization. The sum of the surface area of the two rock-mining lakes is known to be approximately $1.24 * 10^7$ sq ft (Herrera, 2000). Therefore in the model, together they are considered to be a thin strip of two miles (10,560 ft) wide by approximately 0.22 miles (1,175 ft) long. While the lakes actual shapes are in fact very different, for the purposes of the model flow balances, only the surface area is important. Also evident in the table and the figure is the fact that an addititional seepage term is incorporated into the model conceptualization of the lake box. This seepage term, while drawn as a vertical flow in the figure, in fact incorporates both movement through the bottom of the

lakes and any inflow from the horizontal difference between the deeper semi-confining layer and the base of the lakes (approximately five to ten feet). In this regard, it is impossible for the model to distinguish between horizontal and vertical flow across the boundary between box 3 and box 4. While the lakes box incorporates an additional seepage term, the canal box does not. Canal seepage is considered to be only through the sides of the canal. This arrangement is considered to physically describe the system given that hydraulic gradients are very flat in the area of the canal resulting in horizontal flow lines. Furthermore this conceptualization is consistent with the existing MODBRANCH model of the study site as developed by Nemeth (2000) and modified by Herrera (2000). This model utilizes the reach transmissivity relationship which models canal seepage through the side channels of a canal rather than the bottom. A comparison between complex box model output and flow in the MODBRANCH model is performed later in this section.

Results of the complex box model for the 1998 and the overall average data sets (Figures 5.2.4 and 5.2.5) indicate that water leaving the Everglades and seeping under Levee 31N preferentially moves in the layer between the deeper semi-confining layer and the base of the Biscayne Aquifer. This is seen by a flow ratio of ten to one in the “deep” groundwater as compared to “shallow” groundwater for the model run using all the data. Water in this semi-confined layer travels east until moving into the vicinity of the rock mining lakes. As the

lakes cut through the deeper semi-confining layer, the model indicates nearly sixty percent of the “deep” groundwater flow travels up into the lake. Water from both the lake and the “deep” groundwater channel then migrate eastward into control volume number five, the urban box. Here the model flow terms indicate that the pumping well draws water from surrounding urban “shallow” groundwater, the lakes and “deep” groundwater.

The complex model is in many ways an improvement over the simple model. It incorporates rainfall and evapo-transpiration data. In addition, it accounts for the presence of both “deep” groundwater flow and the rock mining lakes. Another positive aspect of the complex box model is that it utilizes data from several of the isotope monitoring stations rather than only two as in the simple box model.

Despite all of the positive aspects of the complex box model, it is still only a conceptualization that does not fully account for north/south water migration or surficial Everglades flow. In addition, some of the sites used in the complex box model were not monitored until the start of 1998 or later. As a result, at sites such as G-3660 too few data points are available to accurately perform additional model runs such as those done for the simple model that assess the impact of seasonal or conditional variations on the system. It is also important to note that the areal size of the complex model was chosen so as to incorporate the rock mining lakes, the West Wellfield and Everglades isotope monitoring stations. As

such, redefining the boundaries of the model could result in different model output.

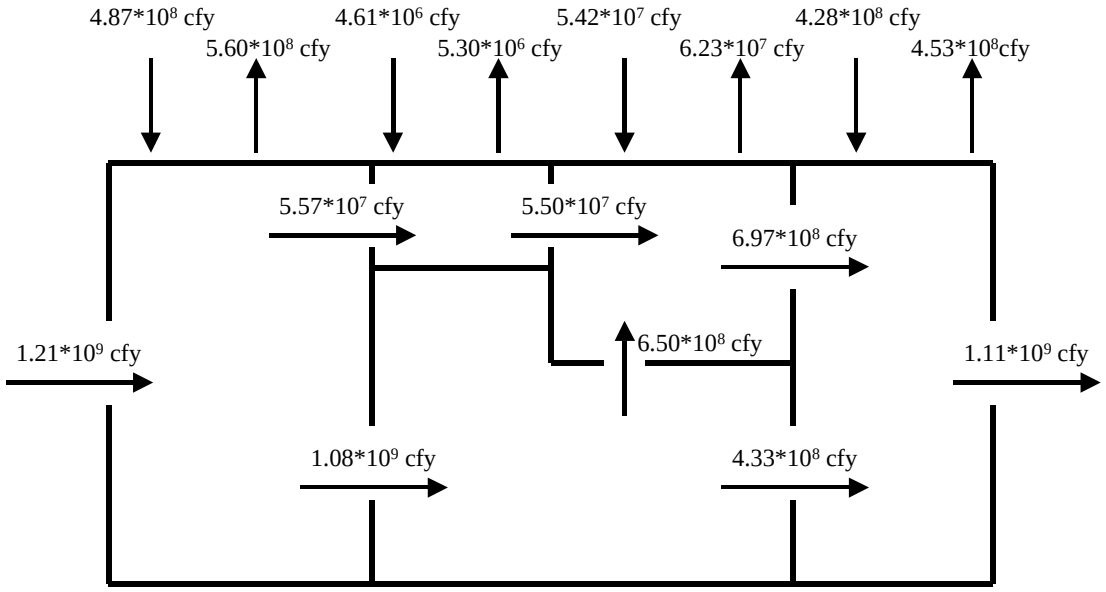

Figure 5.2.4 Complex Box Model Results for 1998

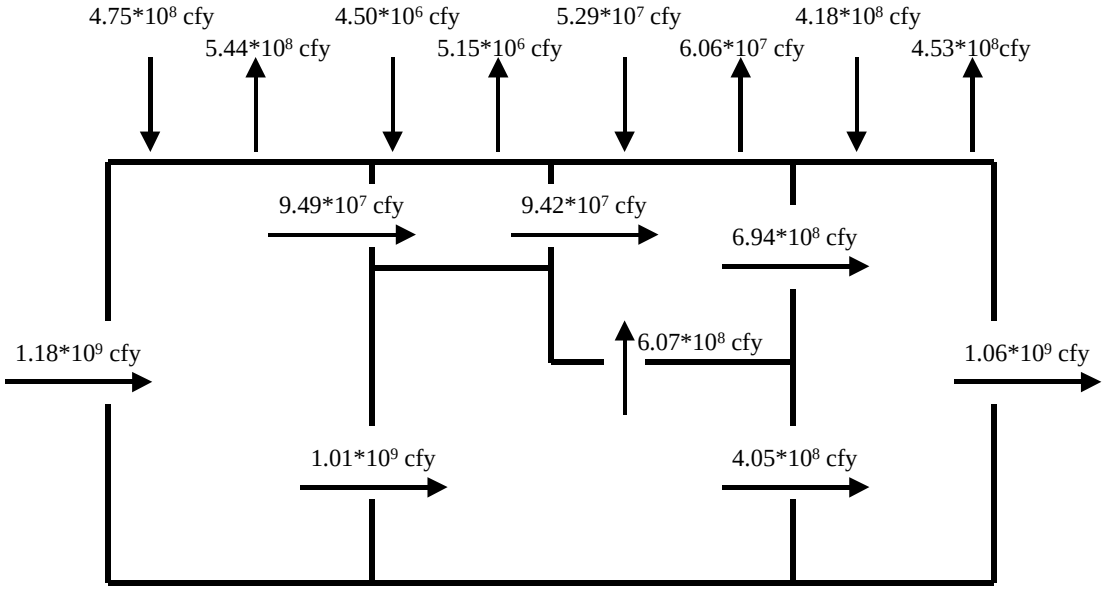

Figure 5.2.5 Complex Box Model Results for All Data

5.3 Comparison of the Complex Box and MODBRANCH Models

One of the goals of creating the complex box model was to compare the results obtained from an isotopic and volumetric flow balance of the study site to the results of the existing MODBRANCH model of the site (Nemeth et al., 2000 and Herrera, 2000). This was accomplished by comparing cumulative flow values of the overall average run of the complex box model and the MODBRANCH model calibrated for 1997 data at two locations. These results, provided in Table 5.3.1, measured the seepage under L-31N and the outflow from the rock mining lakes. In the table, the cumulative sums for the MODBRANCH model are the sums of the outflow terms for model boxes as outlined in Appendix C. As the table illustrates, the sum of the "shallow" and "deep" flow layers for both the seepage under L-31N and the lake outflow are similar when comparing the complex box model to the MODBRANCH model. The results are both of the same order of magnitude with the seepage case having a 35% difference in the complex box model relative to the MODBRANCH model and the lake outflow case having only a 26% difference in the MODBRANCH model relative to the complex box model.

Differences evident in the distribution between "shallow" and "deep" layers predominantly come from two sources. The major cause for these differences is that the complex box model assumes a vertical seepage component to the lakes (as RL1 and RL3 do not reach a depth extending to the base of the

Biscayne aquifer) while the MODBRANCH model assumes that the lakes are fully penetrating. As a result, the deeper groundwater seepage component of the lake (S) in the complex box model cannot be compared to the MODBRANCH model. It is most likely that the increased "deep" seepage under L-31N in the complex box model is a result of the flow balance required to provide the upflow component to the lake box. Another difference between the models is observed in the yearly input data. While the complex model is conceptually dependent on at least some data from 1998 (such as at G-3660 where no data is available before 1998), the MODBRANCH model is based on data from 1996 and calibrated to data from 1997. Differences in rainfall, evaporation rates, etc. between different years could lead to changes in the cumulative flow volumes. Despite these differences, the results of the complex box model and the MODBRANCH simulation do match up well.

Table 5.3.1 Comparison of Complex Box Model and MODBRANCH Model

Location		Complex Box Model for Overall Average Cumulative Flow (cfy)	MODBRANCH Model for 1997 Cumulative Flow (cfy)
Seepage Under L-31N	"Shallow"	$9.50 * 10^7$	$1.01 * 10^9$
	"Deep"	$1.02 * 10^9$	$7.06 * 10^8$
	Sum	**$1.12 * 10^9$**	**$1.71 * 10^9$**
RL1 and RL3 Lake Outflow	"Shallow"	$6.94 * 10^8$	$5.33 * 10^8$
	"Deep"	$6.08 * 10^7$ *	$4.86 * 10^8$
	Sum	**$7.55 * 10^8$**	**$1.02 * 10^9$**

* Depth averaged percentage based on lake penetration into "Deep" layer (taken as 15% of total flow)

6

Summary and Conclusions

In order to examine whether municipal well operation or rock mining practices will affect the northeastern portion of Everglades National Park, an assessment of the hydrology in the area of the West Wellfield of Miami-Dade County and Levee 31N was performed. This thesis incorporated data from a study period spanning from January 1996 to December 1998 and included a hydrogeologic review of the area, the use of stable isotopes as water tracers and development of a series of box models to quantify flows to various areas within the study site. It draws upon, combines and enhances the isotopic and modeling work of previous students along with more recent research in order to obtain a more complete understanding of water movement in the study area. In an effort to achieve this goal, various investigative, experimental and analytical methods were employed to obtain and scrutinize data as presented in this thesis.

As it is necessary to condense this myriad of data and information offered in the thesis into a feasible final set of conclusions and present these findings in a meaningful way, a cartoon-type sketch of water movement in the area of L-31N is provided in Figure 6.1. Results of the hydrogeologic review indicate the presence of two semi-confining layers in the otherwise highly permeable

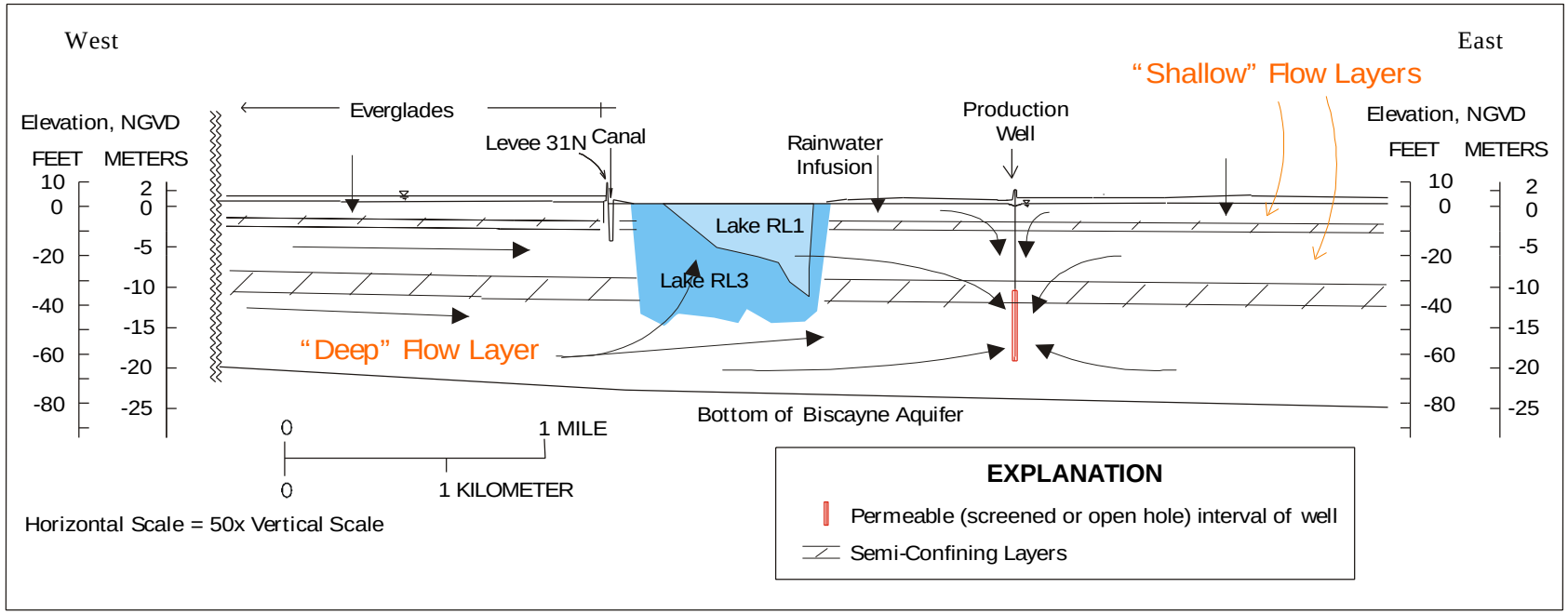

Figure 6.1 Cartoon Sketch of Water Movement in Study Site (Cross Section View)

Biscayne Aquifer. As such, these hard layers are incorporated into Figure 6.1. The meteoric water plots show that the majority of water in the site is coming from local rainfall (both Everglades and urban) with additional water most likely the result of infusion of water at gate S333 from northern water conservation areas. It is known from regional water table maps, measured head differentials, and MODBRANCH modeling simulations of the area that water in the study site moves in general from northwest to southeast on the Everglades side of L-31N and from west to east on the urban side of L-31N.

Isotopically heavy Everglades surface water, primarily comprised of rainfall and water from the conservation areas that has been affected by evaporation, infuses into shallow and deep water flow layers present in the Biscayne aquifer underlying the Everglades. It has been observed that localized geologic disturbances can cause this infusion to occur very rapidly, such as in the vicinity of USGS monitoring wells G-3577 and G-3663. This is evidenced by the observed isotopic behavior in the five-day plots of $\delta^{18}O$ vs. rainfall vs. average flow through S333. Localized rapid infusion of rainfall results in the formation of "conduits" of isotopically light water that travel along with the predominant groundwater flow pattern, gradually mixing with the surrounding groundwater until it comes into isotopic equilibrium. This is seen in the thirty-day plots of $\delta^{18}O$ vs. rainfall vs. average flow.

Upon nearing Levee 31N, Everglades groundwater begins to travel in a more easternly pattern, moving nearly horizontally with very little vertical migration in the geologic layers comprising the Biscayne aquifer. The results of the complex box model and the MOBRANCH model both indicate that a substantial amount of the water is seeping under Levee 31N into the urban side of the study site. Results of the models show that on the order of a billion cubic feet of water per year is seeping under the portion of L-31N between mile 3 and mile 5 (adjacent to the West Wellfield). This water moves in the both the "shallow" flow layers above the deeper semi-confining layer outlined in the hydrogeologic review of the site and the "deep" flow layer between the deeper semi-confining layer and the base of the Biscayne Aquifer. Isotopic and volumetric balances suggest that Everglades water is preferentially moving into the "deep" flow layer prior to seeping under the Levee. This indicates that the L-31N canal, which cuts through a portion of the "shallow" groundwater flow, does not act as a hydrologic boundary between Everglades and urban waters. Additionally, the relative isotopic similarity between canal water and surrounding "shallow" groundwater on both the Everglades and urban sides of L-31N seem to indicate that the canal is mixing with groundwater rather than acting as a boundary.

Once on the urban side of L-31N, rainwater infuses into the "shallow" flow layer, progressively mixing with groundwater and making it isotopically

lighter as it travels east. The plot of $\delta^{18}O$ values vs. distance from the pumping wells shows that this effect is also seen in the "deep" flow layer, however not as drastically. Near the lakes, the "breaks" in the hard layers that are a by-product of rock mining allow "deep" Everglades water to mix with the lake water. This process is aided by the fact that the lakes have greater hydraulic conductivity than does the aquifer, causing some of the "deep" groundwater to migrate into the lake. The inflow of "deep" water in conjunction with the evaporation effects evident in the plot of $\delta^{18}O$ values vs. distance (Figure 4.2.1) make the lakes isotopically heavy. Results of the complex box model agree with this assertion, illustrating that some water is indeed moving up into the lakes from a "deep" groundwater source.

Water from both the lakes and the "deep" groundwater continue to migrate to the east until the operations of the municipal pumping wells at the West Wellfield causes some of this water to be drawn into the production well intakes. These intakes are screened to a depth well below the deeper semi-confining layer and consequently draw upon not only "shallow" urban water (predominantly comprised of urban rainfall) and lake water (having influences from both urban rainfall and Everglades water) but also "deep" water that originated in the Everglades. In fact, results of the simple box model indicate that more than sixty percent of the water being pumped by the West Wellfield ultimately originates in the Everglades. Additionally, during drier weather

conditions, the proportion of Everglades water at the West Wellfield is seen to increase as urban rainfall is not as readily available to recharge the Biscayne Aquifer. The combined examination of the hydrogeology, isotopic characteristics, and water migration patterns in the immediate vicinity of L-31N and the West Wellfields of Miami-Dade County leads to the conclusion that Everglades water, both directly through groundwater flow in “deep” semi-confined units of the Biscayne Aquifer and indirectly through mixing with rock-mining lakes in the area, is indeed being drawn into the operating municipal wellfields.

The conclusions that Everglades water is being pulled into municipal pumping wells and that rock mining practices in the area serve to mix groundwater vertically point to the need for further research near the West Wellfield and Everglades National Park. Perhaps a more in-depth isotopic study of the region between the rock-mining lakes and the wellfield would be useful in further evaluating groundwater flow between these locations. Also, as the pending Everglades Restoration Project seeks to alter the surface water flow pattern through the Everglades, there will most likely be changes in the delivery of water to the northeast Everglades National Park. It seems feasible that a future isotopic water tracing study could help to assess the impact of these changes over time.

References

Axum 6.0 User's Guide. Accompanying Manual to *Axum* 6.0 Software. MathSoft, Inc., Seattle.

Baertschi, P., 1976. "Absolute ^{18}O Content of Standard Mean Ocean Water." *Earth Planet Sci Lett* 31:341-344.

Bigeleisen, J., Perlman, M.L., and Prosser, H.C., 1952. "Conversion of Hydrogenic Materials to Hydrogen for Isotopic Analysis." *Analytical Chemistry*, 24(2): 1356-1357.

Bottinga, Y. and Craig H., 1969. "Oxygen Isotope Fractionation Between CO_2 and Water and the Isotopic Composition of Marine Atmosphere." *Earth Planet Sci Lett* 5:285-295.

Causaras, C.R., 1987. Geology of the surficial aquifer system, Dade County, Florida: U.S. Geological Survey Water-Resources Investigations Report 86-4126, 240 p, 3 sheets.

Clark, I. and Fritz, P., 1997. *Environemtnal Isotopes in Hydrogeology*. Lewis Press, Boca Raton.

Coplen, T.B., Wildman, J.D., and Chen, J., 1991. Imprrvements in the Gaseous Hydrogen-Water Equilibration Technique for Hydrogen Isotope Ratio Analysis. *Analytical Chemistry*, 63:910-912.

Craig, H., 1961. "Isotopic Variations in Meteroic Water." *Scienc*e, 133: 1702-1703.

Cunningham, Kevin. 1998, U.S. Geological Survey, personal communication

Epstein, S., and Mayeda, T., 1953. "Variation of O^{18} Content of Waters from Natural Sources." *Geochimica et Cosmochimica Acta*, 4:213-224.

Fish, J.E., and Stewart, M., 1991. Hydrogeology of the surficial aquifer system, Dade County, Florida: U.S. Geological Survey Water-Resources Investigations Report 90-4108, 50 p.

Garlick, G.D., 1969. The stable isotopes of oxygen. In: Wedepohl, K.H., ed. *Handbook of Geochemistry*, 8B. Springer, Berlin.

Gehre, M., Hoefling, R., Kowski, P., and Strauch, G., 1996. "Sample Preparation Device for Quantitative Hydrogen Isotope Analysis Using Chromium Metal." *Analytical Chemistry*, 68, 4414 - 4417.

Gonfiantini, R., 1986. "Environmental Isotopes in Lake Studies." In *Handbook of Environmental Isotope Geochemistry*. Elsevier, New York.

Hagemann, R., Nief, G., and Roth, E., 1970. "Absolute Isotopic Scale for Deuterium Analysis of Natural Waters. Absolute D / H Ratios for SMOW." *Tellus* 22:712-715.

Herrera, A., 2000. *The Limnology of Two Rockmining Lakes*. Master of Science Thesis. University of Miami, Coral Gables, FL. (In Preparation).

Hoefs, J., 1997. *Stable Isotope Geochemistry, Fourth Edition*. Springer-Verlag, New York.

Hoefs, J., 1987. *Stable Isotope Geochemistry, Third Edition*. Springer-Verlag, Berlin.

Ibler, G., Solo-Gabriele, H., and Sternberg, L., 1999. "A Hydrologic Analysis of the West Wellfield and Vicinity Using Stable Isotopes as Tracers." *Proceedings of the International Symposium on Isotope Techniques in Water Resources Development and Management, Vienna, Austria, May 10-14, 1999.* IAEA-SM-361, p. 152-153.

Jakli, G. and Staschewski, D., 1977. "Vapour Pressure of $H_2{}^{18}O$ ice (-50 to 0°C) and $H_2{}^{18}O$ water (0 to 170°C)." *J. Chem. Soc., Faraday Trans. 1*, 73"1505-1509.

Kakiuchi, M. and Matsuo, S., 1979. "Direct Measurements of D / H and $^{18}O / ^{16}O$ Fractionation Factors Between Vapor and Liquid Water in the Temperature Range from 10 to 40°C." *Geochem., J.*, 13:307-311.

Klein, Howard, and Sherwood, C.B., 1961. Hydrologic conditions in the vicinity of Levee 30, northern Dade County, Florida, Florida Bureau of Geology Report on Investigations No. 24, 24 p.

Krupa, Amanda. 1997. South Florida Water Management District, personal communication

Labowski, J.L., 1988. Geology, hydrology, and water monitoring program, northwest wellfield protection area. Metropolitan Dade County Department of Environmental Resources Management Technical Report 88-3, 53 p.

Majoube, M., 1971. "Fractionation of Oxygen-18 and Deuterium Between Water and Vapor Forms." *J. Chim. Phys.*, 197: 1423-1436.

Matsui, E., 1980. "A Simple Method Using a Disposable Syringe to Prepare Samples for $\delta^{18}O$ Measurements in Water Samples." *Analytica Chimica Acta*, 120: 423-425.

Maurrasse, F., 1976. Hydrogeologic assessment of the environmental impacts of quarry-pit lakes at the Maule Industries Pennsuco Site North Dade County Florida, 76 p.*Part III of:* Jackson, D.F. and Maurrasse, F. 1976, Man-Made lakes of Dade County, friends or foes? An environmental assessment. Florida International University, Miami.

Mazor, E. 1991. *Applied Chemical and Isotopic Groundwater Hydrology*. Halsted Press, New York.

Merritt, M.L., 1995. Simulation of the water-table altitude in the Biscayne aquifer, southern Dade County, Florida, water years 1945-89: U.S. Geological Survey Open-File Report 95-337, 88 p.

Murphy, Bill 1997. Kendall Properties, personal communication

Nemeth, M.., 2000. *Use of the Reach Transmissivity Leakage Relationship to Quantify the Exchange Between Groundwater and Surface Water.* Doctor of Philosophy Dissertation. University of Miami, Coral Gables, FL. (Pending Publication).

Nemeth, M.S., Wilcox, W.M., and Solo-Gabriele, H.M., 2000. Methods for quantifying ground-water seepage beneath Levee 31N, Miami-Dade County, Florida: U.S. Geological Survey Water-Resources Investigations Report (Under Review).

Oxtoby, D., Nactrieb, N., Freeman, W., 1990. *Chemistry: Science of Change.* Saunders College Publishing, Philadelphia.

Randazzo, Anthony F. and Douglas S. Jones, eds., 2000. *The Geology of Florida.* University Press of Florida, Gainesville.

Schroeder, M.C., Klein, H., and Hoy, N.D., 1958. Biscayne Aquifer of Dade and Broward Counties, Florida: Florida Geological Survey Report of Investigations no 17, 56 p.

Sokal, R. and James, F., 1995. *Biometry: The Principles and Practices of Statistics in Biological Research, Third Edition*. W.H. Freeman and Co., New York.

Solo-Gabriele, H.M., 1998. *Sources of Water to the West Wellfield.* Interim Technical Report for Isotope Study, Phase I. University of Miami, Coral Gables, FL. Submitted to the South Florida Water Management District, West Palm Beach, FL.

Solo-Gabriele, H.M., and Herrera, A., 2000. *An Isotopic Study of Two Rock Mining Lakes*. Interim Technical Report for Isotope Study, Phase I. University of Miami, Coral Gables, FL. Submitted to Kendall Properties and Associates, Lauderhill, FL.

Solo-Gabriele, H.M., and Sternberg, L., 1998. "Tracers of Everglades Waters." *WEFTEC'98, Proceedings of the Water Environment Federation 71th Annual Conference & Exposition, Orlando, FL.* Volume 4: 323-333.

Solo-Gabriele, H.M., and Wilcox, W.M.., 2000. *An Isotopic Study of Northeast Everglades National Park and Adjacent Urban Areas*. Third Interim Technical Report for Isotope Study, Phase I. University of Miami, Coral Gables, FL. Prepared for Everglades National Park, FL.

Sonenshein R., 2000. Methods to quantifying seepage beneath Levee 30, Miami-Dade County, Florida: U.S. Geological Survey Water-Resources Investigations Report (Under Review).

Sternberg, Leonel. 1999. University of Miami, personal communication

Swain, E.D., Howie, B. amd Dixon, J., 1996. Description and field analysis of a coupled ground-water / surface-water flow model (MODFLOW / BRANCH) with modifications for structures and wetlands in southern Dade County, Florida. U.S. Geological Survey Water-Resources Investigation Report 96-41118, 67 p.

Switanek, M., 1997, Ongoing investigation by the South Florida Water Management District in the Pennsuco Region of the Dade Lakebelt rock mining area, dade County, Florida.

U.S. Army Corps of Engineers, 1951. Agricultural and conservation areas, geology and soils: Partial Definite Project Report, Central and Southern Florida Project, part 1, supplement 1, Mimeograph Rept., December 6.

U.S. Army Corps of Engineers, 1952. Test levee investigations: Partial Definite Project Report, Central and Southern Florida Project, part 1, supplement 5, Mimeograph Report, March 28.

U.S. Army Corps of Engineers, 1953. Agricultural and conservation areas, design memorandum, permeability investigation by well-pumping tests: Partial Definite Project Report, Central and Southern Florida Project, part 1, supplement 7, Mimeograph Report, February 16.

U.S. Army Corps of Engineers, 1954. Design memorandum, Hydrology and hydraulic design canals in Greater Miami area; Partial Definite Project Report, Central and Southern Florida Project, part 5, supplement 12, Mimeograph Report, March 23.

U.S. Army Corps of Engineers, 1976. Coastal areas south of St. Lucie Canal Supplement 56--Detail Design Memorandum Levee 30, Borrow Canal Enlargement, and Control Structures 32 A and 337: Central and Southern Florida Project, part 5, supplement 56, March 18.

Way, K., Fano, L., Scott, M.R., and Thew, K., 1950. “Nuclear Data. A Collection of Experimental Values of Halflifes, Radiation Energies, Relative Isotope Abundances, Nuclear Moments and Cross-sections.” *National Bureau of Standards U.S. Circ. 499.*

Appendix A

Isotope Calculations and Data

A.1 Calculation of dD relative to VSMOW

In order to calculate the δD of a sample relative to VSMOW ($\delta_{S,VSMOW}$), several steps are necessary. A calibration is performed once a year in order to reference the lab standard (LS) to the VSMOW standard. The equations used are the following:

$$\delta_{LS,gas} = (R_{LS} / R_{gas} - 1)10^3 \qquad \text{(Equation A.1.1)}$$

$$\delta_{VSMOW,\,gas} = (R_{VSMOW} / R_{gas} - 1)10^3 \qquad \text{(Equation A.1.2)}$$

The ratio which is desired is the ratio of the lab standard to the VSMOW standard; in order to obtain this ratio, equations A.1.1 and A.1.2 are rearranged to solve for the R terms and then equation A.1.1 is divided by equation A.1.2. This results in the following equation:

$$\delta_{LS,VSMOW} = [(\delta_{LS,gas}\, 10^{-3} + 1) / (\delta_{VSMOW,\,gas}\, 10^{-3} + 1) - 1]10^3$$

(Equation A.1.3)

This calibration allows the desired delta value of the sample (S) relative to VSMOW ($\delta_{S,VSMOW}$) to be calculated. In terms of the ratios, the equation used is:

$$\delta_{S,VSMOW} = (R_{LS} / R_{gas} - 1)10^3 / [(R_{LS} / R_{gas} - 1)10^3 / (R_{LS} / R_{VSMOW} - 1)10^3]$$

(Equation A.1.4)

Replacing the ratio notation with the delta notation gives the following equation:

$$\delta_{S,VSMOW} = [(\delta_{S,gas}\ 10^{-3} + 1) / [(\delta_{LS,gas}\ 10^{-3} + 1) / (\delta_{LS,VSMOW}\ 10^{-3} + 1)] - 1]10^{3}$$

(Equation A.1.5)

The $\delta_{S,gas}$ term is the mass spectrometer output value of the sample being tested and the $\delta_{LS,gas}$ term is the lab standard run per batch of samples run on the mass spectrometer. The $\delta_{LS,VSMOW}$ term is the calibration performed once a year, found to be –4.796526. As all terms on the right of equation A.1.5 are now available, it is possible to calculate $\delta_{S,VSMOW}$.

A.2 Calculation of $d^{18}O$ relative to VSMOW

The calculation of $\delta^{18}O$ is very similar to that of δD, but is complicated by the equilibration of the CO_2 gas with the water. Due to fractionation effects, a conversion must be made from CO_2 to water. The first step is to determine the ratio value (R) of the carbon dioxide tank to be used. For his study, the value was determined to be 40.78775. The next step is to determine the value of the lab standard relative to the VSMOW standard. As is the case with deuterium, this is done once a year only. Since the sample water of interest is in equilibrium with carbon dioxide, calculations can be done in either water or carbon dioxide. The reason why it does not matter whether the calculations are being performed as carbon dioxide or water is shown in the following proof:

It is necessary to show that:

$$[(R_{LS} / R_{gas}) / (R_{VSMOW} / R_{gas})]^{CO2} = [(R_{LS} / R_{gas}) / (R_{VSMOW} / R_{gas})]^{water}$$

(Equation A.2.1)

The fractionation factor for water in equilibrium with carbon dioxide is:

$$R_{CO2} / R_{H2O} = 1.0412 \qquad \text{(Equation A.2.2)}$$

It is therefore possible to replace the terms on the right-hand side of equation A.2.1 with the delta notations and obtain the following:

$$[(\delta^{CO2}{}_{LS} - 41.2)10^{-3} / 1.0412 + 1] / [(\delta^{CO2}{}_{VSMOW} - 41.2)10^{-3} / 1.0412 + 1$$

(Equation A.2.3)

This term is manipulated to give the following term:

$$[(R^{CO2}{}_{ST} / 1.0412) / R_{gas}] / [(R^{CO2}{}_{VSMOW} / 1.0412) / R_{gas}] \qquad \text{(Equation A.2.4)}$$

The fractionation factors cancel out, leaving the same quantity as the left-hand side of equation A.2.1.

Since it does not matter in which substance delta calculations are performed, carbon dioxide will be used for the following example. The equation needed to calculate the δ of sample water with respect to VSMOW is:

$$\delta^{water}{}_{LS, VMSOW} = [(\delta^{CO2}{}_{LS, gas} + 1) / (40.78775*10^{-3} + 1) - 1]10^{3} \qquad \text{(Equation A.2.5)}$$

In order to determine the delta value of the standard relative to VMSOW in terms of carbon dioxide, this equation is multiplied by 1.0412 and then 41.2 is added.

$$\delta^{CO2}{}_{LS, VMSOW} = 1.0412(\delta^{water}{}_{LS, VMSOW}) + 41.2 \qquad \text{(Equation A.2.6)}$$

The next step is to determine the value of the sample relative to VSMOW in terms of carbon dioxide. The following equation, presented in delta notation, is used:

$$\delta^{CO2}{}_{S,\,VMSOW} = [(\delta^{CO2}{}_{S,\,gas}\,10^{-3}+1)(\delta^{CO2}{}_{LS,\,VSMOW}\,10^{-3}+1) / (\delta^{CO2}{}_{LS,\,gas}\,10^{-3}+1) - 1]10^{3}$$

(Equation A.2.7.)

In this equation, the $\delta^{CO2}{}_{S,\,gas}$ and $\delta^{CO2}{}_{LS,\,gas}$ terms are both determined with each batch by using the mass spectrometer output to calculate the δ^{CO2} values as outline in the deuterium section. The remaining term in the equation is the calibration performed once a year as outlined in the deuterium section.

As it is now possible to calculate $\delta^{CO2}{}_{S,\,VMSOW}$, the final step in the calculation is the conversion from carbon dioxide to water. This is accomplished through the following equation:

$$\delta^{H2O}{}_{S,\,VMSOW} = (\delta^{CO2}{}_{S,\,VMSOW} - 41.2) / 1.0412 + n_c / n_w(\delta^{CO2}{}_{S,\,VMSOW} - \delta^{CO2}{}_{Tank})$$

(Equation A.2.8)

where n_c and n_w are the mole fractions for carbon dioxide and water respectively and $\delta^{CO2}{}_{Tank}$ is the delta value for the carbon dioxide tank used in the sample preparation. The value for n_c is 1.63408×10^{-4} and for n_w is 0.055444. This final conversion gives the desired $\delta^{H2O}{}_{S,\,VMSOW}$ term.

A.3 Complete Isotope Data Tables

Complete data as analyzed by Wilcox, Ibler, Herrera, Solo-Gabriele, Sternberg and Ewe. For Site Information, please refer to Table 3.2.1 in main text.

Table A.3.1 – 1996 Oxygen-18 Data

Site	1/31/ 1996	3/26/ 1996	4/19/ 1996	6/24/ 1996	8/28/ 1996	10/1/ 1996
G3551	1.96	1.73		1.76	1.04	1.55
G3552	1.67	0.92		0.87	1.52	0.70
G3553	1.08	0.70		0.67	1.82	0.41
G3554				0.55	0.94	0.29
G3555		0.66		0.25	-0.05	-0.09
WELL 29/30		1.27			2.21	1.34
2M3	1.43	1.61		0.98		
3M4	1.78	1.78	2.14	0.44	1.39	1.67
4M5	1.38	1.66		0.59		
G3575	2.10	2.27		-0.02	1.71	1.52
G3577			2.43			

Table A.3.2 – 1996 Deuterium Data

Site	1/31/ 1996	3/26/ 1996	4/19/ 1996	6/24/ 1996	8/28/ 1996	10/1/ 1996
G3551	4.70	15.42		11.64	7.85	11.06
G3552	-1.00	3.16		7.00	4.63	4.96
G3553	3.70	-2.01		1.69	6.50	5.97
G3554				4.39	3.14	-1.81
G3555		9.25		2.08	0.73	0.99
WELL 29/30		11.26			11.74	10.22
2M3	10.90	4.71		6.45		
3M4	2.20	14.01	14.46	1.97	7.99	11.96
4M5	1.80	15.71		5.56		
G3575	5.70	7.92		-2.16	7.21	10.68
G3577			16.54			

Table A.3.3 – 1997 Oxygen-18 Data

Site	2/6/ 1997	3/4/ 1997	4/8/ 1997	5/5/ 1997	6/4/ 1997	7/3/ 1997	7/30/ 1997	9/10/ 1997	10/9/ 1997	11/6/ 1997	12/3/ 1997
G3551	1.02	1.04	1.04	1.54	1.22	1.04	-0.13	0.88	0.55	0.39	0.65
G3552	0.75	1.04	1.13	1.18	1.14	0.96	1.23	1.14	2.24	0.40	0.44
G3553	0.61	0.49	0.71	0.72	0.75	0.36	0.98	0.75	0.42	0.31	0.43
G3554	0.28	0.07	0.34	0.78	0.31	0.02	0.76	0.73	0.26	0.55	0.49
G3555	-0.43	-0.51	-0.57	-0.29	-0.45	-0.67	-0.02	-0.62	-2.11	-1.70	-1.09
WELL 29/30	1.02	1.25	1.07	1.28	1.50	1.40	1.52	1.41	1.40	1.15	0.86
G618				2.12	2.72	2.39	2.55	1.68	2.07	1.63	1.32
2M3			1.41	1.13	1.79	-1.82	0.39	0.87	0.38	0.88	1.31
3M4	0.91	0.87	1.36	1.03	1.81	-0.67	0.78	0.98	0.23	1.08	0.69
4M5			1.18	1.42	1.75	-0.03	0.36	1.00	0.56	1.01	0.86
G3439				0.56	0.42	-2.25	-1.84	-0.13	-0.19	0.06	0.33
G3575	0.87	1.00	0.66	0.82	0.87	-3.46	0.49	1.74	1.28	0.42	0.99
G3577							-1.07	1.36	-0.57	0.22	-0.85
G3663											-0.03
G3578							2.05	1.87	2.08	1.71	0.57
G3664											1.66
RAIN-WW								-4.70	-1.44	-0.94	-2.98
RL1											1.3

Table A.3.4 – 1997 Deuterium Data

Site	2/6/ 1997	3/4/ 1997	4/8/ 1997	5/5/ 1997	6/4/ 1997	7/3/ 1997	7/30/ 1997	9/10/ 1997	10/9/ 1997	11/6/ 1997	12/3/ 1997
G3551	14.02	12.65	15.33	7.73	8.65	8.06	1.03	-0.54	-0.63	1.54	1.67
G3552	13.39	8.95	12.02	8.02	6.74	9.42	8.20	1.16	0.06	-1.24	-0.07
G3553	9.22	4.26	9.60	1.81	2.88	3.93	6.10	1.18	3.81	9.40	1.40
G3554	6.18	7.03	4.73	2.31	2.79	1.63	8.43	1.44	-0.29	1.17	-1.96
G3555	1.36	3.78	2.50	-1.81	-2.80	-5.34	9.18	-3.68	-10.50	-7.40	-9.94
WELL 29/30	9.03	10.54	14.06	6.52	5.40	5.80	5.12	0.94	0.80	1.23	1.25
G618				13.90	15.07	15.49	17.80	7.39	14.60	9.54	4.00
2M3			8.77	11.32	10.66	-9.30	3.97	6.47	0.42	4.86	4.48
3M4	15.66	16.46	15.80	6.85	11.23	-10.97	5.16	1.60	0.16	9.02	0.05
4M5			9.23	11.40	11.42	2.60	4.61	6.90	1.32	7.44	2.34
G3439				3.38	1.02	-23.00	-11.79	-10.97	-12.26	-2.38	-7.62
G3575	15.09	10.57	13.58	5.97	4.89	-28.00	2.55	2.40	-5.77	4.98	5.71
G3577							-8.34	4.06	-3.37	-1.50	-6.63
G3663											-4.33
G3578							16.65	6.05	8.44	16.88	-1.02
G3664											3.82
RAIN-WW								-28.43	7.22	8.78	-17.11
RL1											4.14

Table A.3.5 – 1998 Oxygen-18 Data

Site	1/6/ 1998	2/10/1 998	3/3/ 1998	4/7/ 1998	5/5/ 1998	6/1/ 1998	7/6/ 1998	8/3/ 1998	9/1/ 1998	9/24/ 1998	10/6/ 1998	11/10/ 1998	12/10/ 1998
G3551	0.64	1.37	0.24	0.83	1.07	1.44	1.64	1.78	2.70		1.83	1.31	0.88
G3552	0.50	1.33	0.86	-0.06	0.21	1.22	1.02	1.27	0.72		1.08	1.55	1.39
G3661	1.14	1.03	0.68	0.99	1.53	1.38	1.27	0.93	1.65		1.23	1.56	1.32
G3553	0.76	1.11	0.81	0.38	0.70	1.07	1.30	0.78	0.61		1.09	1.18	1.27
G3554	0.72	0.65	0.77	0.29	0.64	1.02	0.50	0.41	0.41		0.61	1.03	0.57
G3662	1.91	1.15	0.89	1.52	1.20	0.81	0.98	0.66	0.95		1.04	1.38	1.30
G3555	-1.20	-0.68	-0.61	-0.31	0.00	0.41	0.30	-0.17	-0.13		-0.31	0.10	-0.84
WELL 29/30	2.06	1.27	0.85	1.59	1.14	1.43	1.24	0.98	0.78		1.63	1.56	1.61
G618	1.55	1.17	1.47	1.52	2.29	3.43	3.04	2.42	2.74		2.43	2.00	2.16
2M3	0.81	1.15	0.69	1.26	2.05	2.97	1.84	1.83	1.56		0.08	0.83	1.18
3M4	0.68	0.99	0.68	0.97	2.03	2.53	1.60	2.09	2.02		0.37	1.22	1.28
4M5	0.97	0.94	0.58	1.08	1.84	2.73	1.43	1.74	1.77		0.82	0.89	1.16
G3439	0.37	0.54	-0.96		0.32	0.44	0.01		1.27		-1.05	0.02	0.34
G3575	0.71	0.75	0.65	1.81	3.08	4.17	3.28	1.69	1.78		0.16	0.57	1.61
G3660						0.69	1.40	0.97	1.61		1.86	1.59	1.44
G3577	0.36	1.36	1.40	1.49	3.39	3.77	3.55	1.86	2.04		0.53	0.86	1.09
G3663	0.06	0.84	0.99	0.13	0.28	0.21	1.25	0.31	0.22		-0.07	0.22	0.25
G3578	1.82	1.81	1.13	1.57	2.74	2.91	2.25	1.91	1.88		1.38	2.07	2.09
G3664	1.87	1.71	1.86	1.84	1.83	1.84	2.11	1.35	2.09		1.94	1.92	1.95
RAIN-WW	-4.41	-2.76	-0.29	-2.92	-1.71	-2.05	-1.77	-2.30	-1.38	-4.54	-2.99	-2.10	-0.56
RAIN-G618						-2.39	-1.53	-3.43	-1.30	-3.90	-3.72	-2.99	-1.27
S3575									2.22		0.96	0.59	1.43
S3577							4.08	4.11	2.77		0.67	-0.18	1.52
S3578							2.66	2.72	2.42		0.77	0.35	1.25
RL1	1.22	1.05	0.85	1.01	1.4	1.36	1.93	1.53	1.56		2.06	2.02	1.95
RL3	1.06	1.25	1.49	1.08	1.3	1.49	1.6	1.66	1.22		1.99	1.65	1.47

Table A.3.6 – 1998 Deuterium Data

Site	1/6/ 1998	2/10/1 998	3/3/ 1998	4/7/ 1998	5/5/ 1998	6/1/ 1998	7/6/ 1998	8/3/ 1998	9/1/ 1998	9/24/ 1998	10/6/ 1998	11/10/ 1998	12/10/ 1998
G3551	6.42	0.36	-0.43	2.67	4.65	5.35	11.41	15.94	13.22		19.38	6.57	4.14
G3552	12.62	1.60	1.25	-0.99	4.68	3.08	3.46	7.88	-2.17		7.46	10.11	10.15
G3661	5.26	-2.45	-4.84	0.36	5.98	1.69	1.61	6.57	5.37		9.72	10.78	14.42
G3553	8.86	0.48	-0.34	-1.49	1.49	0.22	4.36	8.60	-0.83		7.19	8.12	5.21
G3554	1.40	0.58	2.14	0.17	-1.49	2.06	2.91	3.70	1.34		2.73	4.91	5.20
G3662	7.53	9.67	-0.66	-2.61	3.06	0.74	3.21	9.98	1.33		9.85	14.91	14.55
G3555	-6.41	-9.35	-5.13	-7.33	3.81	-5.80	-3.96	2.12	-8.51		8.08	-1.08	-0.29
WELL 29/30	5.91	1.71	3.63	-1.40	4.99	2.88	7.03	4.77	5.52		19.61	14.11	13.67
G618	13.20	3.02	5.83	8.21	4.84	13.94	13.61	21.00	21.38		20.65	19.27	16.85
2M3	4.46	0.37	1.83	5.59	9.09	11.79	13.70	10.40	8.31		-2.24	6.15	8.63
3M4	12.61	-1.34	2.86	4.63	7.62	12.89	11.90	13.26	11.36		8.82	8.89	4.66
4M5	2.63	0.15	3.37	4.62	0.57	10.73	8.41	6.08	7.25		-1.95	4.27	6.60
G3439	2.99	-4.54	-2.14		13.61	-1.51	1.40		6.82		-2.59	-0.19	-1.15
G3575	4.47	1.69	5.94	-3.53	14.96	14.73	12.97	9.80	10.46		-0.34	5.13	12.51
G3660						2.75	10.66	6.36	6.46		10.26	7.23	4.95
G3577	4.76	5.70	9.46	9.61	6.25	17.39	18.95	9.07	11.84		-1.05	5.77	11.88
G3663	4.65	-0.35	-2.51	0.70	10.91	-1.25	0.74	2.43	2.90		2.19	0.82	5.23
G3578	7.63	3.57	6.71	8.44	5.36	11.74	12.61	15.19	10.23		15.14	17.21	13.50
G3664	20.77	2.08	5.19	8.09	6.98	7.94	12.16	9.24	5.54		15.65	7.81	8.37
RAIN-WW	-20.79	-9.54	4.09	-11.69	0.78	-16.35	-3.97	-14.70	-2.78	-32.93	-15.31	-13.05	-5.65
RAIN-G618						-13.71	0.52	-17.20	-4.87	-18.56	-26.86	-9.91	4.89
S3575									13.57		9.21	2.65	11.43
S3577							16.03	16.96	19.88		1.83	-0.24	14.22
S3578							9.82	7.10	13.30		8.39	5.09	14.97
RL1	4.05	5.35	5.95	6.16	8.68	6.64	8.48	10.96	9.51		9.44	6.25	9.17
RL3	3.46	3.27	3.99	3.72	5.04	6.24	7.58	6.70	8.75		7.68	6.8	8.54

A.4 Quality Assurance / Quality Control (QAQC)

As this thesis is the continuation of previous research, results of the QAQC have been previously reported in "An Isotopic Study of Two Rock Mining Lakes" (Solo-Gabriele and Herrera, 2000). Included below is an excerpt from this report. Tables A.4.1 through A.4.4 report the results of the QAQC as analyzed by Walter Wilcox and Albert Herrera.

> "An extensive effort was placed in quality assurance and quality control. This effort involved internal laboratory calibration of standards and a split sampling exercise with the U.S. Geological Survey (USGS) Isotope Laboratory located in Reston, Virginia. The sample splits submitted to the USGS laboratory were analyzed for deuterium using a hydrogen equilibration technique (Coplen *et al.* 1991) and the oxygen ratios were measured using the CO_2 equilibration method of Epstein and Mayeda, 1953. Results from both the University of Miami and USGS laboratories are reported relative to Vienna Standard Mean Ocean Water (VSMOW).
>
> The internal calibration involved simultaneous analyses of the lab standard (LS) and VSMOW purchased from the National Institute of Standards and Technology (NIST). Results from the calibration are provided in table *A.4.1* for oxygen-18 and table *A.4.2* for deuterium. The $\delta^{18}O$ value of the lab standard was determined as -0.9‰ and for δD the value was determined as -4.8 ‰. The split samples were labeled UM1, UM2, UM3, and UM4. UM1 corresponded to an isotopically light sample of rain water collected on September 29th, 1997 at site G3553. UM2 and UM3 were both collected from RL1 on June 1st, 1998. UM2 was collected from the water's surface and UM3 was collected from a depth of 30 feet. UM4 corresponds to an isotopically heavy sample collected from a groundwater well (G-618) located within the Everglades on July 3rd, 1997. Results from the split sampling effort (tables *A.4.3* and *A.4.4*) indicate that the standard deviation of the oxygen analysis was 0.19 ‰ and the 95% confidence limits were ± 0.24 ‰. For hydrogen analysis the standard deviation was 1.64 ‰ and the 95% confidence limits were ± 2.0 ‰. Overall the split sampling exercise was considered a success indicating that both laboratories provided results that were statistically equivalent (at 95% confidence). On average the University of Miami laboratory was heavier in oxygen-18 by 0.07 ‰ and lighter in deuterium by 0.79 ‰. Both differences are considered insignificant relative to the precision of the analysis."

Table A.4.1 Calibration of Lab Standard for Oxygen-18 Relative to VSMOW

Sample ID	Analysis Date	Mass Spec. Precision	Sample Values Relative to CO_2, $^{Sample}R_{ref\ gas}$	Sample Values Relative to H_2O, $^{Sample}R_{ref\ gas}$	Average for VSMOW $^{Sample}R_{ref\ gas}$	Lab Standard Relative to VSMOW, ‰		
						Individual Analysis	Average	Std Dev.
VSMOW	3/11/99	0.064	40.7570	-0.3869	-0.3573			
		0.010	40.7370	-0.4062				
		0.029	40.8550	-0.2925				
		0.016	40.8020	-0.3435				
LS	3/11/99	0.086	39.8940	-1.2183		-0.8613	-0.9013	0.177
		0.089	40.0810	-1.0381		-0.6811		
		0.014	39.6440	-1.4591		-1.1023		
		0.046	39.7910	-1.3175		-0.9606		

Table A.4.2 Calibration of Lab Standard for Deuterium Relative to VSMOW

Sample	Analysis Date	Mass Spec. Precision	Mass Spec Value $^{Sample}R_{ref\ gas}$		Lab Standard Relative to VSMOW, ‰		
				Average for VSMOW	Individual Analysis	Average	Std Dev.
VSMOW	3/24/99	0.272	468.492	466.756			
		0.270	467.580				
		0.226	467.247				
		0.492	463.705				
LS	3/24/99	0.141	459.007		-5.283	-4.797	0.892
		0.196	458.925		-5.339		
		0.383	461.230		-3.767		

Table A.4.3 Oxygen-18 Results from the Split Sampling Exercise

Sample ID	Analysis Date	Sample Values Relative to CO_2, $^{Sample}R_{ref\ gas}$			Sample Values Relative to H_2O, $^{Sample}R_{ref\ gas}$		Sample Values Relative to VSMOW, ‰			USGS Laboratory Results ‰ VSMOW			Difference (U.Miami-USGS) ‰
		Individual Analysis	Average	Std Dev.	Individual Analysis	Average	Individual Analysis	Average	Std Dev.	Individual Analysis	Average	Std Dev.	
LS		39.3890	39.4673	0.068	-1.7048	-1.6293							
		39.5150			-1.5834								
		39.4980			-1.5998								
UM1	1/15/99	35.5400	35.4118	0.104	-5.4129		-4.6876	-4.7046	0.259	-4.91	-4.89	0.032	0.19
		35.4130			5.5352		-4.8100			-4.84			
		35.2500			-5.6922		-4.9672			-4.91			
		35.9650			-5.0034		-4.2779			-4.9			
		35.4440			-5.5053		-4.7802						
UM2	1/15/99	41.8550	41.7660	0.138	0.6709		1.4006	1.4041	0.240	1.25	1.26	0.034	0.14
		41.6750			0.4975		1.2271			1.26			
		41.5940			0.4194		1.1490			1.31			
		42.2290			1.0312		1.7612			1.23			
		41.9400			0.7528		1.4825						
UM3	1/15/99	41.2970	41.2968	0.067	0.1333		0.8626	0.9203	0.145	0.97	1.00	0.032	-0.08
		41.2230			0.0620		0.7913			1.04			
		41.2640			0.1015		0.8308			1.01			
		41.5970			0.4223		1.1519			0.98			
		41.4030			0.2354		0.9648						
UM4	1/15/99	43.0650	42.8868	0.111	1.8366		2.5671	2.3649	0.127	2.34	2.34	0.005	0.02
		42.7600			1.5428		2.2731			2.34			
		42.8640			1.6429		2.3733			2.34			
		42.7290			1.5129		2.2432			2.35			
		42.8580			1.6372		2.3676						

Table A.4.4 Deuterium Results from the Split Sampling Exercise

Sample ID	Analysis Date*	Mass Spec Value $^{Sample}R_{ref\ gas}$		Sample Values Relative to VSMOW, ‰			USGS Laboratory Results ‰ VSMOW			Difference (U.Miami-USGS) ‰
		Individual Values	Ave. for Standards	Individual Values	Ave.	Std Dev.	Individual Values	Ave.	Std Dev.	
LS1	1/7/99	469.751	469.791							
		470.117								
		469.505								
LS1	1/10/99	468.725	469.892							
		469.838								
		471.112								
LS2	3/18/98	459.5	458.775							
		457.2								
		458.9								
		459.5								
LS2	7/9/98	472.611	473.444							
		474.277								
UM1	1/7/99 (LS1)	439.939		-25.009	-27.769	1.92	-27.83	-28.208	0.94	0.439
	1/10/99 (LS1)	435.304		-28.214			-29.62			
	1/10/99 (LS1)	433.490		-29.443			-27.69			
	1/10/99 (LS1)	435.018		-28.408			-27.69			
UM2	1/10/99 (LS1)	488.490		7.796	6.934	0.76	9.72	8.985	0.65	-2.051
	1/10/99 (LS1)	486.334		6.336			9.09			
	1/10/99 (LS1)	486.828		6.670			8.98			
							8.15			
UM3	1/7/99(LS1)	486.822		6.735	6.111	1.59	6.94	7.235	0.35	-1.124
	1/7/99(LS1)	489.779		8.737			7.41			
	1/10/99 (LS1)	482.869		3.990			6.94			
	1/10/99 (LS1)	486.231		6.266			7.65			
	1/10/99 (LS1)	485.215		5.578						
	1/10/99 (LS1)	484.892		5.360						
UM4	1/7/99(LS1)	500.094		15.722	16.778	2.12	18.64	17.190	1.14	-0.412
	1/7/99 (LS1)	499.604		15.390			17.27			
	3/18/98 (LS2)	489.000		19.222			15.88			
							16.97			

* Note LS1 del value relative to VSMOW = -4.797 ‰

** Note LS2 del value relative to VSMOW = -1.467 ‰

A.5 Sampling Date Site Information

The subsequent pages provide data organized according to sampling date. For each sampling date, a cross section of the study site corresponding to Figure A.5.1 provides values for collected oxygen-18 and deuterium delta values. Also given are values for rainfall and flow through gate S333 for various time increments preceding sampling as well as the groundwater stage across the study site at the time of sampling. Note: bottom of lakes in figures do not reflect lake bathymetry.

Figure A.5.1 Cross Section of Study Area Including Isotope Monitoring Wells

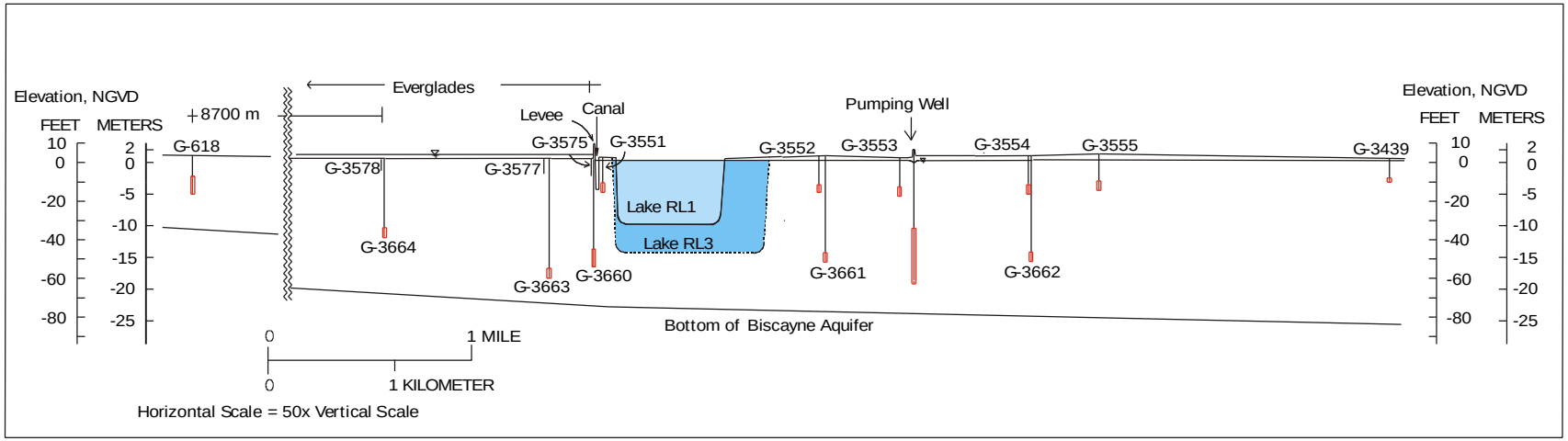

Sampling Date - January 31 , 1996

Ambient Rainfall (in)
- Previous Day - 0.02
- Previous 5 Days - 0.33
- Previous 30 Days - 1.80

Average Flow Through Gate S333 (cfs)
- Previous Day - 273.00
- Previous 5 Days - 87.16
- Previous 30 Days - 14.53

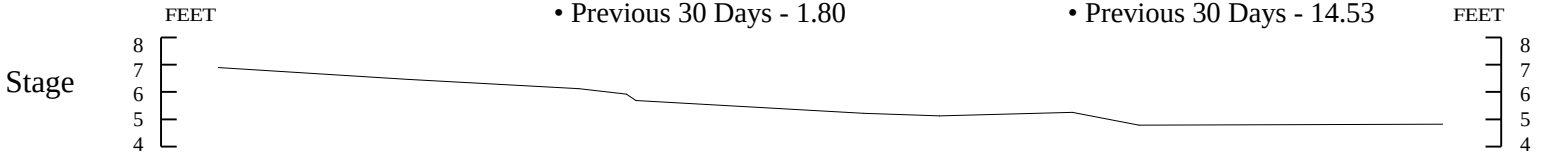

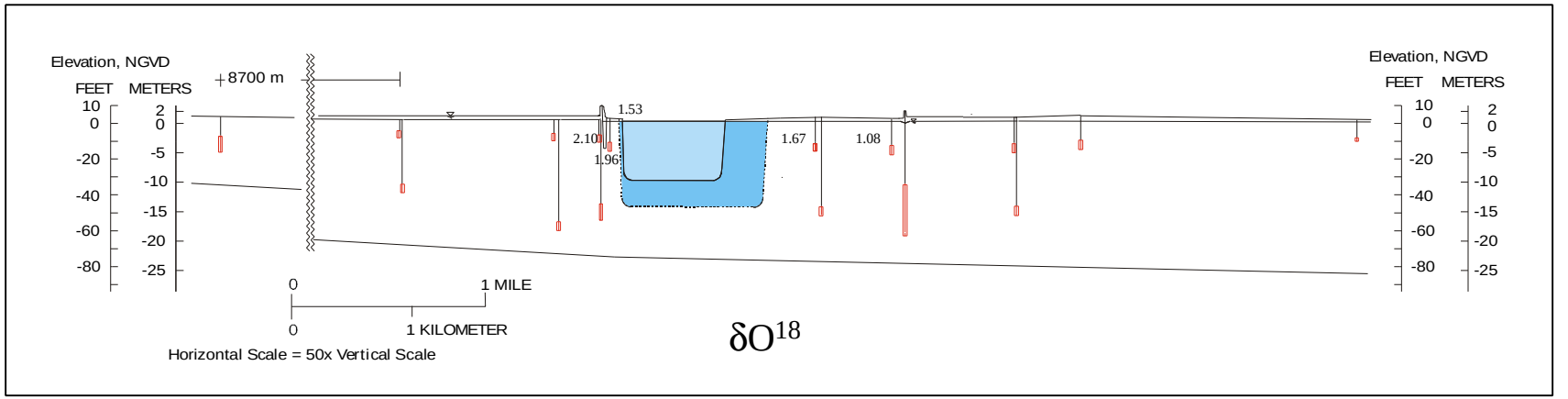

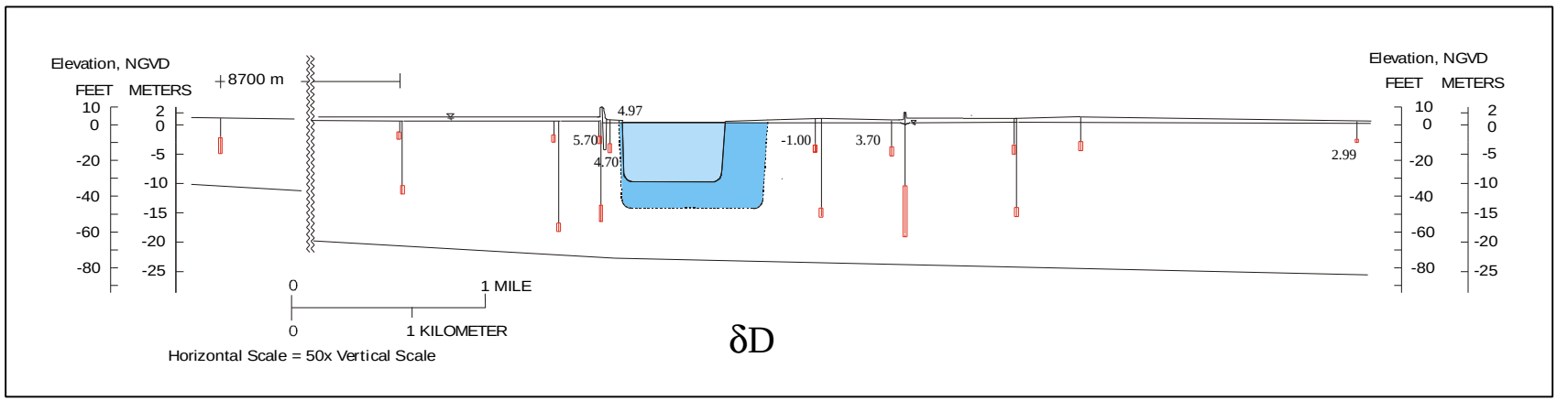

Sampling Date - March 26, 1996

Ambient Rainfall (in)
- Previous Day - 0.00
- Previous 5 Days - 0.00
- Previous 30 Days - 0.84

Average Flow Through Gate S333 (cfs)
- Previous Day - 379.00
- Previous 5 Days - 382.20
- Previous 30 Days - 304.57

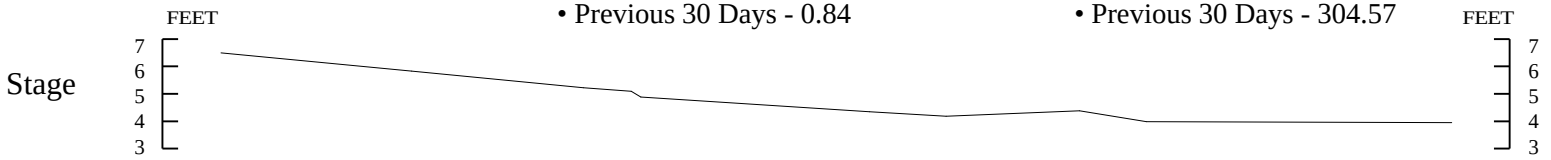

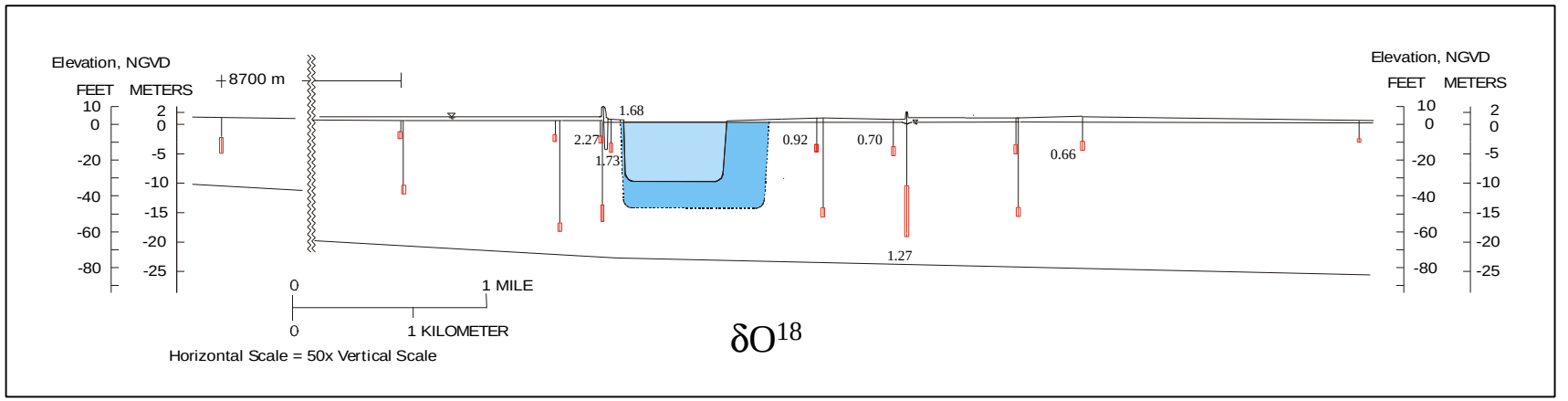

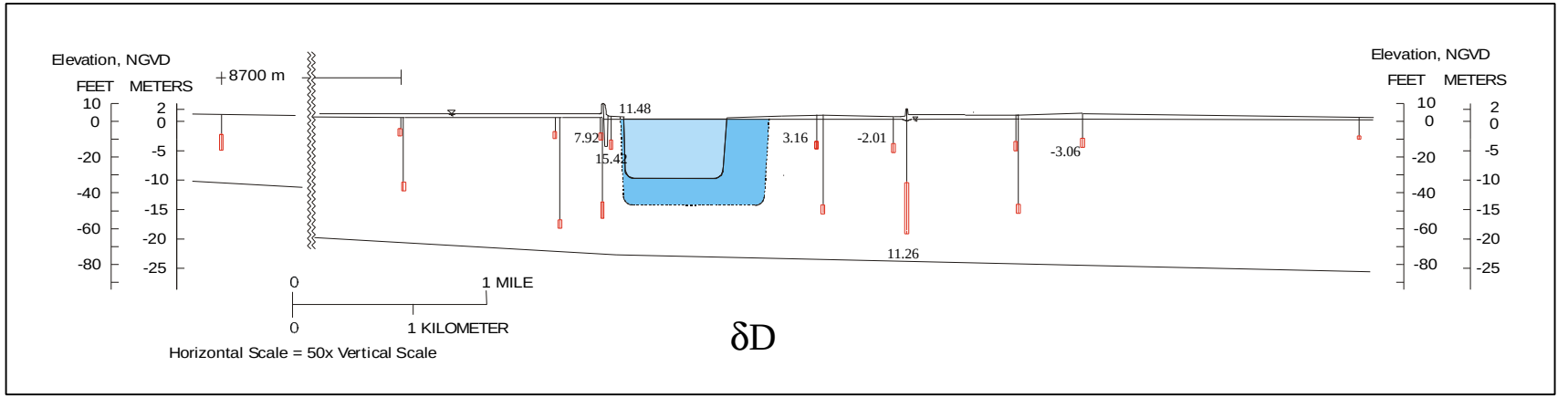

Sampling Date - June 24, 1996

Ambient Rainfall (in)
- Previous Day - 0.00
- Previous 5 Days - 0.05
- Previous 30 Days - 4.51

Average Flow Through Gate S333 (cfs)
- Previous Day - 0.00
- Previous 5 Days - 207.00
- Previous 30 Days - 299.90

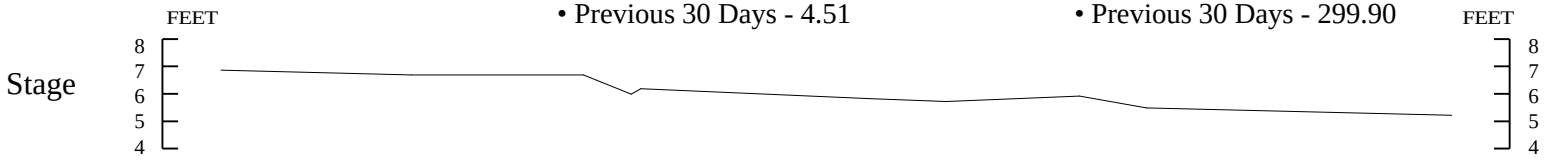

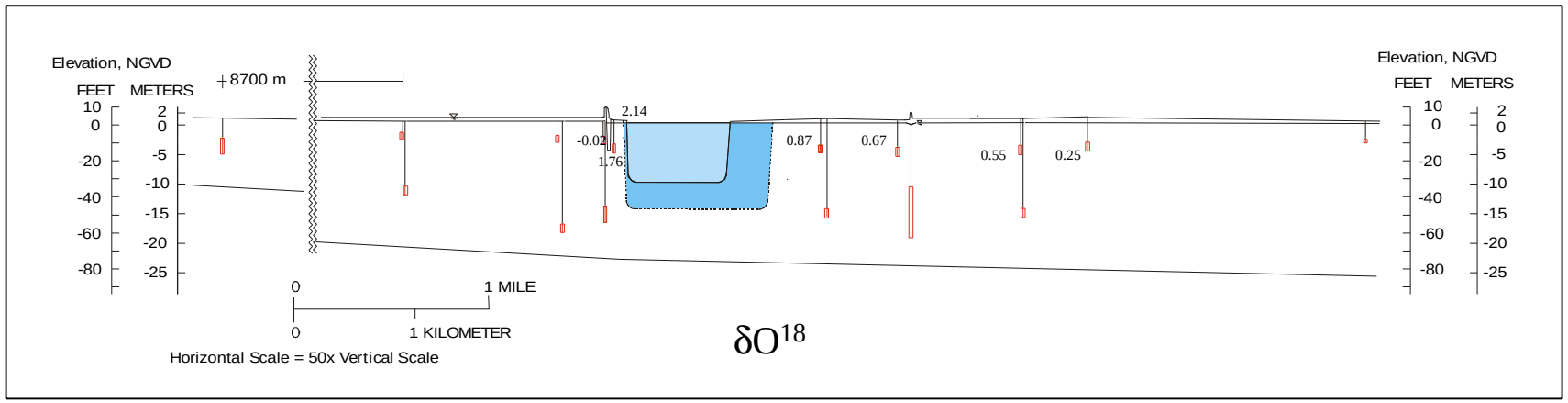

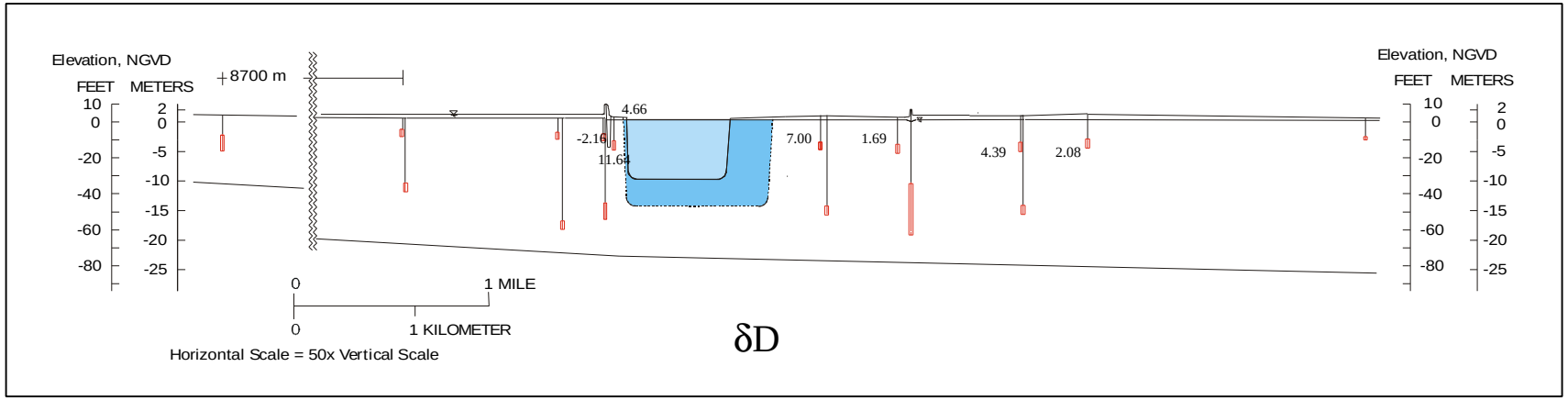

Sampling Date - August 28, 1996

Ambient Rainfall (in)
- Previous Day - 0.05
- Previous 5 Days - 1.11
- Previous 30 Days - 8.46

Average Flow Through Gate S333 (cfs)
- Previous Day - 240.00
- Previous 5 Days - 297.80
- Previous 30 Days - 377.63

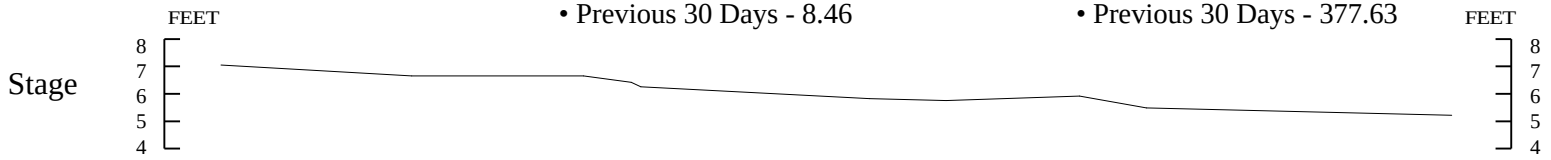

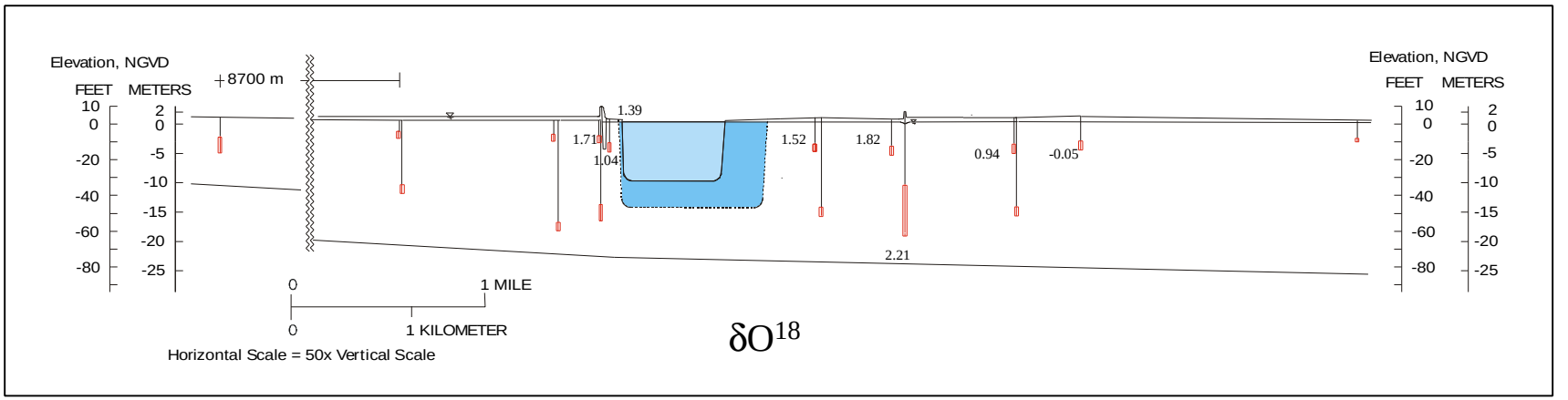

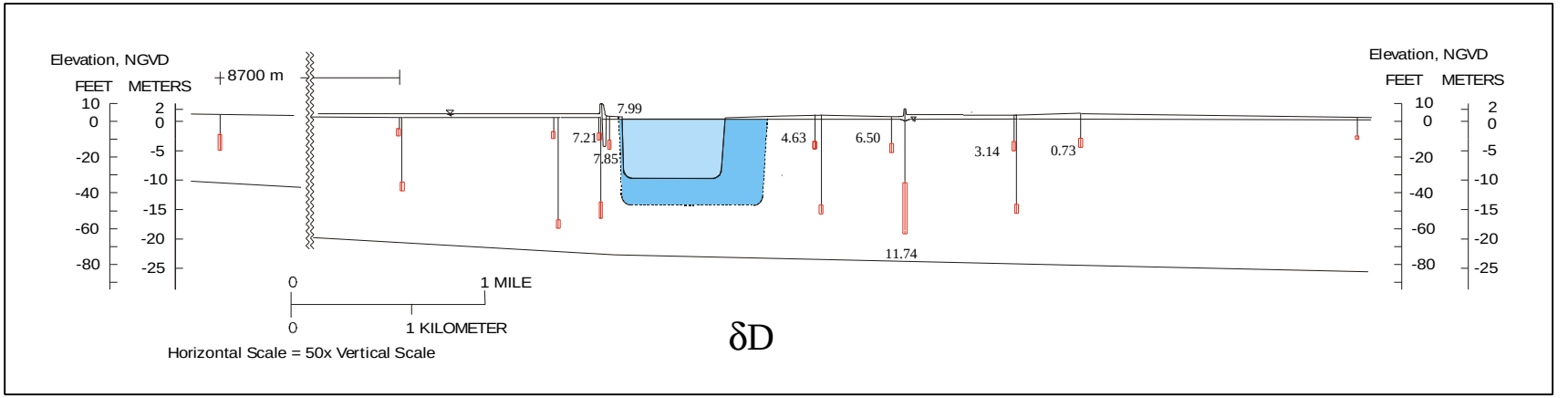

Sampling Date - October 1, 1996

Ambient Rainfall (in)
- Previous Day - 0.72
- Previous 5 Days - 0.72
- Previous 30 Days - 5.61

Average Flow Through Gate S333 (cfs)
- Previous Day - 0.00
- Previous 5 Days - 0.00
- Previous 30 Days - 46.63

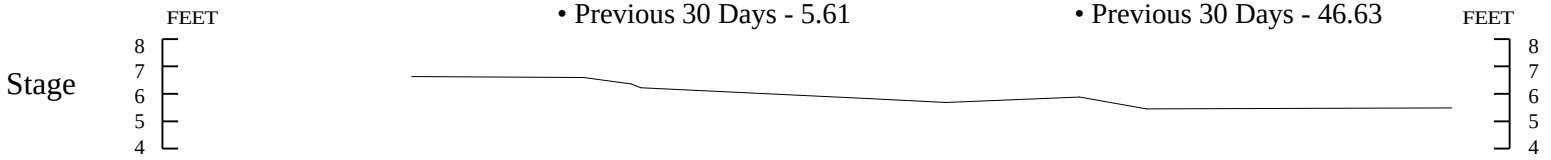

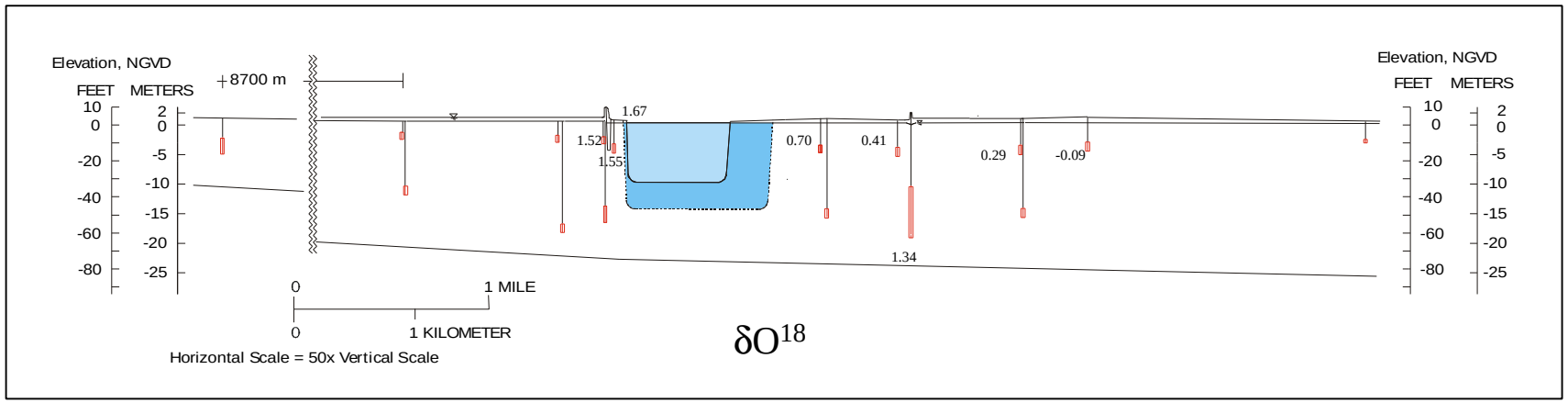

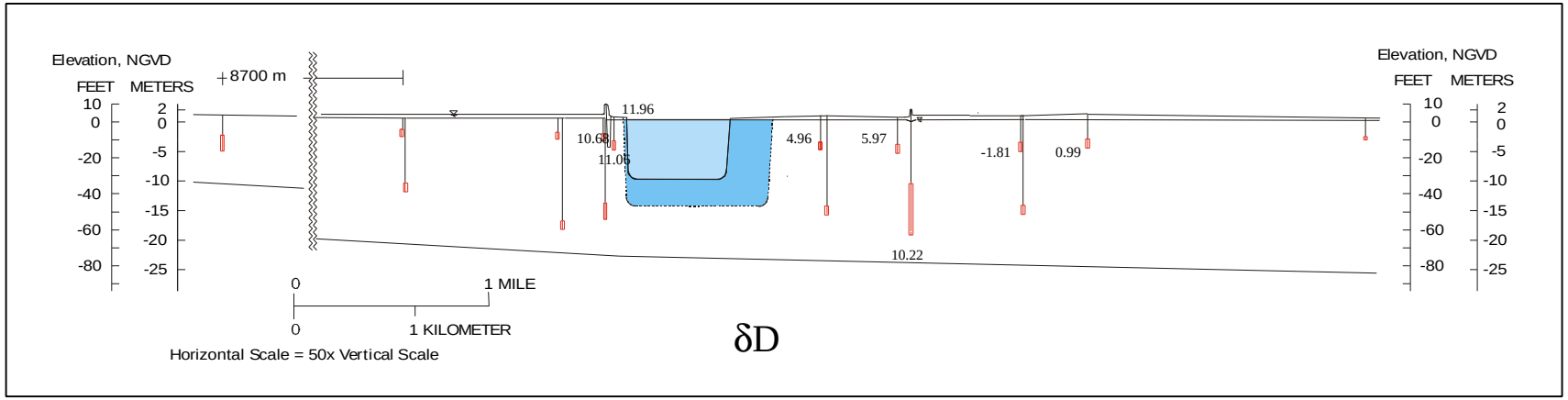

Sampling Date - February 6, 1997

Ambient Rainfall (in)
- Previous Day - 0.06
- Previous 5 Days - 0.13
- Previous 30 Days - 1.45

Average Flow Through Gate S333 (cfs)
- Previous Day - 168.00
- Previous 5 Days - 167.80
- Previous 30 Days - 162.13

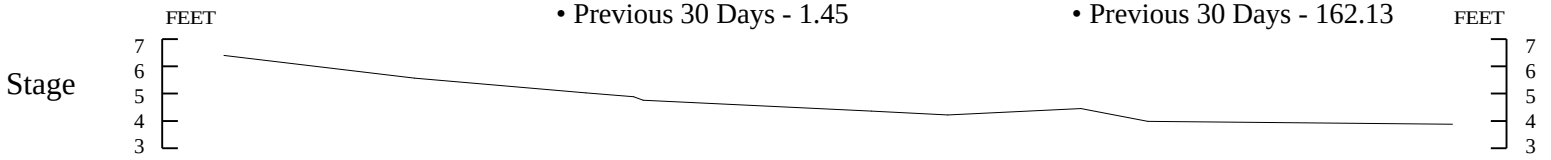

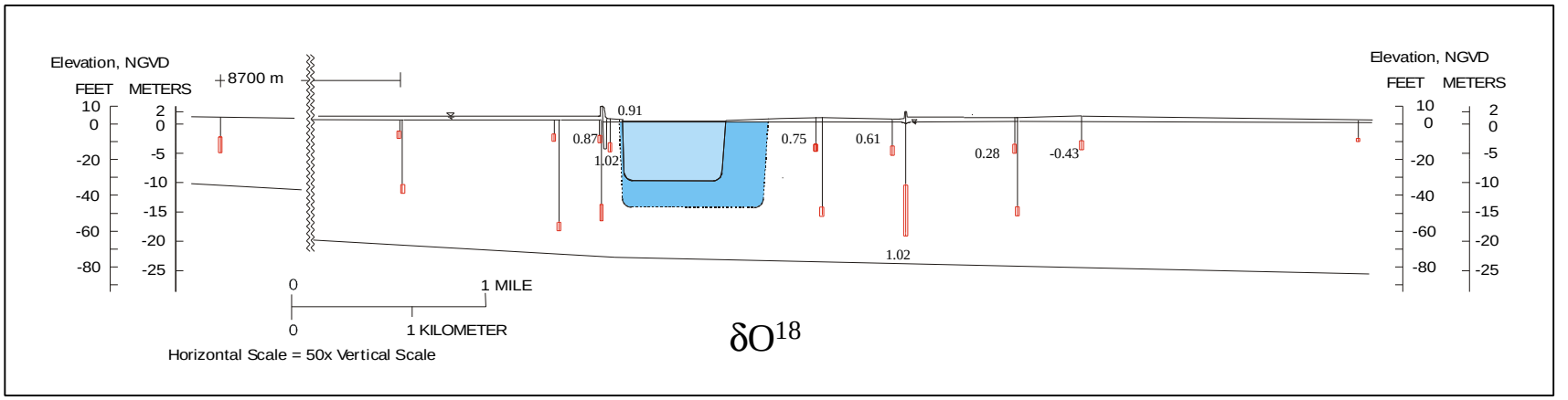

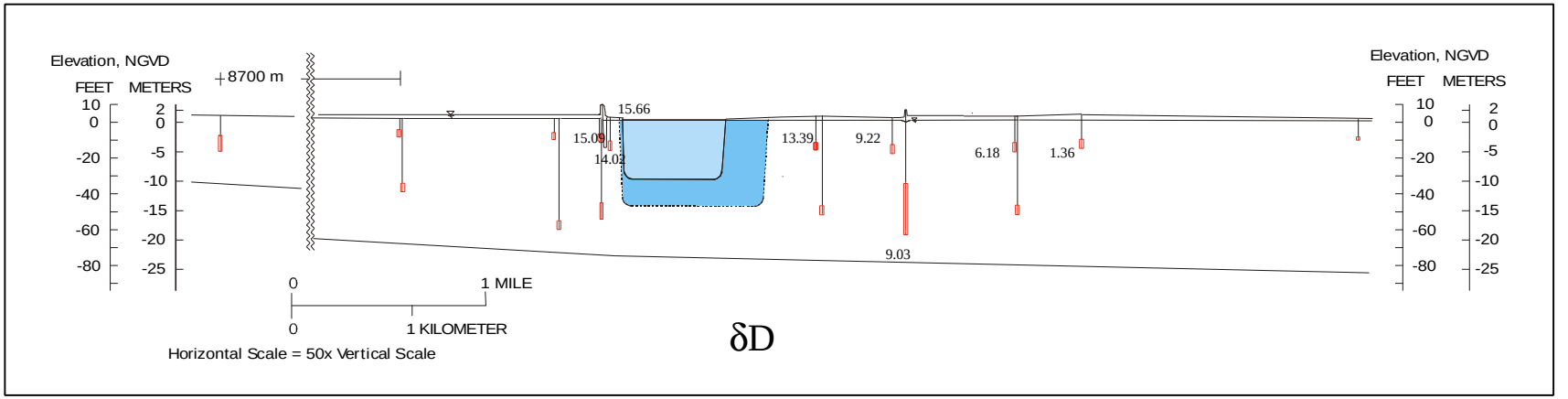

Sampling Date - March 4, 1997

Ambient Rainfall (in)
- Previous Day - 0.00
- Previous 5 Days - 0.07
- Previous 30 Days - 0.63

Average Flow Through Gate S333 (cfs)
- Previous Day - 110.00
- Previous 5 Days - 110.60
- Previous 30 Days - 133.73

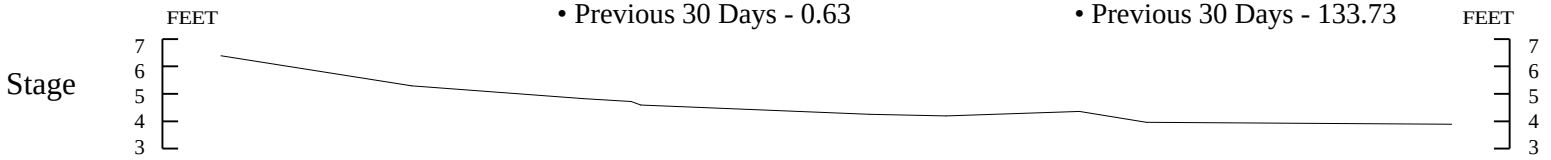

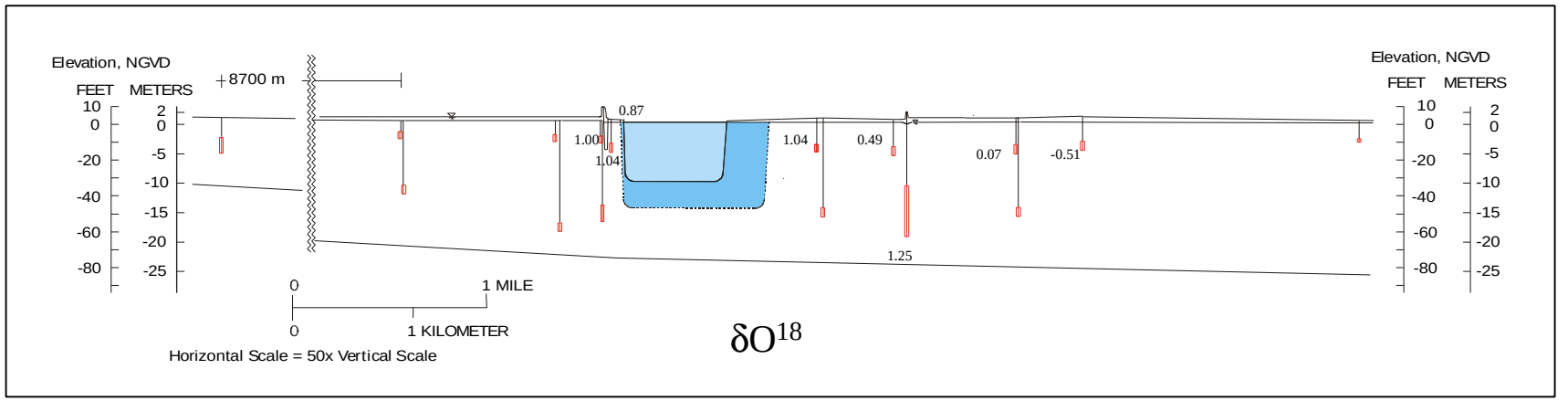

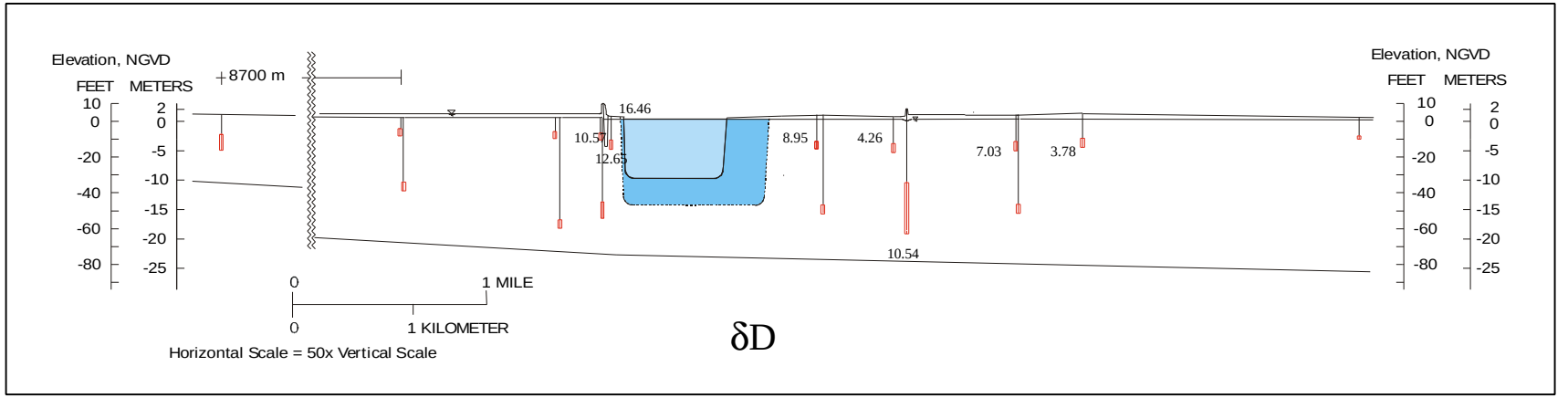

Sampling Date - April 8, 1997

Ambient Rainfall (in)
- Previous Day - 0.00
- Previous 5 Days - 0.00
- Previous 30 Days - 3.22

Average Flow Through Gate S333 (cfs)
- Previous Day - 170.00
- Previous 5 Days - 172.00
- Previous 30 Days - 124.70

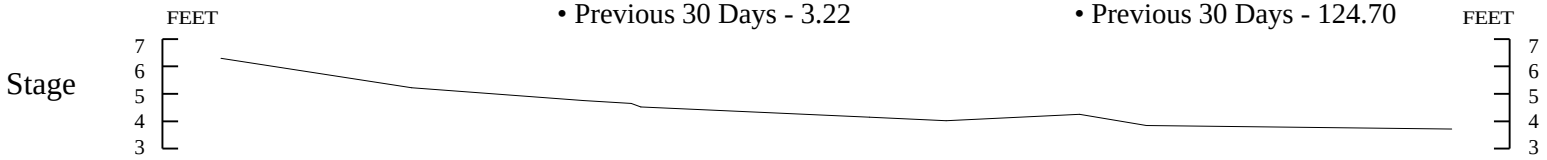

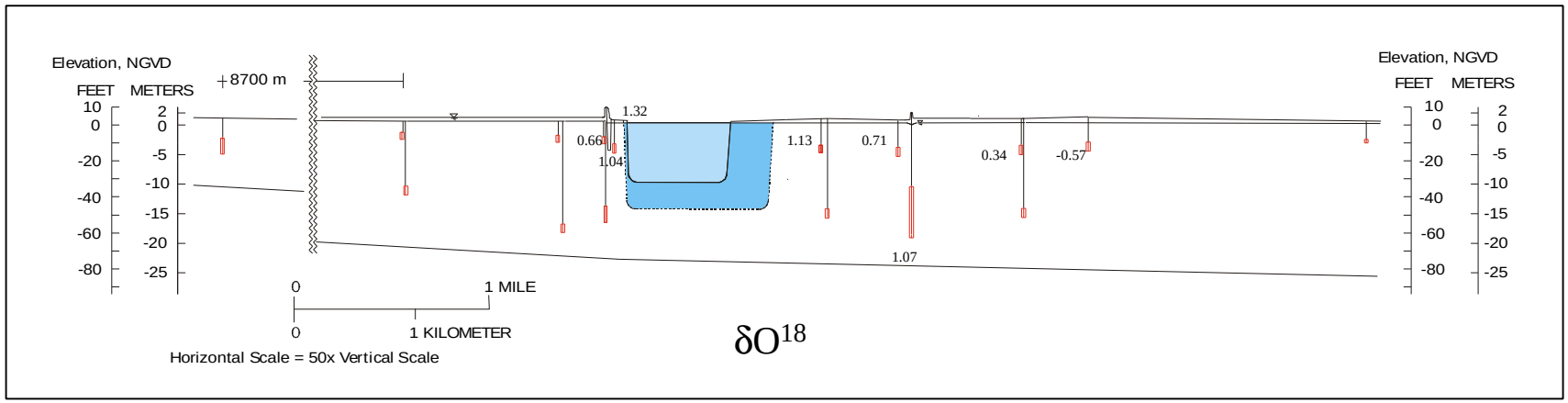

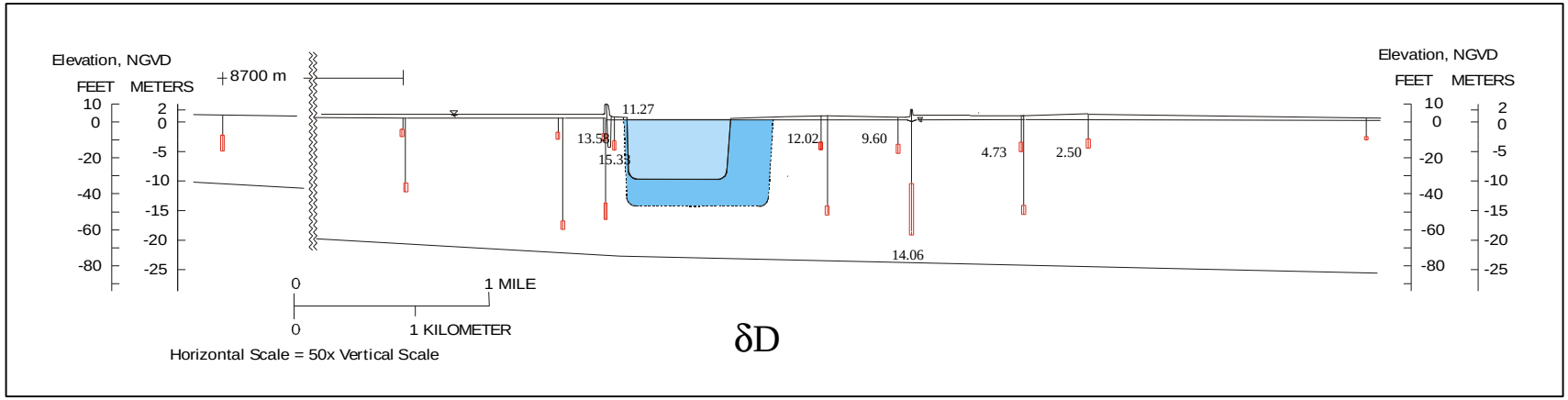

Sampling Date - May 5, 1997

Ambient Rainfall (in)
- Previous Day - 0.00
- Previous 5 Days - 0.00
- Previous 30 Days - 4.73

Average Flow Through Gate S333 (cfs)
- Previous Day - 199.00
- Previous 5 Days - 199.60
- Previous 30 Days - 157.93

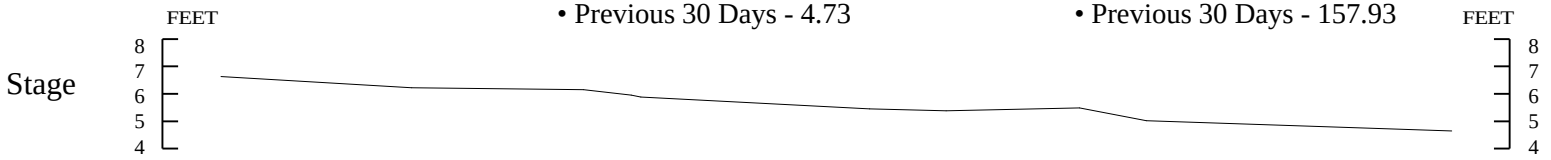

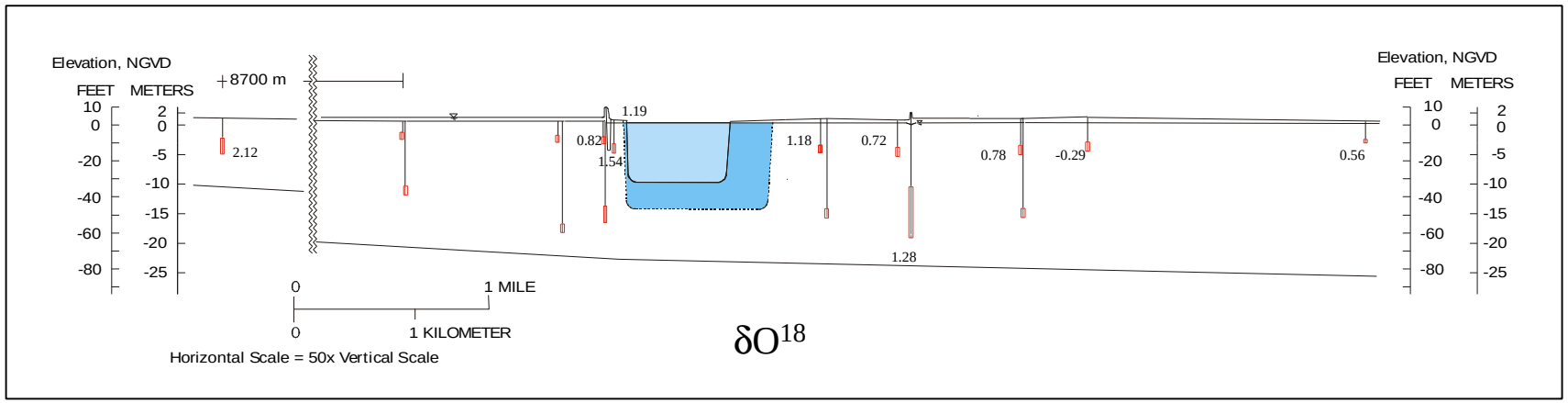

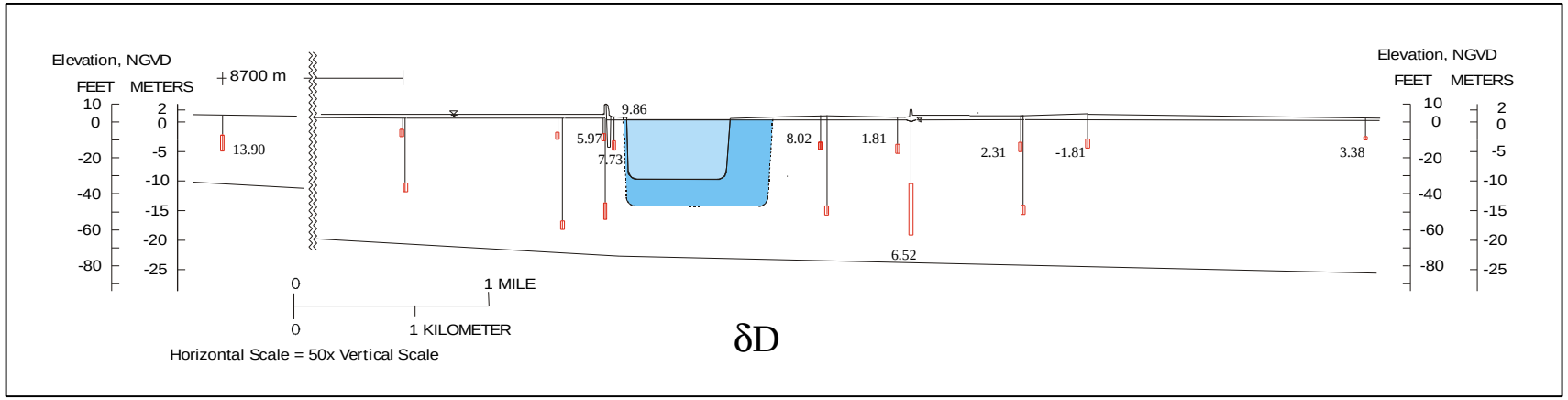

Sampling Date - June 4, 1997

Ambient Rainfall (in)
- Previous Day - 0.01
- Previous 5 Days - 1.31
- Previous 30 Days - 4.20

Average Flow Through Gate S333 (cfs)
- Previous Day - 293.00
- Previous 5 Days - 306.20
- Previous 30 Days - 270.50

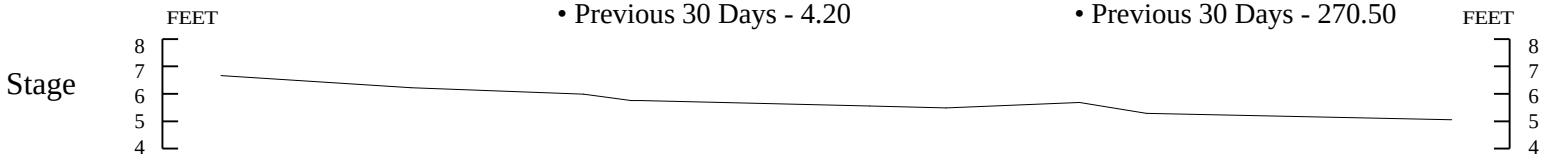

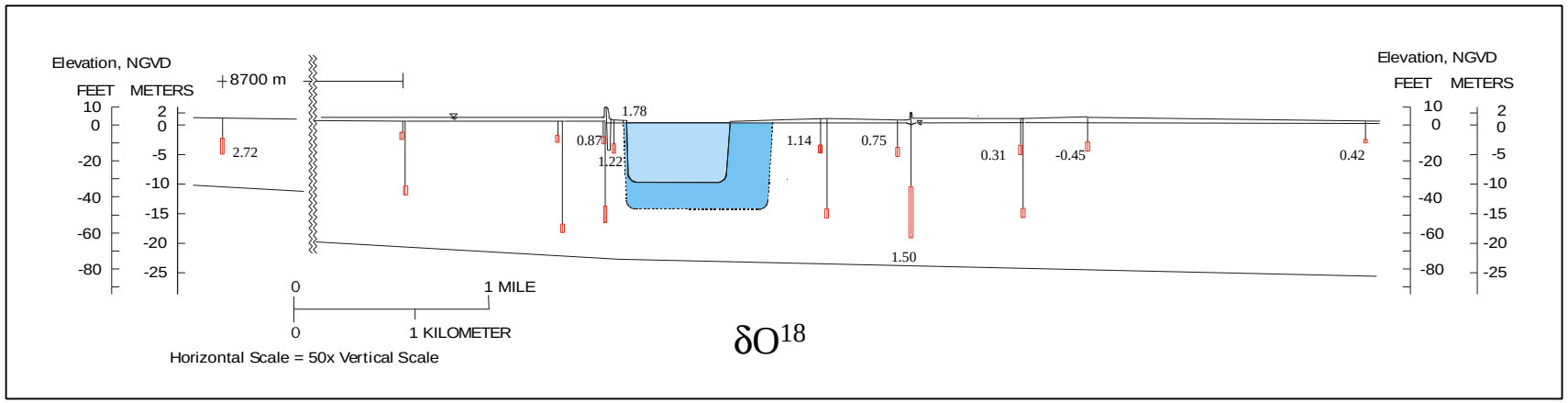

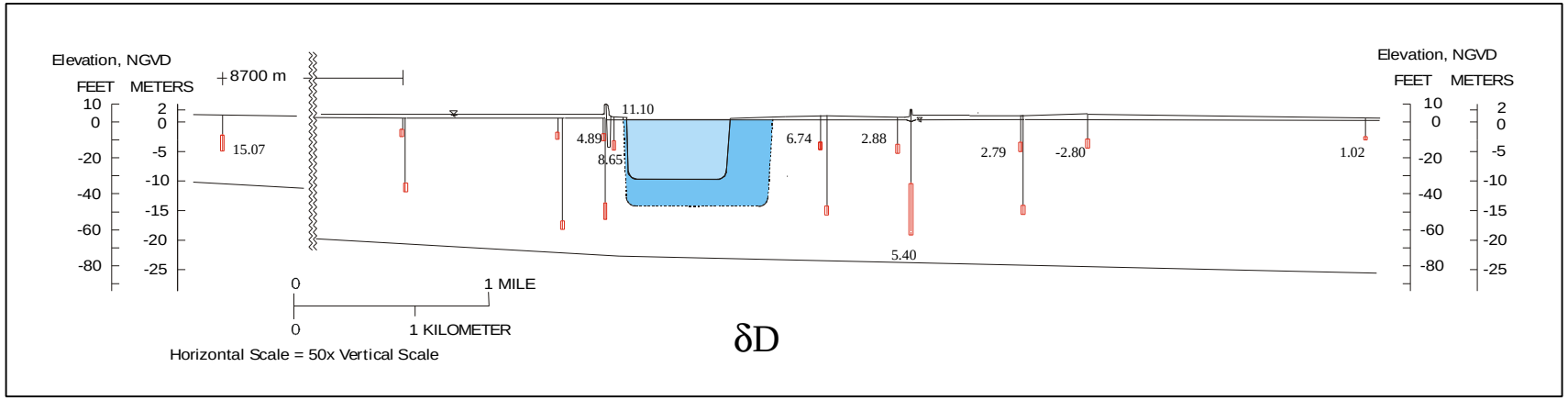

Sampling Date - July 3, 1997

Ambient Rainfall (in)
- Previous Day - 0.01
- Previous 5 Days - 0.09
- Previous 30 Days - 12.17

Average Flow Through Gate S333 (cfs)
- Previous Day - 0.00
- Previous 5 Days - 0.00
- Previous 30 Days - 72.33

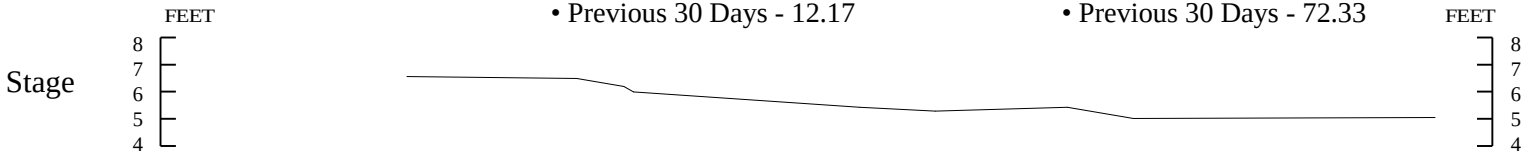

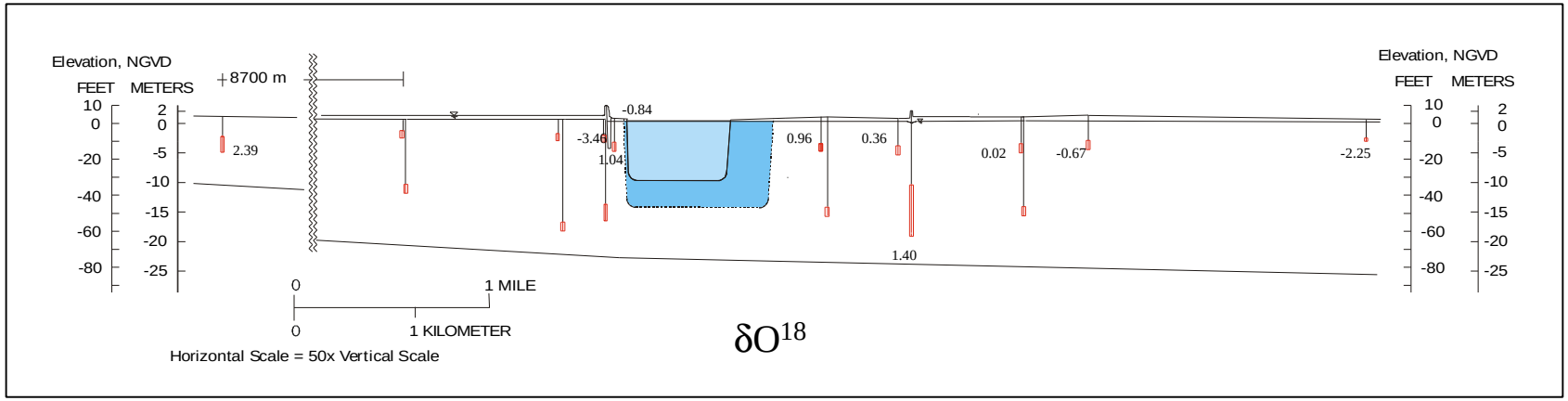

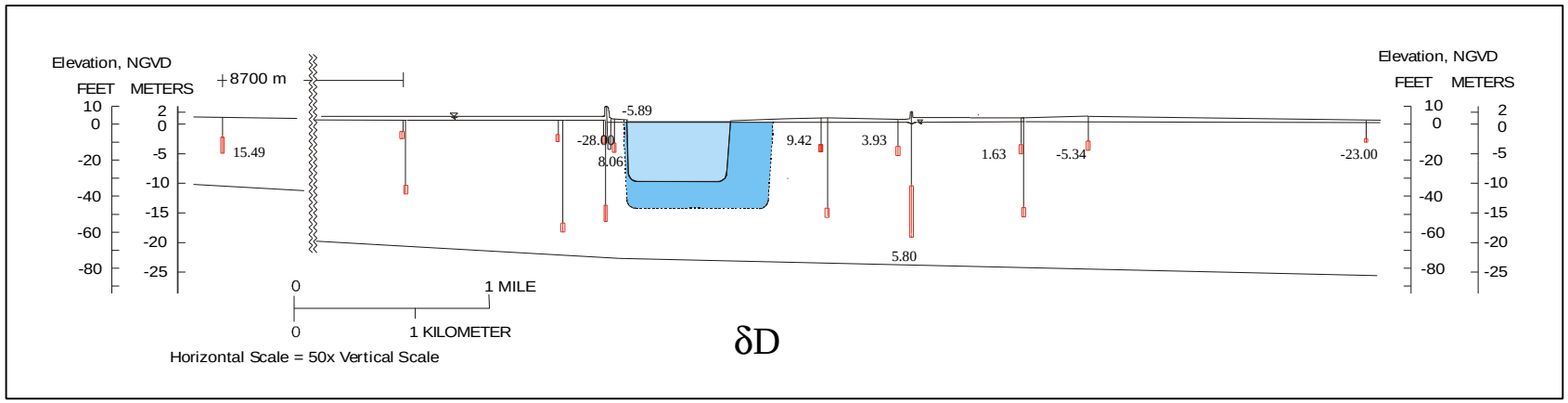

Sampling Date - July 30, 1997

Ambient Rainfall (in)
- Previous Day - 0.14
- Previous 5 Days - 1.07
- Previous 30 Days - 5.84

Average Flow Through Gate S333 (cfs)
- Previous Day - 0.00
- Previous 5 Days - 0.00
- Previous 30 Days - 184.10

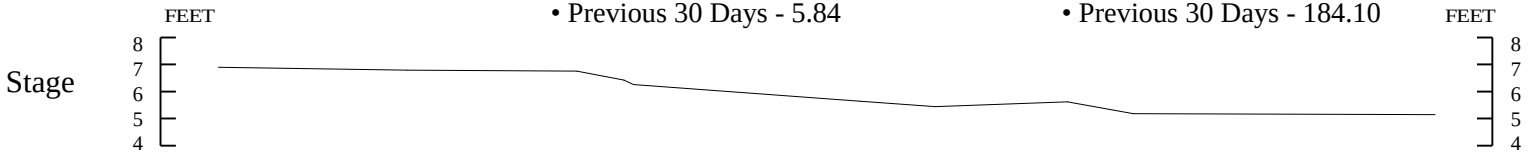

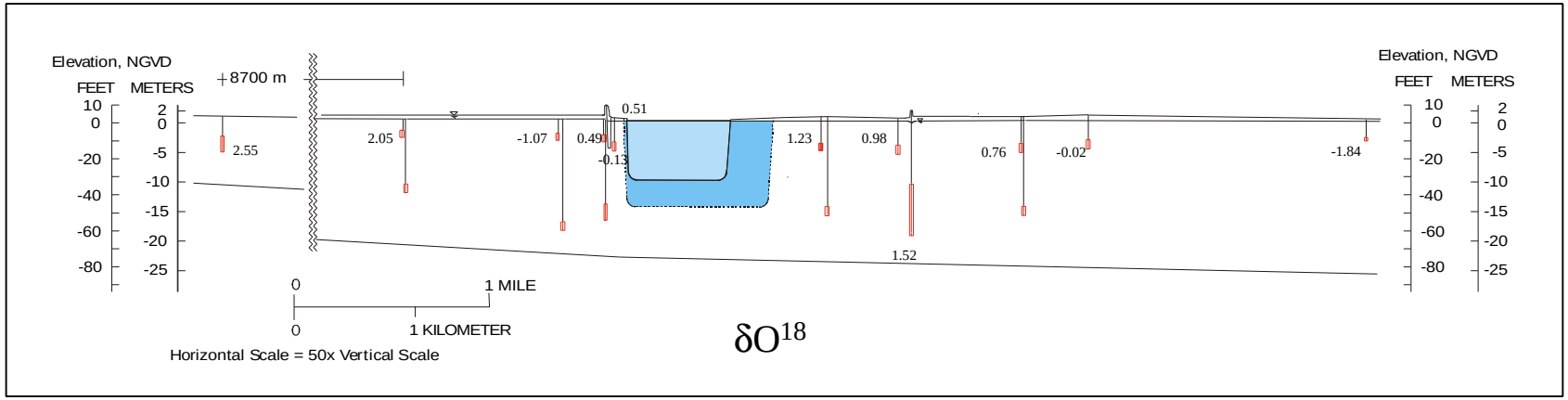

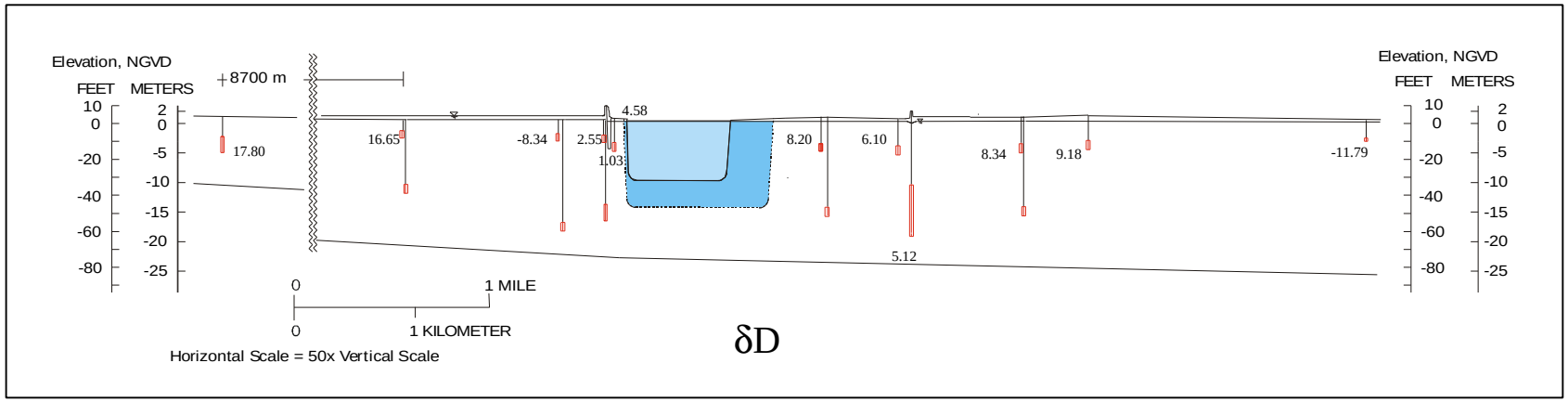

Sampling Date - September 10, 1997

Ambient Rainfall (in)
- Previous Day - 0.00
- Previous 5 Days - 0.78
- Previous 30 Days - 7.61

Average Flow Through Gate S333 (cfs)
- Previous Day - 0.00
- Previous 5 Days - 0.00
- Previous 30 Days - 0.00

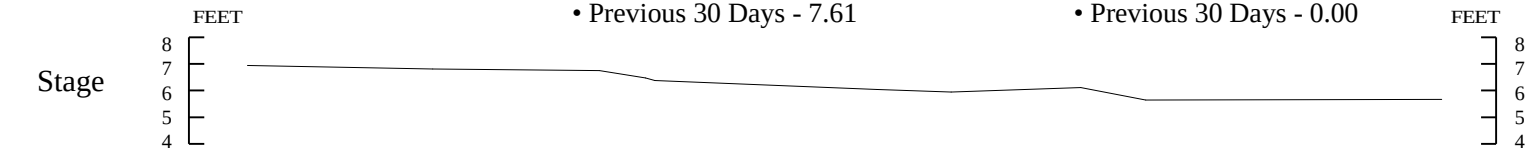

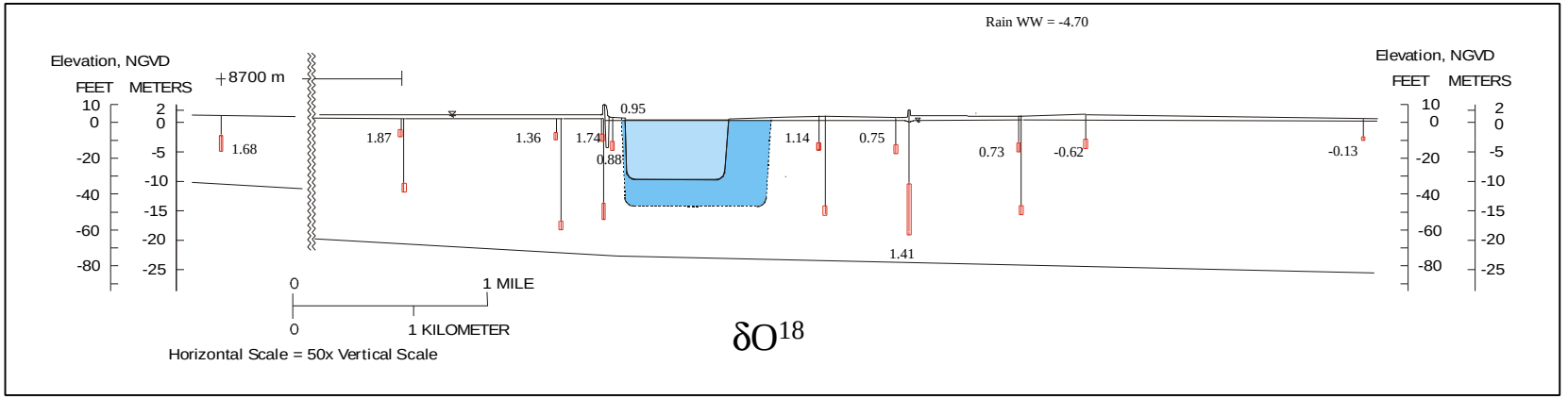

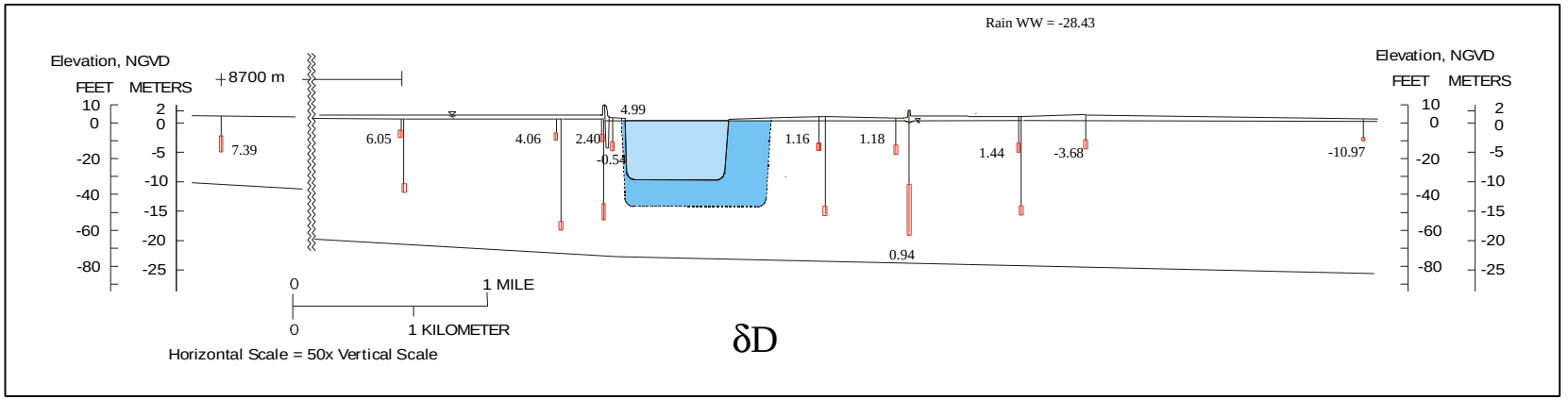

Sampling Date - October 9, 1997

Ambient Rainfall (in)
- Previous Day - 0.00
- Previous 5 Days - 0.07
- Previous 30 Days - 6.86

Average Flow Through Gate S333 (cfs)
- Previous Day - 0.00
- Previous 5 Days - 0.00
- Previous 30 Days - 0.00

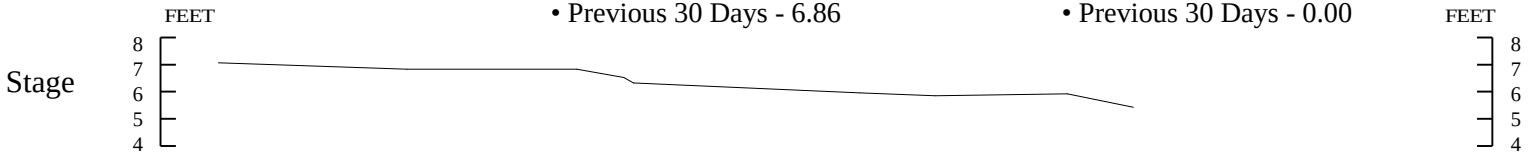

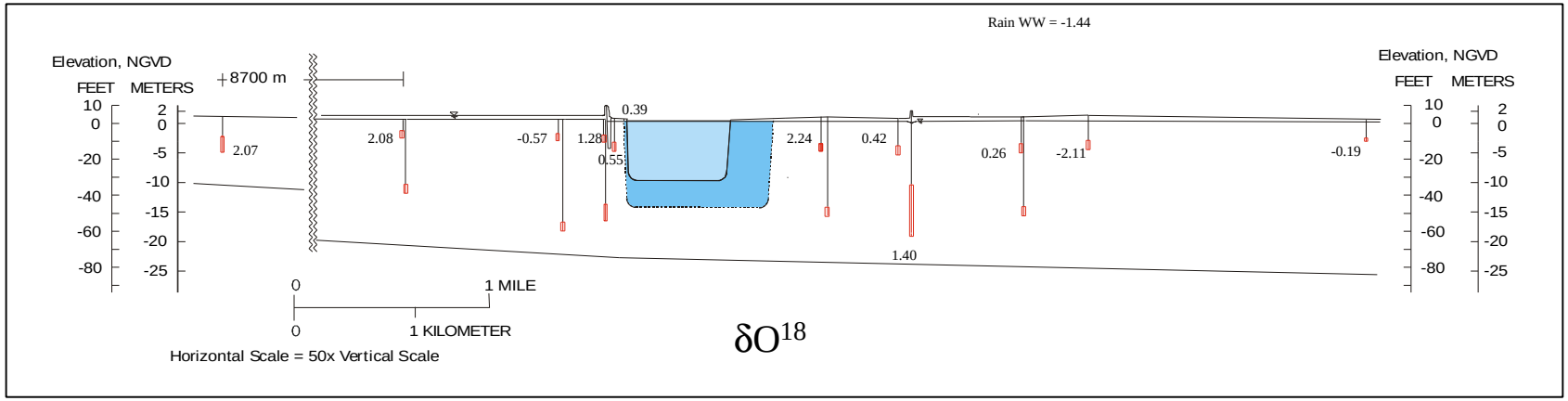

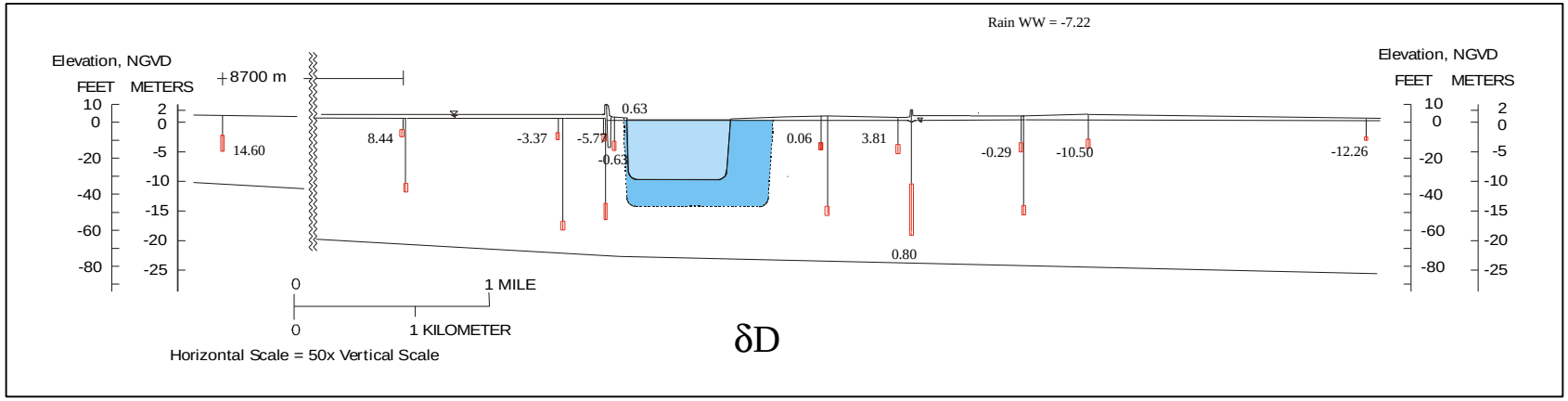

Sampling Date - November 6, 1997

Ambient Rainfall (in)
- Previous Day - 0.01
- Previous 5 Days - 0.02
- Previous 30 Days - 0.50

Average Flow Through Gate S333 (cfs)
- Previous Day - 408.00
- Previous 5 Days - 217.00
- Previous 30 Days - 36.17

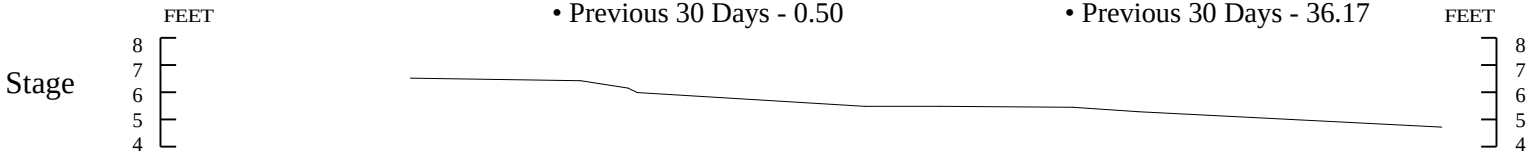

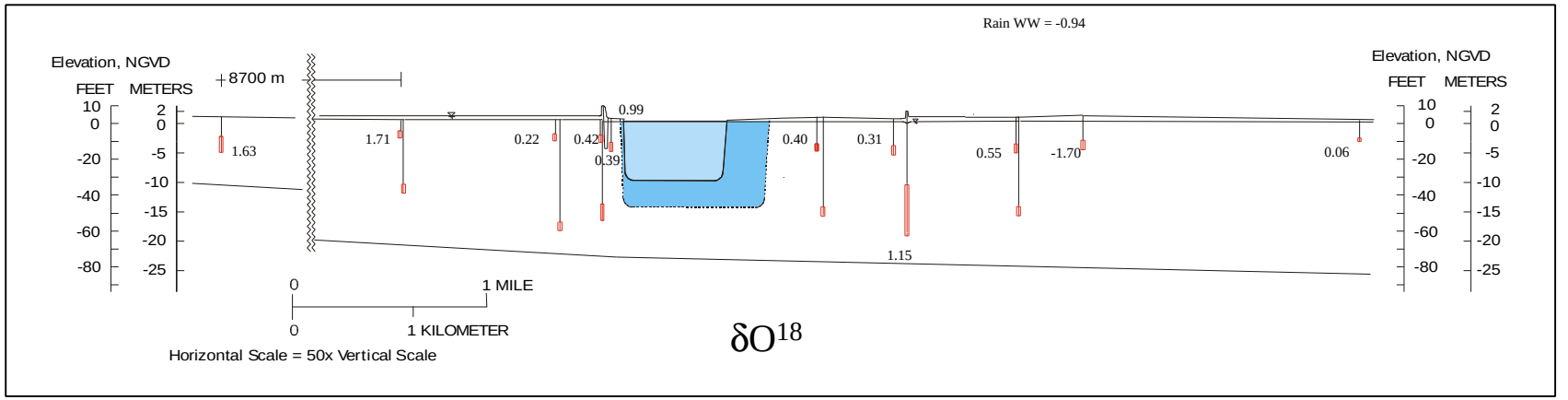

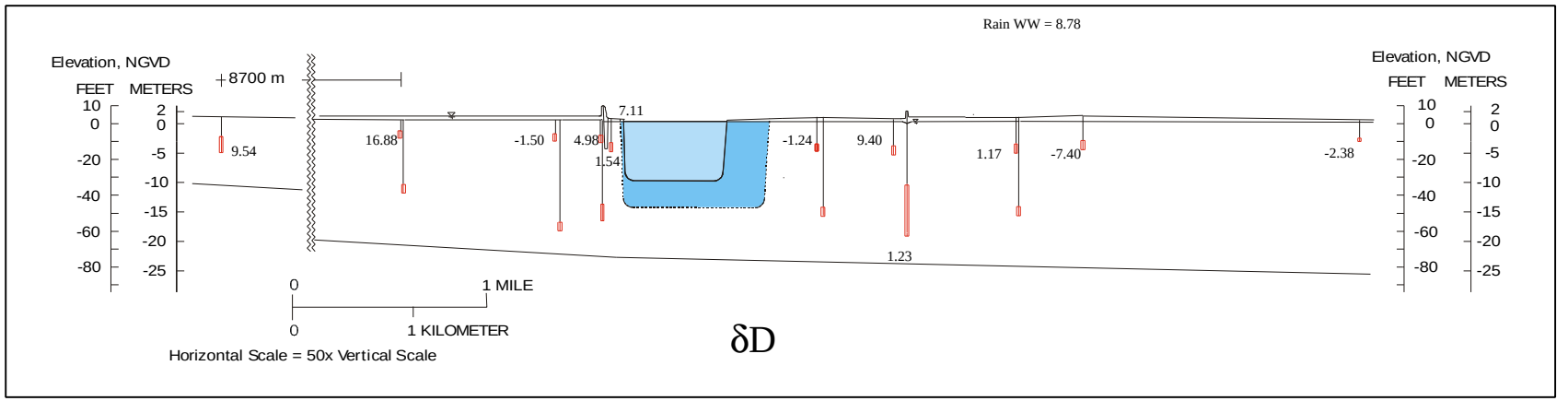

Sampling Date - December 3, 1997

Ambient Rainfall (in)
- Previous Day - 0.00
- Previous 5 Days - 1.99
- Previous 30 Days - 2.42

Average Flow Through Gate S333 (cfs)
- Previous Day - 0.00
- Previous 5 Days - 0.00
- Previous 30 Days - 289.93

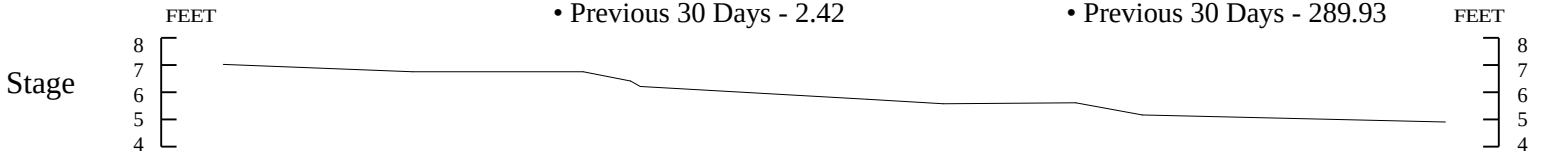

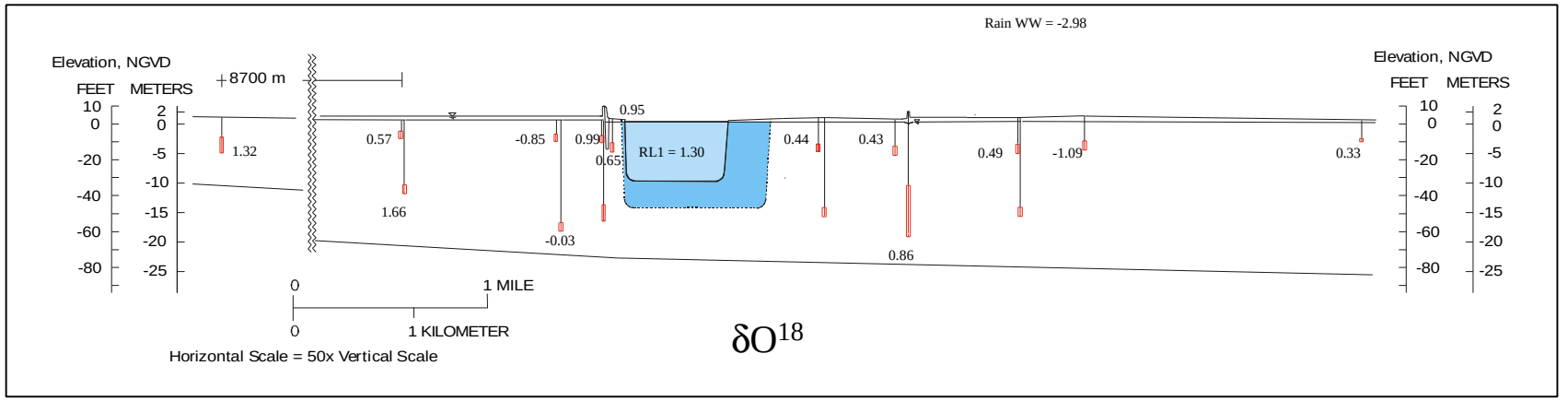

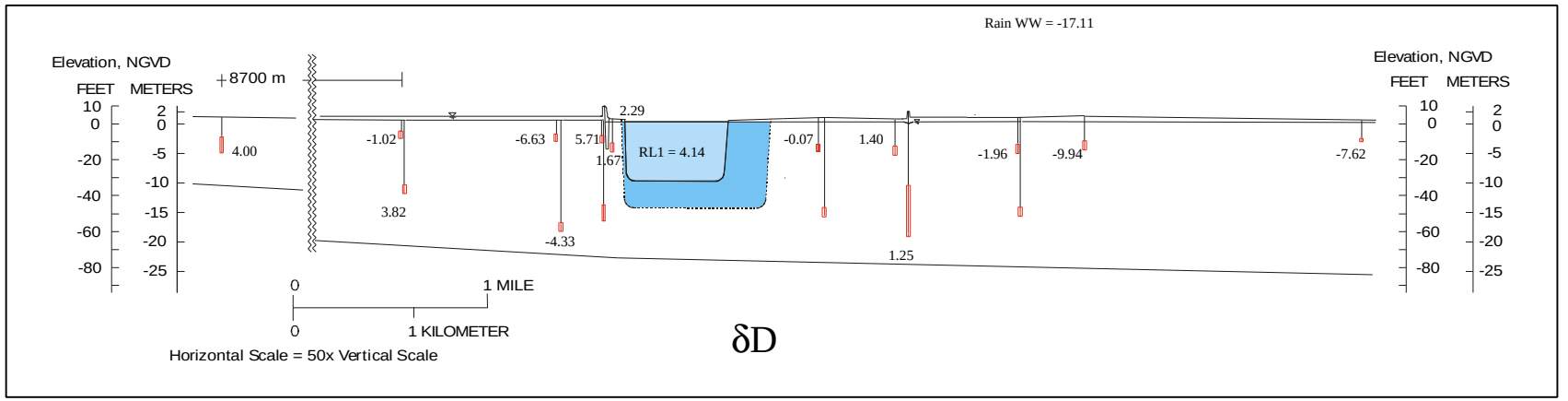

Sampling Date - January 6 , 1998

Ambient Rainfall (in)
- Previous Day - 0.00
- Previous 5 Days - 0.01
- Previous 30 Days - 1.89

Average Flow Through Gate S333 (cfs)
- Previous Day - 0.00
- Previous 5 Days - 0.00
- Previous 30 Days - 0.00

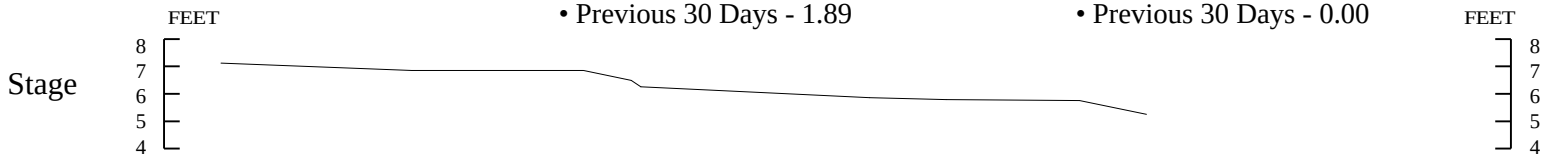

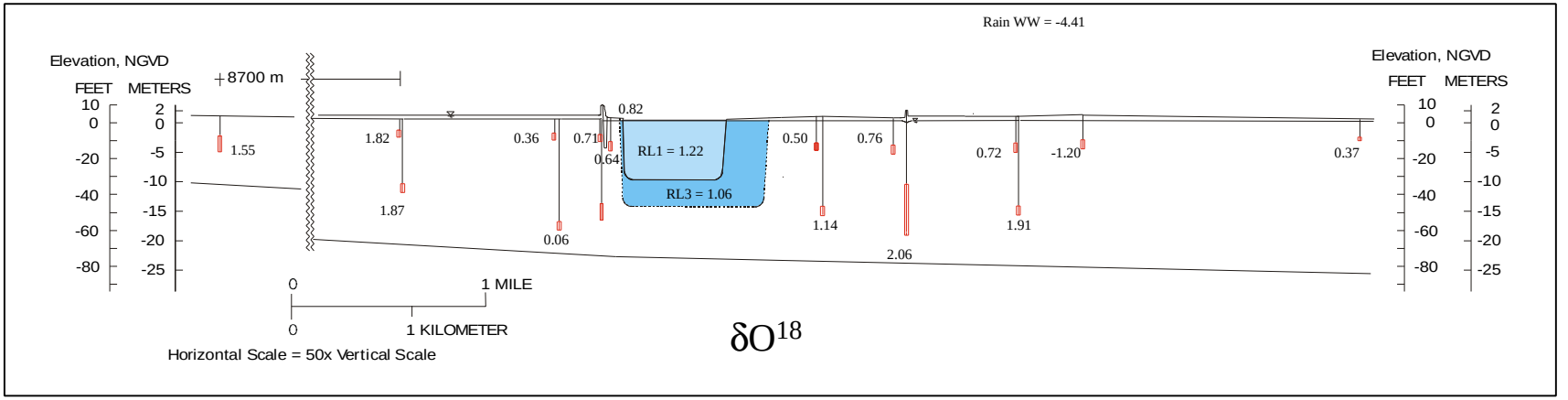

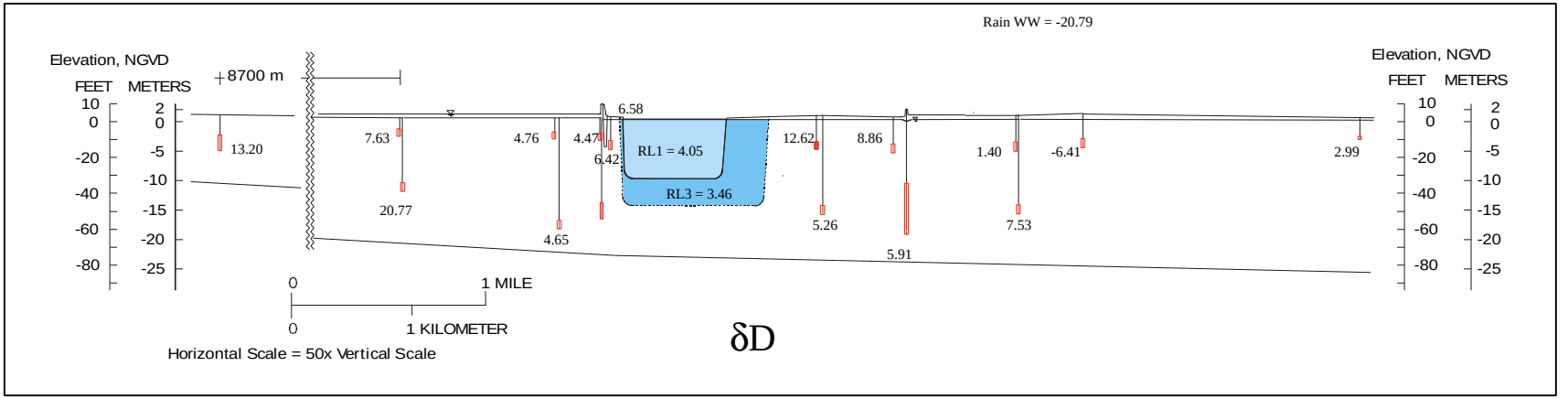

Sampling Date - February 10, 1998

Ambient Rainfall (in)
- Previous Day - 0.00
- Previous 5 Days - 0.25
- Previous 30 Days - 3.58

Average Flow Through Gate S333 (cfs)
- Previous Day - 0.00
- Previous 5 Days - 0.00
- Previous 30 Days - 211.16

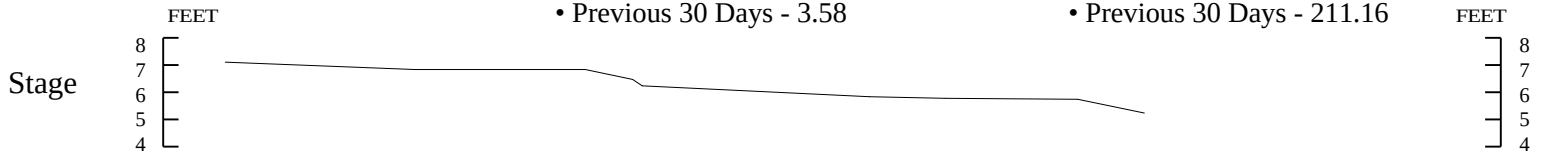

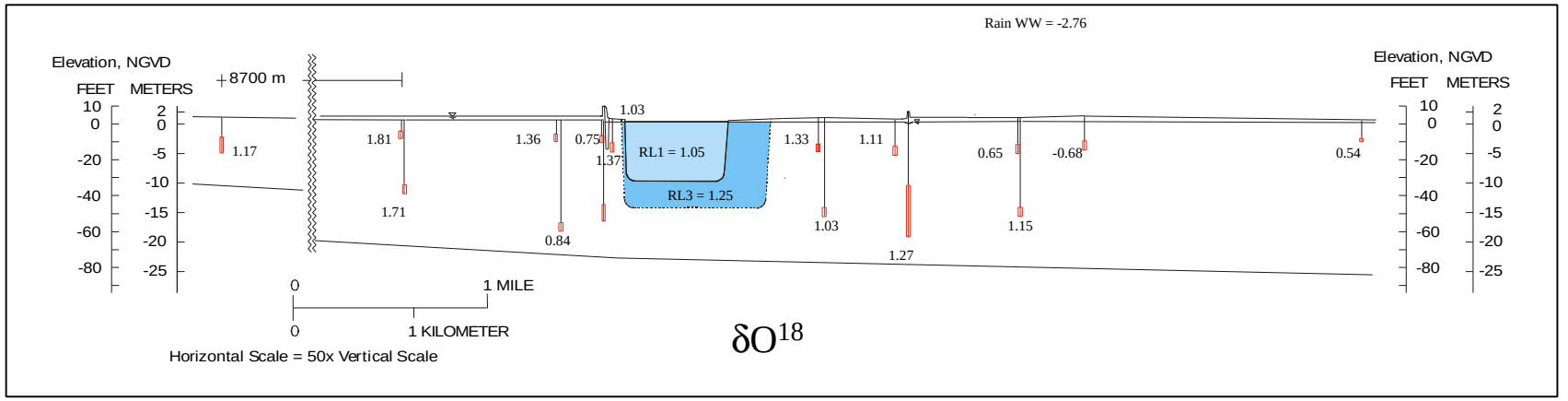

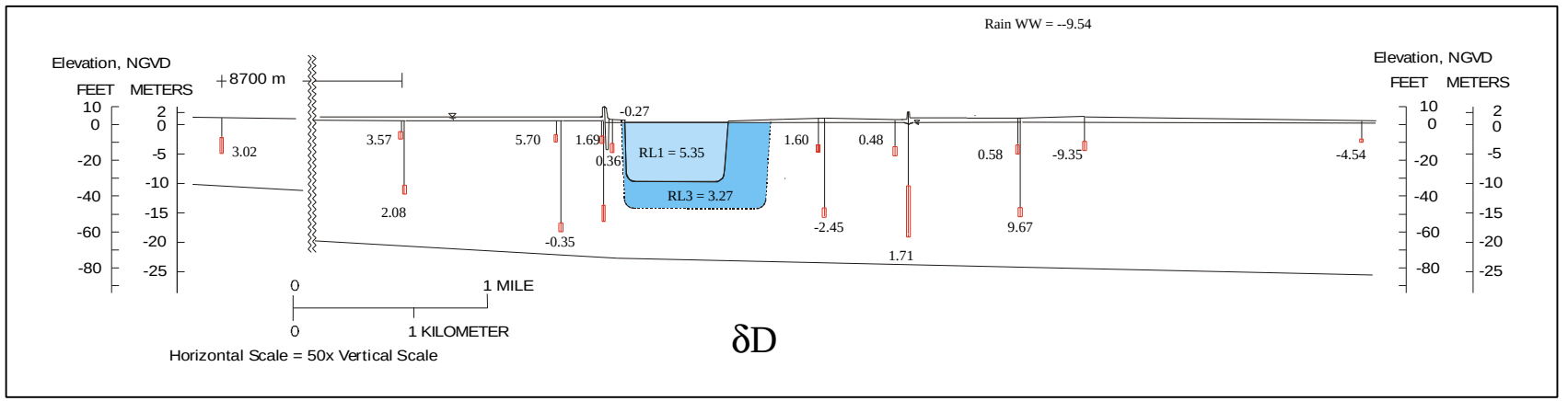

Sampling Date - March 3, 1998

Ambient Rainfall (in)
- Previous Day - 0.41
- Previous 5 Days - 0.47
- Previous 30 Days - 4.56

Average Flow Through Gate S333 (cfs)
- Previous Day - 0.00
- Previous 5 Days - 0.00
- Previous 30 Days - 11.29

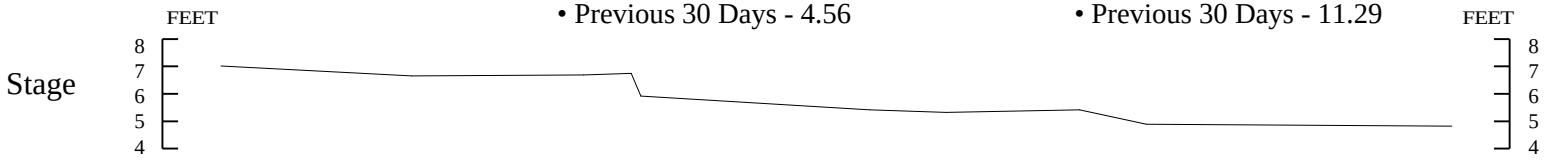

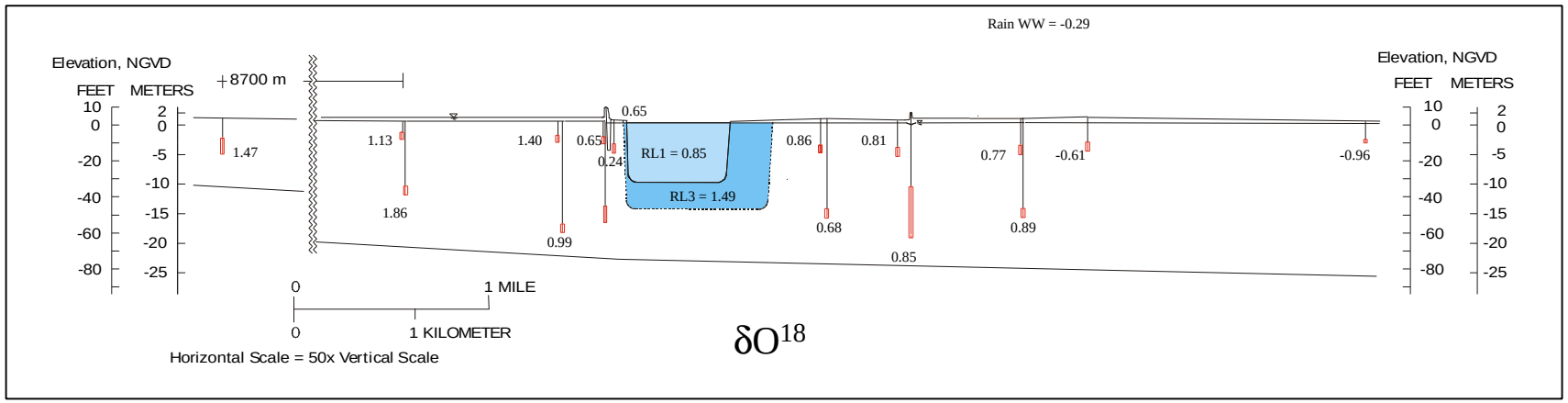

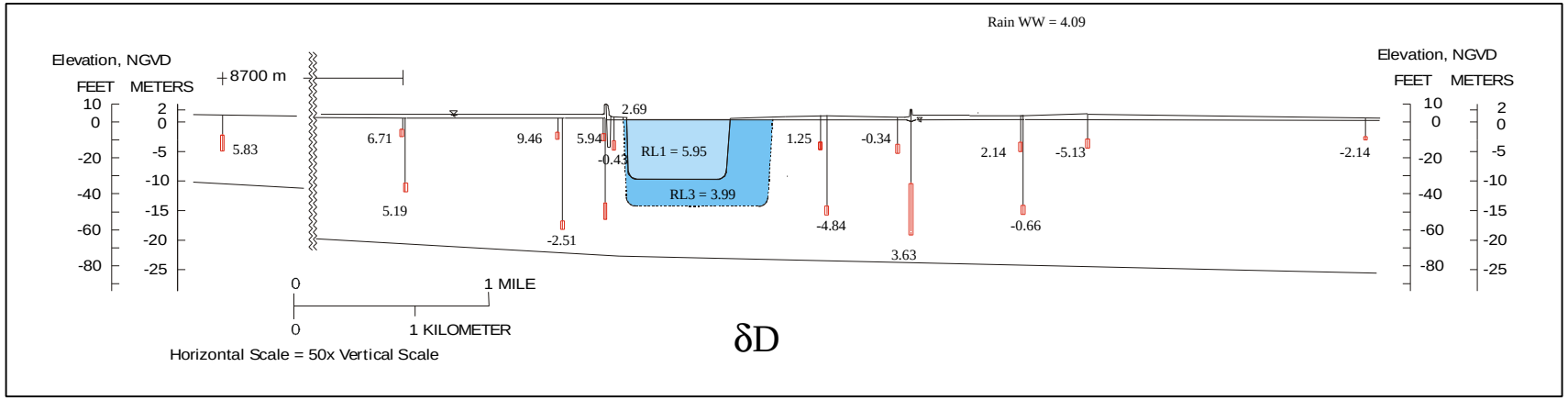

Sampling Date - April 7, 1998

Ambient Rainfall (in)
- Previous Day - 0.00
- Previous 5 Days - 0.00
- Previous 30 Days - 4.97

Average Flow Through Gate S333 (cfs)
- Previous Day - 345.71
- Previous 5 Days - 276.98
- Previous 30 Days - 51.54

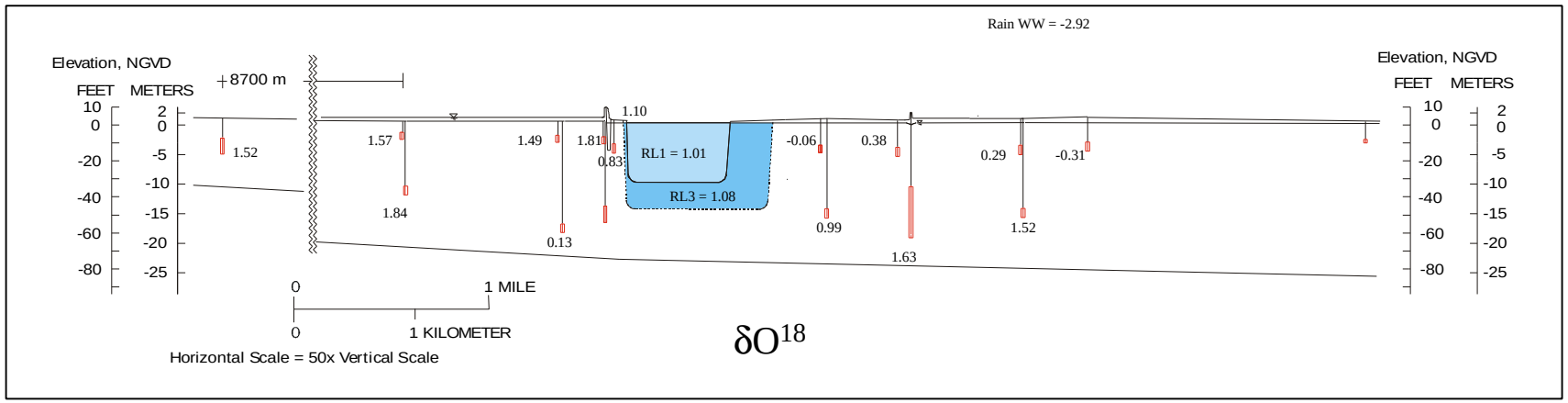

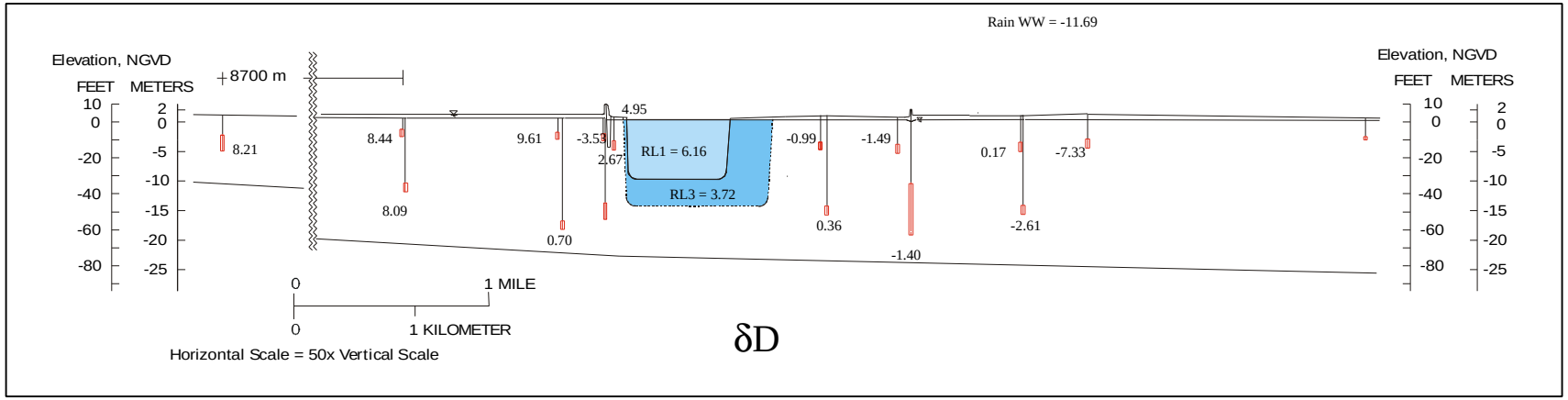

Sampling Date - May 5, 1998

Ambient Rainfall (in)
- Previous Day - 0.00
- Previous 5 Days - 0.68
- Previous 30 Days - 0.70

Average Flow Through Gate S333 (cfs)
- Previous Day - 1091.83
- Previous 5 Days - 1067.41
- Previous 30 Days - 926.04

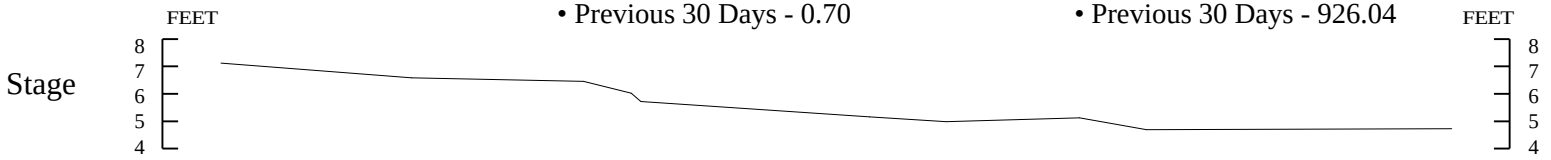

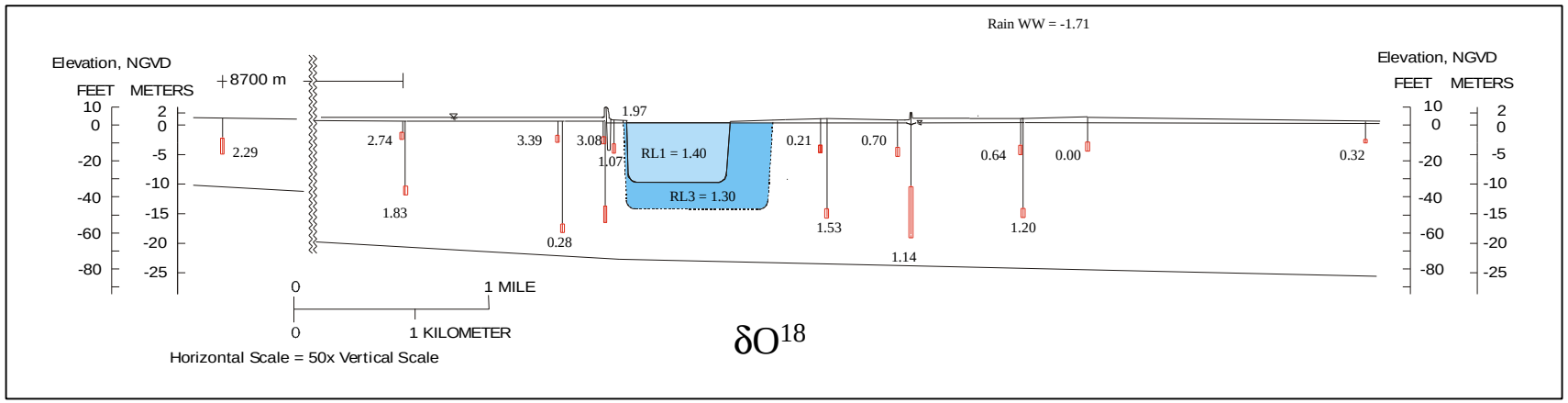

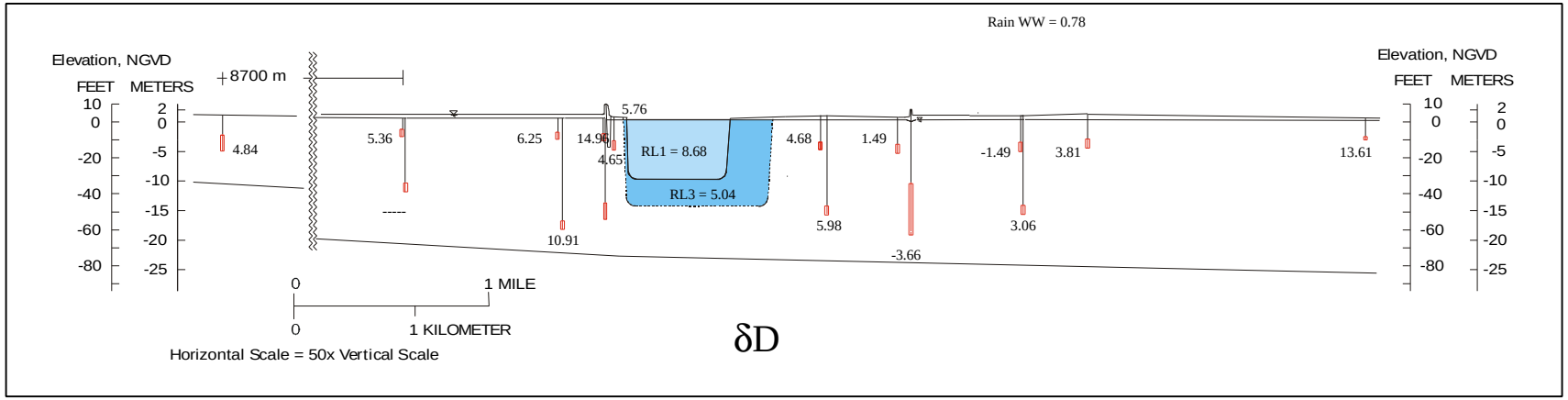

Sampling Date - June 1, 1998

Ambient Rainfall (in)
- Previous Day - 0.00
- Previous 5 Days - 1.47
- Previous 30 Days - 3.08

Average Flow Through Gate S333 (cfs)
- Previous Day - 431.63
- Previous 5 Days - 437.31
- Previous 30 Days - 717.83

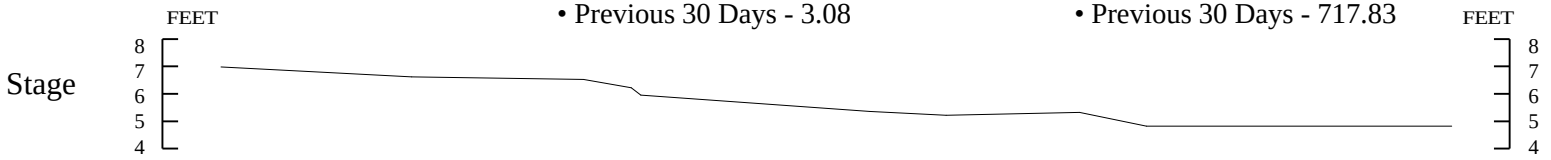

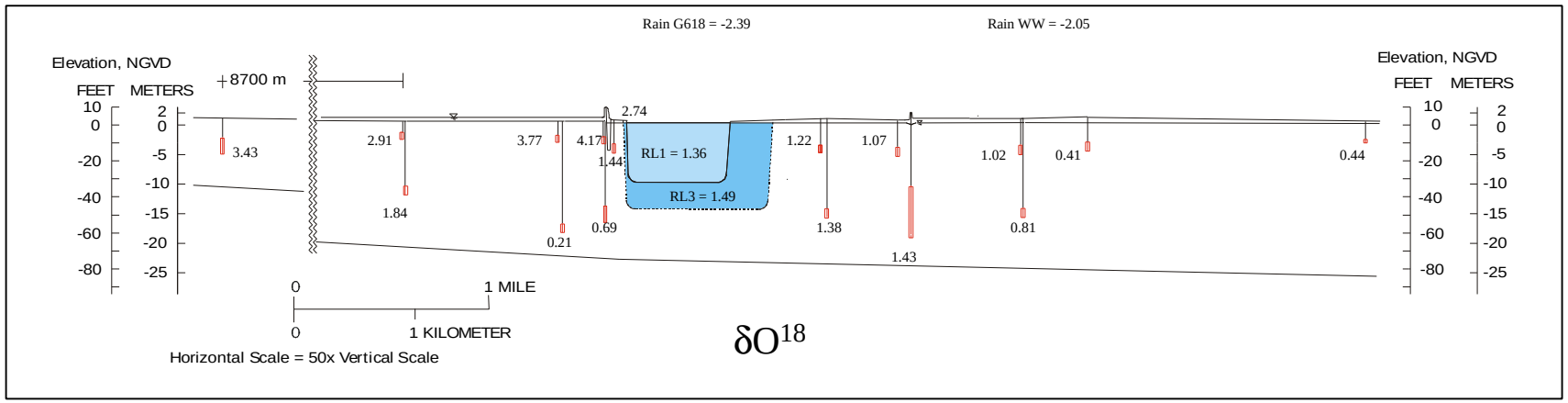

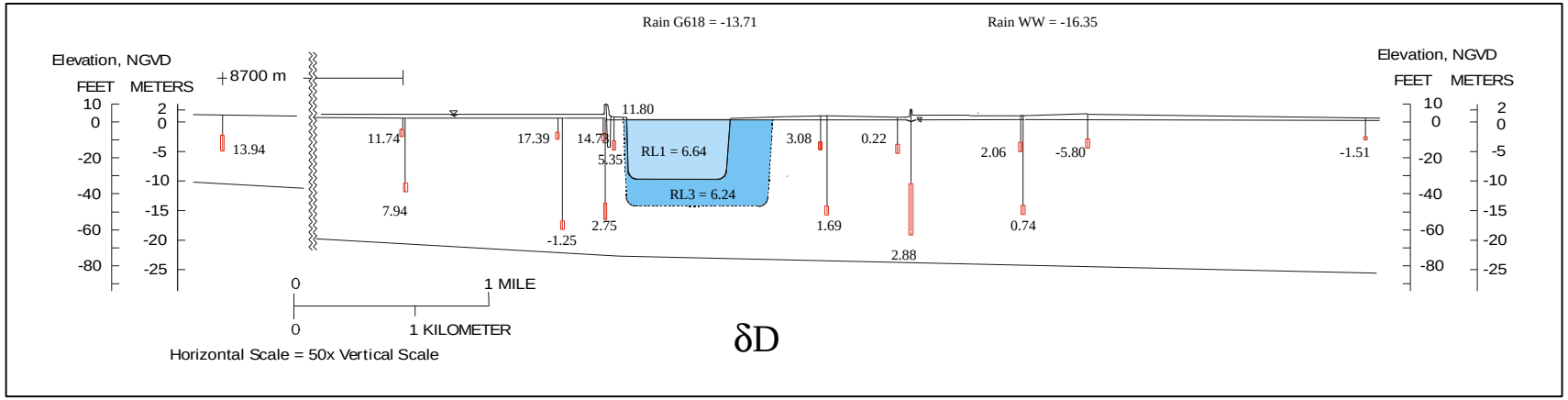

Sampling Date - July 6, 1998

Ambient Rainfall (in)
- Previous Day - 0.74
- Previous 5 Days - 0.93
- Previous 30 Days - 7.20

Average Flow Through Gate S333 (cfs)
- Previous Day - 0.00
- Previous 5 Days - 0.00
- Previous 30 Days - 53.88

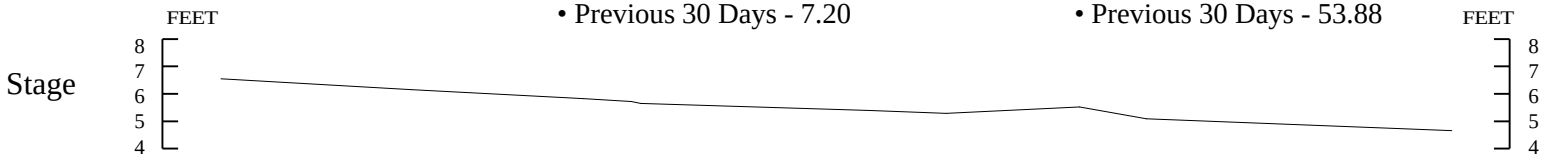

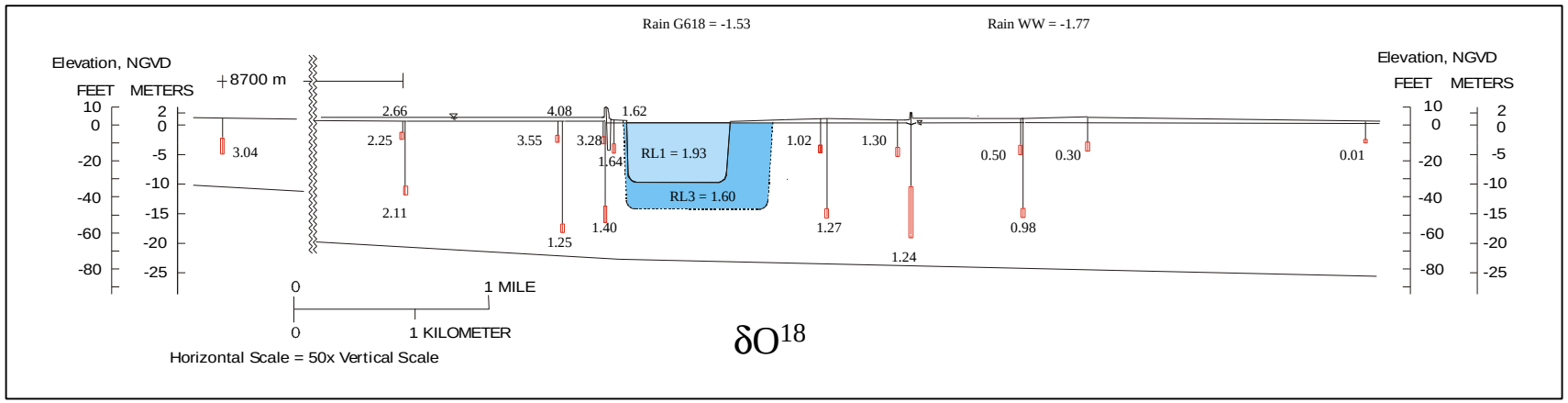

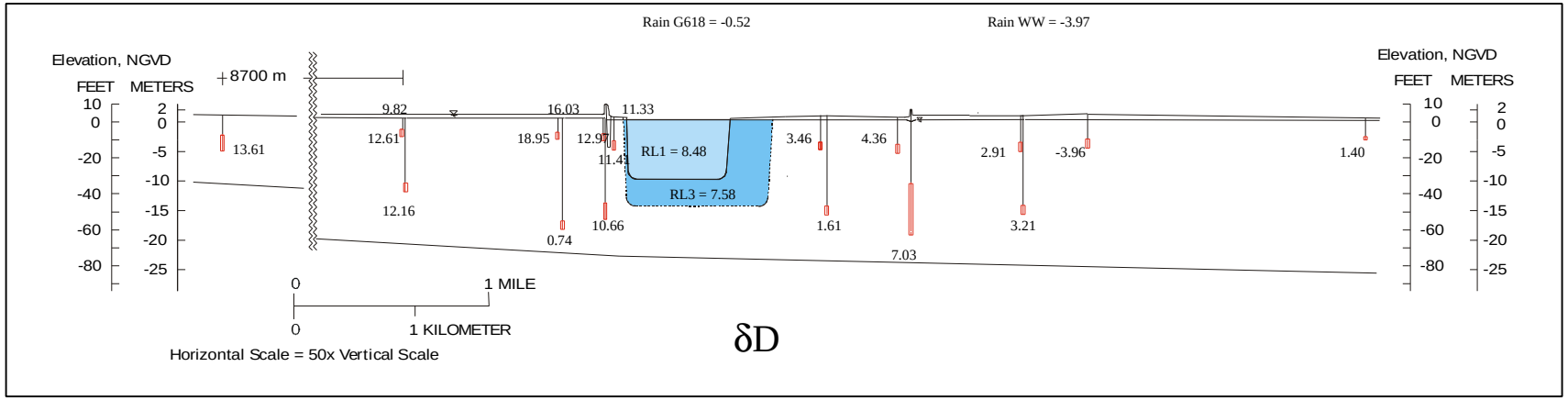

Sampling Date - August 3, 1998

Ambient Rainfall (in)
- Previous Day - 0.00
- Previous 5 Days - 0.16
- Previous 30 Days - 7.47

Average Flow Through Gate S333 (cfs)
- Previous Day - 243.69
- Previous 5 Days - 231.53
- Previous 30 Days - 38.59

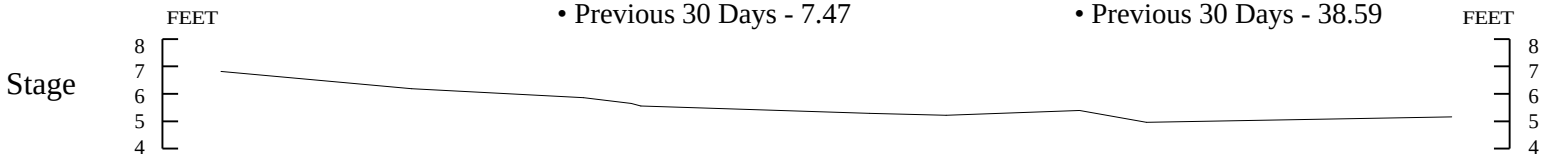

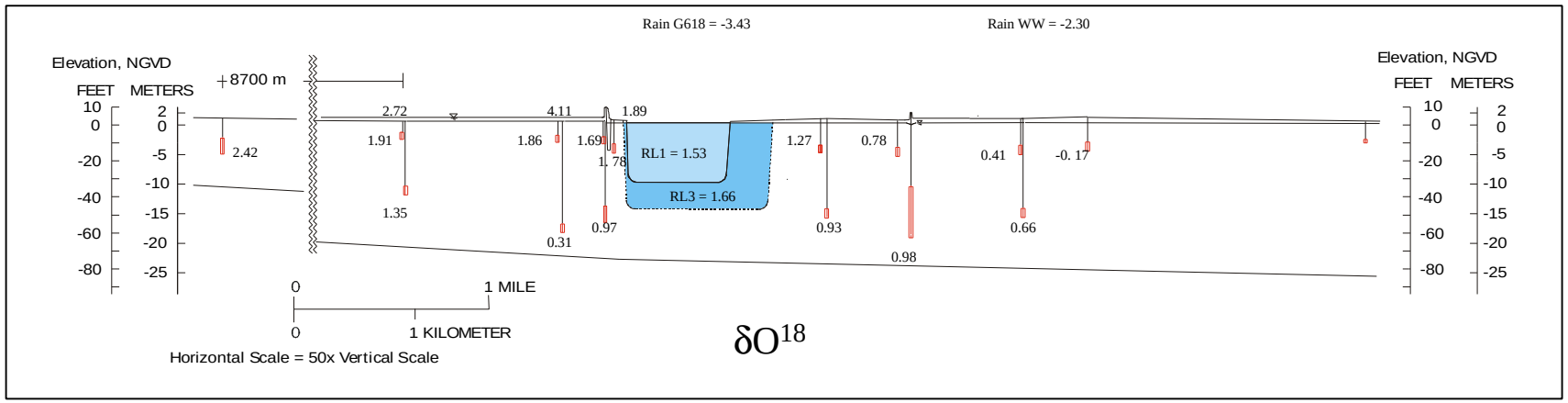

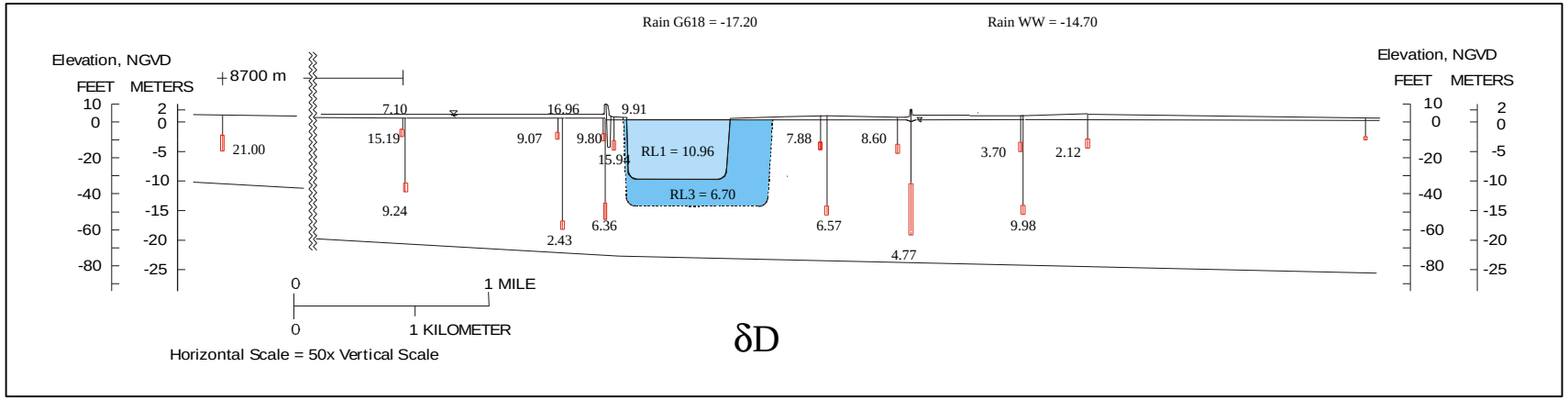

Sampling Date - September 1, 1998

Ambient Rainfall (in)
- Previous Day - 0.00
- Previous 5 Days - 0.04
- Previous 30 Days - 5.04

Average Flow Through Gate S333 (cfs)
- Previous Day - 377.65
- Previous 5 Days - 377.74
- Previous 30 Days - 275.42

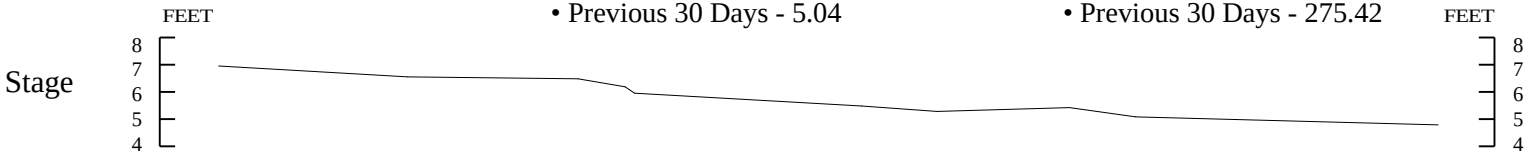

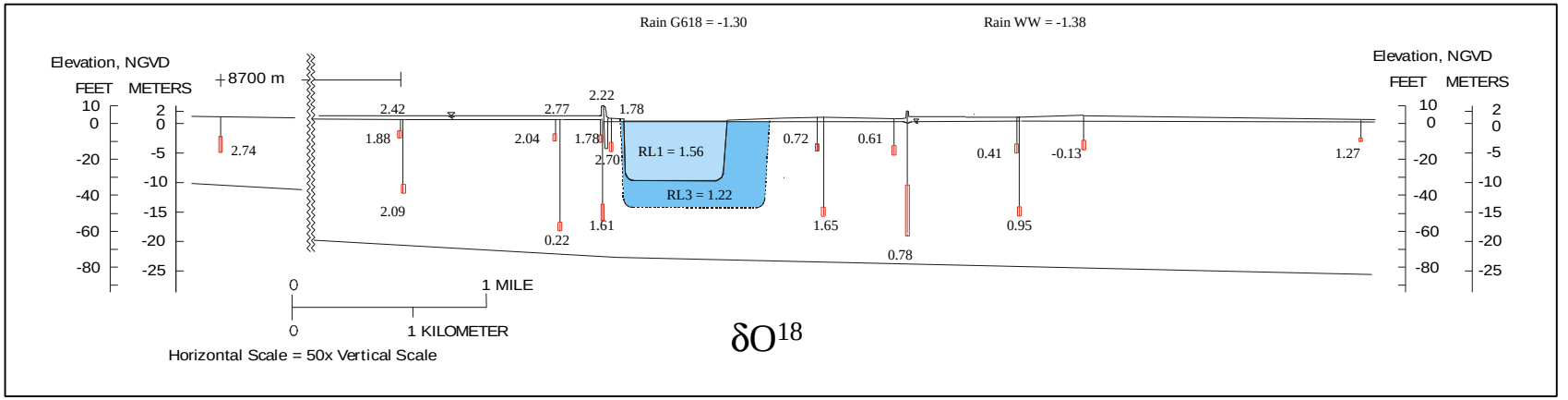

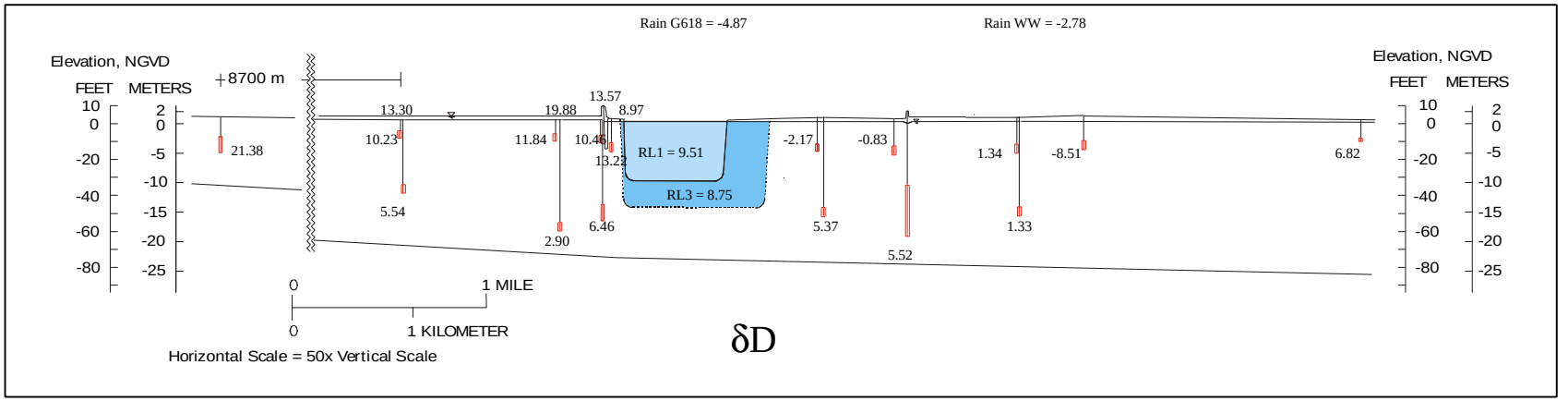

Sampling Date - October 6, 1998

Ambient Rainfall (in)
- Previous Day - 0.00
- Previous 5 Days - 0.03
- Previous 30 Days - 7.94

Average Flow Through Gate S333 (cfs)
- Previous Day - 0.00
- Previous 5 Days - 0.00
- Previous 30 Days - 81.81

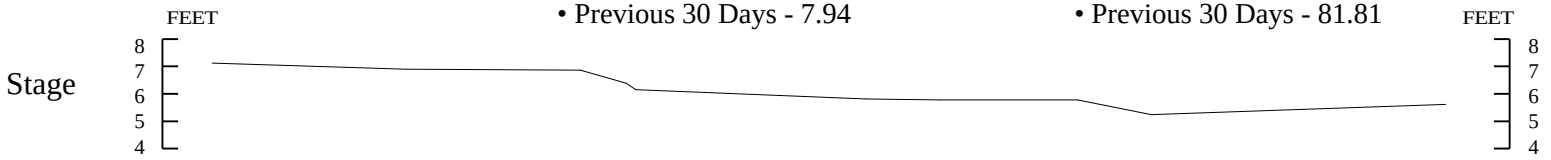

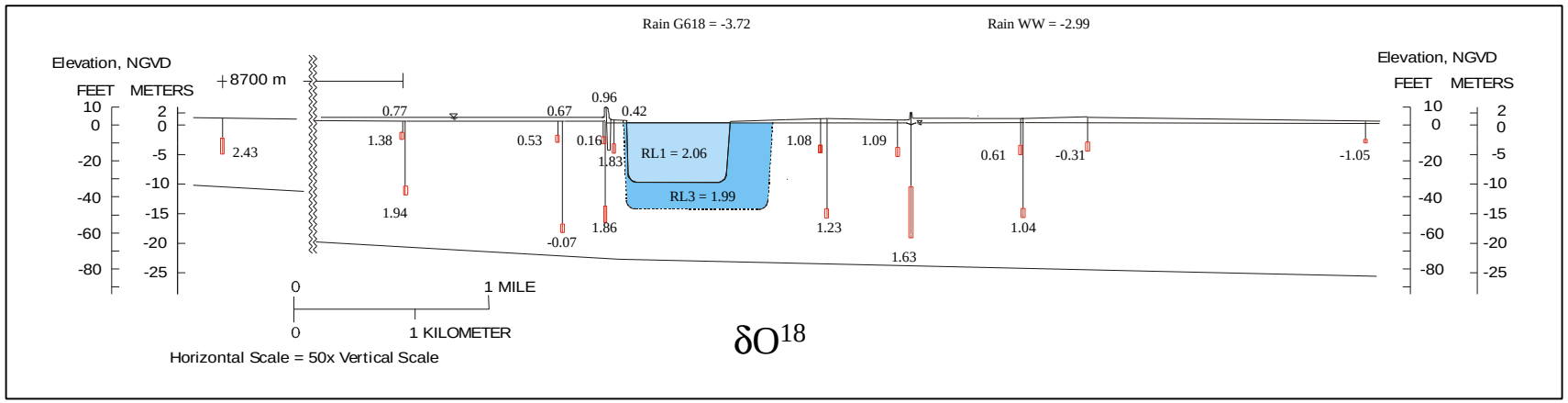

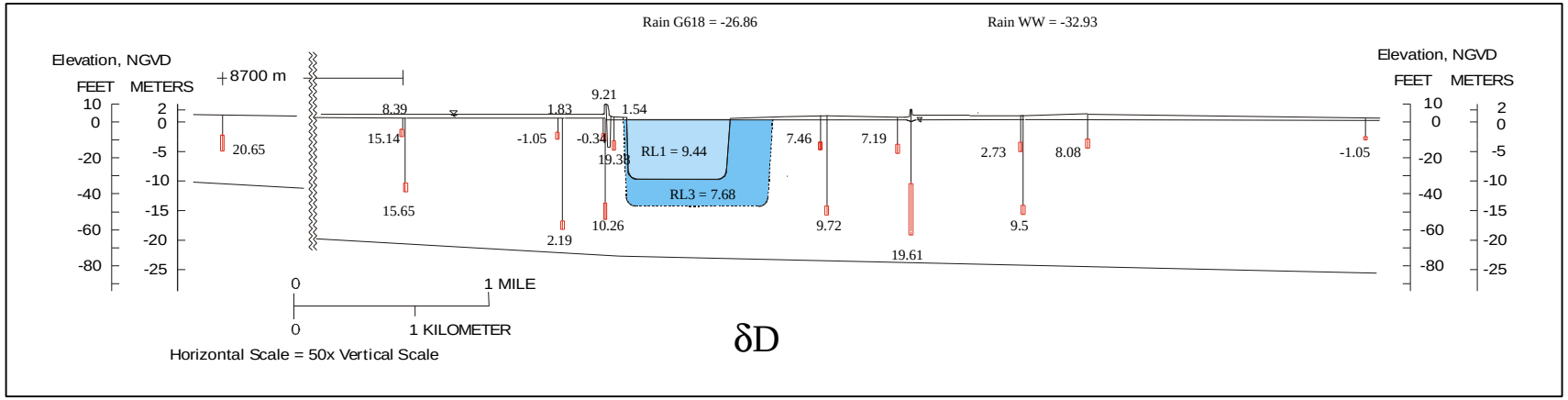

Sampling Date - November 10, 1998

Ambient Rainfall (in)
- Previous Day - 0.04
- Previous 5 Days - 3.21
- Previous 30 Days - 5.00

Average Flow Through Gate S333 (cfs)
- Previous Day - 0.00
- Previous 5 Days - 25.70
- Previous 30 Days - 91.86

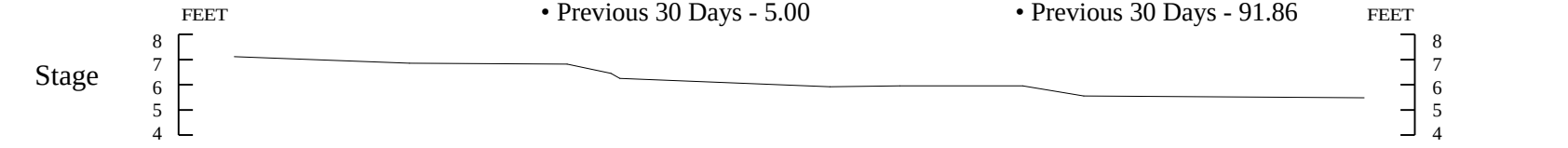

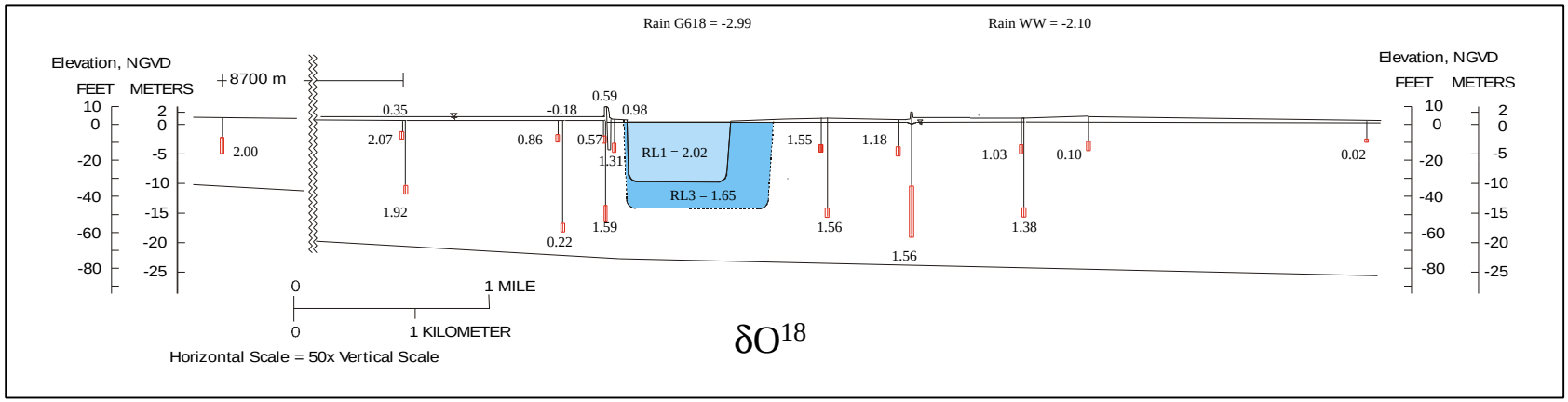

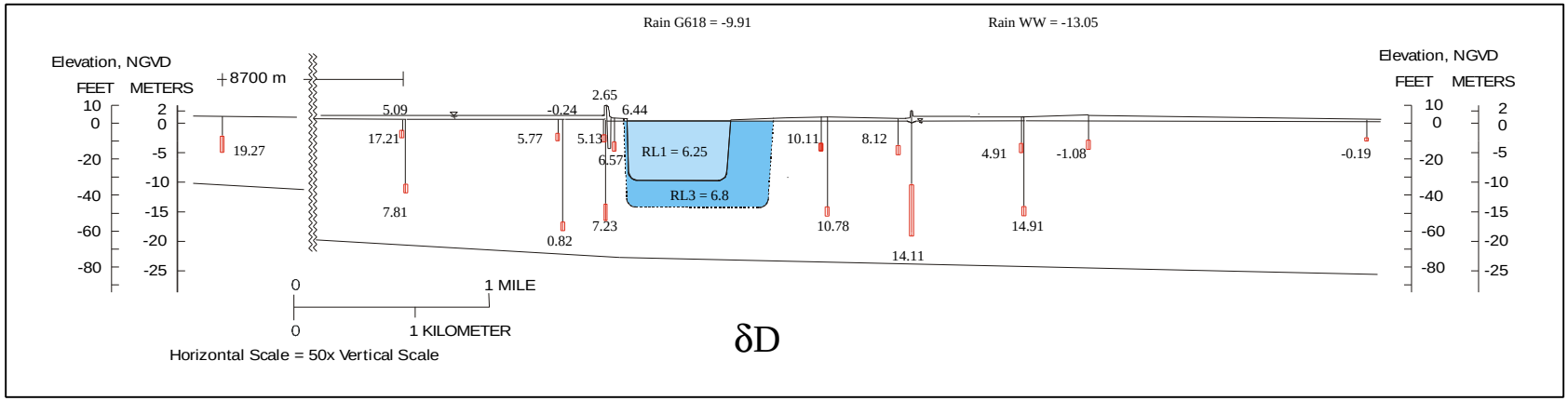

Sampling Date - December 10, 1998

Ambient Rainfall (in)
- Previous Day - 0.02
- Previous 5 Days - 0.07
- Previous 30 Days - 0.30

Average Flow Through Gate S333 (cfs)
- Previous Day - 566.27
- Previous 5 Days - 347.98
- Previous 30 Days - 99.95

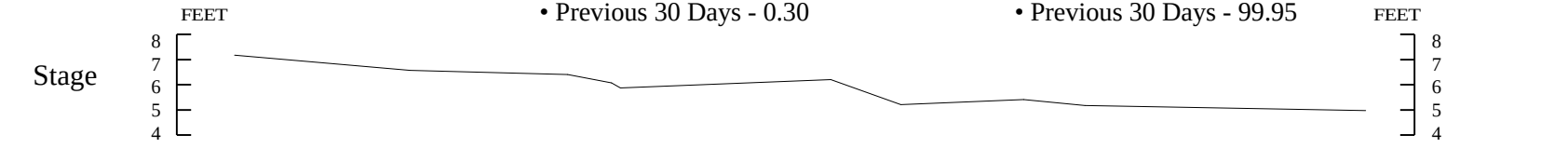

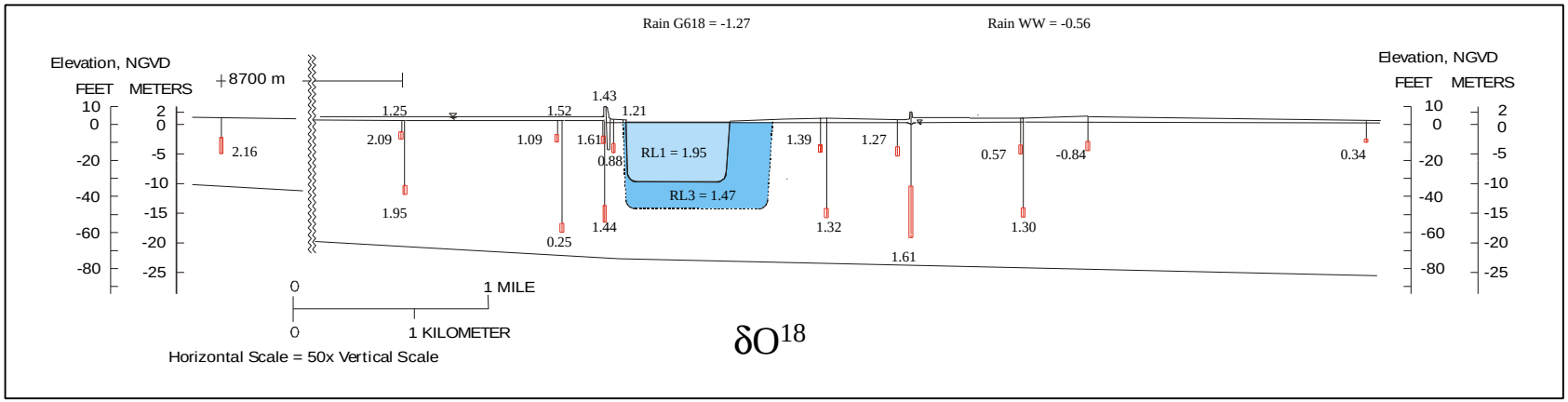

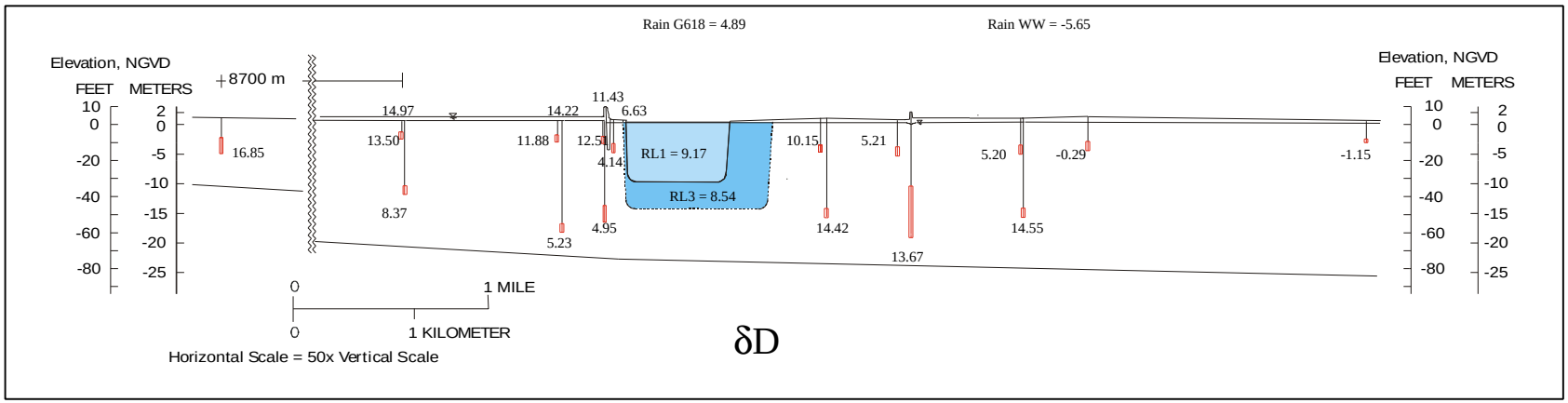

A.6 Isotope Tables for Samples Analyzed by Walter Wilcox

Table A.6.1 Oxygen-18 Sample Analysis

Month	Site	Incubation Date	Sample Value $^{Sample}R_{ref\ gas}$	Lab Standard Value $^{LS}R_{ref\ gas}$	Sample Values Relative to VSMOW, ‰
Jul-97	G3551	6/10/1999	40.4760	39.6720	-0.13
	G3552	6/10/1999	41.8850	39.6720	1.23
	G3553	6/10/1999	41.6260	39.6720	0.98
	G3554	6/10/1999	41.4000	39.6720	0.76
	G3555	6/10/1999	40.5890	39.6720	-0.02
	WELL 29	12/6/1998	41.2170	38.7030	1.52
	G618	12/6/1998	42.2760	38.7030	2.55
	2M3	6/10/1999	41.0160	39.6720	0.39
	3M4	6/10/1999	41.4210	39.6720	0.78
	4M5	6/10/1999	40.9760	39.6720	0.36
	G3439	6/10/1999	38.6960	39.6720	-1.84
	G3575	6/10/1999	41.1200	39.6720	0.49
	G3577	6/10/1999	39.4920	39.6720	-1.07
	G3578	6/10/1999	42.7290	39.6720	2.05
Sep-97	G3551	5/3/1999	41.6210	39.7720	0.88
	G3552	5/3/1999	41.8920	39.7720	1.14
	G3553	5/3/1999	41.4890	39.7720	0.75
	WELL 30	5/3/1999	42.1740	39.7720	1.41
	G3554	5/3/1999	41.4610	39.7720	0.73
	G3555	5/3/1999	40.0600	39.7720	-0.62
	G3575	5/3/1999	42.5130	39.7720	1.74
	G3577	5/3/1999	42.1140	39.7720	1.36
	G3578	5/3/1999	42.6460	39.7720	1.87
	2M3	5/3/1999	41.6140	39.7720	0.87
	3M4	5/3/1999	41.7260	39.7720	0.98
	4M5	5/3/1999	41.7450	39.7720	1.00
	G618	5/3/1999	42.4460	39.7720	1.68
	G3439	5/3/1999	40.5710	39.7720	-0.13
Nov-97	G3439	12/6/1998	40.0930	38.7030	0.44
Dec-97	2M3	12/6/1998	40.9950	38.7030	1.31
Jan-98	G3551	6/7/1999	41.3480	39.7490	0.64
	G3352	6/7/1999	41.1980	39.7490	0.50
	G3661	6/7/1999	41.8650	39.7490	1.14
	G3553	6/7/1999	41.4740	39.7490	0.76
	G3554	6/7/1999	41.4360	39.7490	0.72
	G3662	6/7/1999	42.6620	39.7490	1.91
	G3555	6/7/1999	39.4410	39.7490	-1.20

Month	Site	Incubation Date	Sample Value $^{Sample}R_{ref\ gas}$	Lab Standard Value $^{LS}R_{ref\ gas}$	Sample Values Relative to VSMOW, ‰
	WELL 29	6/7/1999	42.8260	39.7490	2.06
	G618	6/7/1999	42.2950	39.7490	1.55
	2M3	6/7/1999	41.5250	39.7490	0.81
	3M4	6/7/1999	41.3870	39.7490	0.68
	4M5	6/7/1999	41.6940	39.7490	0.97
	G3439	6/7/1999	41.0630	39.7490	0.37
	G3575	6/7/1999	41.4170	39.7490	0.71
	G3577	6/7/1999	41.0540	39.7490	0.36
	G3663	6/7/1999	40.7490	39.7490	0.06
	G3578	6/10/1999	42.4940	39.6720	1.82
	G3664	6/7/1999	42.6240	39.7490	1.87
	RAIN-WW	6/7/1999	35.8230	39.7490	-4.69
Feb-98	G3551	12/4/1998	40.9080	38.5530	1.37
	G3352	12/4/1998	40.8660	38.5530	1.33
	G3661	12/4/1998	38.7650	38.5530	1.03
	G3553	12/4/1998	40.6410	38.5530	1.11
	G3554	12/4/1998	40.1590	38.5530	0.65
	G3662	12/4/1998	40.6790	38.5530	1.15
	G3555	12/4/1998	38.7830	38.5530	-0.68
	WELL 29	12/4/1998	40.8010	38.5530	1.27
	G618	12/4/1998	40.7040	38.5530	1.17
	2M3	12/4/1998	40.6840	38.5530	1.15
	3M4	12/4/1998	40.5080	38.5530	0.99
	4M5	12/4/1998	36.1840	38.5530	0.94
	G3439	12/4/1998	40.0510	38.5530	0.54
	G3575	12/4/1998	40.2670	38.5530	0.75
	G3577	12/4/1998	40.8950	38.5530	1.36
	G3663	12/4/1998	40.3570	38.5530	0.84
	G3578	12/4/1998	41.3650	38.5530	1.81
	G3664	12/4/1998	41.2560	38.5530	1.71
	RAIN-WW	12/4/1998	36.8560	38.5530	-2.54
Mar-98	G3551	10/2/1998	41.0750	39.8940	0.24
	G3552	10/2/1998	39.5560	39.8940	0.86
	G3661	10/2/1998	41.5370	39.8940	0.68
	G3553	12/6/1998	40.5320	38.7030	0.86
	G3554	12/6/1998	40.5840	38.7030	0.91
	G3662	12/6/1998	40.5570	38.7030	0.89
	G3555	12/6/1998	39.0010	38.7030	-0.61
	WELL 30	12/6/1998	40.6780	38.7030	1.00
	G618	5/3/1999	42.2290	39.7720	1.47
	2M3	10/2/1998	41.2220	39.8940	0.38

Month	Site	Incubation Date	Sample Value $^{Sample}R_{ref\ gas}$	Lab Standard Value $^{LS}R_{ref\ gas}$	Sample Values Relative to VSMOW, ‰
	3M4	10/2/1998	41.5400	39.8940	0.68
	4M5	12/6/1998	40.2430	38.7030	0.58
	G3439	10/2/1998	39.8320	39.8940	-0.96
	G3575	10/2/1998	41.5040	39.8940	0.65
	G3577	10/2/1998	42.2780	39.8940	1.40
	G3663	10/10/1998	41.8560	39.8940	0.99
	G3578	10/10/1998	41.4590	39.3507	1.13
	G3664	10/10/1998	42.2120	39.3507	1.86
Apr-98	G3551	10/10/1998	41.1450	39.3507	0.83
	G3552	10/10/1998	40.2240	39.3507	-0.06
	G3661	5/3/1999	41.7320	39.7720	0.99
	G3553	10/10/1998	40.6770	39.3507	0.38
	G3554	10/10/1998	40.5870	39.3507	0.29
	G3662	10/10/1998	41.8570	39.3507	1.52
	G3555	10/10/1998	39.9620	39.3507	-0.31
	WELL30	10/10/1998	41.9380	39.3507	1.59
	G618	12/6/1998	41.2080	38.7030	1.52
	2M3	10/10/1998	41.5910	39.3507	1.26
	3M4	10/10/1998	41.2920	39.3507	0.97
	4M5	10/10/1998	41.4050	39.3507	1.08
	G3575	10/10/1998	42.1580	39.3507	1.81
	G3577	10/10/1998	41.8260	39.3507	1.49
	G3663	12/6/1998	39.8150	38.7030	0.17
	G3578	10/10/1998	41.9110	39.3507	1.57
	G3664	10/10/1998	42.1900	39.3507	1.84
	RAIN-WW	12/6/1998	36.6150	38.7030	-2.92
May-98	G3551	10/10/1998	41.3990	39.3507	1.07
	G3552	10/10/1998	40.5000	39.3507	0.21
	G3661	10/10/1998	41.8710	39.3507	1.53
	G3553	2/11/1999	41.1110	39.4470	0.70
	G3554	2/11/1999	41.0430	39.4470	0.64
	G3662	2/11/1999	41.6300	39.4470	1.20
	G3555	2/11/1999	40.3780	39.4470	0.00
	WELL 30	2/11/1999	41.5670	39.4470	1.14
	G618	2/11/1999	42.7620	39.4470	2.29
	2M3	2/11/1999	42.5060	39.4470	2.05
	3M4	2/11/1999	42.4830	39.4470	2.03
	4M5	2/11/1999	42.2930	39.4470	1.84
	G3439	2/11/1999	40.7150	39.4470	0.32
	G3575	2/11/1999	43.5790	39.4470	3.08
	G3577	2/11/1999	43.9020	39.4470	3.39

Month	Site	Incubation Date	Sample Value $^{Sample}R_{ref\ gas}$	Lab Standard Value $^{LS}R_{ref\ gas}$	Sample Values Relative to VSMOW, ‰
	G3663	2/11/1999	40.6680	39.4470	0.28
	G3578	2/11/1999	43.2250	39.4470	2.74
	G3664	5/3/1999	42.6080	39.7720	1.83
	RAIN-WW	2/11/1999	38.6090	39.4470	-1.71
Jun-98	G3551	2/8/1999	41.7310	39.2990	1.44
	G3552	2/8/1999	41.5030	39.2990	1.22
	G3661	8/20/1998	41.7150	39.3507	1.38
	G3553	2/8/1999	41.3430	39.2990	1.07
	G3554	2/8/1999	41.2870	39.2990	1.02
	G3662	8/20/1998	41.1260	39.3507	0.81
	G3555	2/8/1999	40.6600	39.2990	0.41
	WELL 30	2/8/1999	41.7130	39.2990	1.43
	G618	2/8/1999	43.7910	39.2990	3.43
	2M3	2/8/1999	43.3130	39.2990	2.97
	3M4	2/8/1999	42.8550	39.2990	2.53
	4M5	2/8/1999	43.0670	39.2990	2.73
	G3439	2/8/1999	40.6910	39.2990	0.44
	G3575	2/8/1999	44.5540	39.2990	4.17
	G3660	9/11/1998	40.8070	39.1520	0.69
	G3577	5/17/1999	44.3930	39.5310	3.77
	G3663	5/17/1999	40.6920	39.5310	0.21
	G3578	5/17/1999	43.4940	39.5310	2.91
	G3664	5/17/1999	42.3850	39.5310	1.84
	RAIN-WW	5/17/1999	38.3550	39.5310	-2.05
	RAIN-G618	5/17/1999	37.9970	39.5310	-2.39
Jul-98	G3551	2/1/1999	42.0320	39.3960	1.64
	G3552	2/1/1999	41.3900	39.3960	1.02
	G3661	2/1/1999	41.6440	39.3960	1.27
	G3553	2/1/1999	41.6770	39.3960	1.30
	G3554	2/1/1999	40.8500	39.3960	0.50
	G3662	2/1/1999	41.3460	39.3960	0.98
	G3555	2/1/1999	40.6390	39.3960	0.30
	WELL 30	2/4/1999	41.6680	39.4450	1.24
	G618	2/1/1999	43.4890	39.3960	3.04
	2M3	2/4/1999	42.2860	39.4450	1.84
	3M4	2/1/1999	41.9910	39.3960	1.60
	4M5	5/3/1999	42.1950	39.7720	1.43
	G3439	2/1/1999	40.3410	39.3960	0.01
	G3575	2/1/1999	43.7340	39.3960	3.28
	G3660	2/4/1999	41.8320	39.4450	1.40
	G3577	2/4/1999	44.0650	39.4450	3.55

Month	Site	Incubation Date	Sample Value $^{Sample}R_{ref\ gas}$	Lab Standard Value $^{LS}R_{ref\ gas}$	Sample Values Relative to VSMOW, ‰
	G3663	2/1/1999	41.6230	39.3960	1.25
	G3578	2/1/1999	42.6630	39.3960	2.25
	G3664	2/4/1999	42.5690	39.4450	2.11
	RAIN-WW	2/4/1999	38.5390	39.4450	-1.77
	RAIN-G618	2/4/1999	38.7920	39.4450	-1.53
	S3577	2/4/1999	44.6110	39.4450	4.08
	S3578	2/4/1999	43.1420	39.4450	2.66
Aug-98	G3551	4/27/1999	42.5770	39.7960	1.78
	G3552	4/27/1999	42.0500	39.7960	1.27
	G3661	4/27/1999	41.6950	39.7960	0.93
	G3553	4/27/1999	41.5410	39.7960	0.78
	G3554	4/27/1999	41.1610	39.7960	0.41
	G3662	4/27/1999	41.4150	39.7960	0.66
	G3555	4/27/1999	40.5540	39.7960	-0.17
	WELL 29	4/27/1999	41.7440	39.7960	0.98
	G618	4/27/1999	43.2450	39.7960	2.42
	2M3	4/27/1999	42.6330	39.7960	1.83
	3M4	4/27/1999	42.9020	39.7960	2.09
	4M5	4/27/1999	42.5400	39.7960	1.74
	G3575	4/27/1999	42.4860	39.7960	1.69
	G3660	4/27/1999	41.7330	39.7960	0.97
	G3577	4/27/1999	42.6610	39.7960	1.86
	G3663	4/27/1999	41.0530	39.7960	0.31
	G3578	4/27/1999	42.7180	39.7960	1.91
	G3664	4/27/1999	42.1300	39.7960	1.35
	RAIN-WW	4/27/1999	38.3420	39.7960	-2.30
	RAIN-G618	4/27/1999	37.1710	39.7960	-3.43
	S3577	4/27/1999	44.9920	39.7960	4.11
	S3578	4/27/1999	43.5520	39.7960	2.72
Sep-98	G3551	9/8/1998	43.0810	39.3507	2.70
	G3552	9/8/1998	41.0290	39.3507	0.72
	G3661	9/8/1998	42.0000	39.3507	1.65
	G3553	9/8/1998	40.9150	39.3507	0.61
	G3554	9/8/1998	40.7080	39.3507	0.41
	G3662	9/8/1998	41.2690	39.3507	0.95
	G3555	9/8/1998	40.1500	39.3507	-0.13
	WELL 29	9/8/1998	41.0940	39.3507	0.78
	G618	9/8/1998	38.9770	39.3507	2.74
	2M3	2/4/1999	41.9990	39.4450	1.56
	3M4	2/4/1999	42.4750	39.4450	2.02
	4M5	2/4/1999	42.2130	39.4450	1.77

Month	Site	Incubation Date	Sample Value $^{Sample}R_{ref\ gas}$	Lab Standard Value $^{LS}R_{ref\ gas}$	Sample Values Relative to VSMOW, ‰
	G3439	9/8/1998	41.5980	39.3507	1.27
	G3575	2/4/1999	42.2220	39.4450	1.78
	G3660	2/4/1999	42.0480	39.4450	1.61
	G3577	2/4/1999	42.4940	39.4450	2.04
	G3663	2/4/1999	40.6060	39.4450	0.22
	G3578	2/4/1999	42.3290	39.4450	1.88
	G3664	2/4/1999	42.5490	39.4450	2.09
	RAIN-WW	2/8/1999	38.8070	39.2990	-1.38
	RAIN-G618	2/8/1999	38.8860	39.2990	-1.30
	S3575	2/11/1999	42.6850	39.4470	2.22
	S3577	2/8/1999	43.1020	39.2990	2.77
	S3578	2/8/1999	42.7410	39.2990	2.42
	RAIN-WW/24	2/11/1999	35.6760	39.4470	-4.54
	RAIN-G618/24	2/11/1999	36.3350	39.4470	-3.90
Oct-98	G3551	4/13/1999	42.2790	39.4500	1.83
	G3552	4/13/1999	41.5040	39.4500	1.08
	G3661	4/13/1999	41.6590	39.4500	1.23
	G3553	4/13/1999	41.5130	39.4500	1.09
	G3554	4/13/1999	41.0170	39.4500	0.61
	G3662	4/13/1999	41.4670	39.4500	1.04
	G3555	4/13/1999	40.0660	39.4500	-0.31
	WELL 30	4/13/1999	42.0740	39.4500	1.63
	G618	4/13/1999	42.9010	39.4500	2.43
	2M3	5/3/1999	40.7880	39.7720	0.08
	3M4	4/13/1999	40.7710	39.4500	0.37
	4M5	4/13/1999	41.2360	39.4500	0.82
	G3439	4/13/1999	39.2930	39.4500	-1.05
	G3575	4/13/1999	40.5480	39.4500	0.16
	G3660	4/13/1999	42.3150	39.4500	1.86
	G3577	4/13/1999	40.9340	39.4500	0.53
	G3663	4/13/1999	40.3130	39.4500	-0.07
	G3578	4/13/1999	41.8180	39.4500	1.38
	G3664	4/15/1999	42.0410	39.0970	1.94
	RAIN-WW	4/15/1999	36.9310	39.0970	-2.99
	RAIN-G618	4/15/1999	36.1710	39.0970	-3.72
	S3575	4/15/1999	41.0240	39.0970	0.96
	S3577	4/15/1999	40.7290	39.0970	0.67
	S3578	4/15/1999	40.8280	39.0970	0.77
Nov-98	G3551	4/15/1999	41.3900	39.0970	1.31
	G3552	4/15/1999	41.6420	39.0970	1.55

Month	Site	Incubation Date	Sample Value $^{Sample}R_{ref\ gas}$	Lab Standard Value $^{LS}R_{ref\ gas}$	Sample Values Relative to VSMOW, ‰
	G3661	4/15/1999	41.6440	39.0970	1.56
	G3553	4/15/1999	41.2580	39.0970	1.18
	G3554	4/15/1999	41.0990	39.0970	1.03
	G3662	4/15/1999	41.4650	39.0970	1.38
	G3555	4/21/1999	40.4140	39.3790	0.10
	WELL 30	4/21/1999	41.9280	39.3790	1.56
	G618	4/21/1999	42.3830	39.3790	2.00
	2M3	4/21/1999	41.1780	39.3790	0.83
	3M4	4/21/1999	41.5770	39.3790	1.22
	4M5	4/21/1999	41.2390	39.3790	0.89
	G3439	4/21/1999	40.3340	39.3790	0.02
	G3575	4/21/1999	40.9050	39.3790	0.57
	G3660	4/21/1999	41.9680	39.3790	1.59
	G3577	4/21/1999	41.2080	39.3790	0.86
	G3663	4/21/1999	40.5460	39.3790	0.22
	G3578	4/21/1999	42.4650	39.3790	2.07
	G3664	4/21/1999	42.3000	39.3790	1.92
	RAIN-WW	4/21/1999	38.1330	39.3790	-2.10
	RAIN-G618	4/21/1999	37.2170	39.3790	-2.99
	S3575	4/21/1999	40.9220	39.3790	0.59
	S3577	4/21/1999	40.1290	39.3790	-0.18
	S3578	5/20/1999	40.6550	39.3460	0.35
Dec-98	G3551	5/17/1999	41.3920	39.5310	0.88
	G3552	5/17/1999	41.9220	39.5310	1.39
	G3661	5/17/1999	41.8500	39.5310	1.32
	G3553	5/17/1999	41.7950	39.5310	1.27
	G3554	5/20/1999	40.8880	39.3460	0.57
	G3662	5/20/1999	41.6400	39.3460	1.30
	G3555	5/20/1999	39.4220	39.3460	-0.84
	WELL 30	5/20/1999	41.9630	39.3460	1.61
	G618	5/20/1999	42.5320	39.3460	2.16
	2M3	5/20/1999	41.5180	39.3460	1.18
	3M4	5/20/1999	41.6170	39.3460	1.28
	4M5	5/20/1999	41.4970	39.3460	1.16
	G3439	5/20/1999	40.6450	39.3460	0.34
	G3575	5/20/1999	41.9630	39.3460	1.61
	G3660	5/20/1999	41.7820	39.3460	1.44
	G3577	5/20/1999	41.4190	39.3460	1.09
	G3663	5/20/1999	40.5490	39.3460	0.25
	G3578	5/20/1999	42.4630	39.3460	2.09
	G3664	5/20/1999	42.3190	39.3460	1.95

Month	Site	Incubation Date	Sample Value $^{Sample}R_{ref\ gas}$	Lab Standard Value $^{LS}R_{ref\ gas}$	Sample Values Relative to VSMOW, ‰
	RAIN-WW	5/20/1999	39.7170	39.3460	-0.56
	RAIN-G618	5/20/1999	38.9800	39.3460	-1.27
	S3575	5/20/1999	41.7730	39.3460	1.43
	S3577	5/20/1999	41.8650	39.3460	1.52
	S3578	5/20/1999	41.5870	39.3460	1.25

Table A.6.2 Deuterium Sample Analysis
(All samples analyzed using the chromium method)

Month	Site	Analysis Date	Sample Value $^{Sample}R_{ref\ gas}$	Lab Standard Value $^{LS}R_{ref\ gas}$	Sample Values Relative to VSMOW, ‰
Mar-96	G3551	08/26/99	493.6610	463.9260	15.42
	G3552	08/26/99	475.6360	463.9260	3.16
	G3553	08/26/99	468.0300	463.9260	-2.01
	Well29	08/26/99	487.5430	463.9260	11.26
	2M3	08/26/99	477.9130	463.9260	4.71
	3M4	08/26/99	491.5970	463.9260	14.01
	4M5	08/26/99	494.0920	463.9260	15.71
	G3575	08/26/99	482.6290	463.9260	7.92
Apr-96	3M4	08/26/99	492.2540	463.9260	14.46
	G3577	08/26/99	495.3170	463.9260	16.54
Jun-96	G3551	09/24/99	484.8650	460.7373	11.64
	G3552	09/24/99	478.0450	460.7373	7.00
	G3553	09/24/99	470.2640	460.7373	1.69
	G3554	09/24/99	474.2260	460.7373	4.39
	G3555	09/24/99	470.8240	460.7373	2.08
	2M3	09/24/99	477.2500	460.7373	6.45
	3M4	09/24/99	470.6640	460.7373	1.97
	4M5	09/24/99	475.9440	460.7373	5.56
	G3575	09/24/99	464.6000	460.7373	-2.16
Aug-96	G3551	09/24/99	479.3030	460.7373	7.85
	G3552	09/24/99	474.5760	460.7373	4.63
	G3553	09/24/99	477.3170	460.7373	6.50
	G3554	09/24/99	472.3820	460.7373	3.14
	G3555	09/24/99	468.8550	460.7373	0.73
	Well29	09/24/99	485.0130	460.7373	11.74
	3M4	09/24/99	479.4980	460.7373	7.99
	G3575	09/24/99	478.3560	460.7373	7.21
Oct-96	G3551	09/24/99	484.0090	460.7373	11.06
	G3552	09/24/99	475.0610	460.7373	4.96
	G3553	09/24/99	476.5360	460.7373	5.97
	G3554	09/24/99	465.1170	460.7373	-1.81
	G3555	09/24/99	469.2360	460.7373	0.99
	Well29	09/28/99	475.5720	453.6440	10.22

Month	Site	Analysis Date	Sample Value $^{Sample}R_{ref\ gas}$	Lab Standard Value $^{LS}R_{ref\ gas}$	Sample Values Relative to VSMOW, ‰
	3M4	09/28/99	478.1250	453.6440	11.96
	G3575	09/28/99	476.2500	453.6440	10.68
	Well29	09/28/99	476.6040	453.6440	10.92
Feb-97	G3551	09/28/99	481.1270	453.6440	14.02
	G3552	09/28/99	480.2100	453.6440	13.39
	G3553	09/28/99	474.1100	453.6440	9.22
	G3554	09/28/99	469.6800	453.6440	6.18
	G3555	09/28/99	462.6330	453.6440	1.36
	Well29	09/28/99	473.8390	453.6440	9.03
	3M4	09/28/99	483.5270	453.6440	15.66
	G3575	09/28/99	482.6970	453.6440	15.09
Mar-97	G3551	09/28/99	479.1220	453.6440	12.65
	G3552	09/28/99	473.7160	453.6440	8.95
	G3553	09/28/99	466.8680	453.6440	4.26
	G3554	09/28/99	470.9150	453.6440	7.03
	G3555	09/28/99	466.1740	453.6440	3.78
	Well29	09/28/99	476.0380	453.6440	10.54
	3M4	09/28/99	484.6930	453.6440	16.46
	G3575	09/28/99	476.0840	453.6440	10.57
Apr-97	G3551	09/28/99	483.0400	453.6440	15.33
	G3552	09/28/99	478.2000	453.6440	12.02
	G3553	09/28/99	474.6790	453.6440	9.60
	G3554	09/28/99	467.5610	453.6440	4.73
	G3555	09/28/99	464.2990	453.6440	2.50
	Well29	09/28/99	481.1930	453.6440	14.06
	2M3	10/01/99	480.2110	460.3100	8.77
	3M4	10/01/99	490.5330	460.3100	15.80
	4M5	10/01/99	480.8940	460.3100	9.23
	G3575	10/01/99	487.2760	460.3100	13.58
May-97	2M3	08/26/99	487.6320	463.9260	11.32
	4M5	08/26/99	487.7550	463.9260	11.40
Jun-97	2M3	10/01/99	482.9850	460.3100	10.66
	4M5	10/01/99	484.1040	460.3100	11.42
Jul-97	G3551	10/04/99	473.1860	449.5895	11.40
	G3552	10/04/99	475.1200	449.5895	12.73
	G3553	10/04/99	467.1260	449.5895	7.24

Month	Site	Analysis Date	Sample Value $^{Sample}R_{ref\ gas}$	Lab Standard Value $^{LS}R_{ref\ gas}$	Sample Values Relative to VSMOW, ‰
	2M3	10/01/99	453.7080	460.3100	-9.30
	4M5	10/01/99	471.1590	460.3100	2.60
	G3575	10/01/99	428.6200	460.3100	-26.39
Jul-97	G3551	10/04/99	458.0720	449.5895	1.03
	G3552	10/04/99	468.5240	449.5895	8.20
	G3553	10/04/99	465.4650	449.5895	6.10
	G3554	10/04/99	468.8540	449.5895	8.43
	G3555	10/04/99	469.9500	449.5895	9.18
	2M3	10/04/99	462.3610	449.5895	3.97
	3M4	10/04/99	464.0860	449.5895	5.16
	4M5	10/04/99	463.2920	449.5895	4.61
	G3439	10/04/99	439.3980	449.5895	-11.79
	G3575	10/04/99	460.2900	449.5895	2.55
	G3577	10/04/99	444.4260	449.5895	-8.34
	G3578	10/04/99	480.8310	449.5895	16.65
Sep-97	G3551	10/07/99	472.4830	466.215	-0.54
	G3552	10/07/99	474.9910	466.215	1.16
	G3553	10/07/99	475.0210	466.215	1.18
	G3554	10/07/99	475.4100	466.215	1.44
	G3555	10/07/99	467.8570	466.215	-3.68
	WELL 30	10/07/99	474.6720	466.215	0.94
	G618	10/07/99	484.1640	466.215	7.39
	2M3	10/07/99	482.8100	466.215	6.47
	3M4	10/07/99	475.6390	466.215	1.60
	4M5	10/07/99	483.4450	466.215	6.90
	G3439	10/07/99	457.1240	466.215	-10.97
	G3575	10/07/99	476.8150	466.215	2.40
	G3577	10/07/99	479.2700	466.215	4.06
	G3578	10/07/99	482.1960	466.215	6.05
Oct-97	2M3	10/07/99	473.8970	466.215	0.42
	4M5	10/07/99	475.2310	466.215	1.32
Nov-97	4M5	10/07/99	484.2450	466.215	7.44
Dec-97	G3553	10/07/99	475.3450	466.215	1.40
	2M3	10/07/99	479.8830	466.215	4.48
	4M5	10/07/99	476.7240	466.215	2.34
	G3577	10/07/99	461.2440	466.215	-8.17

Month	Site	Analysis Date	Sample Value $^{Sample}R_{ref\ gas}$	Lab Standard Value $^{LS}R_{ref\ gas}$	Sample Values Relative to VSMOW, ‰
Jan-98	G3551	09/16/99	467.4160	451.0627	6.42
	G3552	09/16/99	476.4590	451.0627	12.62
	G3661	09/16/99	465.7300	451.0627	5.26
	G3553	09/16/99	470.9710	451.0627	8.86
	G3554	09/16/99	460.0990	451.0627	1.40
	G3662	09/16/99	469.0390	451.0627	7.53
	G3555	09/16/99	448.7100	451.0627	-6.41
	WELL 30	09/16/99	466.6710	451.0627	5.91
	G618	09/16/99	477.2980	451.0627	13.20
	2M3	09/16/99	464.5630	451.0627	4.46
	3M4	09/16/99	476.4400	451.0627	12.61
	4M5	09/16/99	461.8880	451.0627	2.63
	G3439	09/16/99	462.4140	451.0627	2.99
	G3575	09/16/99	464.5710	451.0627	4.47
	G3577	09/16/99	465.0030	451.0627	4.76
	G3663	09/16/99	464.8350	451.0627	4.65
	G3578	09/16/99	469.1840	451.0627	7.63
	G3664	09/16/99	488.3390	451.0627	20.77
Feb-98	G3662	09/16/99	472.1560	451.0627	9.67
May-98	G3552	09/16/99	464.8790	451.0627	4.68
	G3664	09/24/99	478.0190	460.7373	6.98
	WELL30	09/24/99	475.0990	460.7373	4.99
Jun-98	RAING618	09/16/99	438.0620	451.0627	-13.71
Jul-98	G3551	7/1/1999	497.4510	473.4514	11.41
	G3552	7/1/1999	485.6820	473.4514	3.46
	G3661	7/1/1999	482.9360	473.4514	1.61
	G3553	7/1/1999	487.0100	473.4514	4.36
	G3554	7/1/1999	484.8590	473.4514	2.91
	G3662	7/1/1999	485.3020	473.4514	3.21
	G3555	7/1/1999	474.6850	473.4514	-3.96
	WELL 30	7/1/1999	490.9620	473.4514	7.03
	G618	7/1/1999	500.7070	473.4514	13.61
	2M3	7/1/1999	500.8420	473.4514	13.70
	3M4	7/1/1999	498.1660	473.4514	11.90
	4M5	7/1/1999	493.0100	473.4514	8.41
	G3439	7/1/1999	482.6190	473.4514	1.40

Month	Site	Analysis Date	Sample Value $^{Sample}R_{ref\ gas}$	Lab Standard Value $^{LS}R_{ref\ gas}$	Sample Values Relative to VSMOW, ‰
	G3575	7/1/1999	499.7570	473.4514	12.97
	G3660	7/1/1999	496.3360	473.4514	10.66
	G3577	7/1/1999	508.6030	473.4514	18.95
	G3663	7/1/1999	481.6530	473.4514	0.74
	G3578	7/1/1999	499.2200	473.4514	12.61
	G3664	7/1/1999	498.5510	473.4514	12.16
	RAIN-WW	7/1/1999	474.6730	473.4514	-3.97
	RAIN-G618	7/1/1999	481.3300	473.4514	0.52
	S3577	7/1/1999	504.2810	473.4514	16.03
	S3578	7/1/1999	495.0860	473.4514	9.82
Aug-98	G3551	7/1/1999	504.1560	473.4514	15.94
	G3552	7/1/1999	492.2210	473.4514	7.88
	G3661	7/1/1999	490.2810	473.4514	6.57
	G3553	7/1/1999	493.2920	473.4514	8.60
	G3554	7/1/1999	486.0340	473.4514	3.70
	G3662	7/1/1999	495.3250	473.4514	9.98
	G3555	7/1/1999	483.6890	473.4514	2.12
	WELL 29	7/1/1999	487.6220	473.4514	4.77
	G618	7/1/1999	511.6440	473.4514	21.00
	2M3	8/3/1999	500.8310	478.2518	10.40
	3M4	8/3/1999	505.0760	478.2518	13.26
	4M5	8/3/1999	494.4140	478.2518	6.08
	G3575	8/3/1999	499.9350	478.2518	9.80
	G3660	8/3/1999	494.8170	478.2518	6.36
	G3577	8/3/1999	498.8540	478.2518	9.07
	G3663	8/3/1999	488.9870	478.2518	2.43
	G3578	8/3/1999	507.9340	478.2518	15.19
	G3664	8/3/1999	499.0990	478.2518	9.24
	RAIN-WW	8/3/1999	463.5460	478.2518	-14.70
	RAIN-G618	8/3/1999	459.8260	478.2518	-17.20
	S3577	8/3/1999	510.5680	478.2518	16.96
	S3578	8/3/1999	495.9220	478.2518	7.10
Sep-98	G3551	8/3/1999	505.0070	478.2518	13.22
	G3552	8/3/1999	482.1460	478.2518	-2.17
	G3661	8/3/1999	493.3510	478.2518	5.37
	G3553	8/3/1999	484.1420	478.2518	-0.83

Month	Site	Analysis Date	Sample Value $^{Sample}R_{ref\ gas}$	Lab Standard Value $^{LS}R_{ref\ gas}$	Sample Values Relative to VSMOW, ‰
	G3554	8/3/1999	487.3640	478.2518	1.34
	G3662	8/3/1999	487.3580	478.2518	1.33
	G3555	8/3/1999	472.7410	478.2518	-8.51
	WELL 29	8/12/1999	475.6440	460.5110	5.52
	G618	8/12/1999	498.9230	460.5110	21.38
	2M3	8/12/1999	479.7520	460.5110	8.31
	3M4	8/12/1999	484.2280	460.5110	11.36
	4M5	8/12/1999	478.1950	460.5110	7.25
	G3439	8/12/1999	477.5620	460.5110	6.82
	G3575	8/12/1999	482.9050	460.5110	10.46
	G3660	8/12/1999	477.0310	460.5110	6.46
	G3577	8/12/1999	484.9280	460.5110	11.84
	G3663	8/12/1999	471.8040	460.5110	2.90
	G3578	8/12/1999	482.5580	460.5110	10.23
	G3664	8/12/1999	475.6850	460.5110	5.54
	RAIN-WW	8/12/1999	463.4740	460.5110	-2.78
	RAIN-G618	8/12/1999	460.4100	460.5110	-4.87
	S3575	8/12/1999	487.4650	460.5110	13.57
	S3577	8/12/1999	496.7270	460.5110	19.88
	S3578	8/12/1999	487.0720	460.5110	13.30
	RAIN-WW/24	8/12/1999	419.2200	460.5110	-32.93
	RAIN-G618/24	8/12/1999	440.3100	460.5110	-18.56
Oct-98	G3551	8/16/1999	493.8880	458.4538	19.38
	G3552	8/16/1999	476.4090	458.4538	7.46
	G3661	8/16/1999	479.7250	458.4538	9.72
	G3553	8/16/1999	476.0170	458.4538	7.19
	G3554	8/16/1999	469.4910	458.4538	2.73
	G3662	8/16/1999	479.9130	458.4538	9.85
	G3555	8/16/1999	477.3240	458.4538	8.08
	WELL 30	8/16/1999	494.2210	458.4538	19.61
	G618	8/16/1999	495.7470	458.4538	20.65
	2M3	8/16/1999	462.2010	458.4538	-2.24
	3M4	8/16/1999	478.4050	458.4538	8.82
	4M5	8/16/1999	462.6200	458.4538	-1.95
	G3439	8/16/1999	461.6910	458.4538	-2.59
	G3575	8/16/1999	464.9870	458.4538	-0.34

Month	Site	Analysis Date	Sample Value $^{Sample}R_{ref\ gas}$	Lab Standard Value $^{LS}R_{ref\ gas}$	Sample Values Relative to VSMOW, ‰
	G3660	8/16/1999	480.5210	458.4538	10.26
	G3577	8/16/1999	463.9400	458.4538	-1.05
	G3663	8/16/1999	468.6990	458.4538	2.19
	G3578	8/16/1999	487.6760	458.4538	15.14
	G3664	8/16/1999	488.4190	458.4538	15.65
	RAIN-WW	8/16/1999	443.0400	458.4538	-15.31
	RAIN-G618	8/16/1999	426.1190	458.4538	-26.86
	S3575	8/16/1999	478.9740	458.4538	9.21
	S3577	8/16/1999	468.1630	458.4538	1.83
	S3578	8/16/1999	477.7820	458.4538	8.39
Nov-98	G3551	8/17/1999	477.3520	460.6640	6.57
	G3552	8/17/1999	482.5400	460.6640	10.11
	G3661	8/17/1999	483.5290	460.6640	10.78
	G3553	8/17/1999	479.6240	460.6640	8.12
	G3554	8/17/1999	474.9100	460.6640	4.91
	G3662	8/17/1999	489.5940	460.6640	14.91
	G3555	8/17/1999	466.1160	460.6640	-1.08
	WELL 30	8/17/1999	488.4130	460.6640	14.11
	G618	8/17/1999	495.9820	460.6640	19.27
	2M3	8/17/1999	476.7320	460.6640	6.15
	3M4	8/17/1999	480.7570	460.6640	8.89
	4M5	8/17/1999	473.9730	460.6640	4.27
	G3439	8/17/1999	467.4240	460.6640	-0.19
	G3575	8/17/1999	475.2340	460.6640	5.13
	G3660	8/17/1999	478.3110	460.6640	7.23
	G3577	8/17/1999	476.1670	460.6640	5.77
	G3663	8/17/1999	468.9020	460.6640	0.82
	G3578	8/17/1999	492.9610	460.6640	17.21
	G3664	8/17/1999	479.1630	460.6640	7.81
	RAIN-WW	8/17/1999	448.5510	460.6640	-13.05
	RAIN-G618	8/17/1999	453.1540	460.6640	-9.91
	S3575	8/26/1999	474.8780	463.9260	2.65
	S3577	8/26/1999	470.6280	463.9260	-0.24
	S3578	8/26/1999	478.4670	463.9260	5.09
Dec-98	G3551	8/26/1999	477.0720	463.9260	4.14
	G3552	8/26/1999	485.9140	463.9260	10.15

Month	Site	Analysis Date	Sample Value $^{Sample}R_{ref\ gas}$	Lab Standard Value $^{LS}R_{ref\ gas}$	Sample Values Relative to VSMOW, ‰
	G3661	8/26/1999	492.1880	463.9260	14.42
	G3553	8/26/1999	478.6410	463.9260	5.21
	G3554	8/26/1999	478.6380	463.9260	5.20
	G3662	8/26/1999	492.3860	463.9260	14.55
	G3555	8/26/1999	470.5500	463.9260	-0.29
	WELL 30	8/26/1999	491.0860	463.9260	13.67
	G618	8/26/1999	495.7730	463.9260	16.85
	2M3	8/26/1999	483.6770	463.9260	8.63
	3M4	8/26/1999	477.8340	463.9260	4.66
	4M5	8/26/1999	480.6890	463.9260	6.60
	G3439	8/26/1999	469.2890	463.9260	-1.15
	G3575	8/26/1999	489.3840	463.9260	12.51
	G3660	8/26/1999	478.2670	463.9260	4.95
	G3577	8/26/1999	488.4500	463.9260	11.88
	G3663	8/26/1999	478.6790	463.9260	5.23
	G3578	8/26/1999	490.8420	463.9260	13.50
	G3664	8/26/1999	483.2880	463.9260	8.37
	RAIN-WW	8/26/1999	462.6740	463.9260	-5.65
	RAIN-G618	8/26/1999	478.1780	463.9260	4.89
	S3575	8/26/1999	487.7940	463.9260	11.43
	S3577	8/26/1999	491.9030	463.9260	14.22
	S3578	8/26/1999	492.9960	463.9260	14.97

Appendix B
Regression Analysis

B.1 Background on Regression Analysis

The linear regression model used to examine the various meteoric water line plots is based upon the Least Squares Method. In this method, a set of *n* observations of response variable y corresponding to predictor variable x is made such that:

$$y^*_i = f^*(x_i) \qquad \text{(Equation B.1.1)}$$

in which y^*_i is the linear response to predictor x_i at the *i*th observation. This linear model is derived such that the sum of the squares of the residuals of individual observations is minimized. A residual is defined as:

$$r_i = y_i - y^*_i \qquad \text{(Equation B.1.2)}$$

in which r_i is the residual and y_i is the observed value at the *i*th observation.

In order to assess the strengths and weaknesses of the modeled regression lines, several diagnostic plots were used. A brief explanation of each of these plots is provided below:

- Residuals vs. Fitted Values

  This graph is helpful in identifying which data points influenced the regression analysis the most. Points that are automatically identified by the plotter are those which had the greatest effect on the regression.

- Square Root of Absolute Residuals vs. Fitted Values

  Much like the Residuals vs. Fitted Values graph, these graphs identify which points had the greatest influence on the regression analysis. However, they do so on an absolute positive scale.

- Normal Quantile Plot of Residuals

  These plots are used to assess whether the errors in the modeled data are normally distributed. If the residuals cluster around the imposed quantile-quantile lines, the errors in the data are indeed normally distributed.

- Residual-Fit Spread Plot

  If the residuals are more closely grouped than the fitted values the regression is valid. A smaller spread in the residuals shows that the modeled line has removed some of the error found in the data set.

- Cook's Distance Plot

  Cook's Distance is a measure of which individual data points influenced the regression coefficients the most. Points the are automatically identified by the plotter are those which had the greatest effect on the regression coefficients.

B.2 Rainfall Regression Analysis

The diagnostic plots (Figures B.2.1 through B.2.5) for the rainfall regression indicate that the points influencing the regression the most were all

collected at the RainWW site near the West Wellfield. The three specific points identified by the plots as the most influential on the regression were collected October 9, 1997, June 1, 1998 and December 10, 1998. Since these values correspond to dates having 6.86", 3.08", and 0.30" respectively in the previous thirty days, it is evident that the regression was not skewed by anomalous data collected solely during drought or flood conditions. This fact coupled with the results of the normal quantile and residual-fit spread plots indicate that the regression is indeed valid.

In conjunction with the diagnostic plots, an analysis of covariance (ANCOVA) was performed on the regression. The ANCOVA indicates that the equation of the rainfall regression line is given by:

$$\delta D = 7.9550\delta^{18}O + 8.9211 \qquad \text{(Equation B.2.1)}$$

The R^2 value of this regression line was calculated to be 0.773. The slope coefficient was found to have a standard error of 0.8878 while the intercept coefficient had a standard error of 2.3982. Overall, the F-statistic of the regression was calculated to be 80.29 on 1 and 23 degrees of freedom. Combined, this statistical analysis shows that the linear rainfall regression is indeed valid and normally distributed (Sokal 1995, *Axum* 6.0).

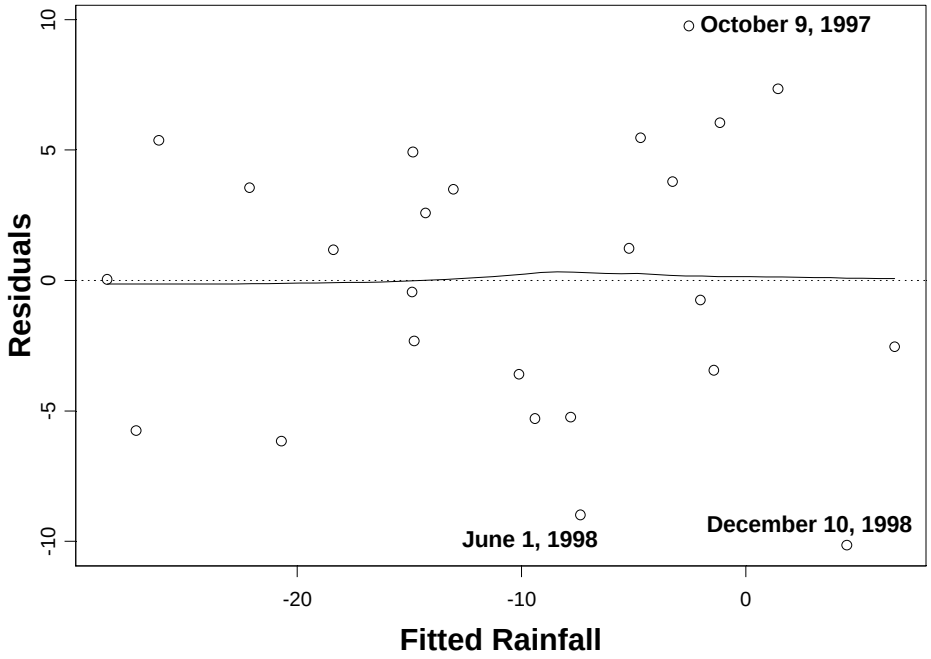

Figure B.2.1 Residuals vs. Fitted Values (Rainfall)

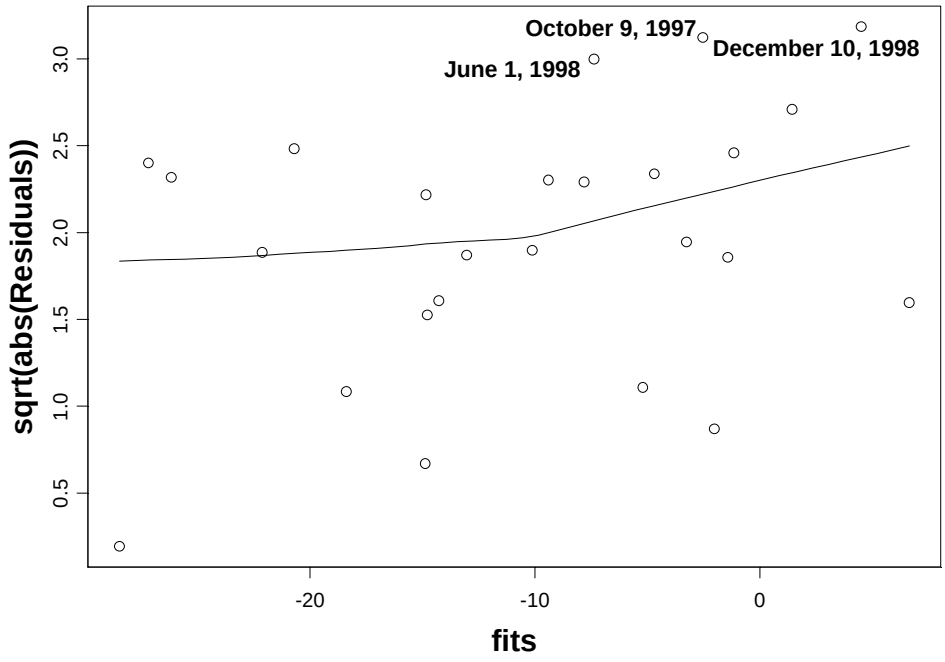

Figure B.2.2 Square Root of Absolute Residuals vs. Fitted Values (Rainfall)

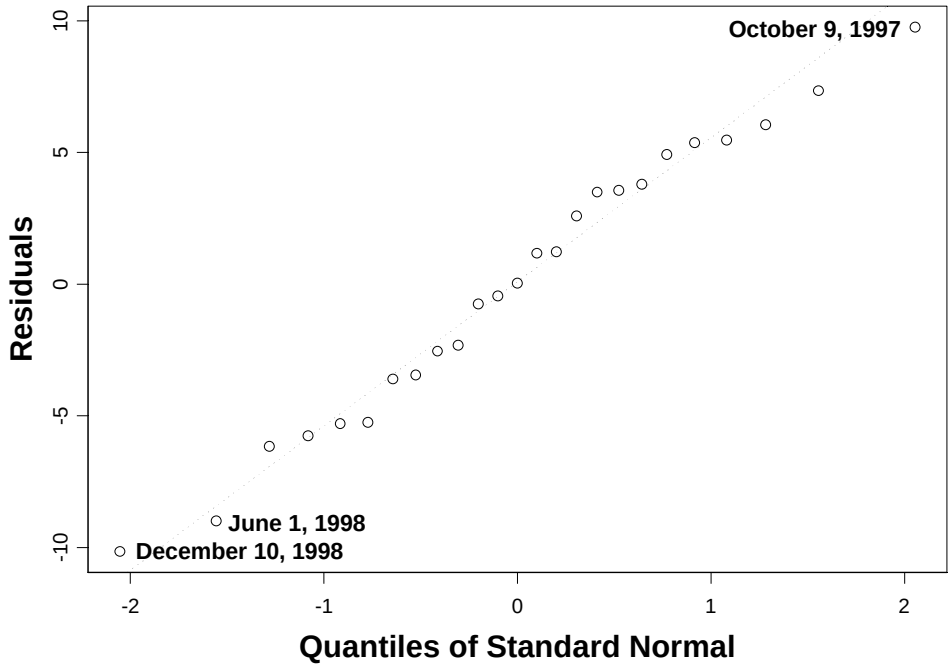

Figure B.2.3 Normal Quantile Plot of Residuals (Rainfall)

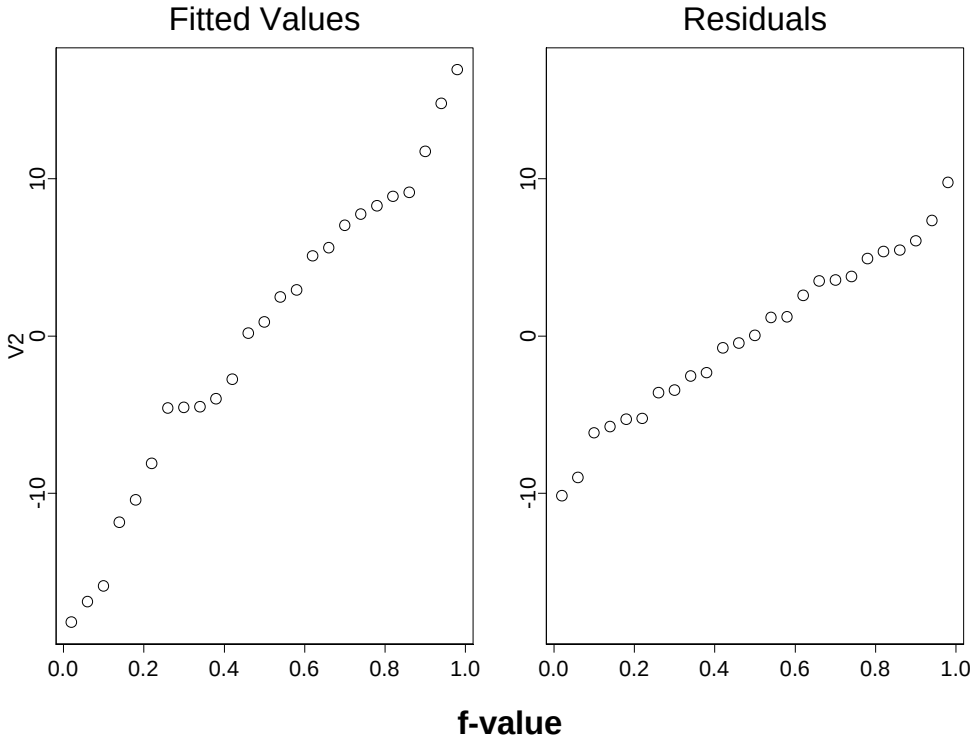

Figure B.2.4 Residual-Fit Spread Plot (Rainfall)

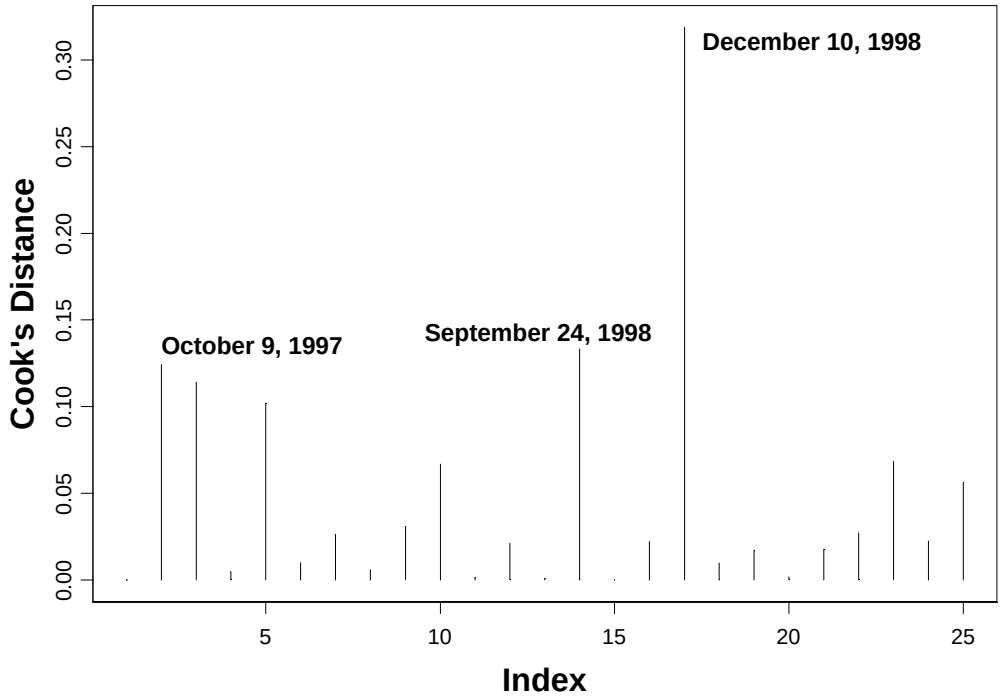

Figure B.2.5 Cook's Distance Plot (Rainfall)

B.3 Sites Regression Line Analysis

The regression line for the average values of the study sites was also used in Section 4.1. Diagnostic plots for this regression (Figures B.3.1 through B.3.5) indicate that G-3661, G3578 and RL3 had the greatest effect on the regression. The regression coefficients for the equation were most affected by G-3554, G-3555 and 3M4. The normal quantile plots and residual-fit spread fits indicate that the distribution of the sites data averages was even more linear than the rainfall

regression. This provides excellent evidence that the conclusions made in Section 4.1 are indeed valid.

ANCOVA analysis shows that the regression line has an equation of:

$$\delta D = 5.7941\delta^{18}O - 0.7369 \qquad \text{(Equation B.3.1)}$$

This regression line has a R^2 value of 0.9215. The slope coefficient was found to have a standard error of 0.3606 while the intercept coefficient had a standard error of 0.4780. The F-statistic of this regression was calculated to be 285.2 on 1 and 22 degrees of freedom. Once again, the statistical analysis shows that the linear sites regression is valid and normally distributed.

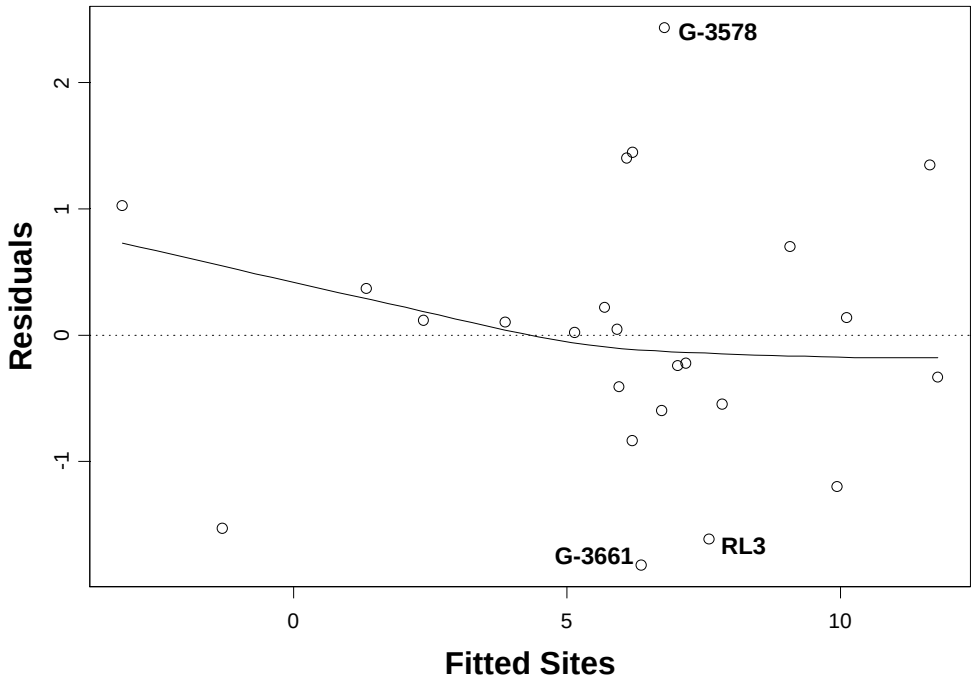

Figure B.3.1 Residuals vs. Fitted Values (Sites)

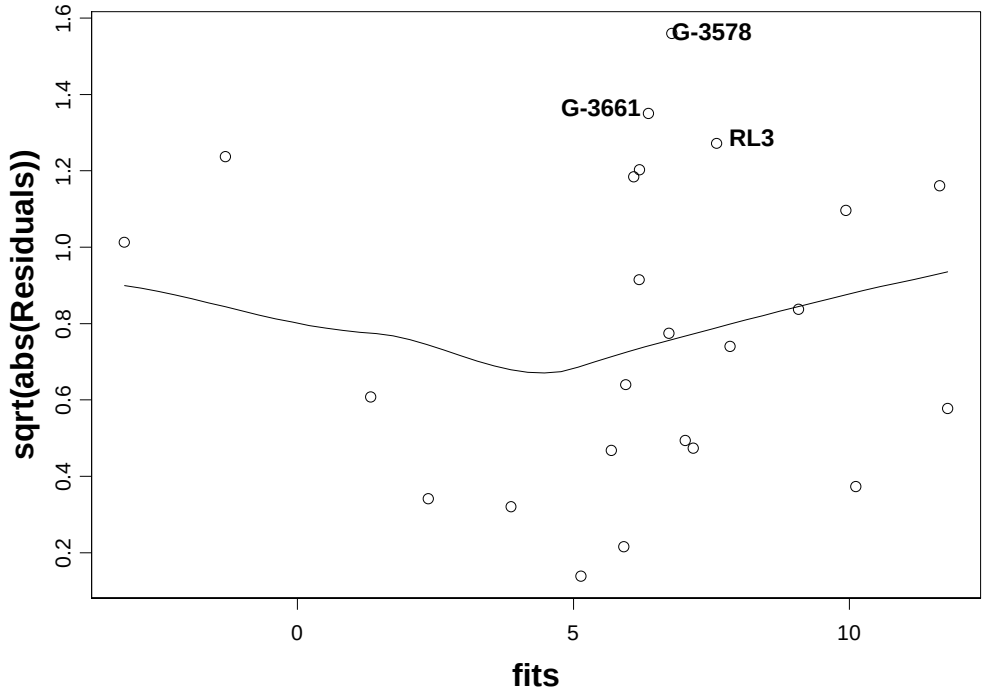

Figure B.3.2 Square Root of Absolute Residuals vs. Fitted Values (Sites)

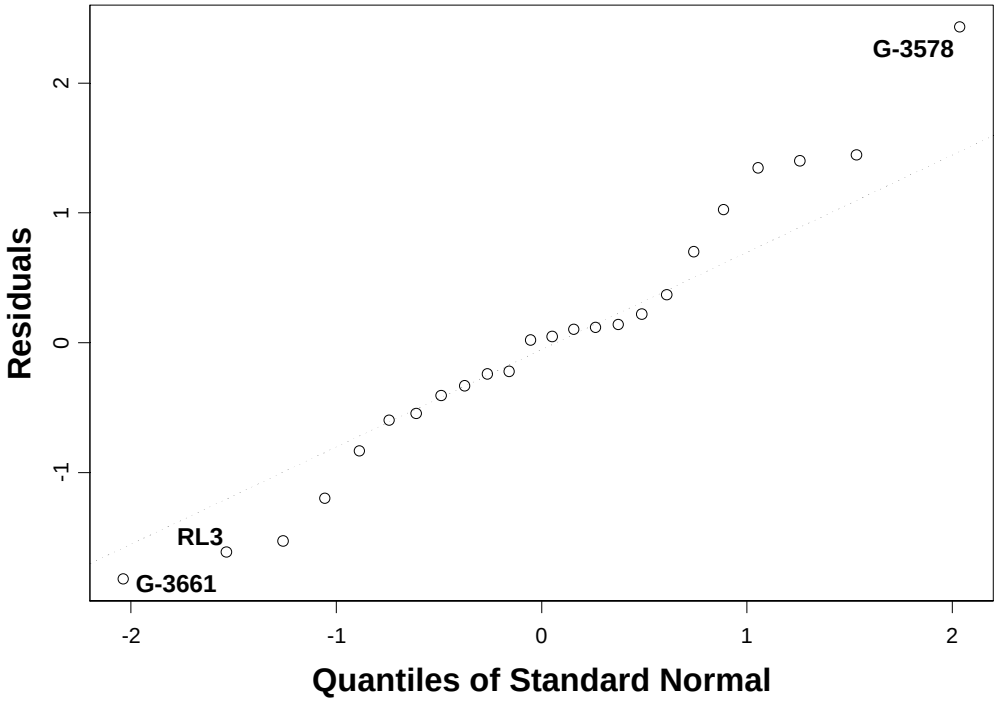

Figure B.3.3 Normal Quantile Plot of Residuals (Sites)

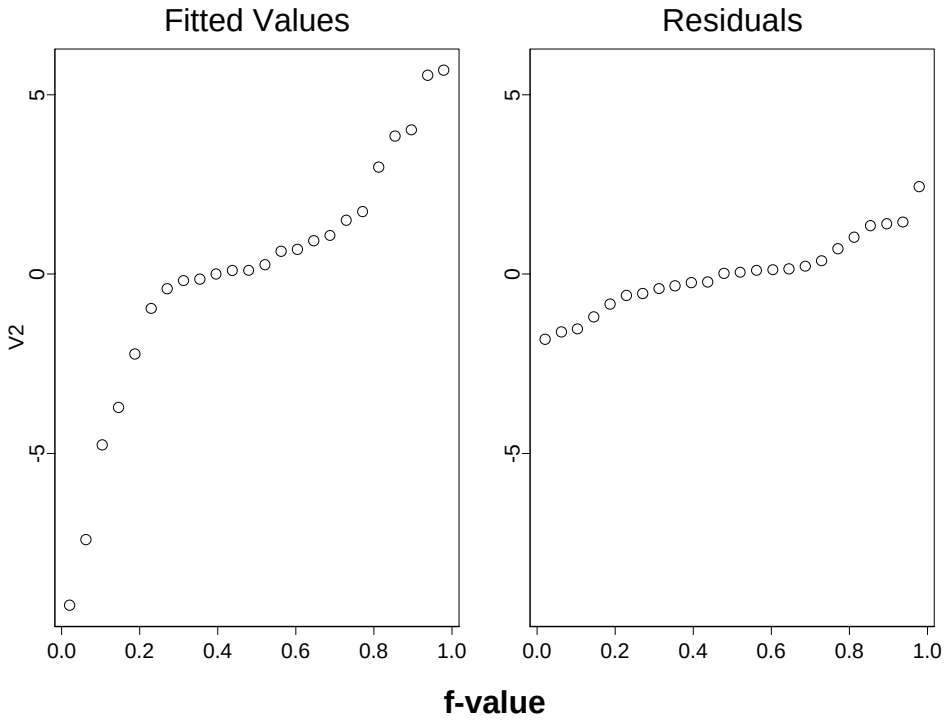

Figure B.3.4 Residual-Fit Spread Plot (Sites)

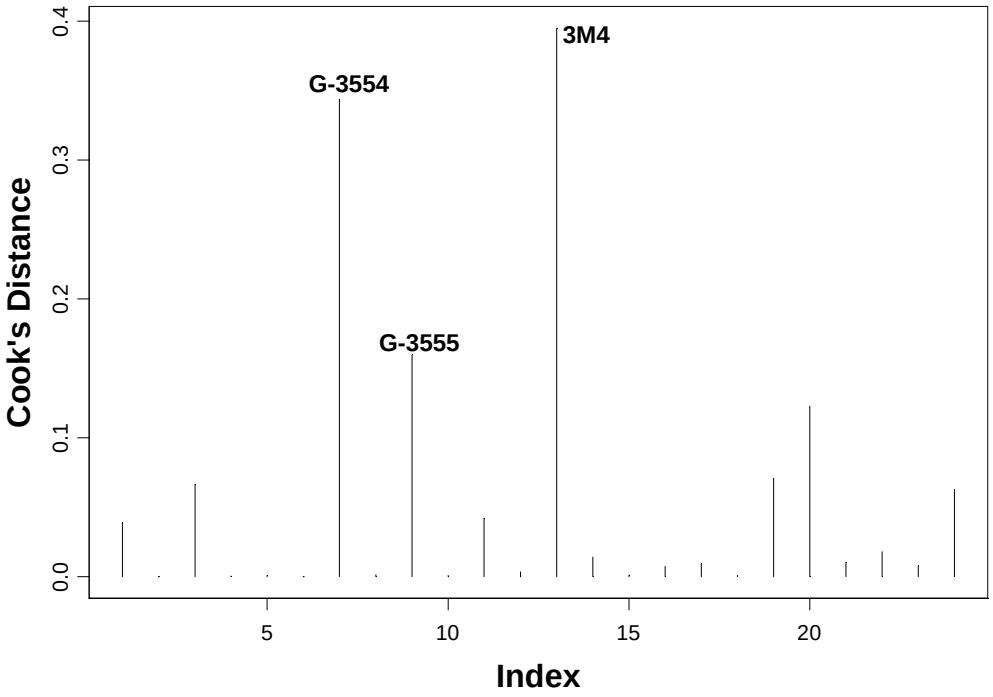

Figure B.3.5 Cook's Distance Plot (Sites)

Appendix C

Complex Box Model Calculations

C.1 Calculation of Evaporated Surface Water d Values

The method for calculation of evaporated surface water δ values as proposed by Gonfiantini (1986) was used to obtain values for the complex box model (δ_{E1}, δ_{E2} and δ_{E3}). The first step in the process is to calculate the equilibrium fractionation factor (α) associated with the evaporative process. This factor is given by the equation:

$$\ln(\alpha) = AT^{-2} + BT^{-1} + C \qquad \text{(Equation C.1.1)}$$

in which T is temperature in Kelvin and A, B and C are empirical coefficients for specific isotopic species. As these coefficients are empirical, different values are available from different studies. In the case of $^{18}O/^{16}O$, a compilation of data from Bottinga and Craig (1969), Majoube (1971), Jakli and Stachewski (1977) and Kakiuchi and Matsuo (1979) indicates that a fractionation factor on the order of 1.0092 is appropriate for approximately 25°C. The fractionation factor can then be used to calculate the equilibrium enrichment factor (ε) using the equation:

$$\varepsilon = (\alpha - 1) * 1000 \qquad \text{(Equation C.1.2)}$$

Knowing the fractionation and enrichment factors, the delta values of air (δ_a) can be calculated from the delta value of rainfall (δ_r):

$$\delta_a = (\delta_r - \varepsilon) / \alpha \qquad \text{(Equation C.1.3)}$$

This calculation is valid because the water vapor which becomes rainfall is in isotopic equilibrium with the surrounding air.

In order to account for the rate of evaporation, the term $\Delta\varepsilon$ is introduced. This term is dependent on humidity and is calculated:

$$\Delta\varepsilon = k(1 - h) \qquad \text{(Equation C.1.4)}$$

in which *h* is humidity (taken to be an average value of 83.73%). This equation includes a proportionality constant (k) which is 14.2 for oxygen-18 calculations.

As all necessary variables are now available, it is possible to calculate the delta value of evaporated water (δ_E) being taken from a surface water of known isotopic composition (δ_s) using the equation:

$$\delta_E = [(\delta_s - \varepsilon)/\alpha - h\delta_a - \Delta\varepsilon]/(1 - h + \Delta\varepsilon) \qquad \text{(Equation C.1.5)}$$

Results of the application of equation C.1.5 in the complex box model provided evaporation oxygen-18 delta values in the range of –0.24 $^{o}/_{oo}$ to 0.02 $^{o}/_{oo}$.

C.2 Volumetric and Isotopic Mass Balances

The complete set of equations for all control volumes in the complex box model is as follows. All variables are defined in Table 4.2.1 in the main text of this thesis. Known versus computed values are provided in Table 4.2.2 of the main text. These equations are solved simultaneously to compute the unknown values.

Volumetric Balances:

CV 1:

$$E + R1*A1 – ET1*A1 – X – Y = 0 \quad \text{(Equation C.2.1)}$$

CV 2:

$$X + R2*A2 – ET2*A2 – Z = 0 \quad \text{(Equation C.2.2)}$$

CV 3:

$$Z + R3*A3 – ET3*A3 – L – S = 0 \quad \text{(Equation C.2.3)}$$

CV 4:

$$Y + S – D = 0 \quad \text{(Equation C.2.4)}$$

CV 5:

$$L + D + R4*A4 – P – U = 0 \quad \text{(Equation C.2.5)}$$

CV 6:

$$E + (R1 – ET1)*A1 + (R2 – ET2)*A2 + (R3 – ET3)*A3 + R4*A4 – U – P = 0$$

(Equation C.2.6)

Isotopic Balances:

CV 1:

$$E*\delta_{G618} + R1*A1*\delta_{Rain\ G618} – ET1*A1*\delta_{E1} – X*\delta_{G3575} – Y*\delta_{G3660} = 0$$

(Equation C.2.7)

CV 2:

$$X*\delta_{G3575} + R2*A2*\delta_{Rain\ WW} – ET2*A2*\delta_{E2} – Z*\delta_{G3551} = 0$$

(Equation C.2.8)

CV 3:

$$Z*\delta_{G3551} + R3*A3*\delta_{Rain\ WW} - ET3*A3*\delta_{E3} - L*\delta_{L} - S*\delta_{L} = 0$$

(Equation C.2.9)

CV 4:

$$Y*\delta_{G3660} + S*\delta_{L} - D*\delta_{G3662} = 0 \qquad \text{(Equation C.2.10)}$$

CV 5:

$$L*\delta_{L} + D*\delta_{G3662} + R4*A4*\delta_{Rain\ WW} - P*\delta_{Well\ 29/30} - U*\delta_{G3555} = 0$$

(Equation C.2.11)

CV 6:

$$E*\delta_{G618} + R1*A1*\delta_{Rain\ G618} - ET1*A1*\delta_{E1} + R2*A2*\delta_{Rain\ WW} - ET2*A2*\delta_{E2} +$$

$$R3*A3*\delta_{Rain\ WW} - ET3*A3*\delta_{E3} + R4*A4*\delta_{Rain\ WW} - P*\delta_{Well\ 29/30} - U*\delta_{G3555} = 0$$

(Equation C.2.12)

C.3 MODBRANCH Flow Sums

A simulation was performed using the MODBRANCH model developed by Nemeth (2000) and modified by Hererra (2000) so as to provide for a means of comparison between the complex box model outlined in Chapter 5 of the main text and the MODBRANCH model. The cumulative flow sums for the MOBRANCH simulation as provided in Table 5.2.3 of the main text were calculated in a similar method as that outlined by Herrera (2000).

As in the Herrera method, the MODBRANCH model was run several times in order to provide output files for flow terms across specified surfaces of the conceptual boxes of the model. The boxes and surfaces examined were selected in order to correspond to the geographic location of the desired boundaries of the complex box model to be used for comparison (Figure C.3.1). In the figure, the grid placed over the study site is the discretization of the MODBRANCH model (Nemeth et al., 2000). The “shallow” flow terms were taken as those of model layers two and four (corresponding to layers two and four in Figure 2.2.2 in the main text). The “deep” flow terms were taken as those of model layer 6 (corresponding to layer six in Figure 2.2.2 in the main text). Boxes meeting the proper geographic, layering, and direction of flow criteria were organized into Tables C.3.1 and C.3.2 where the cumulative flow terms are calculated. Seventeen boxes were chosen as representative of seepage under L-31N while 21 boxes were needed to characterize lake outlfow.

When setting up the simulation, a hypothetical scenario set in 1997 was run in which the pumping wells of the West Wellfield were allowed to pump for one year at their average pumping rate (as used in the input for the complex box model). This scenario used actual rainfall and evaporation from 1997. Instead of obtaining model output values on a monthly basis and computing an average value as done by Herrera, model output was only obtained for two dates, December 31, 1997 and June 30, 1997. The December values were used for

comparison to the complex model while the June values were run as a check on the December values. The flow terms were found to correlate well between the two dates and as such, the December values were used for comparison to the complex box model.

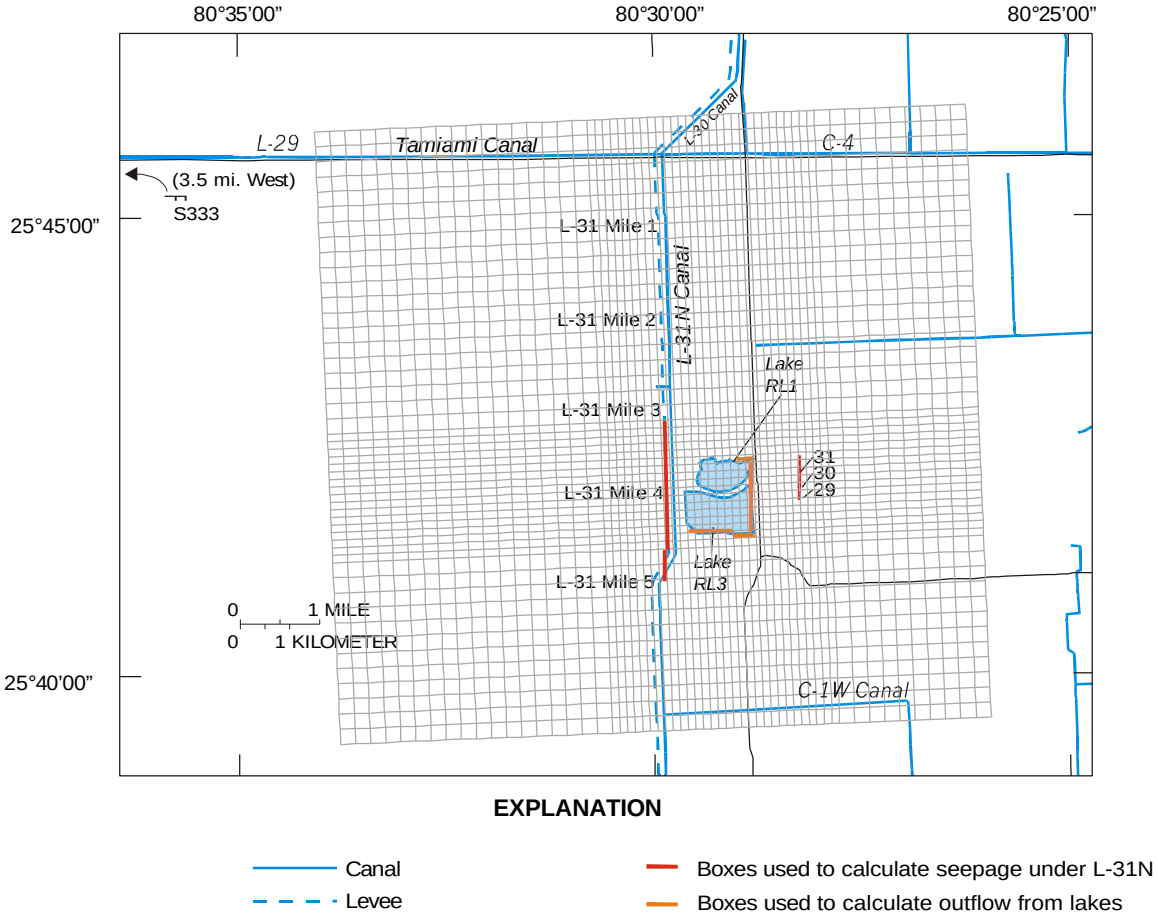

Figure C.3.1 MODBRANCH model boxes used for comparison to complex box model

Table C.3.1 – Seepage Under L-31N MODBRANCH Flow Terms

Model Layer	"Shallow"		"Deep"
	2	4	6
Flow (cf/d) Values were converted to cf/y prior to insertion in Table 4.2.3	6.30E+03	1.10E+05	1.20E+05
	3.40E+03	5.90E+04	6.30E+04
	3.60E+03	6.30E+04	6.60E+04
	3.90E+03	6.80E+04	6.90E+04
	4.30E+03	7.40E+04	7.40E+04
	4.80E+03	8.20E+04	8.00E+04
	5.40E+03	9.30E+04	9.00E+04
	6.30E+03	1.10E+05	1.00E+05
	6.90E+03	1.20E+05	1.20E+05
	9.00E+03	1.60E+05	1.40E+05
	1.10E+04	1.90E+05	1.70E+05
	1.60E+04	2.70E+05	2.30E+05
	1.40E+04	2.40E+05	1.90E+05
	7.80E+03	1.60E+05	9.40E+04
	7.60E+03	1.40E+05	5.90E+04
	7.50E+03	1.40E+05	5.10E+04
	7.50E+03	1.30E+05	4.90E+04
	7.50E+03	1.30E+05	5.00E+04
	1.40E+04	2.70E+05	1.20E+05
Column Sum (cf/d)	1.47E+05	2.61E+06	1.94E+06
Sum (cf/y)	1.01 E+09		7.06 E+08
Cumulative Sum (cf/y)	**1.71 E+09**		

Table C.3.2 – Rock Mining Lake Outflow MODBRANCH Flow Terms

Model Layer	"Shallow"		"Deep"
	2	4	6
Flow (cf / d) Values were converted to cf / y prior to insertion in Table 4.2.3	2.50E+03	2.70E+04	2.30E+04
	2.90E+03	3.10E+04	2.50E+04
	2.90E+03	3.10E+04	2.50E+04
	5.40E+03	5.90E+04	4.60E+04
	4.40E+03	4.80E+04	3.70E+04
	3.80E+03	4.10E+04	3.50E+04
	7.90E+03	8.80E+04	8.00E+04
	7.40E+03	7.90E+04	6.50E+04
	1.80E+04	2.00E+05	2.20E+05
	2.20E+04	2.40E+05	3.20E+05
	1.70E+03	1.30E+04	6.80E+03
	7.60E+00	1.10E+04	1.20E+04
	1.30E+01	1.80E+04	1.90E+04
	1.00E+01	1.50E+04	1.60E+04
	3.00E+03	2.20E+04	9.40E+03
	7.00E+02	7.80E+03	7.00E+03
	2.20E+03	2.20E+04	1.70E+04
	4.10E+03	3.80E+04	2.30E+04
	7.40E+03	5.00E+04	6.80E+03
	5.90E+01	8.40E+04	8.80E+04
	9.00E+01	1.30E+05	1.30E+05
	8.20E+01	1.10E+05	1.20E+05
Column Sum (cf / d)	9.66E+04	1.36E+06	1.33E+06
Sum (cf / y)	5.33 E+08		4.86 E+08
Cumulative Sum (cf/y)	**1.02 E+09**		